Development of Copper Photoredox Catalysis for Defluorinative Carbon–Heteroatom Coupling Reactions

****

(脱フッ素型炭素-ヘテロ原子カップリング反応のための銅光酸化還元触媒の開発)

Priya Saha
Graduate School of Chemical Science and Engineering
Hokkaido University

To my father, and all the people who dedicate themselves
to making life richer and more meaningful.

Contents

Chapter 1
General Introduction

1.1 Photocatalysis

For 100 years, scientists have been exploring ways in which light can be employed as a powerful tool to carry out chemical reactions, which has enabled chemists to construct molecules in new and creative ways. These novel transformations have offered unprecedented opportunities to create new medicines, materials, and numerous other valuable products.[1]

As a result, photocatalysis has attracted a great deal of interest, and practical protocols are continuously being developed during the recent decades. Generally, when the photocatalyst absorbs light (frequently from LEDs or sunlight), it gains energy or becomes "excited." This excited-state species then interacts with substrates and promotes reactions that are otherwise out of reach. By going through these high-energy states, the ground-state thermal barrier can be bypassed, thus allowing for milder reaction conditions. Furthermore, light offers opportunities to achieve high temporal, spatial, and spectral precision, which can be exploited for additional layers of reaction control.[2]

1.2 Photoredox catalysis

Photoredox catalysis is one particular category of photocatalytic reactions, where the excited-state catalyst (PC*) engages redox events with substrates either through an oxidative or reductive quenching process (Scheme 1). As compared to the ground-state catalysts, the excited-state species are more potent reductant and/or oxidant, allowing for reactions with a broader range of substrates.[3] Importantly, following the single-electron reduction or oxidation of organic substrates, the resulting radical intermediates are now set up for reactivity distinct from two-electron mechanisms. As a result, photoredox catalysis unlocks an entire array of new reactivity by accessing radical mechanism under extremely mild conditions.

---

[1] (a) Karkas, M. D.; Porco, J. A., Jr.; Stephenson, C. R. J. *Chem. Rev.* **2016**, DOI: 10.1021/acs.chemrev.5b00760. (b) Bach, T.; Hehn, J. P. *Angew. Chem., Int. Ed.* **2011**, *50*, 1000−1045. (c) Hoffmann, N. *Chem. Rev.* **2008**, *108*, 1052−1103.(d) Roth, H. D. *Angew. Chem., Int. Ed. Engl.* **1989**, *28*, 1193−1207. (e) Trommsdorff, H. *Ann. Pharm.* **1834**, *11*, 190−207. (f) Ciamician, G.; Silber, P. Ber. *Dtsch. Chem. Ges.* **1908**, *41*, 1928−1935.

[2] Shaw, M. H.; Twilton, J.; MacMillan, D. W. C. *J. Org. Chem.* **2016**, *81*, 6898−6926.

[3] (a) Nicewicz, D. A.; MacMillan, D. W. C. *Science* **2008**, *322*, 77–80. (b) Ischay, M. A.; Anzovino, M. E.; Du, J.; Yoon, T. P. *J. Am.Chem. Soc.* **2008**, *130*, 12886–12887.

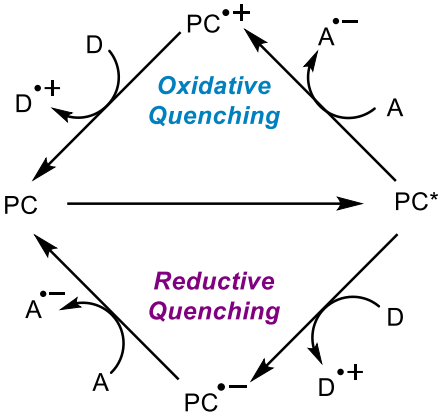

Scheme 1. Oxidative and Reductive quenching cycle of photocatalyst.

Metal complexes [4] and organic dye [5] represent two most widely utilized classes of photoredox catalysts. Redox properties of metal catalysts can be finely tuned by modifying ligands coordinated to the metal centers. Electron-deficient ligands boost oxidizing power of catalysts while electron-rich ligands enhance the ability to reduce substrates. Among all, Ru- and Ir-complexes are the dominant choices. For instance, $Ru(bpy)_3^{2+}$ can act as a strong photo-reductant and relatively weak photo-oxidant. Replacing bipyridine ligands with more electron-deficient bipyrazine ligands significantly increase the oxidizing capability.

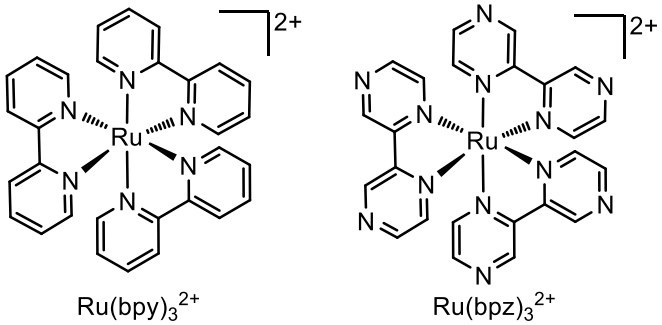

$Ru(bpy)_3^{2+}$

E^*_{ox} = -0.81 V vs SCE

E^*_{red} = +0.77 V vs SCE

$Ru(bpz)_3^{2+}$

E^*_{ox} = -0.26 V vs SCE

E^*_{red} = +1.45 V vs SCE

[4] (a) Schmalzbauer, M.; Marcon, M.; König, B. *Angew. Chem., Int. Ed.*, **2021**, *60*, 6270–6293. (b) Barham, J. P.; Ko¨nig, B. *Angew. Chem., Int. Ed.*, **2020**, *59*, 11732–11747. (c) Crisenza, G.E.M.; Mazzarella, D.; Melchiorre, P. *J. Am. Chem. Soc.*, **2020**, *142*, 5461–5476. (d) Xie, J.; Jin, H.; Hashmi, A. S. K. *Chem. Soc. Rev.*, **2017**, *46*, 5193–5203. (e) Pe´ter, A.; Agasti, S.; Knowles, O.; Pye, E.; Procter, D. J. *Chem. Soc. Rev.*, **2021**, *50*, 5349–5365. (f) Twilton, J.; Le, C.; Zhang, P.; Shaw, M. H.; Evans, R. W. MacMillan, D. W. C. *Nat. Rev. Chem.*, **2017**, *1*, 0052.

[5] (a) Romero, N. A.; Nicewicz, D. A. *Chem. Rev.*, **2016**, *116*, 10075–10166. (b) Prier, C.K.; Rankic, D. A.; MacMillan, D. W. C. *Chem. Rev.*, **2013**, *113*, 5322–5363. (c) McAtee, R. C.; McClain, E. J.; Stephenson, C. R. J. *Trends Chem.*, **2019**, *1*(special issue), 111–129. (d) Marzo, L. S.; Pagire, K.; Reiser, O.; B. Ko¨nig, *Angew. Chem., Int. Ed.*, **2018**, *57*, 10034–10072.

On the other hand, $Ir(ppy)_3$ serves as a potent photo-reductant but possesses weak oxidizing ability. Introduction of electron-withdrawing substituents to the ligands diminishes the reducing power and increases the oxidizing capability.[6] In both cases, excited states persist for several microsecond, which is sufficient for energy or electrons transfer to another transition metal catalyst or directly with an organic molecule. However, the applicability of Ru- and Ir-based photocatalysts can be hindered by their high cost and limited natural abundance.[7] Additionally, tunability can be an issue as in advance preparation of these complexes is required.

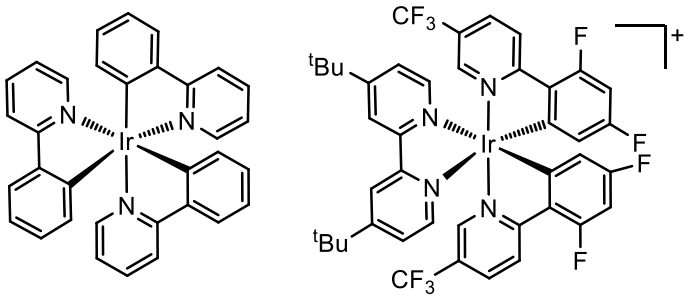

In the design of organic dye photocatalysts, donor-acceptor aromatic structures are frequently employed, and their photochemical and redox characters can often be tuned by varying the electronic properties of the substituents. For example. 3DPA2FBN displays a lower excited-state reduction potential (+0.92 V vs. SCE). Upon replacing diphenylamine groups with carbazole units and introducing nitrile group yields 4CzIPN, a strong photooxidant with an excited state potential of +1.43 V vs. SCE.[8] Although organic dyes offer a metal-free alternative for photoredox catalysis, but it requires laborious molecular design and synthesis to tune the redox properties. Furthermore, organic dye photocatalysts may exhibit inferior photostability.[9]

---

[6] Bell, J. D.; Murphy, J. A. *Chem. Soc. Rev.*, **2021**, *50*, 9540–9685.

[7] (a) Shaw, M. H.; Twilton, J.; MacMillan, D. W. C. *J. Org. Chem.* **2016**, *81*,6898–6926. (b) Flamigni, L.; Barbieri, A.; Sabatini, C.; Ventura, B.; Barigelletti, F. *Top. Curr. Chem.* **2007**, *281*, 143–203. (c) Chan, A. Y.; Perry, I. B.; Bissonnette, N. B.; Buksh, B. F.; Edwards, G. A.; Frye, L. I.; Garry, O. L.; Lavagnino, M. N.; Li, B. X.; Liang, Y. F. et al., *Chem. Rev.* **2022**, *122*, 1485–1542.

[8] (a) Speckmeier, E.; Fischer, T. G.; Zeitler, K. *J. Am. Chem. Soc.*, **2018**, *140*, 15353–15365. (b) Nguyen, J. D.; Matsuura, B. S.; Stephenson, C. R. J. *J. Am. Chem. Soc.*, **2014**, *136*, 1218–1221. (c) Chen, K.; Schwarz, J.; Karl, T. A.; Chatterjee, A.; Ko¨nig, B. *Chem. Commun.*, **2019**, *55*, 13144–13147.

[9] Romero, N. A.; Nicewicz, D. A. *Chem. Rev.* **2016**, *116*, 10075–10166.

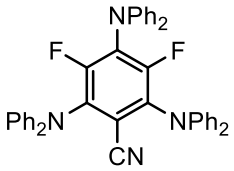

3DPA2FBN

E^*_{ox} = -1.60 V vs SCE

E^*_{red} = +0.92 V vs SCE

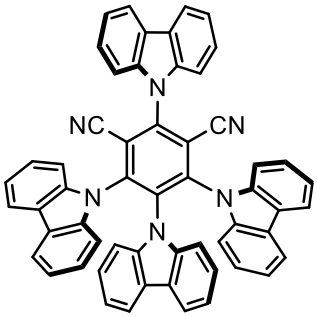

4CzIPN

E^*_{ox} = -1.18 V vs SCE

E^*_{red} = +1.43 V vs SCE

1.3 Base metal photoredox catalyst

The high cost and limited availability of Ir- and Ru-based photocatalysts,[10] as well as the synthetic challenges and low photostability associated with organic dyes prompted a growing interest in developing base-metal photoredox catalysts derived from earth-abundant first-row transition metals such as iron,[11] nickel,[12] and copper[13] (Scheme 2). In addition to being a more sustainable and affordable alternative for light-driven chemistry, they offer superior tunability by *in situ* screening of metal precursors and ligands to achieve the desired reactivity and selectivity.[14]

---

[10] Skubi, K. L.; Blum, T. R.; Yoon, T. P. *Chem. Rev.* **2016**, *116*, 10035–10074.

[11] (a) Shepard, S. G.; Fatur, S. M.; Rappe, A. K.; Damrauer, N. H. *J. Am. Chem. Soc.* **2016**, *138*, 2949−2952. (b) Liu, Y. Z.; Harlang, T.; Canton, S. E.; Chabera, P.; Suarez Alcantara, K.; Fleckhaus, A.; Vithanage, D. A.; Goransson, E.; Corani, A.; Lomoth, R.; Sundstrom, V.; Warnmark, K. *Chem. Commun.* **2013**, *49*, 6412−6414. (c) Duchanois, T.; Etienne, T.; Cebrian, C.; Liu, L.; Monari, A.; Beley, M.; Assfeld, X.; Haacke, S.; Gros, P. C. *Eur. J. Inorg. Chem.* **2015**, 2469−2477. (d) Liu, L.; Duchanois, T.; Etienne, T.; Monari, A.; Beley, M.; Assfeld, X.; Haacke, S.; Gros, P. C. *Phys. Chem. Chem. Phys.* **2016**, *18*, 12550−12556.

[12] (a) Welin, E. R.; Le, C.; Arias-Rotondo, D. M.; McCusker, J. K.; MacMillan, D. W. C. *Science* **2017**, *355*, 380−384. (b) Shields, B. J.; Kudisch, B.; Scholes, G. D.; Doyle, A. G. *J. Am. Chem. Soc.* **2018**, *140*, 3035−3039. (c) Grubel, M.; Bosque, I.; Altmann, P. J.; Bach, T.; Hess, C. R. *Chem. Sci.* **2018**, *9*, 3313−3317.

[13] (a) Armaroli, N. *Chem. Soc. Rev.* **2001**, *30*, 113−124. (b) Cuttell, D. G.; Kuang, S. M.; Fanwick, P. E.; McMillin, D. R.; Walton, R. A. *J. Am. Chem. Soc.* **2002**, *124*, 6−7. (c) Creutz, S. E.; Lotito, K. J.; Fu, G. C.; Peters, J. C. *Science* **2012**, *338*, 647−651.

[14] (a) Wenger, O. S. *J. Am. Chem. Soc.* **2018**, *140*, 13522–13533. (b) Larsen, C. B.; Wenger, O. S. *Chemistry* **2018**, *24*, 2039–2058.

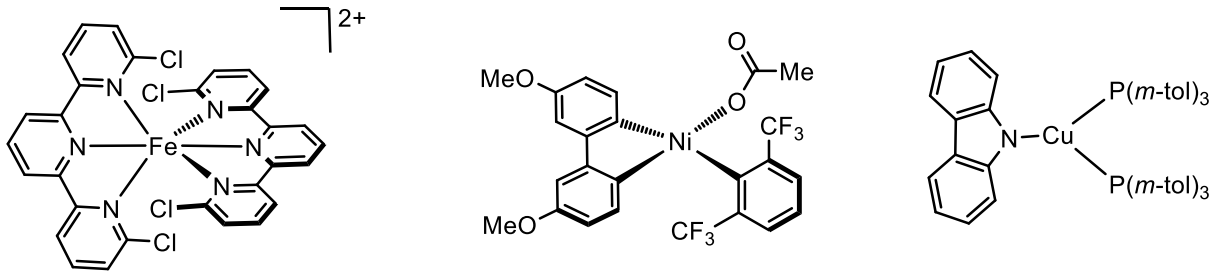

$Fe(dctpy)_2]^{2+}$ — *Damrauer*

$[Ni(MeObpy)(ArCF_3)(OCOMe)]$ — *MacMillan and McCuske*

$[Cu(cbz)(P(m\text{-}tol)_3)_2$ — *Peters and Fu*

Scheme 2. Examples of base metal photocatalyst.

1.4 Copper(I) complexes functioning as independent photocatalysts

Among all base-metal photoredox catalysts, copper has recently gained broad popularity.[15] Accessibility to Cu(I/II/III) oxidation states allows for engagement with substrates under both photochemical and thermal conditions. The ability of copper to complex with a wide range of ligand classes also facilitate their flexibility and tunability.

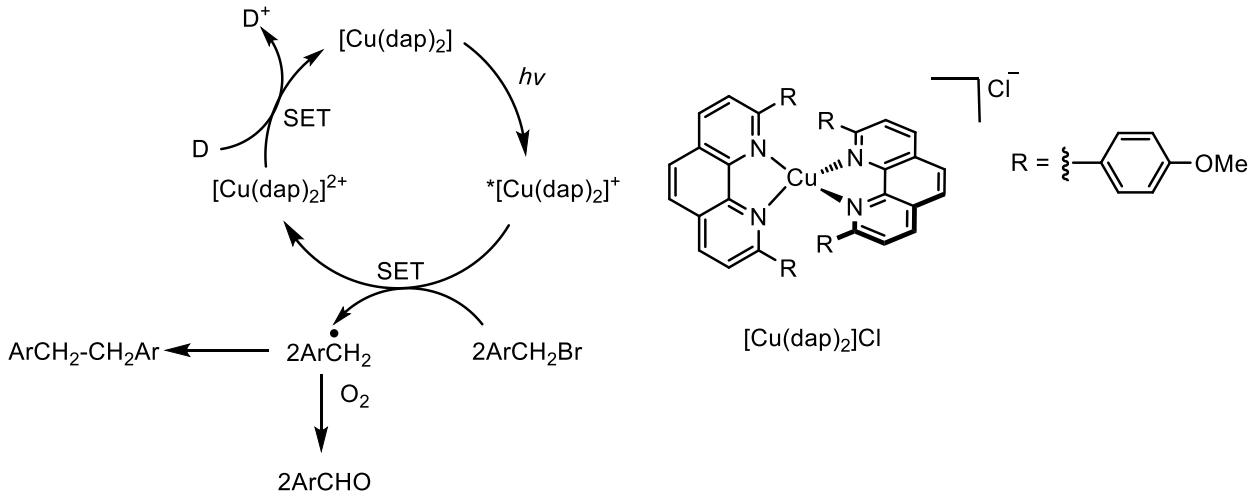

$[Cu(dap)_2]Cl$

Scheme 3. $[Cu(dap)_2]Cl$ catalysed reductive coupling of aryl bromide.

In 1977, McMillin et al. reported an early study on copper(I) complex $[Cu(dmp)_2]BF_4$ (dmp = 2,9-dimethyl-1,10-phenanthroline). Upon 454-nm photoexcitation, this complex reaches a metal-

[15] Hossain, A.; Bhattacharyya, A.; Reiser, O. *Science*, **2019**, *364*, eaav9713. (b) SandovalPauker, C.; Molina-Aguirre, G.; Pinter, B. *Polyhedron*, **2021**, *199*, 115105. (c) Beaudelot, J.; Oger, S.; Peruško, S.; Phan, T.-A.; Teunens, T.; Moucheron, C.; Evano, G. *Chem. Rev.*, **2022**, 122, 16365.

to-ligand-charge-transfer (MLCT) excited state, enabling the reduction of Co(III) to Co(II).[16] About a decade later, Sauvage (Scheme 3) developed $[Cu(dap)_2]Cl$ (dap = phenanthroline with anisyl groups) that shows enhanced lifetime of its MLCT excited state (up to 270 ns) and a potent reducing strength (–1.43 V vs. SCE in MeCN), and its catalytic activity was showcased in a reductive coupling of nitrobenzyl bromide to the corresponding bibenzylic coupling product..[17] Following these pioneering studies, numerous publications have established the role of copper(I) complexes in catalyzing light-driven reactions such as bifunctionalization of olefins,[18] Cu(sp^2)-heteroatom cross coupling,[19] and Sonogashira-type couplings (Scheme 4).[20]

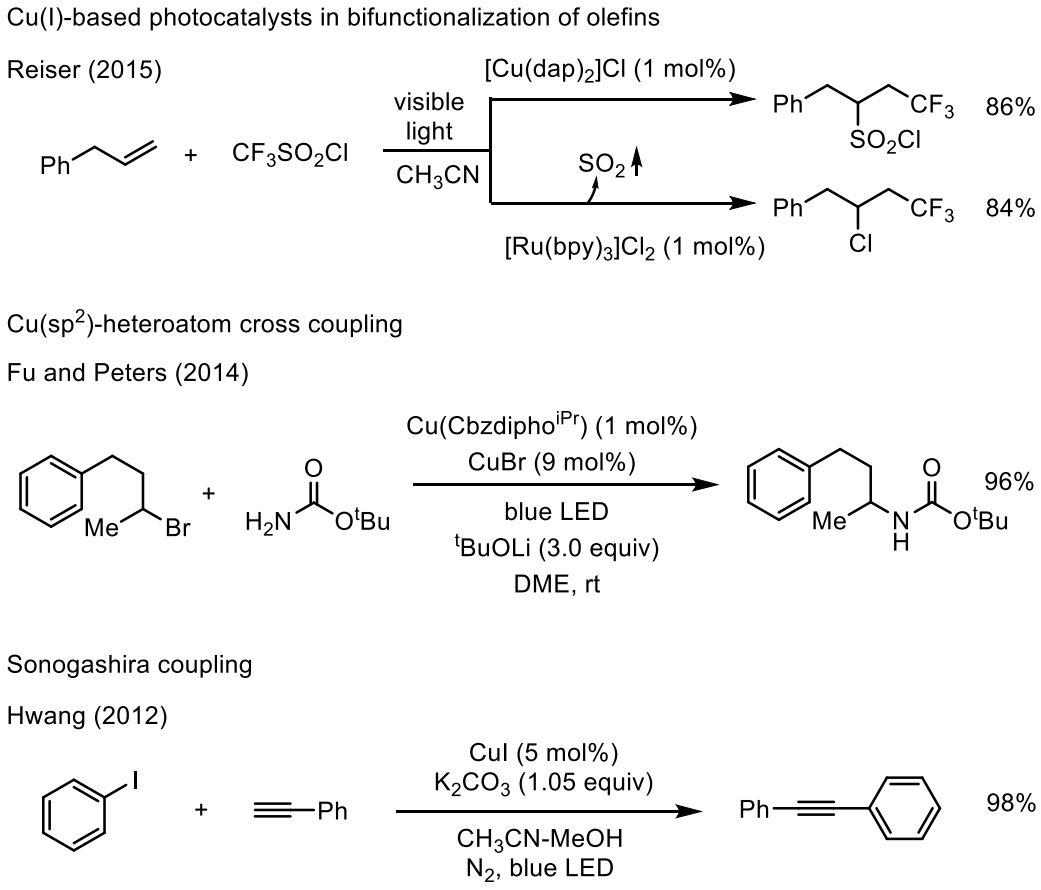

Scheme 4. Examples of copper(I) complexes as photocatalyst.

---

[16] McMillin, D. R. M.; Buckner, T.; Ahn, B. T. *Inorg. Chem.* **1977**, *16*, 943–945.
[17] Kern, J.-M.; Sauvage, J.-P. *J. Chem. Soc. Chem. Commun.* **1987**, *8*, 546–548.
[18] Bagal, D. B.; Kachkovskyi, G.; Knorn, M.; Rawner, T.; Bhanage, B. M.; Reiser, O. *Angew. Chem., Int. Ed.* **2015**, *54*, 6999−7002.
[19] Ahn, J. M.; Peters, J. C.; Fu, G. C. *J. Am. Chem. Soc.* **2017**, *139*, 18101– 18106,
[20] Sagadevan, A.; Hwang, K. C. *Adv. Synth. Catal.* **2012**, *354*, 3421–3427.

As can be seen from the above examples, recent attention has shifted to utilizing copper as dual role catalysts (Scheme 5). On one hand, copper complexes can serve as photocatalysts to activate the substrate and generate radical intermediates. On the other hand, copper can act to catalyze thermal reaction (e.g. cross coupling). This flexibility thus allows for the design of sophisticated mechanistic schemes within a single catalytic system:

- Light Activation: A copper(I) complex with appropriate ligands absorbs visible light and is promoted to the excited state.
- Electron Transfer: The photoexcited complex undergoes single-electron transfer to the substrate, producing a radical intermediate (R•) and concurrently oxidizing copper (I) to copper (II).
- Pathway 1: The Cu(II) complex reacts with a nucleophilic cross-coupling partner (Nu) to form a Cu–Nu intermediate. An outersphere attack by the radical (R•) then affords the final product (R–Nu) and regenerates the starting copper(I) catalyst
- Pathway 2: This innersphere mechanism involves the radical (R•) added to the copper (II) complex, form a copper (III) intermediate. Ligand exchange with the nucleophile (Nu) followed by a reductive elimination then produces the cross-coupled product (R–Nu) and regenerates the original copper (I) state.[11,21]

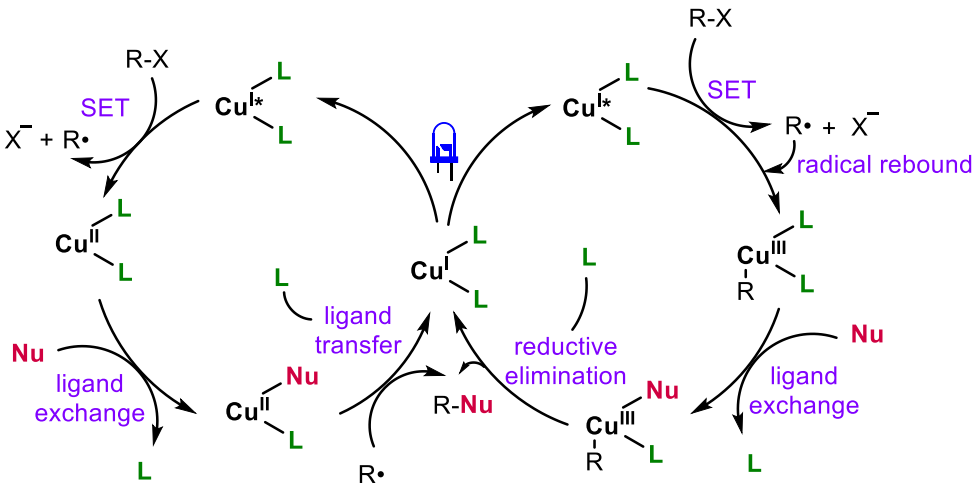

Scheme 5. The plausible mechanism of Cu(I) photocatalysts for cross-coupling reactions.

[21] Mitani, M.; Kato, I.; Koyama, K. *J. Am. Chem. Soc.* **1983**, *105*, 6719–6721.

1.5 Fluorine containing Compounds

For the last few decades, fluorinated organic molecules have gained lots of attention across many fields. Due to the unique physical, chemical, and biological properties fluorine substituents impart, these molecules are widely used in the production of pharmaceuticals, agrochemicals, and functional materials.[22]

In particular, there is a huge impact of fluorine in pharmaceutical industry. It is estimated that one-fifth of the drugs presently being used in clinic contain fluorine. What is even more compelling is the fact that nearly 30% of the 30 most profitable drugs on the global market have at least one fluorine atom in their structures.[23] Notable examples of currently marketed fluorine-containing drugs include fluoxetine (antidepressant), celebrex (anti-inflammatory drug), efavirenz (used to treat HIV), atorvastatin (used for blocking enzyme needed to make cholesterol), fluticasone propionate (used in asthma inhalers).[24]

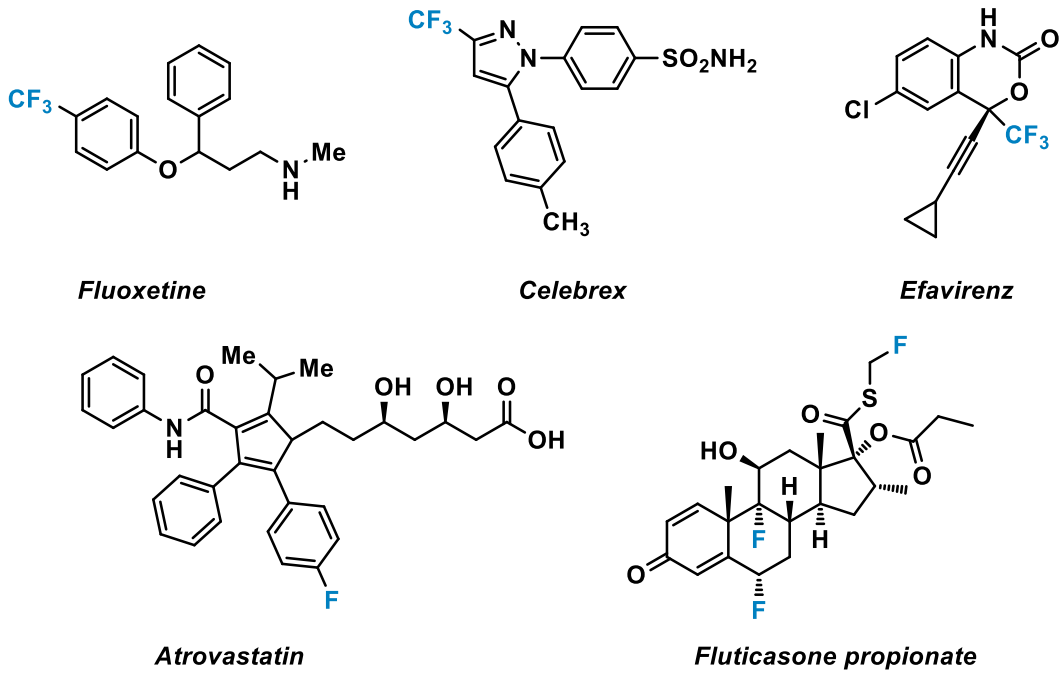

Scheme 6. Some fluorine-containing pharmaceutical molecules.

---

[22] (a) Uneyama, K. Organofluorine Chemistry, Blackwell, Oxford, **2006**. (b) Kirsch, P. Modern Fluoroorganic Chemistry: Synthesis, Reactivity, Applications, Wiley-VCH, Weinheim, **2013**.

[23] Hagan, D. O. *J. Fluorine Chem.* **2010**, *131*, 1071–1081.

[24] (a) Prakash, V.R. Organofluorine Compounds in Biology and Medicine, Elsevier, **2015**. (b) Wang, J.; Sánchez-Roselló, M.; Aceña, J.L.; Pozo, Cd.; Sorochinsky, A.E.; Fustero, S.; Soloshonok, V.A.; Liu, H. *Chem. Rev.* **2014**, 114, 2432–2506.

In general, fluorine-containing drugs are more effective in comparison with the non-fluorinated counterpart due to the following reasons:

- Improved binding to the drug targets
- Improved metabolic stability
- Improved bioavailability
- Improved membrane permeability

CF_3 group containing drugs have emerged as a topic of remarkable significance for the medical and fluorine chemists to investigate, as such drugs typically manifest improved biological properties and are better suited for the development of pharmaceuticals.[20]

1.6 Difluoromethylene group

Trifluoromethyl group has been a prestigious motif in functional molecules and is widely included in drug molecules and advanced materials. Recent efforts to expand the chemical space have focused on difluoromethylene group (–CF_2–).[25] This moiety can serve as an structural isostere of an ether or hydroxy group.

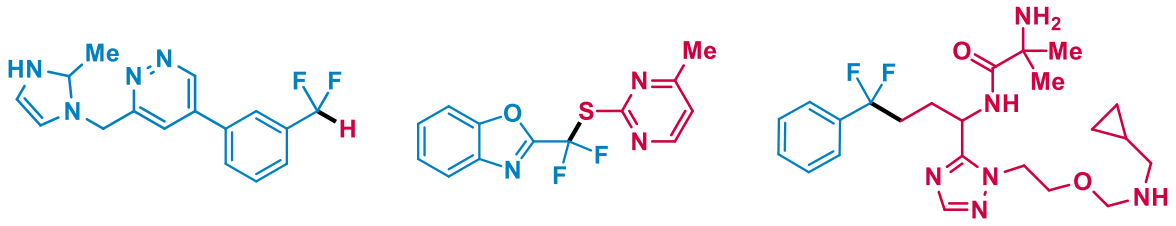

NR2B antagonist | *HIV-1 reverse transcriptase inhibitor* | *growth hormone secretatgogue*

Scheme 7. Drugs containing difluoromethyl motif**.**

Given their importance, efficient preparation of CF_2 groups has thus become a highly desirable goal[26]. To this end, selective breaking of a C–F bond in trifluoromethyl (–CF_3)

[25] (a) Hu, J.; Zhang, W.; Wang, F. *Chem. Commun*. **2009**, *48*, 7465–7478. (b) Ni, C.; Hu, J. *Synthesis* **2014**, 842–863. (c) Ni, C.; Zhu, L.; Hu, J. *Acta Chim. Sinica* **2015**, *73*, 90–115. (d) Chen, B.; Vicic, D.A. *Top. Organomet. Chem.* **2015**, *52*, 113–142. (e) Belhomme, M.-C.; Besset, T.; Poisson, T.; Pannecoucke, X. *Chem. Eur. J.* **2015**, 21, 12836–12865.

[26] (a) Xu, P.; Guo, S.; Wang, L.; Tang, P. *Angew. Chem. Int. Ed.* **2014**, *53*, 5955–5058. (b) Feng, Z.; Xiao, Y.-L.; Zhang, X. *Acc. Chem. Res.* **2018**, *51*, 2264–2278. (c) Sumino, S.; Uno, M.; Fukuyama, T.; Ryu, I.; Matsuura, M.; Yamamoto, A.; Kishikawa, Y. *J. Org. Chem.* **2017**, *82*, 5469–5474.

compounds to generate difluoromethyl compounds represents an attractive strategy given the prevalence of CF_3-containing compounds.

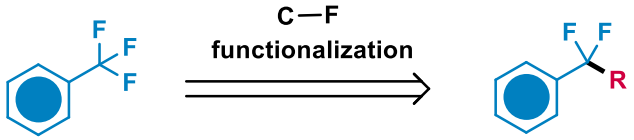

Scheme 8. Selective C–F bond functionalization.

Nevertheless, this approach can be challenging since the carbon–fluorine bond is one of the strongest single bonds in organic chemistry (Scheme 9). Furthermore, in the course of the defluorination, if one fluorine atom is removed, the rest of the C–F bonds are weakened, which inevitably leads to over-defluorination.[27] Therefore, the quest for efficient and selective methods for selectively substituting only one fluorine remains a highly sought-after topic.

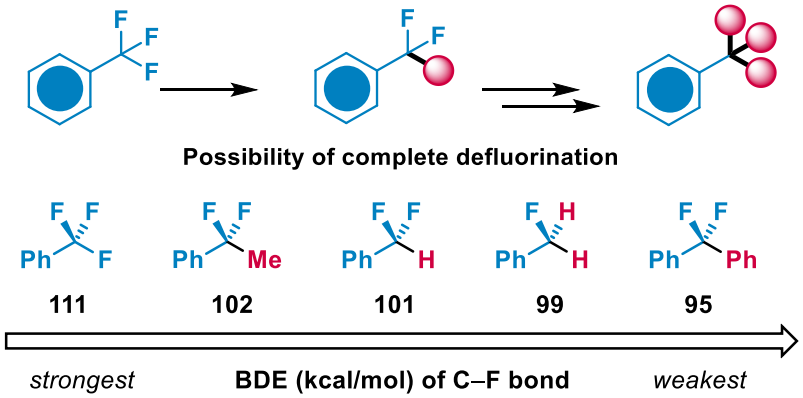

Scheme 9. Bond dissociation energies of C-F bond in fluoroalkylated arenes.

[27] Luo, C.; Bandar, J. S. *J. Am. Chem. Soc.* **2019**, *141*, 14120−14125.

Many different strategies have been explored to activate the C–F bond with the help of reducing metals, [28] frustrated Lewis pairs, [29] silicon Lewis acids, [30] remote substitution, [31] electrocatalysis,[32] and photoredox catalysis.[33]

In particular, photoredox catalysis has been an emerging strategy for selective C–F functionalization (Scheme 10). The excited photocatalyst undergoes SET to trifluoromethylarenes, followed by mesolytic cleavage to form a key difluoromethyl radical (·CF_2). This radical intermediate can subsequently be participate in a wide range of reactions, leading to many different difluoromethylated products.[34]

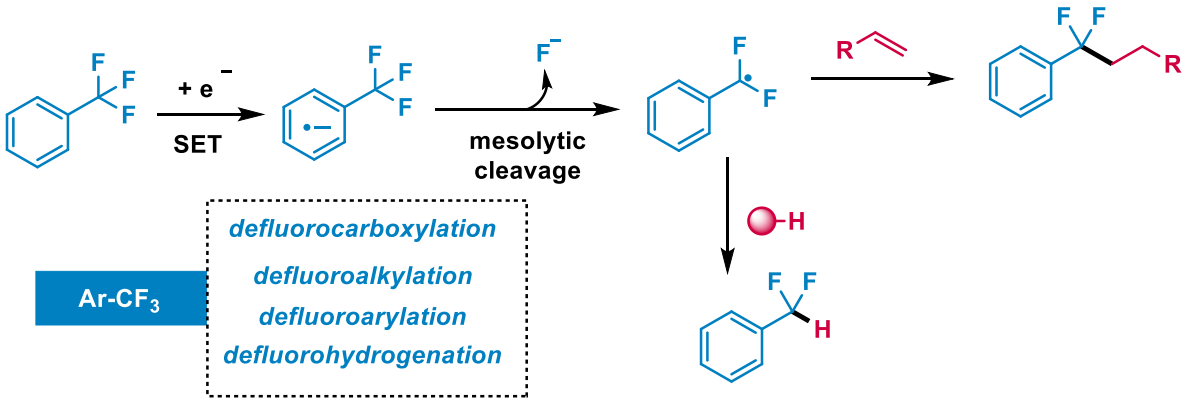

Scheme 10. SET approach for selective activation of trifluoromethyl arene.

---

[28] Munoz, S. B.; Ni, C.; Zhang, Z.; Wang, F.; Shao, N.; Mathew,T.; Olah, G. A.; Prakash, G. K. S. *Eur. J. Org. Chem.* **2017**, 2322−2326.

[29] (a) Mallov, I.; Ruddy, A. J.; Zhu, H.; Grimme, S.; Stephan, D.W. *Chem. Eur. J.* **2017**, *23*, 17692−17696. (b) Mandal, D.;Gupta, R.; Jaiswal, A. K.; Young, R. D. *J. Am. Chem. Soc.* **2020**, *142*, 2572−2578.

[30] (a) Dang, H.; Whittaker, A. M.; Lalic, G. *Chem. Sci.* **2016**, *7*,505−509. (b) Wright, S. E.; Bandar, J. S. *J. Am. Chem. Soc.* **2022,** *144*, 13032−13038.

[31] Jesani, M. H.; Schwarz, M.; Kim, S.; Evans, F. L.; White, A.;Browning, A.; Abrams, R.; Clayden, J. *Angew. Chem., Int. Ed.* **2024**, *63*, No. e202403477.

[32] (a)Box, J. R.; Avanthay, M. E.; Poole, D. L.; Lennox, A. J. J. *Angew.Chem., Int. Ed.* **2023**, *62*, No. e202218195. (b) Saboureau, C.; Troupel, M.; Sibille, S.; Périchon, J. *J. Chem. Soc. Chem. Commun*. **1989**, 1138–1139. (c) Sock, O.; Troupel, M.; Périchon, J. *Tetrahedron Lett*. **1985**, *26*,1509–1512. (d) Hebri, H.; Duñach, E.; Périchon, J. *Synth. Commun*. **1991**, *21*,2377–2382. (e) Andrieux, C. P.; Le Gorande, A.; Savéant, J. M. *J. Am. Chem. Soc.* **1992**, *114*, 6892–6904. (f) Andrieux, C. P.; Combellas, C.; Kanoufi, F.; Savéant, J. M.; Thiébault, A. *J. Am. Chem. Soc.* **1997**, *119*, 9527–9540. (g) Clavel, P.; Léger-Lambert, M. P.; Biran, C.; Serein-Spirau, F.; Bordeau, M.; Roques, N.; Marzouk, H. *Synthesis (Stuttg*). **1999**, 829–834. (h) Clavel, P.; Lessene, G.; Biran, C.; Bordeau, M.; Roques, N.; Trévin, S.; de Montauzon, D. *J. Fluorine Chem.* **2001**, *107,* 301–310.

[33] (a)Vogt, D. B.; Seath, C. P.; Wang, H.; Jui, N. T. *J. Am.Chem. Soc.* **2019**, *141*, 13203−13211. (b) Sap, J. B. I.; Straathof, N. J.W.; Knauber, T.; Meyer, C. F.; Médebielle, M.; Buglioni, L.; Genicot,C.; Trabanco, A. A.; Noël, T.; am Ende, C. W.; Gouverneur, V. *J. Am. Chem.Soc.* **2020**, *142*, 9181−9187. (c) Liu, C.; Shen, N.; Shang, R. *Nat. Commun.* **2022**, *13*, 354−361. (d) Liu, C.; Li, K.; Shang, R. *ACS Catal.* **2022**, *12*, 4103−4109. (e) Li, S.-Y.; Yang, X.-Y.; Shen, P.-H.; Xu, L.; Xu, J.; Zhang, Q.; Xu, H.-J. *J.Org. Chem.* **2023**, *88*, 17284−17296.

[34](a) Zhou, L. *Molecules* **2021**, *26*, 7051. (b) Wang, Z.; Sun, Y.; Shen, L.-Y.; Yang, W.-C.; Meng, F.; Li, P. *Org. Chem. Front.* **2022**, *9*, 853−873. (c) Wang, F.; Wang, Q.; Wang. L. *Tetrahedron* **2024**, *163*, 134155.

The groups of Jui, Gouverneur, and Shang recently made notable progresses by utilizing photoredox catalysis for selective hydrodefluorination and defluoroalkylation. These methods offer improved yields and selectivity but remain restricted to substrates possessing suitable redox properties as dictated by the photocatalytic systems.[29]

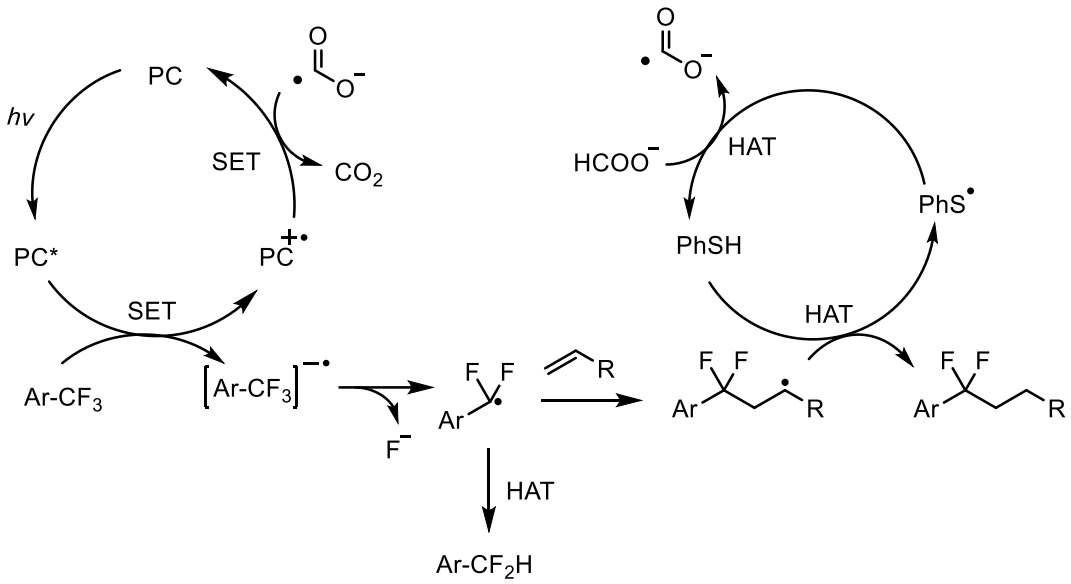

Scheme 11. Proposed photocatalytic cycles for defluoroalkylation and hydrodefluorination.

Chapter 2

Defluorinative C−O Coupling between Trifluoromethylarenes and Alcohols via Copper Photoredox Catalysis

2.1 Introduction

Compounds containing fluorine play a prominent role in modern society. Among all fluorinated functional groups, trifluoromethylarenes have been shown to be a prestigious motif. Selective defluorinative functionalization of trifluoromethylarenes for accessing difluoromethylene moieties can thus expand the chemical space but is limited due to their high reduction potential and susceptibility to overdefluorination.[35]

Among all transformations,[36] construction of CF_2-heteroatom motifs is underdeveloped but can afford novel functional groups. We decided to pursue the selective replacement of one of the C–F bonds of trifluoromethylarenes with oxygen, which will yield difluoroalkylether (R_1–CF_2O–R_2) structures. These modifications lead to new materials incorporating fantastic unique electronic, optical, and liquid crystalline properties. For example, difluoroalkylether (R1–CF2O–R2) structures can be found in liquid crystal materials[37] and anti-cancer drug molecule.[38]

[35] (a) Purser, S.; Moore, P. R.; Swallow, S.; Gouverneur,V. *Chem. Soc. Rev.* **2008**, *37*, 320–330. (b) Gillis, E. P. K.; Eastman, J.; Hill, M. D.; Donnelly, D. J.; Meanwell, N. A. *J. Med. Chem.* **2015**, *58*, 8315–8359. (c) Berger, R.; Resnati, G.; Metrangolo, P.; Weber, E.; Hulliger, J. *Chem. Soc. Rev.* **2011**, *40*, 3496–3508. (d) Zhou, Y.; Wang, J.; Gu, Z.; Wang, S.; Zhu, W.; Ace˜na, J. L.; Soloshonok, V. A.; Izawa, K.; Liu, H. *Chem. Soc. Rev.* **2016**, *116*, 422 –518. (e) Meanwell, N. A. *J. Med. Chem.* **2018**, *61*, 5822–5880.

[36] Zhao, F.; Zhou, W.; Zuo, Z. *Adv. Synth. Catal.* **2022**, *364*, 234–267.

[37] (a) Kuroboshi, M.; Kanie, K.; Hiyama, T. *Adv. Synth. Catal.* **2001**, *343*, 235–250. (b) Kirsch, P.; Bremer, M.; Taugerbeck, A.; Wallmichrath, T. *Angew. Chem. Int. Ed.* **2001**, *40*, 1480–1484. (c) Kirsch, P.; Huber, F.; Lenges, M.; Taugerbeck, A. *J. Fluor. Chem.* **2001**, *112*, 69–72. (d) Kirsch, P. *J. Fluor. Chem.* **2015**, *177*, 29–36.

[38] a) Lien, V. T.; Pettersen, S.; Haugen, M. H.; Olberg, D. E.; Mælandsmo, G. M.; Klaveness, J. *Arch. Pharm. Chem. Life Sci.* **2019**, *35*, 1900101. (b) Gray, N. S.; Zhang, T.; Fan, M.; Che, J.; Lu, W.; Dhepaganon, S.; Kwiatkowski, N. P. (Dana-Farber Cancer Institute, Inc.), WO 2022/232088 A1, **2022.**

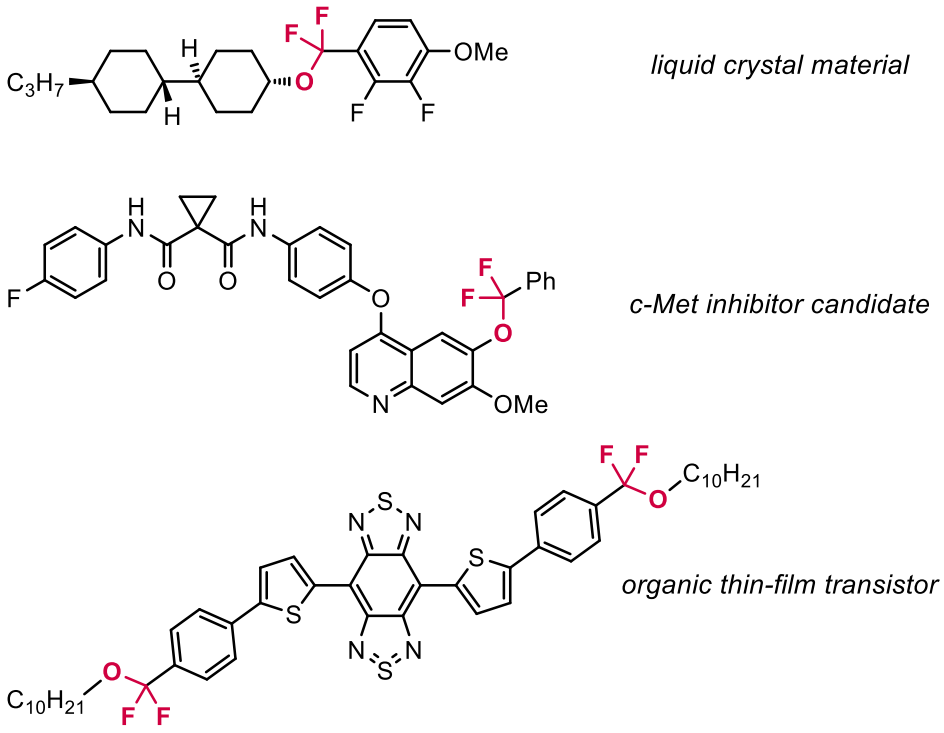

Scheme 12. Functional molecules containing CF_2O group.

The direct transformation of carbonyl groups of aldehydes and ketones into gem-difluorides typically require harsh conditions and result in low yields when applied to electron-deficient ketones, esters, and amides.[39] Alternative approaches involve the reaction of carbonyl-derived hydrazones[40] and diazo compounds[41] with strong oxidative fluorinating agents, iodine monofluoride or fluorine. ArCF2OR can also be synthesized via oxidative desulfurization-fluorination of ortho-thioesters,[42] dithiolanes,[43] and thiocarbonyl derivatives using electrophilic halonium species in the presence of fluoride ions.[44] Later reports showed that diethylaminosulfur

[39] (a) Boswell, G. A. Jr.; Ripka, W. C.; Scribner, R. M.; Tullock, C. W. *Org. React.* **1974**, *21*, 1–124. (b) Hudlicky, M. *Org. React.* **1988**, *25*, 513–637.
[40] Rozen, S.; Brand, M.; Zamir, D.; Hebel, D. *J Am. Chem. Soc.* **1987**, *109*, 896–897.
[41] Patrick, T. B.; Schiebel, J. J.; Cantrell, G. L. *J. Org. Chem.* **1981**,*46*, 3917–3918.
[42] (a) Patrick, T. B.; Hudson, C. M. *Heteroat. Chem.* **1999**, *10*, 1. (b) Matthews, D. P.; Whitten, J. P.; McCarthy, J. R. *Tetrahedron Lett.* **1986**, *27*, 4861–4864.
[43] Katzenellenbogen, J. A.; Sondej, S. C. *J. Org. Chem.* **1986**, *51*, 3508–3513. (b) Chambers, R. D.; Sandford, G.; Sparrowhawk, M. E.; Atherton, M. J. *J. Chem. Soc., Perkins Trans. 1* **1996**, 1941–1944.
[44] (a) Kuroboshi, M.; Hiyama, T. *Chem. Lett.* **1992**, 827–830. (b)Kuroboshi, M.; Hiyama, T. *Tett. Lett.* **1994**, *35*, 3983–3986. (c) Kuroboshi, M.; Suzuki, K.; Hiyama, T. *Tett. Lett.* **1992**, *33*, 4173–4176. (d) Kuroboshi, M.; Hiyama, T. *Tetrahedron Lett.* **1992**, *33*, 4177–4178. (e) Rozen, S.; Mishani, E. *J. Chem. Soc., Chem. Commun.* **1994**, 2081. (f) Kanie, K.; Mizuno,K.; Kuroboshi, M.; Hiyama, T. *Bull. Chem. Soc. Jpn.* **1998**, *71*, 1973–1991.

trifluoride (DAST),[45] Deoxofluor,[46] HF/NIS, AgF used in the conversion of thioesters into R,R-difluoroethers However, these multi-step protocols suffer from poor step economy.[47]

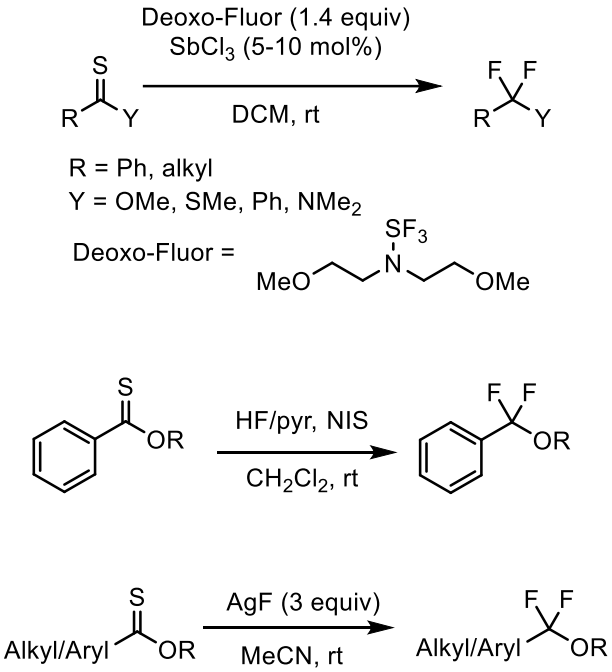

Scheme 13. Strategies of conversion of thioester to CF_2O compounds.

A direct coupling between trifluoromethyl arene and alcohols would represent the most desirable strategy to prepare $ArCF_2OR$ motifs. The transformation faces the same challenges in C–F functionalization such as strong C–F bond strength and overdefluorination side reactions. Furthermore, the C–O bond formation must be compatible with conditions for C–F activation. There have only been limited publications in this direction. In a recent paper in 2023, Xu et al. reported a photoredox approach, but the scope was restricted to electron rich phenols, presumably due to the requirement for more stable radicals in radical-radical coupling. [48]

[45] Bunnelle, W. H.; McKinnis, B. R.; Narayanan, B. A. *J. Org. Chem.* **1990**, *55*, 768–770.
[46] (a) Lal, G. S.; Lobach, E.; Evans, A. *J. Org. Chem.* **2000**, *65*, 4830–4832. (a) Mishani, E. *J. Chem. Soc., Chem. Commun.,* **1993**, 1761–1772.
[47] (a) Newton, J. J.; Britton, R.; Friesen, C. M. *J. Org. Chem.* **2018**, *83*, 12784–12792. (b) Newton, J. J.; Driedger, D.; Nodwell, M. B.; Schaffer, P.; Martin, R. E.; Britton, R.; Friesen, C. M. *Chem. Eur. J.* **2019**, *25*, 15993–15997.
[48] Xu, J.; Liu, J.-W.; Wang, R.; Yang, J.; Zhao, K.-K.; Xu, H.-J. *ACS Catal.* **2023**, *13*, 7339−7346.

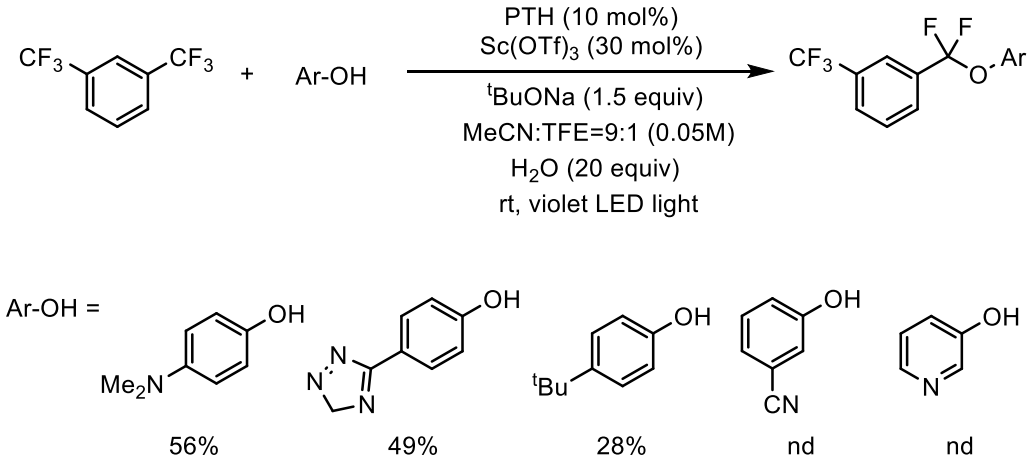

Scheme 14. Defluoroetherification of trifluoromethyls.

More recently in 2024, Nishimoto, Yasuda and co-workers developed a C–O coupling reaction of perfluoroalkylarenes, which is only limited to TEMPO, a stable radical species, as the coupling partner.[49] While these studies provide foundational insights, they lack generality in the coupling partners such as aliphatic alcohols, which are crucial in drug and material synthesis.

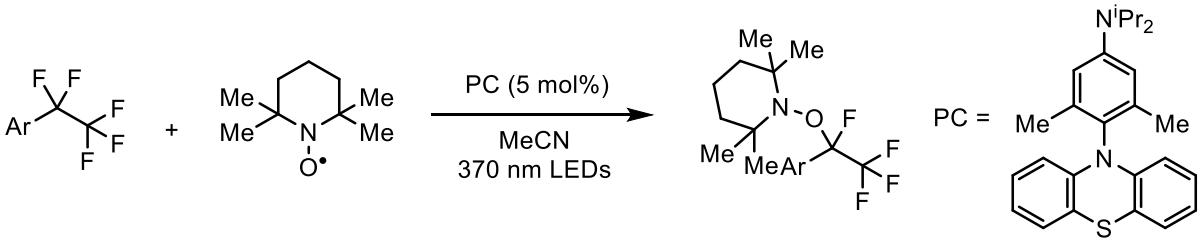

Scheme 15. Photo-catalyzed aminoxylation of perfluoroalkylarene with TEMPO.

We envisioned that the above challenges can be addressed by implementing copper as dual role catalysis. First, copper can act as the photoredox catalyst for C–F activation via single electron transfer. Additionally, copper can serve as a cross-coupling catalyst, further promoting C–O coupling. Along this line, in 2023, Xie and coworkers reported a photoexcited copper catalyzed C–F bond activation of trifluoromethylarenes for C–N coupling, but the scope is limited to carbazoles (Scheme 16).[50]

[49] Sugihara, N.; Nishimoto, Y.; Osakada, Y.; Fujitsuka, M.; Abe, M.; Yasuda, M. *Angew. Chem. Int. Ed.* **2024**, *63*, e202401117.
[50] Huang, J.; Gao, Q.; Zhong, T.; Chen, S.; Lin, W.; Han, J.; Xie, J. *Nat. Commun.* **2023**, *14*, 8292–8302.

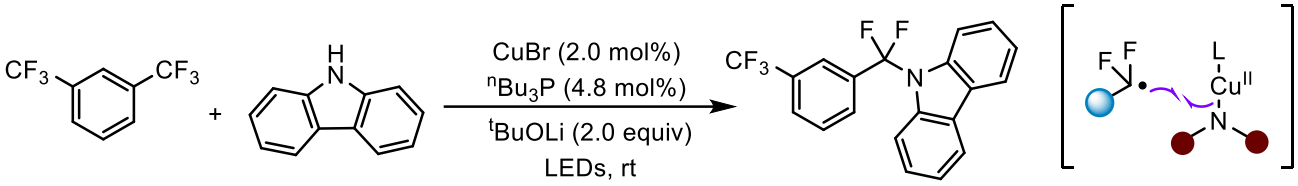

Scheme 16. Photoinduced copper-catalyzed C-N coupling.

A mechanistic scheme can be drawn in which a single copper system mediates two cooperative catalytic cycles: the selective C–F activation cycle and the C–O bond formation cycle (Scheme 17).

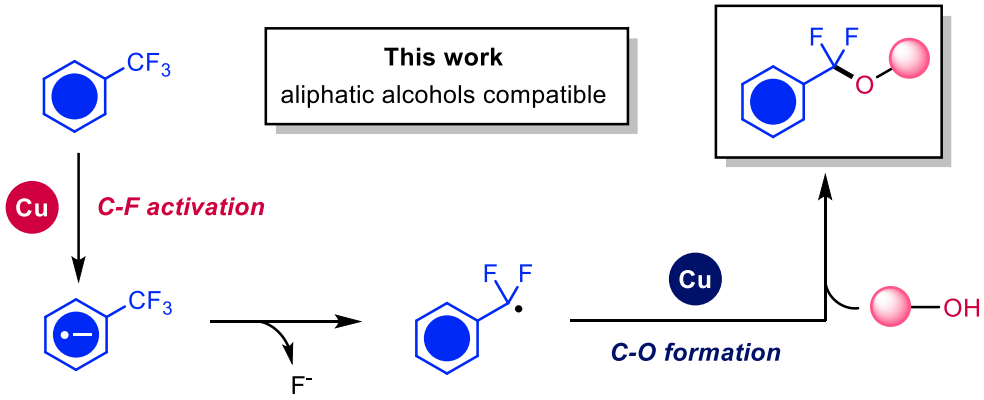

Scheme 17. Strategy for photoinduced copper catalyzed C-O coupling via C-F bond functionalization.

2.2 Optimization Studies

We initiated the optimization studies by identifying a suitable combination of copper and ligands. Furthermore, Lewis acid additives were screened since they may aid the C–F activation.

Copper source and ligand screening

To begin with, we selected the coupling between trifluoromethylarene **1a** and alcohol **2a** as the model reaction. Various copper sources were screened as potential catalysts. A wide range of copper salts were evaluated in combination of a phosphine ligand under 390-nm LED irradiation (Table 1). It was discovered that CuI is uniquely effective in this protocol.

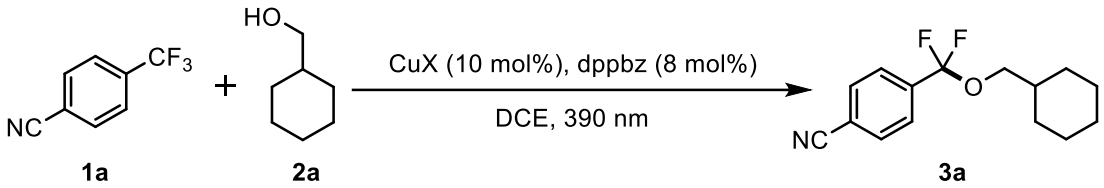

1a 2a 3a

CuX	Yield (%)
Cu_2O	<3
Cu powder	<3
CuI	10
$CuCl_2$	<3
CuCl	<3
CuCN	<3
$Cu(CH_3CN)BF_6$	<3
$Cu(BF_4)_2.2H_2O$	<3
$Cu(OTf)_2$	<3
$Cu(OAc)_2.H_2O$	<3
CuBr	<3

Table 1. Reactions were carried out using 0.05 mmol of **1a** and 25 equiv of **2a** in DCE under irradiation with violet LEDs (390 nm) for 24 h at rt. Yields were determined by ^{19}F-NMR analysis of the crude mixture using (trifluoromethoxy)benzene as the standard.

Next, using CuI as the metal precursor, we evaluated various N-, P-, and O-ligand. It was found that bisphosphines are ligand class of choice, and among all, 1,2-bis(diphenylphosphino)benzene (dppbz) is the best performer.

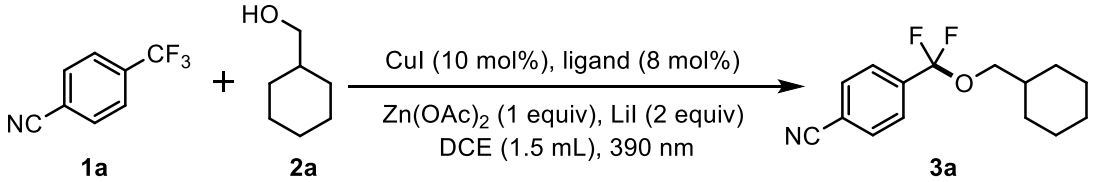

1a 2a 3a

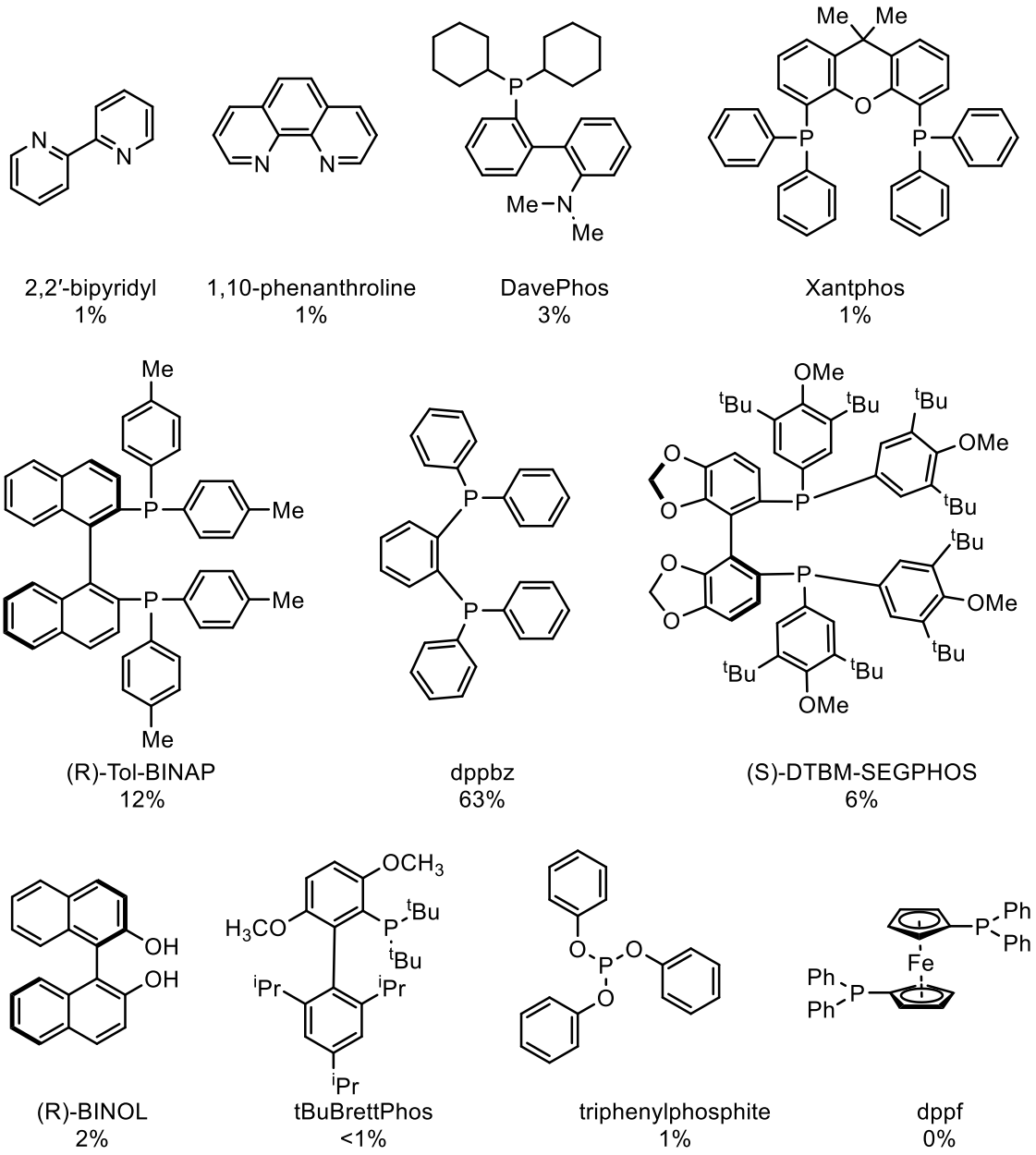

Table 2. Reactions were carried out using 0.05 mmol of **1a** and 25 equiv of **2a** in DCE under irradiation with violet LEDs (390 nm) for 24 h at rt. Yields were determined by ^{19}F-NMR analysis of the crude mixture using (trifluoromethoxy)benzene as the standard.

Metal iodides

Next, we moved to select a suitable fluorophilic metal, hoping to trap the fluoride ion resulting from the mesolytic cleavage of reduced trifluoromethylarene ($ArCF_2^{\bullet -}$) to drive the equilibrium to $ArCF_2^{\bullet}$ side while preventing overdefluorination. We screened various metal iodide

additives, of which LiI emerged as the best. NaI and KI gave slightly diminished yields, and almost no product was obtained with ZnI_2 as an additive.

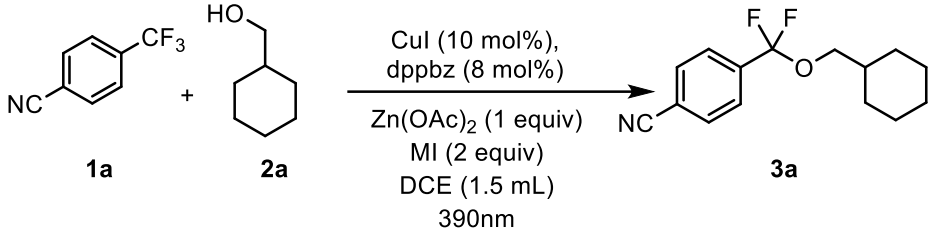

Entry[a]	Metal Iodide	Yield (%)[b]
1	LiI	51
2	NaI	45
3	KI	43
4	ZnI_2	No product

Table 3. [a]Reactions were carried out using 0.05 mmol of **1a** and 5 equiv of **2a** in DCE under irradiation with violet LEDs (390 nm) for 24 h at rt. [b]Yields were determined by ^{19}F-NMR analysis of the crude mixture using (trifluoromethoxy)benzene as the standard.

LiI loading

The loading of LiI was screened, and it was observed that with increased equivalents of LiI, the yield of difluorobenzyl ether product drastically decreased. Upon closer examination, we discovered an intriguing side reaction, formation of $ArCF_2I$, that occurs with excess LiI.

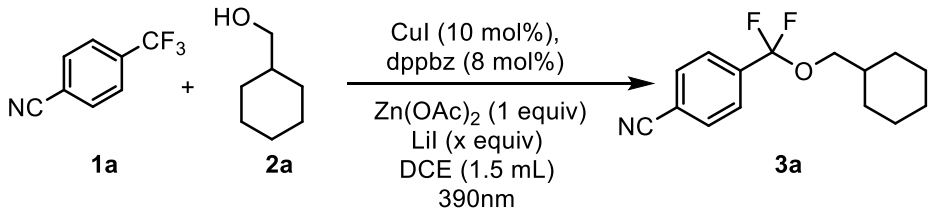

Entry[a]	LiI (equiv)	Yield (%)[b]
1	2	50
2	4	25
3	6	12
4	8	1

Table 4. [a]Reactions were carried out using 0.05 mmol of **1a** and 5 equiv of **2a** in DCE under irradiation with violet LEDs (390 nm) for 24 h at rt. [b]Yields were determined by ^{19}F-NMR analysis of the crude mixture using (trifluoromethoxy)benzene as the standard.

Zinc salts

Further screening of zinc salts was performed, identifying $Zn(OAc)_2$ as the best additive to afford 55% yield.

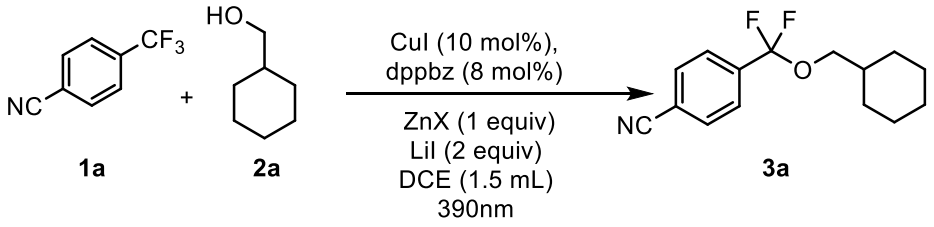

Entry[a]	ZnX	Yield (%)[b]
1	$Zn(OAc)_2$•$2H_2O$	49
2	$Zn(hfac)_2$	10
3	ZnI_2	No product
4	$Zn(OTf)_2$	34
5	$Zn(OAc)_2$	55
6	Zinc powder	22
7	ZnPc	<2
8	ZnTPP	37
9	$ZnCl_2$	37
10	$ZnBr_2$	37

Table 5. [a]Reactions were carried out using 0.05 mmol of **1a** and 5 equiv of **2a** in DCE under irradiation with violet LEDs (390 nm) for 24 h at rt. [b]Yields were determined by ^{19}F-NMR analysis of the crude mixture using (trifluoromethoxy)benzene as the standard.

$Zn(OAc)_2$ loading

Screening of equivalences of $Zn(OAc)_2$ showed that upon increasing the loading, a significant decrease in the yield is observed. As will be discussed in later sections, LiI and $Zn(OAc)_2$ play unique mechanistic role in this protocol.

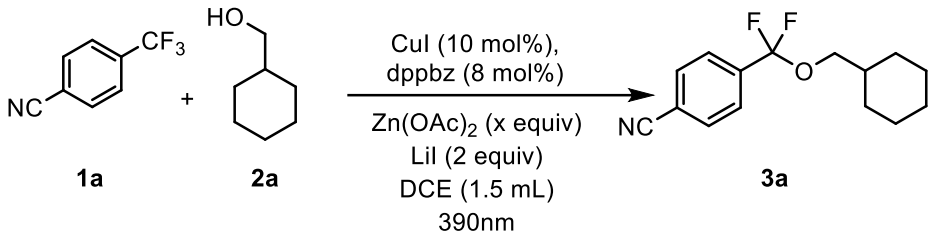

Entry[a]	Zn(OAc)$_2$(equiv)	Yield (%)[b]
1	1	41
2	3	31
3	6	23
4	8	17

Table 6. [a]Reactions were carried out using 0.05 mmol of **1a** and 5 equiv of **2a** in DCE under irradiation with violet LEDs (390 nm) for 24 h at rt. [b]Yields were determined by ^{19}F-NMR analysis of the crude mixture using (trifluoromethoxy)benzene as the standard.

Wavelengths of light

Upon changing the light source to tuna blue or 440 nm instead of 390 nm LED, a decrease in the yield was obtained.

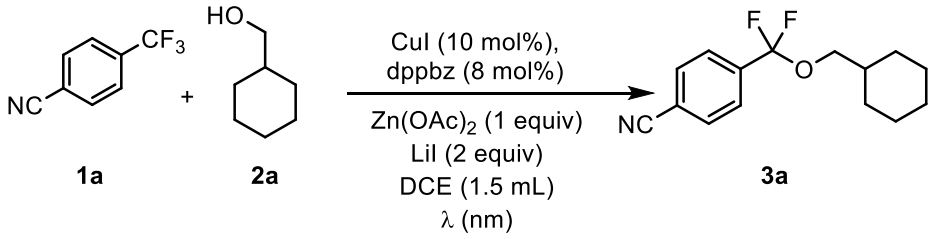

Wavelength	Conversion (%)	Yield (%)
Tuna blue	7	6
440nm	18	14
390nm	49	47

Table 7. [a]Reactions were carried out using 0.05 mmol of **1a** and 5 equiv of **2a** in DCE under irradiation with different Kessil LED lamps for 24 h at rt. [b]Yields were determined by ^{19}F-NMR analysis of the crude mixture using (trifluoromethoxy)benzene as the standard.

Alcohol loading

Alcohol equivalence played a key role in reaction yield. A large excess is necessary for achieving good efficiency, which we hypothesized can be essential for dissolving the metal salts and promoting substitution of Cu–I to Cu–OR in the absence of strong base.

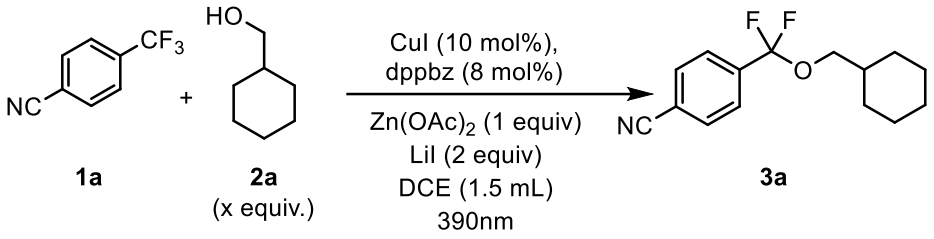

Entry[a]	Alcohol 2a (equiv)	Yield (%)[b]
1	5	49
2	10	62
3	15	63
4	20	58
5	25	71
6	30	60
7	35	60
8	40	66
9	20 equiv of *t*AmOH + 5 equiv of **2a**	22

Table 8. [a]Reactions were carried out using 0.05 mmol of **1a** and x equiv of **2a** in DCE under irradiation with violet LEDs (390 nm) for 24 h at rt. [b]Yields were determined by ^{19}F-NMR analysis of the crude mixture using (trifluoromethoxy)benzene as the standard.

Concentration screening

An increase in the yield is observed with increase in dilution, presumably as it enables the light to penetrate more deeply into the reaction mixture.

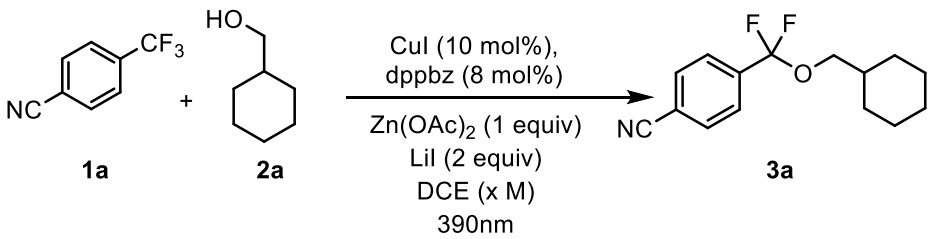

Entry[a]	DCE (M)	Yield (%)[b]
1	0.050	55
2	0.040	65
3	0.033	76
4	0.028	71
5	0.025	68
6	0.022	70
8	0.017	74

Table 9. [a]Reactions were carried out using 0.05 mmol of **1a** and 25 equiv of **2a** in DCE under irradiation with violet LEDs (390 nm) for 24 h at rt. [b]Yields were determined by ^{19}F-NMR analysis of the crude mixture using (trifluoromethoxy)benzene as the standard.

Control experiments

These control experiments demonstrate the essential role of copper, dppbz, LiI, $Zn(OAc)_2$ and light. In certain conditions when the reactions when carried out under air or under heating in dark, the desired product was not formed.

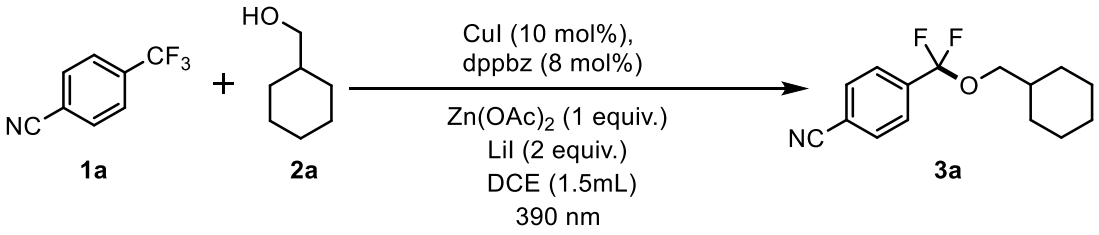

Entry[a]	Experiments	Yield (%)[b]
1	standard conditions	71%
2	no Cu/dppbz	<5%
3	no LiI	<5%
4	no $Zn(OAc)_2$	<5%
5	no light, rt or 80 °C	<5%
6	under air	<5%

Table 10. [a]Reactions were carried out using 0.05 mmol of **1a** and 25 equiv of **2a** in DCE under irradiation with violet LEDs (390 nm) for 24 h at rt. [b]Yields were determined by ^{19}F-NMR analysis of the crude mixture using (trifluoromethoxy)benzene as the standard.

$ArCF_2I$

During the isolation of $ArCF_2OR$ products, we identified an intriguing byproduct, $ArCF_2I$, which is not well studied in the literature but can potentially serve as a useful fluorine-containing intermediate. These iodides have also prospective to be used as halogen bond donors in bioactive molecules. The bulk of the research done on $ArCF_2X$ derivatives concentrates on the chlorides and bromides.[51] Only one recent publication reports the defluorinative iodination of $ArCF_3$ compounds via a carbanion intermediate.[52]

$Zn(OAc)_2$ loading

We decided to employ *t*AmOH as a non-coupling alcohol and optimize the conditions for $ArCF_2I$ production. It was found that the relative equivalence of LiI and $Zn(OAc)_2$ has profound impact on the reaction yield (see the discussion in mechanistic section).

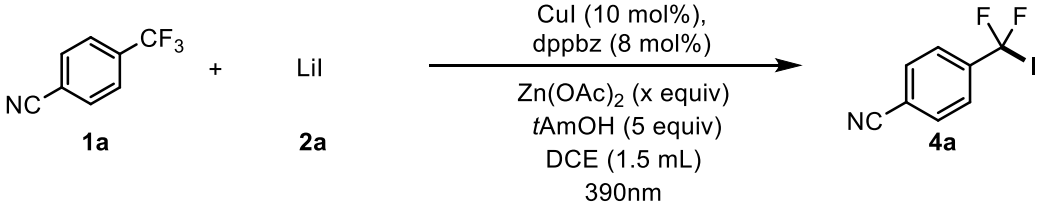

Entry[a]	$Zn(OAc)_2$ (equiv)	Yield (%)[b]
1	0.1	66
2	0.25	64
3	0.5	77
4	1.0	80
5	2.0	45
6	3.0	29
7	4.0	10
8	w/o	54

[51] (a) Dorian, A.; Landgreen, E. J.; Petras, H. R.; Shepherd, J. J.; Williams, F. J. *Chem. Eur. J.* **2021**, *27*, 10839–10843. (b) Yang, R.-Y.; Gao, X.; Gong, K.; Wang, J.; Zeng, X.; Wang, M.; Han, J.; Xu, B. *Org. Lett.* **2022**, *24*, 164–168. (c) Vaas, S.; Zimmermann, M. O.; Schollmeyer, D.; Stahlecker, J.; Engelhardt, M. U.; Rheinganz, J.; Drotleff, B.; Olfert, M.; Lämmerhofer, M.; Kramer, M.; Stehle, T.; Boeckler, F. M. *J. Med. Chem.* **2023**, *66*, 10202–10225.

[52] (a) Muta, K.; Okamoto, K.; Nakayama, H.; Wada, S.; Nagaki, A. *ChemRxiv*, **2024**, DOI: 10.26434/chemrxiv-2024-5ml66-v3. (b) Mandal, D.; Gupta, R.; Jaiswal, A. K.; Young, R. D. *J. Am. Chem. Soc.* **2020**, *142*, 2572–2578.

Table 11. [a]Reactions were carried out using 0.05 mmol of **1a** and 5 equiv of **2a** in DCE under irradiation with violet LEDs (390 nm) for 24 h at rt. [b]Yields were determined by ^{19}F-NMR analysis of the crude mixture using (trifluoromethoxy)benzene as the standard.

<u>*t*AmOH loading</u>

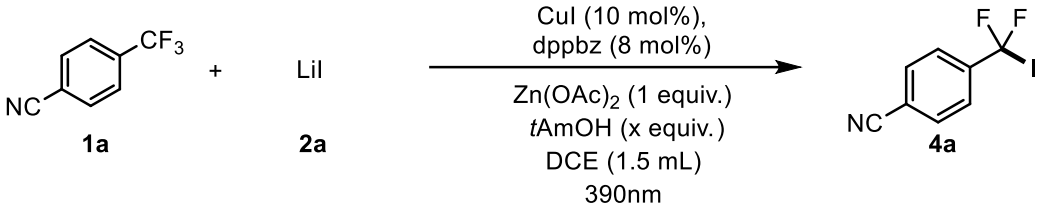

Entry[a]	*t*AmOH (equiv)	Yield (%)[b]
1	0	50
2	0.5	58
3	1	66
4	2	69
5	5	72

Table 12. [a]Reactions were carried out using 0.05 mmol of **1a** and x equiv of **2a** in DCE under irradiation with violet LEDs (390 nm) for 24 h at rt. [b]Yields were determined by ^{19}F-NMR analysis of the crude mixture using (trifluoromethoxy)benzene as the standard.

- Thus, the optimized reaction condition for $ArCF_2OR$ formation includes 10 mol% CuI, 8 mol% dppbz, 1.0 equiv $Zn(OAc)_2$, 2.0 equiv LiI in dichloroethane (DCE) under 390-nm irradiation for 24 h, affording the model ether product **3a** in 71% yield.
- The optimized reaction condition for $ArCF_2I$ formation includes increasing the loading of LiI to 7.0 equiv and applying 2.0 equiv of the non-coupling *tert*-amyl alcohol, the model iodide **4a** could be produced in 70% NMR yield

2.3 Substrate scope

Substrate scope of $ArCF_2OR$

By employing the optimized conditions, we explored the substrate scope of the copper-catalyzed defluorinative C–O coupling reaction (Scheme 18). All non-volatile products were purified by standard column chromatography. Several electron-deficient trifluoromethylarenes, including the anti-cancer drug bicalutamide, were found to be suitable substrates (**3a**–**f**). The reaction also showed good compatibility with a variety of primary and secondary aliphatic alcohols, yielding the corresponding $ArCF_2OR$ products in moderate to good yields. Of great importance, naturally occurring alcohols such as menthol (**3j**) and cholesterol (**3r**), along with amino alcohols (**3p**, **3q**), were found to be effective coupling partners. Phenolic ethers could form under these conditions but only in low yields (**3u**, **3v**). Poor reactivity with tertiary alcohol is a limitation of the method, most likely due to steric crowding at the coupling step (**3w**).

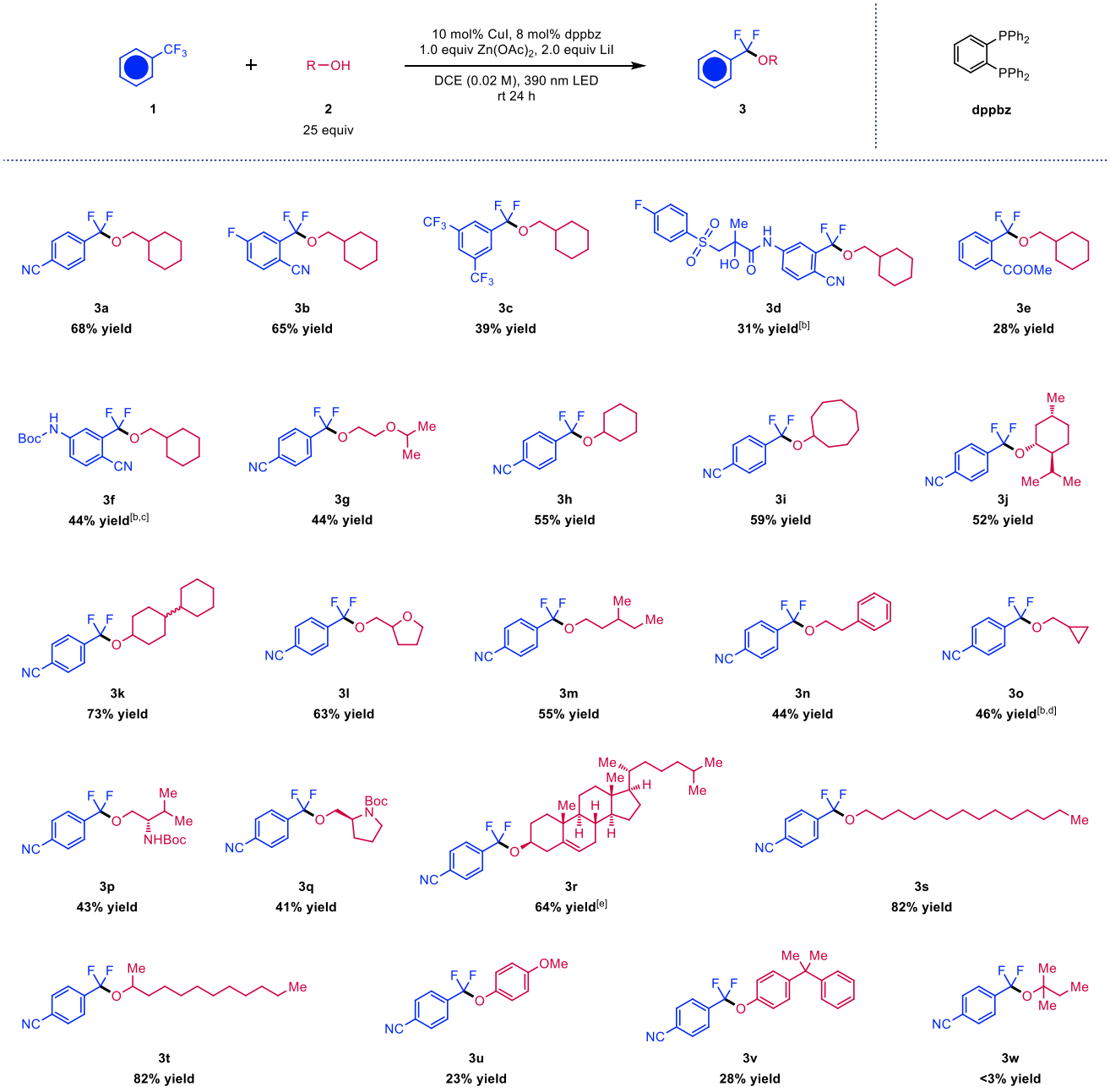

Scheme 18. Substrate scope of photoinduced copper-catalyzed defluorinative C–O coupling reactions.

Liquid crystal molecule

With our defluorinative C–O coupling approach, we could overcome the long, tedious synthetic pathways to directly construct CF_2O linkers from commercially available trifluoromethylarenes and alcohols. As an illustration, we described the synthesis of compound **3x**

in a straightforward one step process, in which $ArCF_3$ **1a** was coupled with *trans*-4-(trans-4-propylcyclohexyl)cyclohexanol **2x**.[53] Compound **3x** was produced as a crystalline solid, and one single crystal suitable for X-Ray diffraction (XRD) structural analysis was obtained. The solid-state structure showed intermolecular packing of CH–π interactions by the cyclohexyl and phenylene parts.

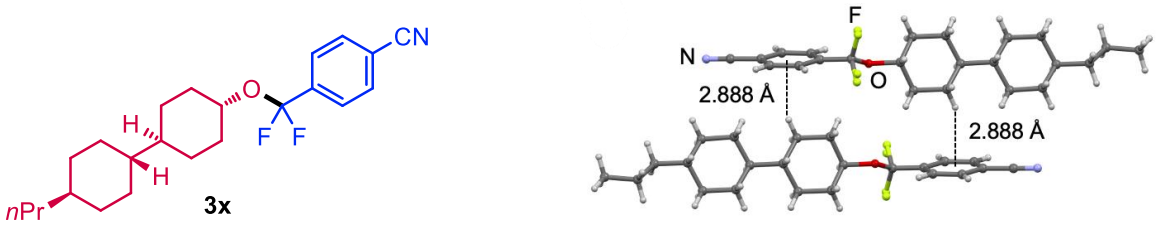

Scheme 19. Molecular and X-ray single crystal structures of **3x**.

It was shown previously that the introduction of CF_2O-bridges into certain molecular frameworks is capable of improving mesophase characteristics by expanding the range of the nematic phase and the clearing temperature while also reducing rotational viscosity, thus making these motifs attractive for liquid crystal applications. Gratifyingly, when the amorphous powder of **3x** was observed under cross-polarized microscopy, it underwent thermotropic phase transition at 140 °C, displaying liquid crystal behavior.

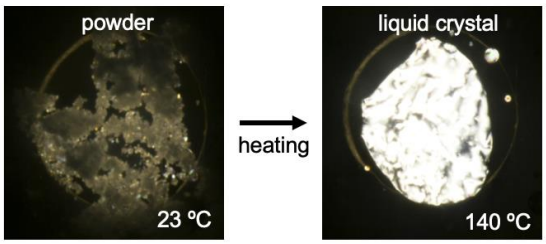

Scheme 20. Cross-polarized microscopy images of **3x** recorded at different temperatures.

Substrate scope of $ArCF_2I$

Despite the instability of $ArCF_2I$ groups, we managed to fully characterize **4a** and **4b** after their isolation. This method thus provides a protocol to synthesize these underexplored moieties for future exploration of their utility. In a notable divergence, the substrate scope for forming

[53] Sasada, Y.; Matsui, S.; Takeuchi, H.; Kubo, Y.; Nakagawa, E. (Chisso Corporation), EP 1 081 123 A2, **2001**.

$ArCF_2I$ did not coincide with that of the $ArCF_2OR$ products. For instance, substrates giving rise to **4b**, **4c**, and **4e** were not suitable for $ArCF_2OR$ formation, which may be due to increased steric hinderance that hampers the C–O coupling.

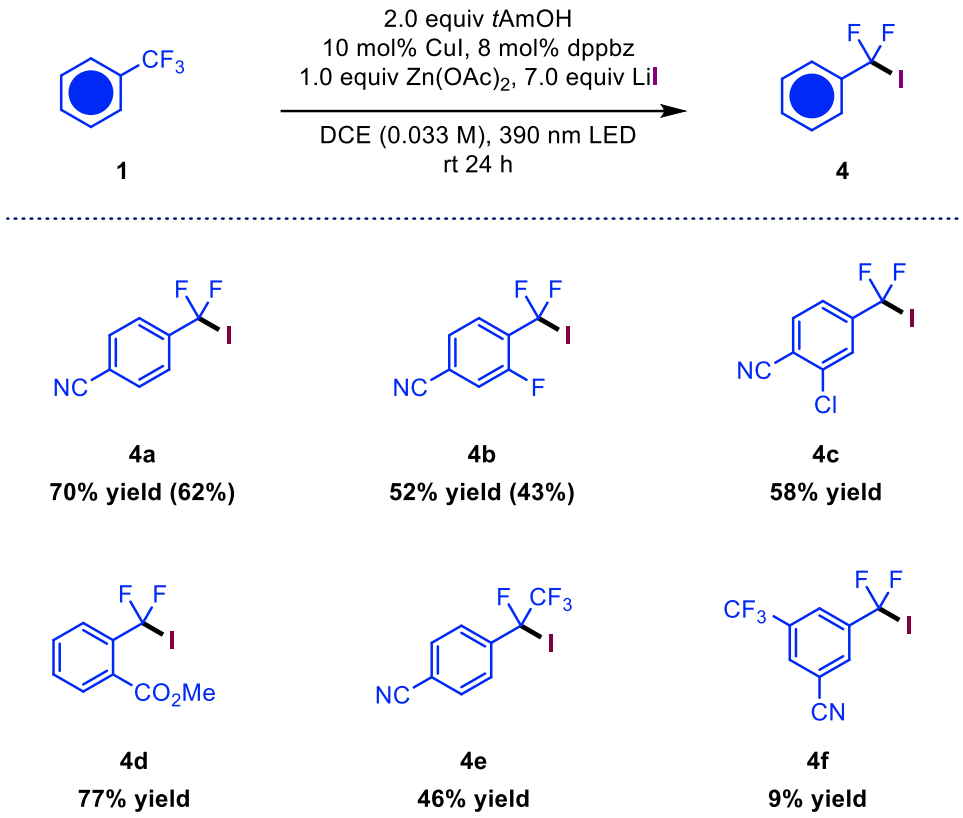

Scheme 21. Substrate Scope of photoinduced copper catalyzed $ArCF_2I$ formation.

2.4 Mechanistic studies

Alcohol and LiI loadings

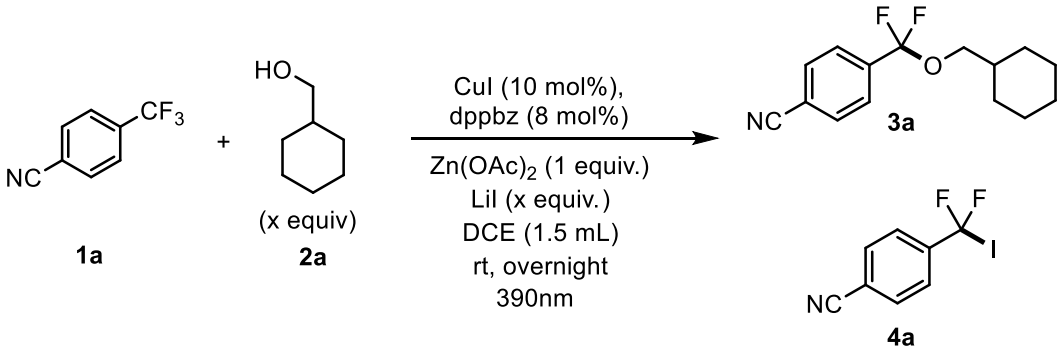

Entry[a]	Alcohol 2a (equiv)	LiI (equiv)	Yield 3a (%)[b]	Yield 4a(%)[b]
1	2	7	0	77
2	9	6	14	54
3	13	5	41	22
4	17	4	46	7
5	21	3	56	3
6	25	2	63	0

Table 13. [a]Reactions were carried out using 0.05 mmol of **1a** and x equiv of **2a** in DCE under irradiation with violet LEDs (390 nm) for 24 h at rt. [b]Yields were determined by ^{19}F-NMR analysis of the crude mixture using (trifluoromethoxy)benzene as the standard.

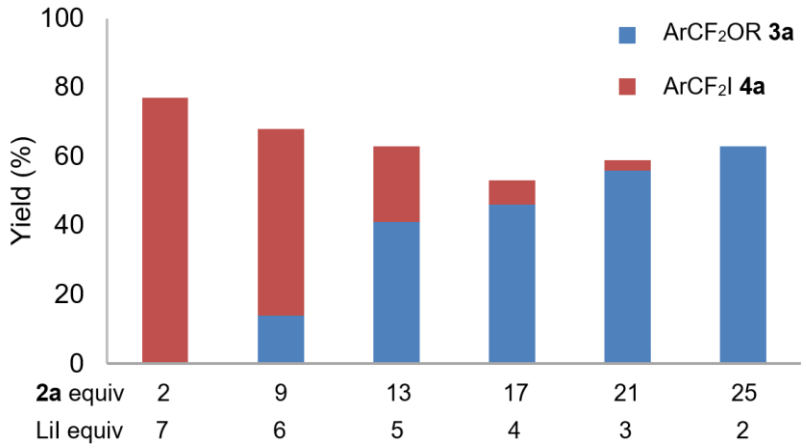

Scheme 22. Studies of $ArCF_2I$ and $ArCF_2OR$.

The generation of $ArCF_2I$ and $ArCF_2OR$ seem to be competitive processes, with increased equiv. of alcohol leading to more $ArCF_2OR$ product while increased equiv. of LiI affording more $ArCF_2I$ product. This result suggests the two products may originate from a common intermediate.

Conversion of $ArCF_2I$ to $ArCF_2OR$

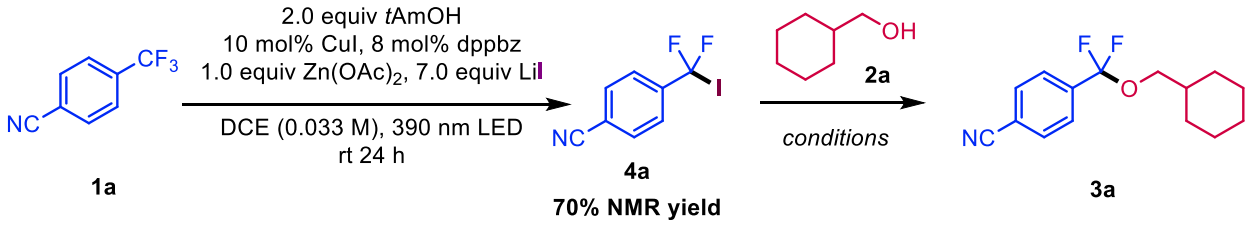

4a → **3a** conditions	**3a** yield (2-step)
dark or 390 nm	<3%
CuI, dppbz, dark or 390 nm	<3%
CuI, dppbz, $Zn(OAc)_2$, dark	<3%
CuI, dppbz, $Zn(OAc)_2$, 390 nm	53%

To further study the mechanistic role of $ArCF_2I$, we then probed its conversion to $ArCF_2OR$. Under dark conditions, even in the presence of CuI, dppbz, and $Zn(OAc)_2$, no product was obtained. This outcome thus disapproves a S_N2-type mechanism between $ArCF_2I$ and alcohol. Only the addition of fresh CuI, dppbz, and $Zn(OAc)_2$ in combination with irradiation condition allowed for the formation of product, suggesting the essential role of light and these catalytic components. The divergent substrate scopes observed for the formation of $ArCF_2I$ and $ArCF_2OR$ products also imply that both products arise from a common intermediate, likely the difluorobenzylic radical, $ArCF_2•$. We hypothesized that $ArCF_2I$ acts as a reservoir for the ephemeral radical $ArCF_2•$ so that this key intermediate can be produced in a controlled manner without losing catalytic efficiency.

Radical trapping studies

Radical trapping experiments with TEMPO and alkene provided supports for the intermediacy of ArCF2•.

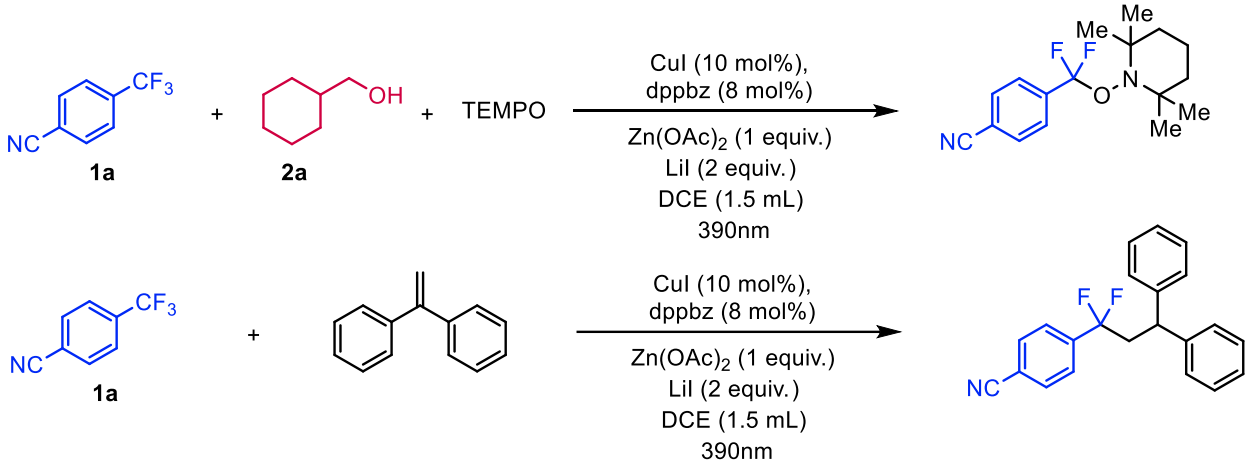

^{31}P NMR spectroscopic studies

To probe more deeply the nature of the active copper catalyst, we performed a series of ^{31}P NMR studies (Scheme 23). On mixing CuI and dppbz in DCE, a peak at –22 ppm was observed,

which concurred the formation of the bis (phosphine)-ligated complex, (dppbz)CuI (**CuP2**). Individual addition of $ArCF_3$ **1a**, alcohol **2a**, LiI, or $Zn(OAc)_2$ did not yield noticeable changes in the ^{31}P NMR spectra. Nevertheless, the addition of both LiI and $Zn(OAc)_2$ to the **CuP2** solution led to the emergence of a new peak at +9 ppm. When all the components of the reaction mixture are present, +9 ppm peak predominates.

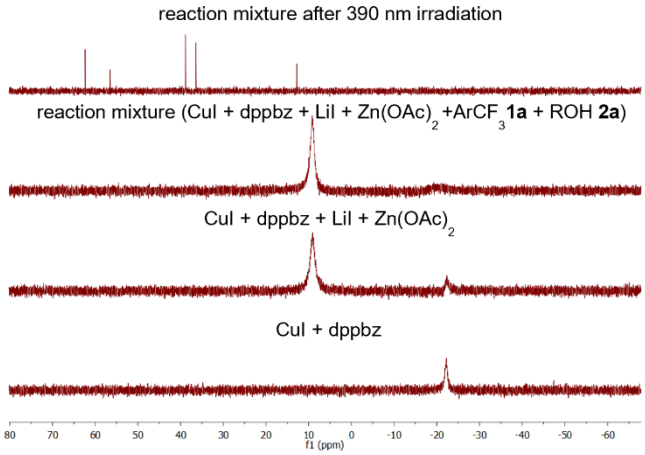

Scheme 23. ^{31}P NMR studies.

Single crystal studies

Structural elucidation via single crystal X-ray diffraction and high-resolution mass spectrometry confirmed the identity of this newly discovered species as a homoleptic copper(I) complex ligated with two dppbz ligands (**CuP4**). The crystal structure of **CuP4** contained a ZnI_3^- counterion, providing mechanistic insight for the requirement of both Zn^{2+} and I^- for converting **CuP2** into **CuP4**.

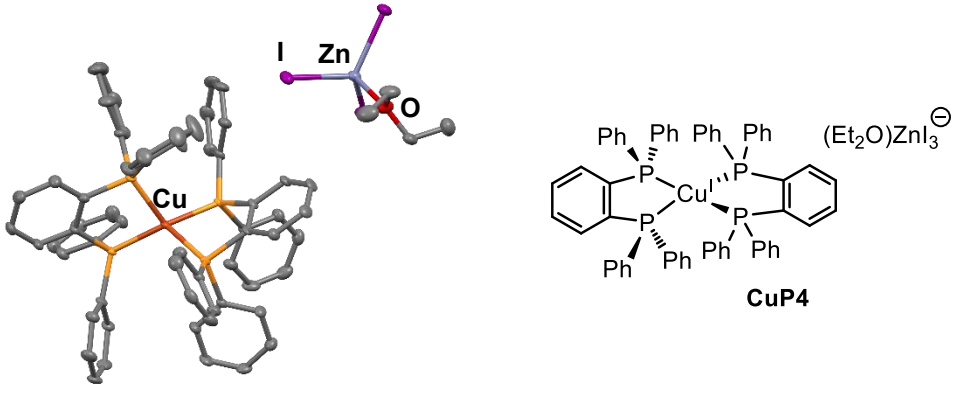

Scheme 24. X-ray structure of CuP4.

UV-Vis studies

Independent synthesis of **CuP4** was attained by combining CuI and dppbz at a molar ratio of 1:2. UV–vis spectroscopy revealed that the addition of both $Zn(OAc)_2$ and LiI to **CuP2** result a significant bathochromic shift beyond 400 nm, and this observed bathochromic shift is consistent to that of **CuP4**, suggesting its indispensable role under the 390-nm irradiation conditions employed in our protocol.

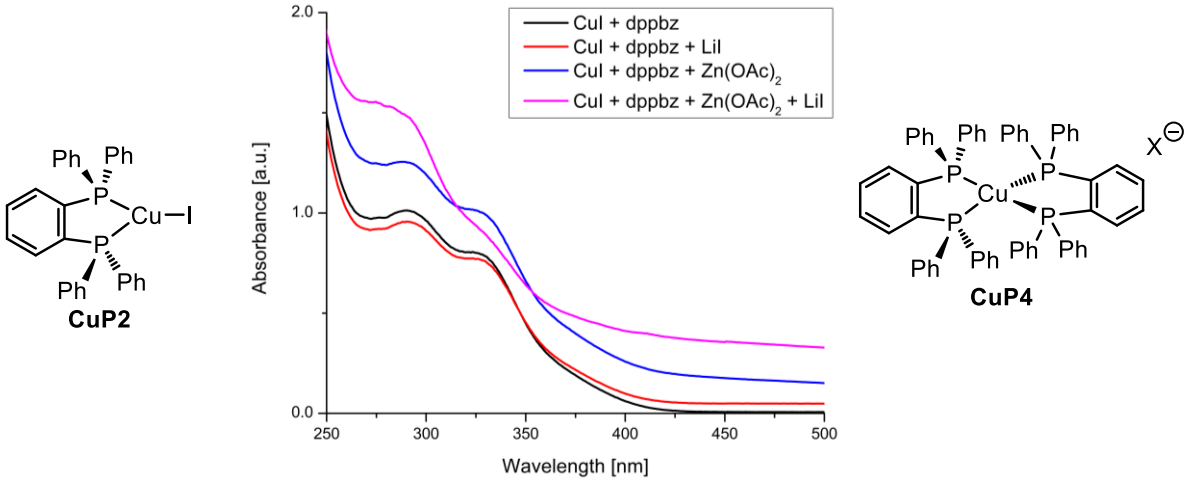

Scheme 25. UV-vis studies

Stern-Volmer quenching studies

Fluorescence quenching experiments were performed using $ArCF_3$ and TBAI as quenchers. Stern-Volmer analysis revealed linear relationship between emission quenching of photoexcited **CuP4** and concentration of $ArCF_3$ **1a**, suggesting an oxidative quenching of excited state **CuP4** by **1a**. Previously, an analogous complex $[Cu(dppbz)_2](BF_4)$ was reported being photoactive with excited-state reduction potential $E_{1/2}(Cu^{II/I*})$ = -2.19 V vs. SCE,[54] which is sufficient to reduce $ArCF_3$ **1a** (-1.92V vs SCE). On the other hand, iodide ions were also found to quench the excite state of CuP4 rather effectively, albeit at higher concentrations compared with $ArCF_3$. Notably, the plot for iodide quenching exhibited concave upward curvature that is indicative of combined

[54] (a) Black, J. R.; Levason, W.; Spicer, M. D.; Webster, M. *J. Chem. Soc. Dalton Trans.* **1993**, 3129–3136. (b) Szłyk, E.; Kucharek, R.; Szymańska, I.; Pazderski, L. *Polyhedron*, **2003**, *22*, 3389–3393. (c) Moudam, O.; Kaeser, A.; Delavaux-Nicot, B.; Duhayon, C.; Holler, M.; Accorsi, G.; Armaroli, N.; Séguy, I.; Navarro, J.; Destruel, P.; Nierengarten, J.-F. *Chem. Commun.*, **2007**, 3077–3084. (d) Kaeser, A.; Moudam, O.; Accorsi, G.; Séguy, I.; Navarro, J.; Belbakra, A.; Duhayon, C.; Armaroli, N.; Delavaux-Nicot, B.; Nierengarten, J.-F. *Eur. J. Inorg. Chem.* **2014**, 1345–1355.

dynamic and static quenching processes likely emerging from iodide coordination with the copper center.[55]

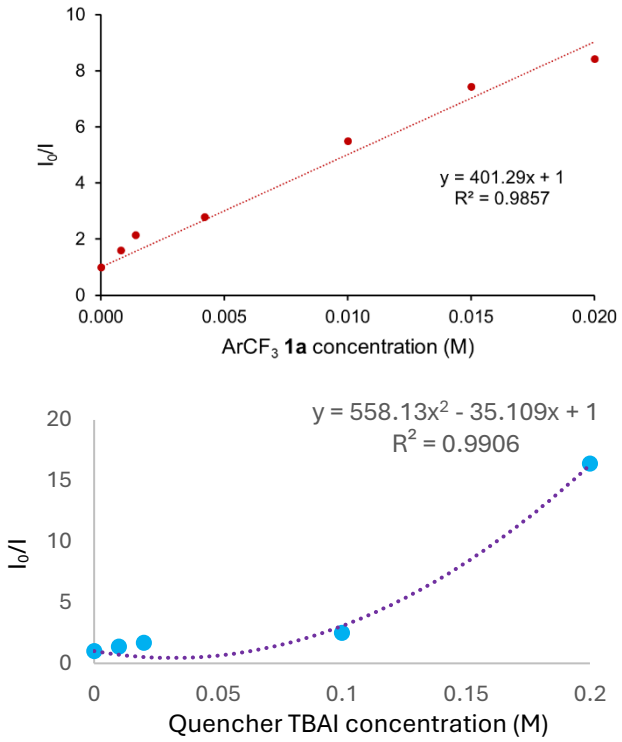

Scheme 26. Stern -Volmer plot

Role of LiI and $Zn(OAc)_2$ in $ArCF_3$ activation

Upon photoexcitation, **CuP4** can engage in SET event to reduce $ArCF_3$ **1a**. Cyclic voltammetry studies further substantiate this hypothesis. It was shown that the reduction potential of $ArCF_3$ **1a** shifted markedly from –1.92 V to –1.84 V vs SCE in the presence of LiI and $Zn(OAc)_2$. NMR spectroscopic analysis supported the coordination of Li^+ and Zn^{2+} cations to the substrate. Additionally, both cations readily form fluoride complexes, thereby facilitating the mesolytic cleavage of C–F bond by driving equilibrium toward radical generation $ArCF_2$•.

[55] (a) Clark, C. C.; Marton, A.; Meyer, G. J. *Inorg. Chem.* **2005**, *44*, 1345–1355. (b) Boschloo, G.; Hagfeldt, A. *Acc. Chem. Res.* **2009**, *42*, 1819–1826. (c) Troian-Gautier, L.; Swords, W. B.; Meyer, G. J. *Acc. Chem. Res.* **2019**, *52*, 170–179.

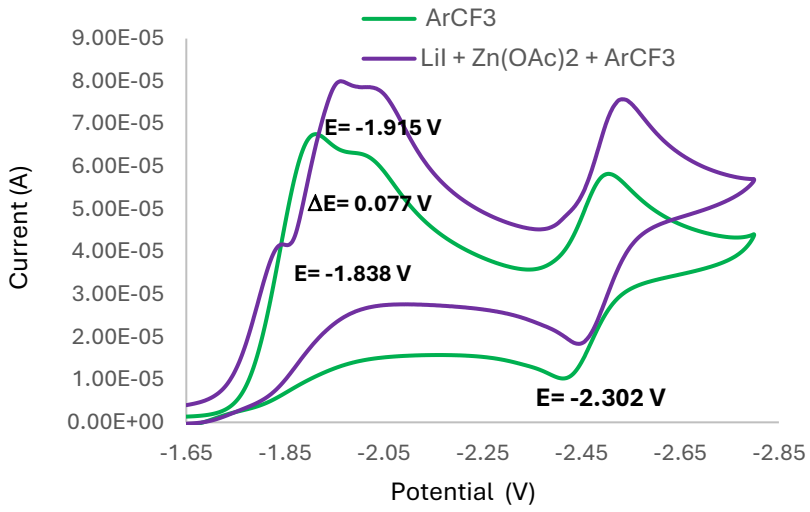

Scheme 27. CV studies

ppm (CD_2Cl_2)	**1a**	**1a** + 2 equiv LiI + 1 equiv $Zn(OAc)_2$	**1a** + 1 equiv $Zn(OAc)_2$	**1a** + 2 equiv LiI
$\Delta\delta$ 134.60 ppm (q)	0	0.18	0.01	0.27
$\Delta\delta$ 133.23 ppm	0	0.08	0.01	0.13
$\Delta\delta$ 126.54 ppm(q)	0	0.05	0.01	0.04
$\Delta\delta$ 123.675 ppm (q)	0	-0.05	-0.03	-0.08
$\Delta\delta$ 117.89 ppm	0	-0.02	0.00	0.09
$\Delta\delta$ 116.58 ppm (q)	0	-0.32	-0.03	-0.52

C–O bond formation step

According to the conversion studies of $ArCF_2I$ to $ArCF_2OR$, CuI, dppbz, $Zn(OAc)_2$, and light are necessary. ^{31}P NMR spectra of a mixture of CuI, dppbz (1:1), $Zn(OAc)_2$, and alcohol **2a** afforded only CuP2 in the absence of light. Under photoirradiation of this mixture, both ^{31}P NMR and mass spectrometric analyses indicated the formation of a copper–alkoxide complex **5**. This result might be due to the absence of strong base, preventing effective substitution of the Cu–I to Cu–OR. This observation also corroborates the necessary large excess of alcohol in the optimized reaction conditions. Various attempts to independently prepare complex **5** were unsuccessful.

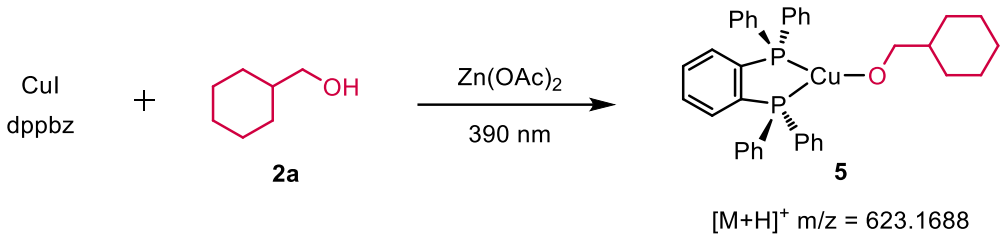

Scheme 28. Formation of Copper-alkoxide Complex **5**.

Proposed mechanism

We propose a dual-cycle mechanism consisting of two separate but parallel pathways: C–F activation and C–O coupling . In the presence of LiI and $Zn(OAc)_2$, the homoleptic copper-bisphosphine complex (**CuP4**) is formed as the predominant species. Upon photoexcitation, **CuP4*** transfers one electron (SET) to $ArCF_3$ (**1**) to generate the radical anion, which in turn undergoes mesolytic C–F bond cleavage to form difluorobenzylic radical intermediate **6**. Meanwhile, in the presence of $Zn(OAc)_2$, upon photoirradiation, **CuP2** reacts with alcohol **2** to produce the copper–alkoxide intermediates **5**. At the crossing point of both cycles, species **5** and CuP4 (**7**) can undergo an electron transfer to give rise to the Cu(II)–alkoxide **8** and recovering **CuP4** ($E_{1/2}$(**CuP4**/**7**) = +1.10 V vs. SCE.

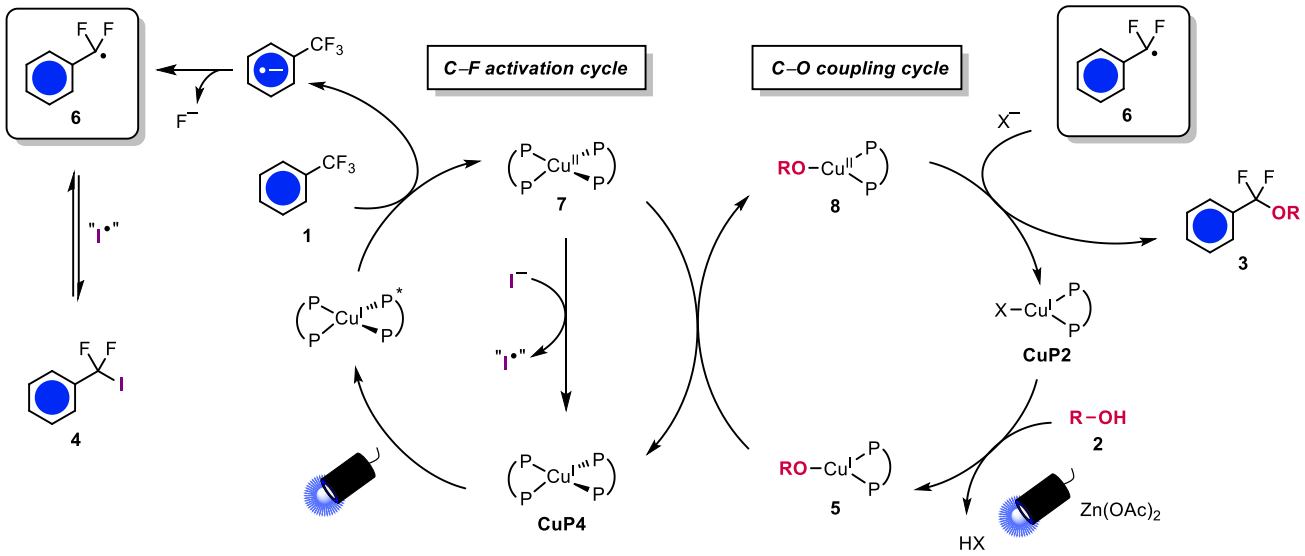

Scheme 29. Proposed mechanism.

$ArCF_2$• radical (**6**) can react with Cu(II)–alkoxide **8** to yield the $ArCF_2OR$ product (**3**), most likely through an outer-sphere radical pathway due to preference from steric factors.[56] Under high concentration of I^-, it is plausible that copper species **7** could alternatively oxidize I^- to yield an iodine radical I• that might be present as $I_2^{\bullet-}$ or metal iodide. This I• can further react with $ArCF_2$• (**6**) in reaction to form $ArCF_2I$ (**4**), which can serve as a radical reservoir for controlling the concentration of **6** and sustaining efficient turnover within the radical processes.

2.5 Conclusion

Both copper species, **CuP4** and **CuP2**, mediate this dual-cycle mechanism. **CuP4** serves as the photocatalyst for C–F activation while **CuP2** acts as the cross-coupling catalyst for the C–O bond formation. Notably, the use of two salt additives (LiI & $Zn(OAc)_2$) permits the synergistic catalysis through bifunctional copper reactivity and the precise generation of both catalytic constituents **CuP2** and **CuP4** from a single Cu-dppbz precursor.

2.6 Outlook

Future research will focus on the rational design and development of more effective **CuP4** based catalysts possessing sufficiently high reduction potentials to efficiently activate electron-rich trifluoromethyl arenes. Efforts will also be directed toward the synthesis of structurally diverse liquid crystalline compounds, accompanied by comprehensive investigation of their physicochemical and mesophase properties. Additionally, optimization of reaction conditions to improve product yields and identification of an appropriate copper-ligand system capable of inducing enantioselectivity in the formation of $ArCF_2O$-derivatives will be pursued. Furthermore, the development of a one-pot transformation strategy enabling the in-situ generation of $ArCF_2I$ intermediates for subsequent conversion to a variety of difluorinated products will be explored.

2.7 Experimental Section

General Methods

Starting materials and reagents were commercially available and used as obtained from Wako Pure Chemical, Kanto Chemical, Sigma-Aldrich, or TCI without further purification. CuI and LiI was obtained from Wako Pure Chemical. $Zn(OAc)_2$ and dppbz were obtained from TCI. Anhydrous

[56] Sterling, A. J.; Ciccia, N. R.; Guo, Y.; Hartwig, J. F.; Head-Gordon, M. *J. Am. Chem. Soc.* **2024**, *146*, 6168–6177.

DCE was obtained from Kanto Chemical. NMR spectra were recorded on a JEOL ESZ-400S spectrometer at 25 °C using residual protonated solvent signals as internal standards for ^{1}H- and ^{13}C-spectra (^{1}H: δ($CHCl_3$) = 7.26 ppm and ^{13}C: δ($CDCl_3$) = 77.16 ppm or δ(CD_2Cl_2) = 53.84 ppm) and chemical shifts are denoted in δ (ppm). Coupling constants J, are denoted in Hz. The splitting patterns are designated as follows: s (singlet); d (doublet); t (triplet); q (quartet); m (multiplet); dd (doublet of doublets); ddd (doublet of doublets of doublets); dt (doublet of triplets); td (triplet of doublets) and br (broad). The UV-vis experiments were performed on a F-7000 FL spectrophotometer (Hitachi, Japan) with a quartz cuvette (10 mm path length). The fluorescence quenching experiments were performed on a F-7000 FL Spectrophotometer (Hitachi, Japan). High resolution mass spectra were measured at the Instrumental Analysis Division of Global Facility Center in Hokkaido University. Thin-layer chromatography (TLC) was performed on commercial Merck 60F, 254 silica gel plates and compounds were visualized with naked eyes or UV light (λ = 254 nm). Kessil PR160L-390nm LED lamps were used for the photoreaction. Single-crystal X-ray diffraction (XRD) analyses were carried out on a Rigaku XtaLAB Synergy diffractometer using graphite monochromated Cu-Kα radiation. The structures were solved with the SHELXT structure solution program using Intrinsic Phasing incorporated in the OLEX2 program package[57] and refined with the SHELXL package[58]. Hydrogen atoms were refined using the riding model.

Cu-catalyzed C-O Coupling of Trifluoromethylarenes

In a nitrogen-filled glovebox, a catalyst solution was prepared in a 9-ml vial by vigorously stirring CuI (9.7 mg, 0.050 mmol, 0.10 equiv) and dppbz (17.9 mg, 0.040 mmol, 0.08 equiv) in DCE (3 mL) for 60 min. To another 50-ml tube were added $Zn(OAc)_2$ (91.7 mg, 0.50 mmol, 1.00 equiv) and LiI (133.9 mg, 1.00 mmol, 2.00 equiv), followed by the addition of a stir bar and DCE (10 mL). The mixture was stirred for 30 min, and then trifluoromethyl arene (0.50 mmol, 1.00 equiv), alcohol (12.5 mmol, 25.00 equiv) were added. The catalyst solution was added to the reaction mixture. The vial was rinsed with DCE (2 ml), which was transferred to the reaction mixture. The tube was sealed with a PTFE-lined septum cap, removed from the glovebox, and then placed at ~5 cm from two 52 W 390nm Kessil LED lamps. The reaction mixture was vigorously stirred while irradiated for 24 h at room temperature (with fan cooling). The resulting yellow turbid mixture

[57]Dolomanov, O. V.; Bourhis, L. J.; Gildea, R. J.; Howard, J. A. K; Puschmann, H. J. *Appl. Crystallogr.* **2009**, *42*, 339–341.
[58]Sheldrick, G. M. *Acta Crystallogr., Sect. A.* **2015**, *71*, 3–8.

was concentrated, and the crude was purified by flash column chromatography (Biotage, 100-g silica gel column, EtOAc in pentane/hexane as the eluent). For the determination of NMR yields, (trifluoromethoxy)benzene (0.05 mmol, 1.00 equiv) was added to the reaction mixture as the standard.

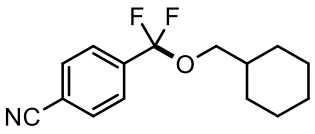

4-((cyclohexylmethoxy)difluoromethyl)benzonitrile (3a). Prepared according to the general procedure (13% of 5% EtOAc/pentane solution in hexane for column chromatography), and the title compound was obtained as a colorless oil (run 1: 93 mg, 70% yield; run 2: 87 mg, 65% yield).

^{1}H NMR (400 MHz, $CDCl_3$) δ (ppm) 7.73 (s, 4H), 3.85 (d, *J* = 6.5 Hz, 2H), 1.85 – 1.66 (m, 6H), 1.34 – 1.15 (m, 3H), 1.08 – 0.96 (m, 2H).

^{13}C NMR (101 MHz, $CDCl_3$) δ (ppm) 138.37 (t, *J* = 35.4 Hz), 132.41, 126.55 (t, *J* = 3.4 Hz), 121.90 (t, *J* = 237.35 Hz), 118.22, 114.35 (t, *J* = 1.5 Hz), 69.52 (t, *J* = 5.3 Hz), 37.58, 29.71, 26.49, 25.80.

^{19}F NMR (376 MHz, $CDCl_3$) *δ* (ppm) -69.29.

HRMS (EI) *m/z* calculated for $C_{15}H_{17}F_2NO^+$ ($[M]^+$): 265.1271, found: 265.1273.

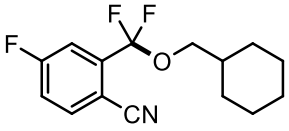

2-((cyclohexylmethoxy)difluoromethyl)-4-fluorobenzonitrile (3b). Prepared according to the general procedure (2% of 5% EtOAc/pentane solution in hexane for column chromatography), and the title compound was obtained as a colorless oil (run 1: 92 mg, 17% EtOAc, 62% yield; run 2: 97 mg, 4.5% hexane, 68% yield).

^{1}H NMR (400 MHz, $CDCl_3$) δ(ppm) 7.79 (dd, *J* = 8.6, 5.2 Hz, 1H), 7.49 (dd, *J* = 8.8, 2.6 Hz, 1H), 7.29 – 7.23 (m, 1H), 3.92 (d, *J* = 6.4 Hz, 2H), 1.86 – 1.65 (m, 6H), 1.33 – 1.17 (m, 3H), 1.09-0.99 (m, 2H).

^{13}C NMR (101 MHz, $CDCl_3$) δ(ppm) 164.40 (d, *J* = 257.8 Hz), 140.28 (td, *J* = 34.8, 8.6 Hz), 136.97 (d, *J* = 9.2 Hz), 121.84 (dd, *J* = 259.9, 2.3 Hz), 118.26 (d, *J* = 22.4 Hz), 115.94, 115.13 (dt, *J* = 25.4, 4.8 Hz), 106.78 (dt, *J* = 3.9, 2.0 Hz), 70.23 (t, *J* = 5.1 Hz), 37.40, 29.67, 26.47, 25.76.

^{19}F NMR (376 MHz, $CDCl_3$) δ (ppm) -69.24 (s, 2F), -101.49 (m, 1F).

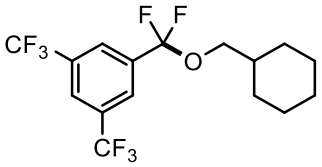

1-((cyclohexylmethoxy)difluoromethyl)-3,5-bis(trifluoromethyl)benzene (3c). Prepared according to the general procedure (100% hexane for column chromatography), and the title compound was obtained as a colourless oil (run 1: 73 mg, 6% EtOAc, 38% yield; run 2: 76 mg, 40% yield).

^{1}H NMR (400 MHz, $CDCl_3$) δ 8.06 (s, 2H), 7.98 (s, 1H), 3.89 (d, J = 6.5 Hz, 2H), 1.85 – 1.67 (m, 6H), 1.35 – 1.17 (m, 3H), 1.08 – 0.98 (m, 2H).

^{13}C NMR (101 MHz, $CDCl_3$) δ (ppm) 137.11 (t, J = 35.1 Hz), 132.24 (q, J = 33.9 Hz), 126.30 – 126.19 (m), 124.62 – 124.40 (m), 123.05 (q, J = 272.7 Hz), 121.43 (t, J = 258.0 Hz), 69.87 (t, J = 5.2 Hz), 37.49, 29.70, 26.48, 25.76.

^{19}F NMR (376 MHz, $CDCl_3$) δ (ppm) -62.90 (s, 6F), -68.69 (s, 2F).

HRMS (EI) *m/z* calculated for $C_{16}H_{16}F_8O^+$ ($[M]^+$): 376.1075, found: 376.1068.

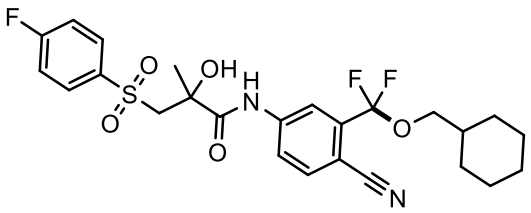

***N*-(4-cyano-3-((cyclohexylmethoxy)difluoromethyl)phenyl)-3-((4-fluorophenyl)sulfonyl)-2-hydroxy-2-methylpropanamide (3d).** Prepared according to the general procedure (48% EtOAc/ hexane for column chromatography), and the title compound was obtained as a white solid (run 1: 83 mg, 1.5% unreacted bicalutamide, 4.5% pentane 7.3% EtOAc, 31% yield).

^{1}H NMR (400 MHz, $CDCl_3$) δ(ppm) 8.99 (s, 1H), 7.90 – 7.86 (m, 2H), 7.79 – 7.71 (m, 3H), 7.15 (t, J = 8.5 Hz, 2H), 5.08 (s, 1H), 3.98 (d, J = 14.5 Hz, 1H), 3.92 (d, J = 6.5 Hz, 2H), 3.49 (d, J = 14.5 Hz, 1H), 1.85 – 1.6 (m, 7H), , 1.34 – 1.16 (m, 6H), 1.09 – 1.00 (m, 1H).

^{13}C NMR (101 MHz, $CDCl_3$) δ (ppm) 171.24, 167.66, 165.09, 140.58, 138.54 (t, J = 34.1 Hz), 135.73, 135.14 (d, J = 3.1 Hz), 131.00 (d, J = 9.9 Hz), 121.01, 120.67, 117.27 (t, J = 4.9 Hz),

116.98 (q, J = 24.2 Hz), 105.86 (t, J = 2.0 Hz), 74.53, 70.14 (t, J = 5.1 Hz), 61.68, 37.41, 29.69, 27.84, 26.49, 25.78.

^{19}F NMR (376 MHz, $CDCl_3$) δ (ppm) -69.45 (s, 2F), -101.26 – -101.36 (m, 1F).

HRMS (ESI) *m/z* calculated for $C_{25}H_{27}F_3N_2O_5NaS^+$ ([M +Na]$^+$): 547.1485, found: 547.1472.

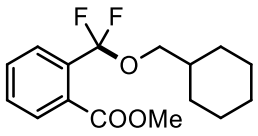

Methyl 2-((cyclohexylmethoxy)difluoromethyl)benzoate (3e). Prepared according to the general procedure (5% EtOAc /hexane for column chromatography), and the title compound was obtained as a dark purple solid (run 1: 49 mg, 10% pentane, 6% $ArCF_2I$, 30% yield; run 2: 42 mg, 11% hexane, 2% $ArCF_2I$, 26% yield; $ArCF_2I$: methyl 2-(difluoroiodomethyl)benzoate).

^{1}H NMR (400 MHz, $CDCl_3$) δ (ppm) 7.74 – 7.72 (m, 1H), 7.57 – 7.55 (m, 1H), 7.52 – 7.49 (m, 2H), 3.90 (s, 3H), 3.81 (d, J = 6.6 Hz, 2H), 1.80 – 1.65 (m, 6H), 1.28 – 1.23 (m, 3H), 1.04 – 0.98 (m, 2H).

^{13}C NMR (101 MHz, $CDCl_3$) δ (ppm) 168.98, 137.06, 132.20, 130.49 (t, J = 1.5 Hz), 130.44, 128.95, 126.75 (t, J = 4.9 Hz), 69.47 (t, J = 5.6 Hz), 52.69, 37.54, 29.72, 26.51, 25.82.

^{19}F NMR (376 MHz, $CDCl_3$) δ (ppm) -66.68.

HRMS (ESI) *m/z* calculated for $C_{16}H_{20}F_2NaO_3^+$ ([M+Na]$^+$): 321.1265, found: 321.1273.

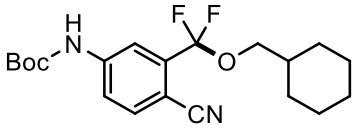

***tert*-butyl (4-cyano-3-((cyclohexylmethoxy)difluoromethyl)phenyl)carbamate (3f).** Prepared according to the general procedure (14% EtOAc/hexane for column chromatography), and the title compound was obtained as a white solid (run 1: 56 mg, 15% ester, 50% **2a**, 44% yield; ester: cyclohexylmethyl 4-((*tert*-butoxycarbonyl)amino)-2-cyanobenzoate).

^{1}H NMR (400 MHz, $CDCl_3$) δ (ppm) 7.68 (s, 1H), 7.67 (s, 2H), 6.78 (s, 1H), 3.89 (d, J = 6.5 Hz, 2H), 1.86 – 1.63 (m, 6H), 1.52 (s, 9H), 1.33 – 1.14 (m, 3H), 1.09 – 1.00 (m, 2H).

^{13}C NMR (101 MHz, CD_2Cl_2) δ (ppm) 151.90, 142.40 (t, J = 82.0 Hz), 138.39, 135.74, 119.21 (t, J = 225.9 Hz), 116.97, 115.90 (t, J = 4.3 Hz), 112.0, 103.70, 82.18, 69.99 (t, J = 5.3 Hz), 37.42, 29.69, 28.33, 26.49, 25.78.

^{19}F NMR (376 MHz, $CDCl_3$) δ (ppm) -69.52.

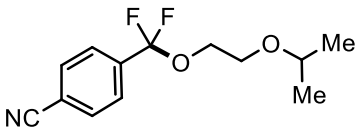

4-(difluoro(2-isopropoxyethoxy)methyl)benzonitrile (3g). Prepared according to the general procedure (7% EtOAc/hexane for column chromatography), and the title compound was obtained as a colorless oil (run 1: 59 mg, 15% hexane, 1.4% ROAc, 43% yield; run 2: 60 mg, 8% hexane, 1.3% ROAc, 45% yield; ROAc: 2-isopropoxyethyl acetate).

^{1}H NMR (400 MHz, $CDCl_3$) δ (ppm) 7.75 (d, J = 8.8 Hz, 2H), 7.72 (d, J = 8.8 Hz, 2H), 4.17 (dd, J = 5.7, 4.5 Hz, 2H), 3.72 – 3.68 (m, 2H), 3.67 – 3.61 (m, 1H), 1.18 (d, J = 6.1 Hz, 6H).

^{13}C NMR (101 MHz, CD_2Cl_2) δ (ppm) 138.55 (t, J = 33.7 Hz), 132.38, 126.62 (t, J = 3.5 Hz), 121.97 (t, J = 258.9 Hz), 118.16, 114.71 (t, J = 1.4 Hz), 72.26, 66.34, 64.03 (t, J = 5.6 Hz), 22.16.

^{19}F NMR (376 MHz, $CDCl_3$) δ (ppm) -69.44.

HRMS (ESI) *m/z* calculated for $C_{13}H_{15}F_2NaO_2^+$ ([M+Na]$^+$): 278.0961, found: 278.0963.

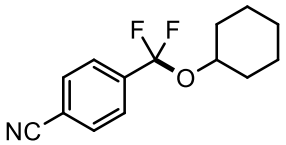

4-((cyclohexyloxy)difluoromethyl)benzonitrile (3h). Prepared according to the general procedure (30% of 5% EtOAc/pentane solution in hexane for column chromatography), and the title compound was obtained as a colorless oil (run 1: 71 mg, 5% hexane, 51% yield; run 2: 74 mg, 3.3% hexane, 58% yield).

^{1}H NMR (400 MHz, $CDCl_3$) δ 7.72 (s, 4H), 4.53 – 4.43 (m, 1H), 2.02 – 1.91 (m, 2H), 1.85 – 1.73 (m, 2H), 1.63 – 1.50 (m, 3H), 1.44 – 1.23 (m, 3H).

^{13}C NMR (101 MHz, $CDCl_3$) δ (ppm) 139.38 (t, J = 34.3 Hz), 132.35, 126.53 (t, J = 3.4 Hz), 122.15 (t, J = 258.0 Hz), 118.24, 114.46 (t, J = 1.4 Hz), 74.64 (t, J = 4.5 Hz), 33.40, 25.33, 23.95.

^{19}F NMR (376 MHz, $CDCl_3$) δ (ppm) -66.40.

HRMS (ESI) *m/z* calculated for $C_{14}H_{15}F_2NNaO^+$ ([M+Na]$^+$): 274.1009, found: 274.1014.

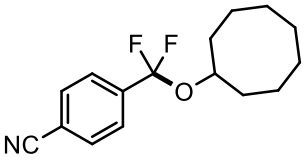

4-((cyclooctyloxy)difluoromethyl)benzonitrile (3i). Prepared according to the general procedure (13% of 5% EtOAc/pentane solution in hexane for column chromatography), and the title compound was obtained as a colorless oil (run 1: 79 mg, 57% yield; run 2: 89 mg, 1.5% hexane, 5% ROAc, 61% yield; ROAc: cyclooctyl acetate).

^{1}H NMR (400 MHz, $CDCl_3$) δ (ppm) 7.72 (s, 4H), 4.71 – 4.64 (m, 1H), 2.02 – 1.83 (m, 5H), 1.81 – 1.69 (m, 2H), 1.65 – 1.49 (m, 7H).

^{13}C NMR (101 MHz, $CDCl_3$) δ (ppm) 139.44 (t, *J* = 34.3 Hz), 132.35, 126.54 (t, *J* = 3.4 Hz), 122.04 (t, *J* = 257.4 Hz), 118.27, 114.42 (t, *J* = 1.4 Hz), 77.05 (t, *J* = 4.0 Hz), 32.83, 27.27, 25.40, 22.76.

^{19}F NMR (376 MHz, $CDCl_3$) *δ* (ppm) -66.70.

HRMS (ESI) *m/z* calculated for $C_{16}H_{19}F_2NNaO^+$ ($[M+Na]^+$): 302.1326, found: 302.1327.

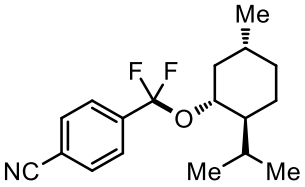

4-(difluoro(((1*R*,2*S*,5*R*)-2-isopropyl-5-methylcyclohexyl)oxy)methyl)benzonitrile (3j). Prepared according to the general procedure (13% of 5% EtOAc/pentane solution in hexane for column chromatography), and the title compound was obtained as a colorless oil (run 1: 81 mg, 5.0% ROAc, 50% yield; run 2: 87 mg, 5.0% ROAc, 54% yield; ROAc: 2-isopropyl-5-methylcyclohexyl acetate).

^{1}H NMR (400 MHz, $CDCl_3$) δ 7.72 (s, 4H), 4.32 – 4.25 (m, 1H), 2.29 – 2.20 (m, 1H), 2.17 – 2.04 (m, 1H), 1.76 – 1.66 (m, 2H), 1.55 – 1.43 (m, 1H), 1.39 – 1.32 (m, 1H), 1.19 (dd, *J* = 23.9, 11.8 Hz, 1H), 1.14 – 1.02 (m, 1H), 0.94 (d, *J* = 6.5 Hz, 3H), 0.92 (d, *J* = 7.1 Hz, 3H) 0.90 – 0.86 (m, 1H), 0.82 (d, *J* = 6.9 Hz, 3H).

^{13}C NMR (101 MHz, $CDCl_3$) δ (ppm) 139.42 (t, *J* = 34.8 Hz), 126.48 (t, *J* = 3.4 Hz), 122.20 (t, *J* = 259.6 Hz), 118.25, 114.46 (t, *J* = 1.4 Hz), 76.71 (t, *J* = 3.5 Hz), 47.97, 43.18, 34.20, 31.77, 25.73, 23.10, 22.24, 21.32, 15.62, 15.59.

^{19}F NMR (376 MHz, $CDCl_3$) δ (ppm) -64.81 (d, J = 152.8 Hz), -65.76 (d, J = 152.9 Hz).

HRMS (ESI) *m/z* calculated for $C_{18}H_{23}F_2NNaO^+$ ($[M+Na]^+$): 330.1638, found: 330.1640.

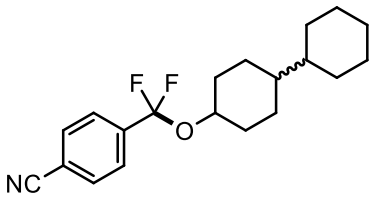

4-(([1,1'-bi(cyclohexan)]-4-yloxy)difluoromethyl)benzonitrile (3k) Prepared according to the general procedure (40% of 5% EtOAc/pentane solution in hexane for column chromatography), and the title compound was obtained as a colorless oil (run 1: 124 mg, 11% ROAc, 10% pentane, dr = 1.00 : 0.91, 67% yield; run 2: 135 mg, 5% ROAc, dr = 1.00 : 0.93, 78% yield; ROAc: [1,1'-bi(cyclohexan)]-4-yl acetate).

^{1}H NMR (400 MHz, $CDCl_3$) δ (ppm) 7.73 (s, 4H), 7.71 (s, 4H*), 4.77 – 4.72 (s, 1H), 4.38 – 4.30 (m, 1H*), 2.16-2.10 (m, 2H), 2.03 – 1.95 (m, 2H*), 1.84 – 1.61 (m, 7H+7H*), 1.54 – 1.38 (m, 2H+2H*), 1.14 (tt, J = 15.5, 10.5 Hz, 7H+7H*), 1.02 – 0.88 (m, 2H+2H*).

^{13}C NMR (100 MHz, $CDCl_3$) δ (ppm) 139.57 (t, J = 34.4 Hz), 139.34 (t, J = 34.2 Hz)*, 132.39, 132.34*, 126.54 (t, J = 3.3 Hz), 126.52 (t, J = 3.3 Hz)*, 122.19 (t, J = 258.1 Hz), 122.13 (t, J = 257.8 Hz)*, 118.27, 118.24*, 114.48 – 114.47 (m, 2C+2C*), 75.79 (t, J = 4.4 Hz), 72.01 (t, J = 4.4 Hz)*, 42.74, 42.58*, 42.22, 42.20*, 33.74, 31.69*, 30.46, 30.39*, 28.13, 26.91*, 26.89, 26.88*, 26.86, 24.32*.

^{19}F NMR (376 MHz, $CDCl_3$) δ (ppm) -66.32, -66.54*.

HRMS (ESI) *m/z* calculated for $C_{20}H_{25}F_2NNaO^+$ ($[M+Na]^+$):356.1797, found: 356.1797.

* denotes the peaks for minor diastereoisomer

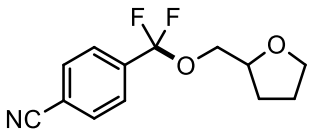

4-(difluoro((tetrahydrofuran-2-yl)methoxy)methyl)benzonitrile (3l). Prepared according to the general procedure (19% EtOAc/hexane for column chromatography), and the title compound was obtained as a colorless oil (run 1: 78 mg, 1.6% pentane, 61% yield; run 2: 82 g, 65% yield).

^{1}H NMR (400 MHz, $CDCl_3$) δ (ppm) 7.75 (d, *J* = 8.7 Hz, 2H), 7.72 (d, *J* = 8.7 Hz, 2H), 4.22 – 4.16 (m, 1H), 4.09 – 3.99 (m, 2H), 3.93 – 3.88 (m, 1H), 3.84 – 3.79 (m, 1H), 2.09 – 2.01 (m, 1H), 1.96 – 1.89 (m, 2H), 1.74 – 1.66 (m, 1H).

^{13}C NMR (101 MHz, $CDCl_3$) δ (ppm) 138.37 (t, *J* = 33.6 Hz), 132.34, 126.55 (t, *J* = 3.6 Hz), 121.85 (t, *J* = 259.1 Hz), 118.08, 114.69 (t, *J* = 1.4 Hz), 76.67, 68.69, 66.42 (t, *J* = 5.2 Hz), 28.07, 25.74.

^{19}F NMR (376 MHz, $CDCl_3$) *δ* (ppm) -69.26 (d, *J* = 151.4 Hz), -69.80 (d, *J* = 151.5 Hz).

HRMS (ESI) *m/z* calculated for $C_{13}H_{13}F_2NNaO_2^+$ ($[M+Na]^+$): 276.0802, found: 276.0807.

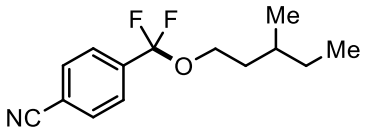

4-(difluoro((3-methylpentyl)oxy)methyl)benzonitrile (3m). Prepared according to the general procedure (21% of 5% EtOAc/pentane solution in hexane for column chromatography), and the title compound was obtained as a colorless oil (run 1: 73 mg, 33% pentane, 51% yield; run 2: 74 mg, 3.7% CH_2Cl_2, 58% yield).

^{1}H NMR (400 MHz, $CDCl_3$) δ (ppm) 7.72 (s, 4H), 4.15 – 4.04 (m, 2H), 1.82 – 1.71 (m, 1H), 1.59 – 1.46 (m, 2H), 1.44 – 1.34 (m, 1H), 1.28 – 1.16 (m, 1H), 0.95 – 0.87 (m, 6H).

^{13}C NMR (101 MHz, $CDCl_3$) δ (ppm) 138.90 (t, *J* = 34.0 Hz), 132.39, 126.52 (t, *J* = 3.5 Hz), 121.92 (t, *J* = 258.1 Hz), 118.18, 114.61 (t, *J* = 1.4 Hz), 62.92 (t, *J* = 5.9 Hz), 35.77, 31.30, 29.49, 19.06, 11.34.

^{19}F NMR (376 MHz, $CDCl_3$) *δ* (ppm) -69.50.

HRMS (ESI) *m/z* calculated for $C_{14}H_{17}F_2NNaO^+$ ($[M+Na]^+$): 276.1168, found: 276.1170.

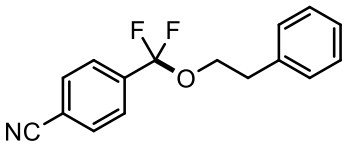

4-(difluoro(phenethoxy)methyl)benzonitrile (3n). Prepared according to the general procedure (39% of 5% EtOAc/pentane solution in hexane for column chromatography), and the title compound was obtained as a colorless oil (run 1: 57 mg, *ca.* 95% purity, 42% yield; run 2: 65 mg, 4.5% hexane, 2% ROAc, 46% yield ROAc: phenethyl acetate).

^{1}H NMR (400 MHz, $CDCl_3$) δ (ppm) 7.71 (d, *J* = 8.7 Hz, 2H), 7.68 (d, *J* = 8.8 Hz, 2H), 7.37 – 7.30 (m, 2H), 7.28 – 7.23 (m, 3H), 4.28 (t, *J* = 7.1 Hz, 2H), 3.04 (t, *J* = 7.1 Hz, 2H).

^{13}C NMR (101 MHz, $CDCl_3$) δ (ppm) 138.62 (t, *J* = 33.7 Hz), 137.55, 132.40, 129.05, 128.70, 126.87, 126.52 (t, *J* = 3.5 Hz), 121.89 (t, *J* = 258.8 Hz), 118.14, 114.70 (t, *J* = 1.4 Hz), 64.92 (t, *J* = 5.7 Hz), 35.88.

^{19}F NMR (376 MHz, $CDCl_3$) *δ* (ppm) -69.41.

HRMS (ESI) *m/z* calculated for $C_{16}H_{13}F_2NNaO^+$ ([M+Na]$^+$): 296.0853, found: 296.0857.

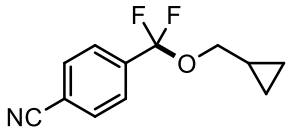

4-((cyclopropylmethoxy)difluoromethyl)benzonitrile (3o). Prepared according to the general procedure, and the yield was determined by ^{19}F NMR analysis (run 1: 46% NMR yield).

^{19}F NMR (376 MHz, $CDCl_3$) *δ* (ppm) -68.93.

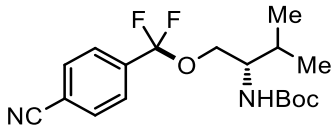

***tert*-Butyl (S)-(1-((4-cyanophenyl)difluoromethoxy)-3-methylbutan-2-yl)carbamate (3p).** Prepared according to the general procedure (8% EtOAc/hexane for column chromatography), and the title compound was obtained as a colorless oil (run 1: 75 mg, 6% pentane, 42% yield; run 2: 77 mg, 44% yield).

^{1}H NMR (400 MHz, $CDCl_3$) δ (ppm) 7.72 (s, 4H), 4.57 (d, *J* = 9.5 Hz, 1H), 4.16 – 4.01 (m, 2H), 3.78 – 3.65 (m, 1H), 1.90 – 1.82 (m, , 1H), 1.43 (s, 9H), 0.99 (d, *J* = 6.8 Hz, 3H), 0.96 (d, *J* = 6.8 Hz, 3H).

^{13}C NMR (101 MHz, CD_2Cl_2) δ (ppm) 155.85, 138.34 (t, *J* = 33.3 Hz), 132.41, 126.55 (t, *J* = 3.5 Hz), 121.83 (t, *J* = 260.6 Hz), 118.09, 114.80, 79.60, 64.80 (t, *J* = 5.0 Hz), 54.89, 29.45, 28.47, 19.53, 18.52.

^{19}F NMR (376 MHz, $CDCl_3$) *δ* (ppm) -68.73 (d, *J* = 152.0 Hz), -70.23 (d, *J* = 152.0 Hz).

HRMS (ESI) *m/z* calculated for $C_{18}H_{24}F_2N_2NaO_3^+$ ([M+Na]$^+$): 377.1640, found: 377.1647.

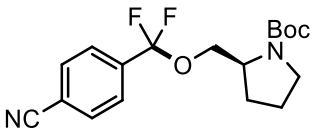

***tert*-Butyl (*S*)-2-(((4-cyanophenyl)difluoromethoxy)methyl)pyrrolidine-1-carboxylate (3q).** Prepared according to the general procedure (6% EtOAc/hexane for column chromatography), and the title compound was obtained as a light green solid (run 1: 71 mg, 41% yield; run 2: 70 mg, 40% yield).

^{1}H NMR (400 MHz, $CDCl_3$) δ(ppm) 7.72 (s, 4H), 4.17 (dd, *J* = 9.3, 3.1 Hz, 1H), 4.16 – 3.90 (m, 2H), 3.49 – 3.29 (m, 2H), 2.09 – 1.92 (m, 2H), 1.91 – 1.82 (m, 2H), 1.47 (s, 9H) (*mixture of rotamers*).

^{13}C NMR (101 MHz, CD_2Cl_2) δ (ppm) 154.90, 134.12 (t, *J* = 7.6 Hz), 132.43, 129.80 (t, *J* = 1.6 Hz), 129.02, 128.03 (t, *J* = 4.6 Hz), 126.58 – 126.42 (m), 121.82 (t, *J* = 260.58 Hz), 118.11 114.80, 79.98, 79.72, 64.79, 64.55, 55.97, 46.98, 46.71, 28.80, 28.58, 27.88, 23.89, 23.06 (*mixture of rotamers*).

^{19}F NMR (376 MHz, $CDCl_3$) *δ* (ppm) -68.31 – -69.70 (m) (*mixture of rotamers*).

HRMS (ESI) *m/z* calculated for $C_{18}H_{22}F_2N_2NaO_3^+$ ([M+Na]$^+$): 375.1491, found: 375.1483.

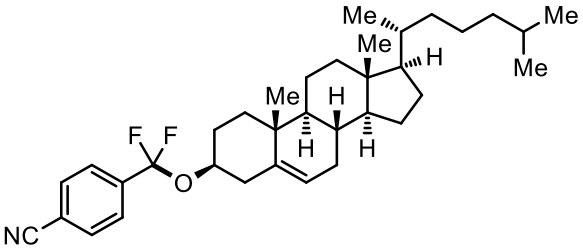

4-((((3*S*,8*S*,9*S*,10*R*,13*R*,14*S*,17*R*)-10,13-dimethyl-17-((*R*)-6-methylheptan-2-yl)-2,3,4,7,8,9,10,11,12,13,14,15,16,17-tetradecahydro-1H-cyclopenta[*a*]phenanthren-3-yl)oxy)difluoromethyl)benzonitrile (3r). Prepared according to the general procedure except that 12.5 equiv of alcohols was used (39% of 5% EtOAc/pentane solution in hexane for column chromatography), and the title compound was obtained as a white solid (run 1: 177 mg, 11% hexane, 7.0% ester, 62% yield; run 2: 216 mg, 30% ROAc, 65% yield; ROAc: (3*S*,8*S*,9*S*,10*R*,13*R*,14*S*,17*R*)-10,13-dimethyl-17-((*R*)-6-methylheptan-2-yl)-2,3,4,7,8,9,10,11,12,13,14,15,16,17-tetradecahydro-1H-cyclopenta[a]phenanthren-3-yl acetate, ester: (3S,8S,9S,10R,13R,14S,17R)-10,13-dimethyl-17-((R)-6-methylheptan-2-yl)-

2,3,4,7,8,9,10,11,12,13,14,15,16,17-tetradecahydro-1H-cyclopenta[a]phenanthren-3-yl 4-cyanobenzoate).

^{1}H NMR (400 MHz, $CDCl_3$) δ 7.72 (s, 4H), 5.39 (dd, *J* = 16.2, 5.1 Hz, 1H), 4.38 – 4.30 (m, 1H), 2.52 – 2.28 (m, 2H), 2.07 – 1.68 (m, 6H), 1.62 – 1.44 (m, 7H), 1.39 – 1.22 (m, 4H), 1.22 – 1.01 (m, 12H), 0.92 (d, *J* = 6.5 Hz, 3H) 0.87 (d, *J* = 1.5 Hz, 3H), 0.86 (d, *J* = 1.6 Hz, 3H), 0.68 (s, 3H).

^{13}C NMR (101 MHz, $CDCl_3$) δ (ppm) 139.87 (t, *J* = 44.3 Hz), 132.38, 126.53 (t, *J* = 3.5 Hz), 123.02, 121.04 (t, *J* = 141.4 Hz), 118.24, 114.54 (t, *J* = 2.0 Hz), 75.93 (t, *J* = 2.4 Hz), 73.11, 56.85, 56.27, 50.20, 42.47, 39.99, 39.86, 39.66, 37.24, 36.62, 36.32, 35.93, 32.08, 31.99, 29.58, 28.38, 28.17, 24.43, 23.96, 22.97, 22.71, 21.18, 19.44, 18.87, 12.01.

^{19}F NMR (376 MHz, $CDCl_3$) *δ* (ppm) -66.08 (d, *J* = 153.5 Hz), -66.53 (d, *J* = 153.5 Hz).

HRMS (ESI) *m/z* calculated for $C_{35}H_{49}F_2NNaO^+$ ($[M+Na]^+$): 560.3675, found: 560.3666.

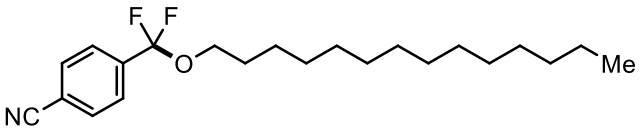

4-(difluoro(tetradecyloxy)methyl)benzonitrile (3s). Prepared according to the general procedure (20% of 5% EtOAc/pentane solution in hexane for column chromatography), and the title compound was obtained as a colorless solid (run 1: 178 mg, 24% ROAc, 15% pentane, 81% yield; run 2: 178 mg, 24% ROAc, 6% hexane, 82% yield; ROAc: tetradecyl acetate).

^{1}H NMR (400 MHz, $CDCl_3$) δ 7.73 (s, 4H), 4.05 (t, *J* = 6.6 Hz, 2H), 1.77 – 1.66 (m, 2H), 1.44 – 1.37 (m, 2H), 1.30 – 1.25 (m, 20H), 0.88 (t, *J* = 6.8 Hz, 3H).

^{13}C NMR (101 MHz, $CDCl_3$) δ (ppm) 138.92 (t, *J* = 34.0 Hz), 132.39, 126.54 (t, *J* = 3.5 Hz), 121.91 (t, *J* = 258.1 Hz), 118.20, 114.60 (t, *J* = 1.4 Hz), 64.56 (t, *J* = 5.8 Hz), 32.07, 29.83, 29.81, 29.80, 29.78, 29.72, 29.66, 29.51, 29.34, 29.29, 25.93, 22.84, 14.27.

^{19}F NMR (376 MHz, $CDCl_3$) *δ* (ppm) -69.43.

HRMS (ESI) *m/z* calculated for $C_{22}H_{33}F_2NNaO^+$ ($[M+Na]^+$): 388.2419, found: 388.2423.

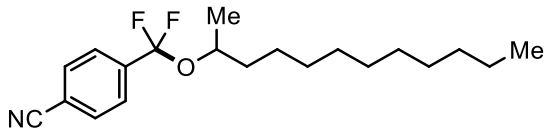

4-((dodecan-2-yloxy)difluoromethyl)benzonitrile (3t). Prepared according to the general procedure (30% of 5% EtOAc/pentane solution in hexane for column chromatography), and the

title compound was obtained as a colorless oil (run 1: 158 mg, 18% ROAc, 10% pentane, 80% yield; run 2: 160 mg, 23% hexane, 0.33% unreacted $ArCF_3$, 10% ROAc, 84% yield; ROAc: dodecan-2-yl acetate).

^{1}H NMR (400 MHz, $CDCl_3$) δ (ppm) 7.72 (s, 4H), 4.63 – 4.56 (m, 1H), 1.71 – 1.62 (m, 1H), 1.59 – 1.50 (m, 1H), 1.35 (d, *J* = 6.2 Hz, 3H), 1.31-1.17 (m, 16H), 0.88 (t, *J* = 6.9 Hz, 3H).

^{13}C NMR (101 MHz, $CDCl_3$) δ (ppm) 139.39 (t, *J* = 34.3 Hz), 132.35, 126.49 (t, *J* = 3.4 Hz), 122.13 (t, *J* = 259.1 Hz), 118.22, 114.49 (t, *J* = 1.4 Hz), 73.29 (t, *J* = 4.3 Hz), 71.22, 37.24, 32.04, 29.73, 29.68, 29.56, 29.47, 25.49, 22.82, 21.85, 14.25.

^{19}F NMR (376 MHz, $CDCl_3$) *δ* (ppm) -66.12 (d, *J* = 153.7 Hz), -66.76 (d, *J* = 153.7 Hz).

HRMS (ESI) *m/z* calculated for $C_{20}H_{29}F_2NNaO^+$ ($[M+Na]^+$): 360.2107, found: 360.2109.

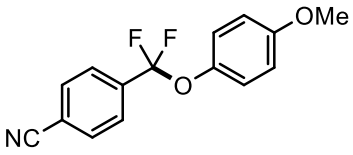

4-(difluoro(4-methoxyphenoxy)methyl)benzonitrile (3u). Prepared according to the general procedure (13% EtOAc/hexane for column chromatography), and the title compound was obtained as a dark purple solid (run 1: 36 mg, 4% unreacted $ArCF_3$, 36% ROAc, 8% hexane, *ca.* 95% purity, 21% yield; run 2: 46 mg, 54.3% ROAc, 25% yield; ROAc: 4-methoxyphenyl acetate).

^{1}H NMR (400 MHz, $CDCl_3$) δ (ppm) 7.85 (d, *J* = 8.2 Hz, 2H), 7.78 (d, *J* = 8.2 Hz, 2H), 7.17 (d, *J* = 8.8 Hz, 2H), 6.89 (d, *J* = 9.1 Hz, 2H), 3.81 (s, 3H).

^{13}C NMR (101 MHz, $CDCl_3$) δ (ppm) 157.74, 143.39 (t, *J* = 2.0 Hz), 138.23 (t, *J* = 33.0 Hz), 132.51, 126.70 (t, *J* = 3.6 Hz), 123.40, 121.17 (t, *J* = 261.4 Hz), 118.05, 115.01 (t, *J* = 1.4 Hz), 114.59, 55.72.

^{19}F NMR (376 MHz, $CDCl_3$) *δ* (ppm) -66.10.

HRMS (EI) *m/z* calculated for $C_{15}H_{11}F_2NO^+$ ($[M]^+$):275.0748, found: 275.0752.

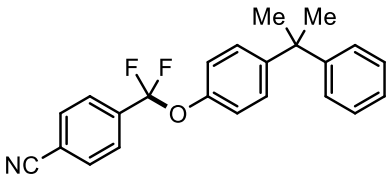

4-(difluoro(4-(2-phenylpropan-2-yl)phenoxy)methyl)benzonitrile (3v). Prepared according to the general procedure (6% EtOAc/hexane for column chromatography), and the title compound was obtained as a white solid (run 1: 53 mg, 12% pentane, 28% yield; run 2: 61 mg, 4% hexane, 0.3% unreacted $ArCF_3$, 35% ROAc: 4-(2-phenylpropan-2-yl)phenyl acetate, 27% yield).

^{1}H NMR (400 MHz, $CDCl_3$) δ(ppm) 7.86 (d, *J* = 8.6 Hz, 2H), 7.78 (d, *J* = 8.7 Hz, 2H), 7.43 – 7.07 (m, 9H), 1.69 (s, 6H).

^{13}C NMR (101 MHz, $CDCl_3$) δ (ppm) 150.34, 148.73, 147.92 (t, *J* = 2.0 Hz), 138.29 (t, *J* = 33.0 Hz), 132.54, 128.24, 128.08, 126.88, 126.70 (t, *J* = 3.7 Hz), 125.95, 121.37, 121.37, 118.06 (t, *J* = 303 Hz), 115.06 (t, *J* = 1.5 Hz), 42.84, 30.95.

^{19}F NMR (376 MHz, $CDCl_3$) *δ* (ppm) -65.82.

HRMS (EI) *m/z* calculated for $C_{23}H_{19}F_2NO^+$ ($[M]^+$):363.1435, found: 363.1425.

Reduced alcohol loading

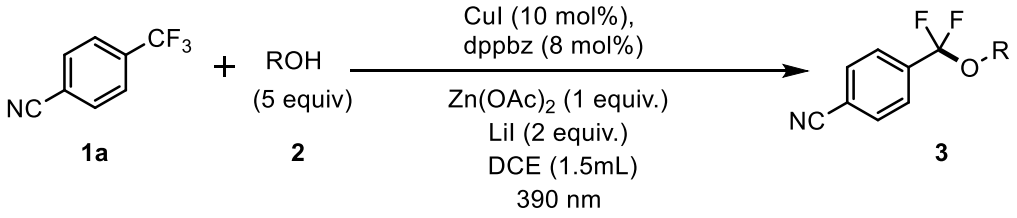

Entry[a]	ROH (5 equiv)	NMR Yield (%)[b]
1	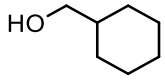	40 (**3a**)
2	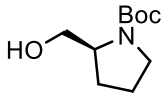	16 (**3q**)
3	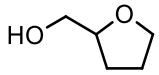	31 (**3l**)
4	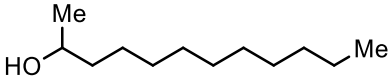	30 (**3t**)
5	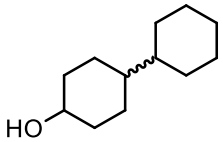	29 (**3k**)
6	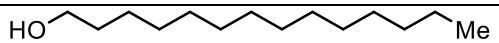	53 (**3s**)

7	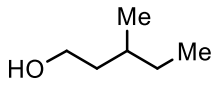	25 (**3m**)
8	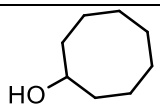	40 (**3i**)

Table 14. [a]Reactions were carried out using 0.15 mmol of **1a** and 5 equiv of **2a** in DCE under irradiation with violet LEDs (390 nm) for 24 h at rt. [b]Yields were determined by ^{19}F-NMR analysis of the crude mixture using (trifluoromethoxy)benzene as the standard.

Unsuccessful substrates

trifluoromethylarenes

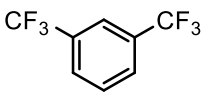

<3% yield

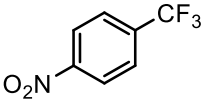

<3% yield

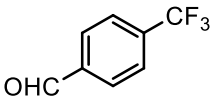

<3% yield

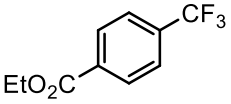

7% yield

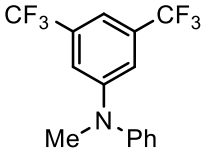

10% yield

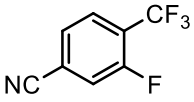

15% yield

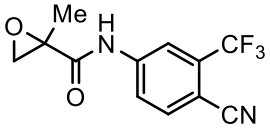

7% yield

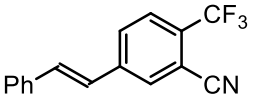

7% yield

alcohols

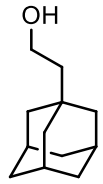

85% yield
isolation issue

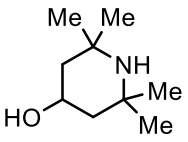

45% yield

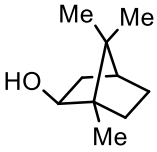

32% yield

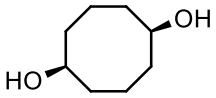

11% yield

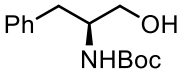

31% yield

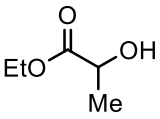

32% yield

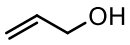

23% yield

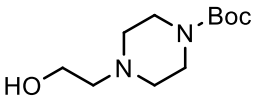

10% yield

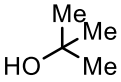

<3% yield

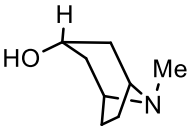

<3% yield

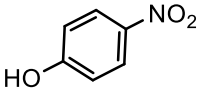

<3% yield

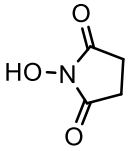

<3% yield

Cu-catalyzed C-I Coupling of Trifluoromethylarenes

In a nitrogen-filled glovebox, a catalyst solution was prepared in a 9-ml vial by vigorously stirring CuI (4.8 mg, 0.025 mmol, 0.10 equiv) and dppbz (8.9 mg, 0.020 mmol, 0.08 equiv) in DCE (1.5 mL) for 60 min. To a 10-ml tube were added $Zn(OAc)_2$ (45.9 mg, 0.25 mmol, 1.00 equiv), LiI (234.2 mg, 1.75 mmol, 7.00 equiv), trifluoromethyl arene (0.25 mmol, 1.00 equiv), *tert*-amyl alcohol (0.054 mL, 0.50 mmol, 2.00 equiv), followed by the addition of a stir bar and DCE (5 mL). The catalyst solution was added to the reaction mixture. The vial was rinsed with DCE (0.5 ml), and the rinse was transferred to the reaction mixture. The tube was sealed with a PTFE-lined septum cap, removed from the glovebox, and placed ~5 cm from two 52 W 390nm Kessil LED lamps. The reaction mixture was vigorously stirred while irradiated for 24 h at room temperature (with fan cooling). The resulting solution was concentrated and purified by flash column chromatography (hexane as the eluent). For the determination of NMR yields, (trifluoromethoxy)benzene (0.25 mmol, 1.00 equiv) was added to the reaction mixture as the standard.

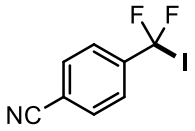

4-(difluoroiodomethyl)benzonitrile (4a). Prepared according to the general procedure (hexane for column chromatography), and the title compound was obtained as a colorless oil (61 mg, 17% DCE, 11 % unreacted $ArCF_3$, 60% hexane, 62% yield).

^{1}H NMR (400 MHz, $CDCl_3$) δ (ppm) 7.75 (dt, *J* = 8.8, 0.7 Hz), 7.67 (dt, *J* = 8.8, 0.7 Hz)

^{13}C NMR (101 MHz, $CDCl_3$) δ (ppm) 145.23 (t, *J* = 22.1 Hz), 132.72, 124.56 (t, *J* = 5.4 Hz), 115.03 (t, *J* = 1.6 Hz), 96.24, 93.12.

^{19}F NMR (376 MHz, $CDCl_3$) *δ* (ppm) -40.61.

HRMS (APCI) *m/z* calculated for $C_8H_5F_2IN^+$ ($[M+H]^+$): 279.9423, found: 279.9429.

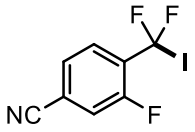

4-(difluoroiodomethyl)-3-fluorobenzonitrile (4b). Prepared according to the general procedure (hexane for column chromatography), and the title compound was obtained as a colorless oil (34 mg, 11 % unreacted $ArCF_3$, 12% hexane, 62% yield).

^{1}H NMR (400 MHz, $CDCl_3$) δ (ppm) 7.61 (t, *J* = 6.9 Hz, 1H), 7.54 (d, *J* = 8.1 Hz, 1H), 7.48 (d, *J* = 9.7 Hz, 1H).

^{13}C NMR (101 MHz, $CDCl_3$) δ (ppm) 157.85 (d, *J* = 260.2 Hz), 133.49 – 132.84 (m), 128.59 (t, *J* = 3.4 Hz), 128.24 (d, *J* = 4.5 Hz), 125.55 (t, *J* = 6.7 Hz), 121.19 (d, *J* = 24.2 Hz), 116.72 (d, *J* = 8.7 Hz), 116.57 – 116.51 (m).

^{19}F NMR (376 MHz, $CDCl_3$) *δ* (ppm) -41.75 (d, *J* = 14.6 Hz, 2F), -107.70 – 107.99 (m, 1F).

HRMS (APCI) *m/z* calculated for $C_8H_4F_3IN^+$ ($[M+H]^+$): 297.9334, found: 279.9335.

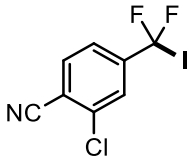

2-chloro-4-(difluoroiodomethyl)benzonitrile (4c). Prepared according to the general procedure, and the title compound was obtained in 58% NMR yield.

^{19}F NMR (376 MHz, $CDCl_3$) δ (ppm) -41.83 (d, J = 8.8 Hz).

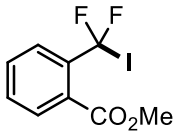

methyl 2-(difluoroiodomethyl)benzoate (4d). Prepared according to the general procedure, and the title compound was obtained in 77% NMR yield.

^{19}F NMR (376 MHz, $CDCl_3$) δ (ppm) -37.11.

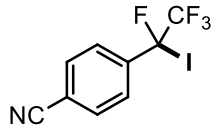

4-(1,2,2,2-tetrafluoro-1-iodoethyl)benzonitrile (4e). Prepared according to the general procedure, and the title compound was obtained in 46% NMR yield.

^{19}F NMR (376 MHz, $CDCl_3$) δ (ppm) -84.43 (s, 3F), -133.55 – -133.73 (m, 1F).

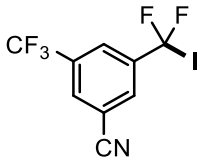

3-(difluoroiodomethyl)-5-(trifluoromethyl)benzonitrile (4f). Prepared according to the general procedure, and the title compound was obtained in 9% NMR yield.

^{19}F NMR (376 MHz, $CDCl_3$) δ (ppm) -41.50 (s, 2F), 63.14 (s, 3F).

Synthesis of Copper Complexes CuP2 and CuP4

Synthesis of Cu(dppbz)I (CuP2)

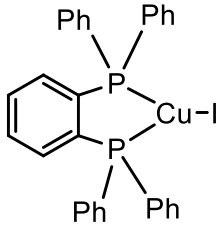

In a nitrogen-filled glovebox, an oven-dried 9-mL flask equipped with a magnetic stir bar was charged with CuI (19.3 mg, 0.1 mmol, 1.0 equiv), dppbz (44.6 mg, 0.1 mmol, 1.0 equiv), and DCE (5 mL). The reaction mixture was allowed to stir at rt for 3 hr. The resulting mixture was filtered,

washed with 0.5 mL hexane, and the filtrate was concentrated to afford the desired complex. The title compound was obtained as a greenish-yellow solid (58 mg, 14 % DCE, 5% hexane, 89% yield).

^{1}H NMR (400 MHz, $CDCl_3$) δ (ppm) 7.35 – 7.21 (m, 12H), 7.18 (t, *J* = 7.3 Hz, 4H), 7.07 (t, *J* = 7.3 Hz, 8H).

^{1}H NMR (400 MHz, CD_2Cl_2) δ (ppm) 7.38 – 7.35 (m, 2H), 7.28 – 7.21 (m, 10H), 7.21 – 7.17 (m, 3H), 7.11 – 7.05 (m, 9H).

^{13}C NMR (101 MHz, CD_2Cl_2) δ (ppm) 143.29 (t, *J* = 29.9 Hz), 134.53 (t, *J* = 4.1 Hz), 134.28 (t, *J* = 7.5 Hz), 133.13 (t, *J* = 15.0 Hz), 130.29, 129.45, 128.33 (t, *J* = 4.6 Hz).

^{31}P NMR (101 MHz, $CDCl_3$) *δ* (ppm) -22.42.

^{31}P NMR (101 MHz, CD_2Cl_2) *δ* (ppm) -22.06.

HRMS (ESI) *m/z* calculated for $C_{30}H_{24}CuINaP_2^+$ ($[M+Na]^+$):658.9574, found: 658.9586.

Synthesis of $[Cu(dppbz)_2]^+I^-$ (CuP4)

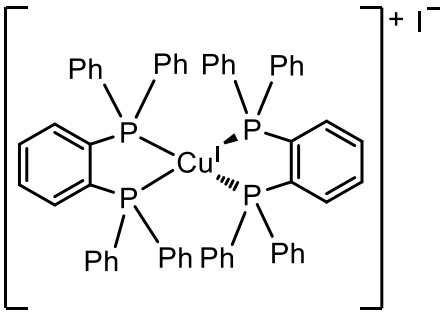

In a nitrogen-filled glovebox, an oven-dried 9-mL flask equipped with a magnetic stir bar was charged with CuI (19.3 mg, 0.1 mmol, 1.0 equiv), dppbz (89.2 mg, 0.2 mmol, 2.0 equiv), and DCE (5 mL). The reaction mixture was then stirred at rt for 3 hr. The resulting mixture was filtered, washed with 0.5 mL hexane, and the filtrate was concentrated to afford the desired complex. The title compound was obtained as a pale yellow solid (95 mg, 12 % DCE, 6% hexane, 87% yield).

^{1}H NMR (400 MHz, $CDCl_3$) δ (ppm) 7.53 (m, 4H), 7.48 (m, 4H), 7.29 (t, *J* = 7.4 Hz, 8H), 7.06 (t, *J* = 7.7 Hz, 16H), 6.97 – 6.90 (m, 16H).

^{13}C NMR (101 MHz, $CDCl_3$) δ (ppm) 141.75, 134.32 – 134.08 (m), 132.76 – 132.47 (m), 131.83, 131.34 (m), 130.37, 129.27 – 128.99 (m).

^{31}P NMR (101 MHz, $CDCl_3$) *δ* (ppm) 8.71.

HRMS (ESI) *m/z* calculated for $C_{60}H_{48}CuP4^+$ ($[M]^+$): 955.1997, found: 955.1997.

X-ray single crystal of **CuP4**

In a nitrogen-filled glovebox, an oven-dried 9-mL flask equipped with a magnetic stir bar was charged with CuI (19.3 mg, 0.1 mmol, 1.0 equiv), dppbz (48.6 mg, 0.1 mmol, 1.0 equiv), and DCE (3.0 mL). The reaction mixture was then stirred at rt for 30 min. Then ZnI_2 (5 equiv) was added to the reaction mixture and the mixture was stirred for 1 h. The resulting heterogeneous mixture was settled, and *ca.* 1.0 ml supernatant was transferred to another vial. A single crystal suitable for X-ray analysis was obtained by vapor diffusion of diethyl ether to the **CuP4** in DCE solution.

Table 15. The crystal data parameters obtained by single crystal XRD of CuP4

Crystal name (CCDC #)	**CuP4** (2382840)
Empirical formula	$C_{64}H_{58}CuI_3OP_4Zn$
Formula weight	1476.59
Temperature/K	153
Crystal system	orthorhombic
Space group	*Pbca*
a/Å	26.4223(2)
b/Å	14.42560(10)
c/Å	31.4049(2)
α/°	90
β/°	90
γ/°	90
Volume/$Å^3$	11970.21(14)
Z	8
$\rho_{calc}g/cm^3$	1.639

μ/mm^{-1}	14.401
F(000)	5824
Crystal size/mm^3	0.7 × 0.7 × 0.7
Radiation	Cu Kα (λ = 1.54184)
2Θ range for data collection/°	5.628 to 152.844
Reflections collected	47044
Independent reflections	12113 [R_{int} = 0.0467]
Data/restraints/parameters	12113/0/670
Goodness-of-fit on F^2	1.044
Final R indexes [I>=2σ (I)]	R_1 = 0.0464, wR_2 = 0.1247
Final R indexes [all data]	R_1 = 0.0483, wR_2 = 0.1283
Largest diff. peak/hole / e Å^{-3}	2.60/-1.53

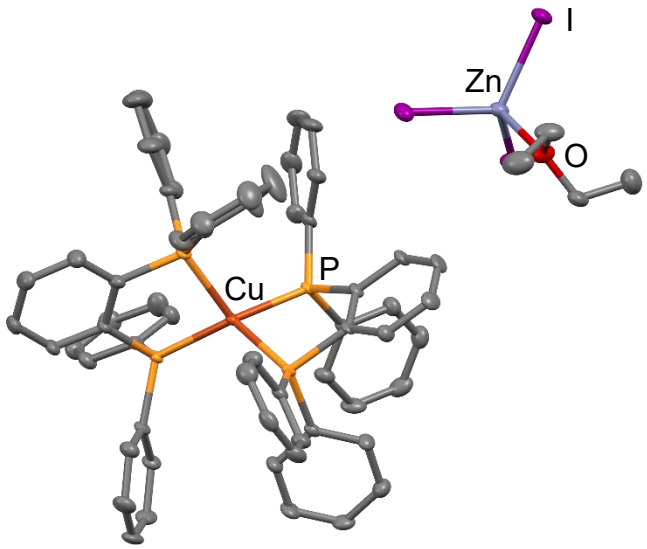

Figure 1. Single crystal structure of **CuP4**

^{31}C NMR Studies of 1a with Salt Additives

To 0.04 mmol of **1a** in a vial, the following salts were added according to the equivalence mentioned. Deuterated dichloromethane (CD_2Cl_2, 3 mL) was added, and the mixture was stirred for 5 hour inside glovebox.

ppm (CD_2Cl_2)	**1a** (Vial **1**)	**1a** + 2 equiv LiI + 1 equiv $Zn(OAc)_2$ (Vial **2**)	**1a** + 1 equiv $Zn(OAc)_2$ (Vial **3**)	**1a** + 2 equiv LiI (Vial **4**)
$\Delta\delta$ 134.60 ppm (q)	0	0.18	0.01	0.27
$\Delta\delta$ 133.23 ppm	0	0.08	0.01	0.13
$\Delta\delta$ 126.54 ppm(q)	0	0.05	0.01	0.04
$\Delta\delta$ 123.675 ppm (q)	0	-0.05	-0.03	-0.08
$\Delta\delta$ 117.89 ppm	0	-0.02	0.00	0.09
$\Delta\delta$ 116.58 ppm (q)	0	-0.32	-0.03	-0.52

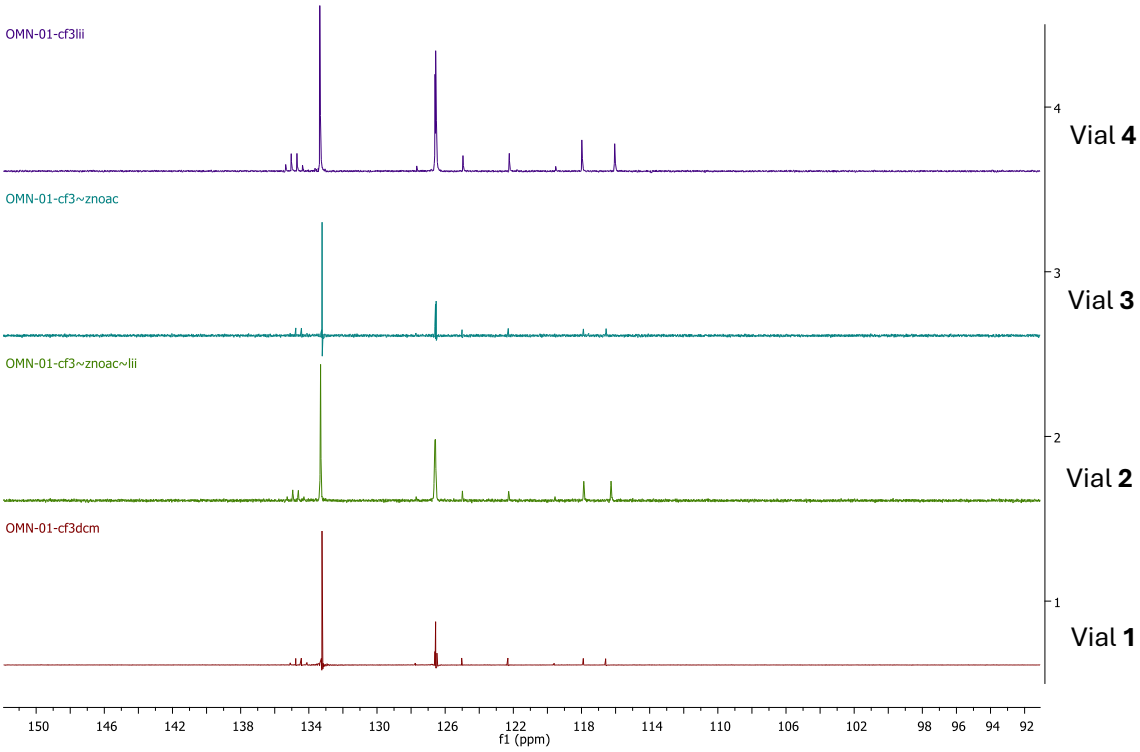

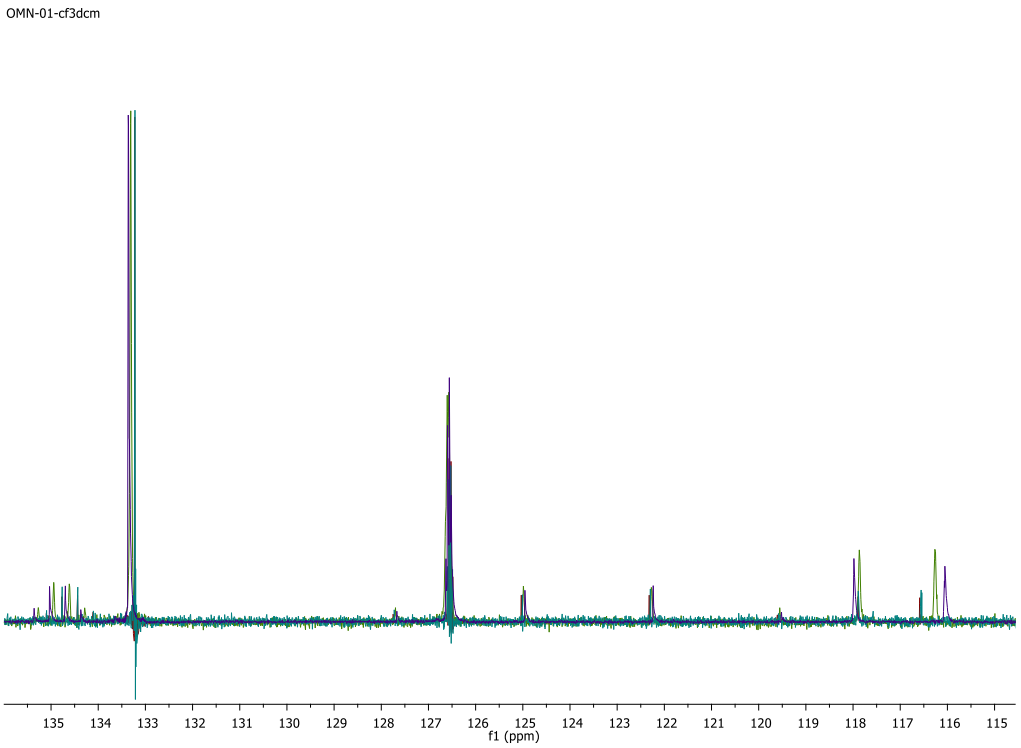

Cyclic Voltammetry Analysis

All the cyclic voltammetry experiments were performed in a batch setup. The analysis was performed with a PalmSens EmStat3+ instrument equipped with a glassy carbon working electrode (3 mm), a platinum wire counter electrode, and a SCE reference electrode. All measurements were carried out at the analyte concentration of 0.06 M in anhydrous MeCN in the presence of an electrolyte (Me_4NPF_6, 0.06M) and with a scan rate of 100 mV/s.

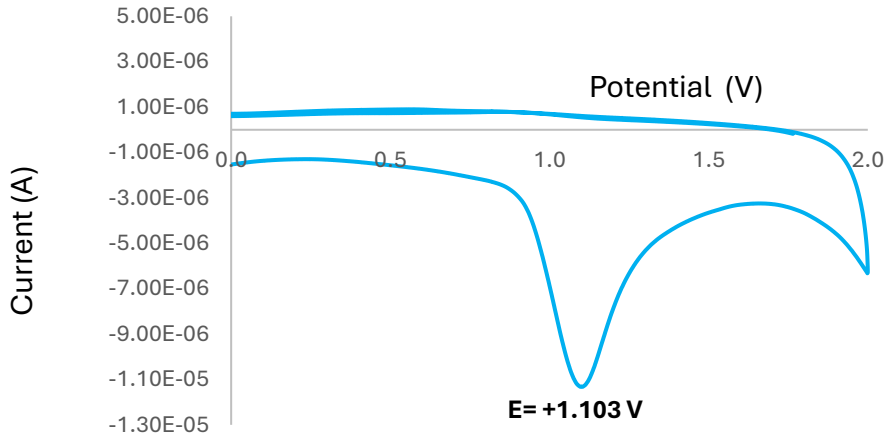

Figure 2. Cyclic voltammetry of **CuP4** in MeCN

Right: from 0.0 V to +2.0 V.

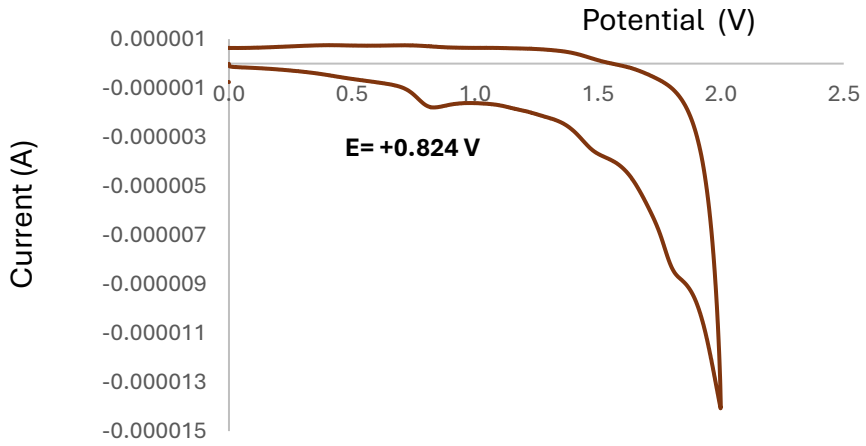

Figure 3. Cyclic voltammetry of **CuP2** in MeCN

Right: from 0.0 V to +2.5 V.

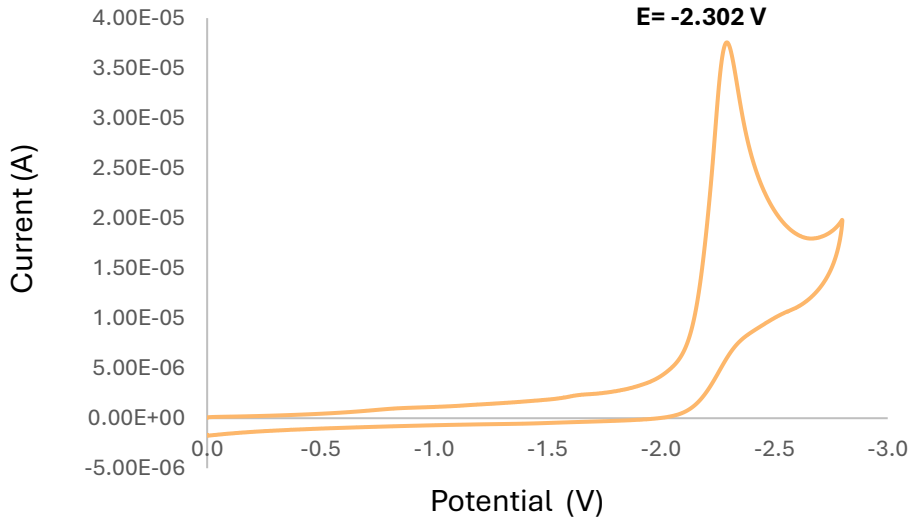

Figure 4. Cyclic voltammetry of LiI in MeCN

Right: from 0.0 V to -3.0 V.

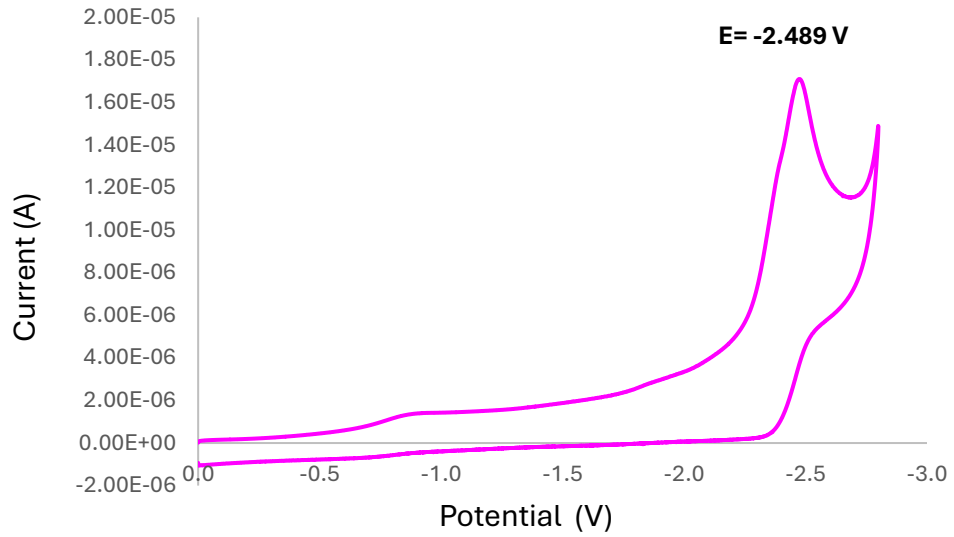

Figure 5. Cyclic voltammetry of $Zn(OAc)_2$ in MeCN

Right: from 0.0 V to -3.0 V.

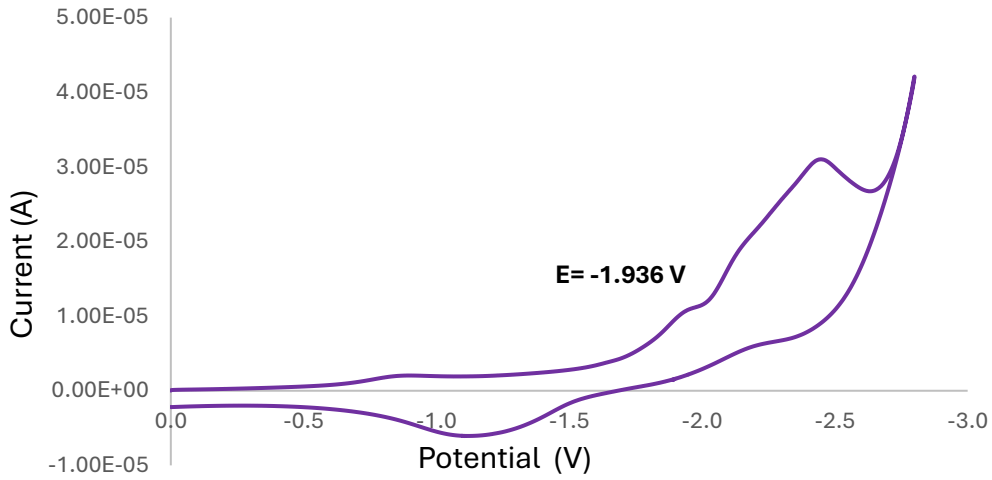

Figure 6. Cyclic voltammetry of $LiI+Zn(OAc)_2$ in MeCN

Right: from 0.0 V to -3.0 V.

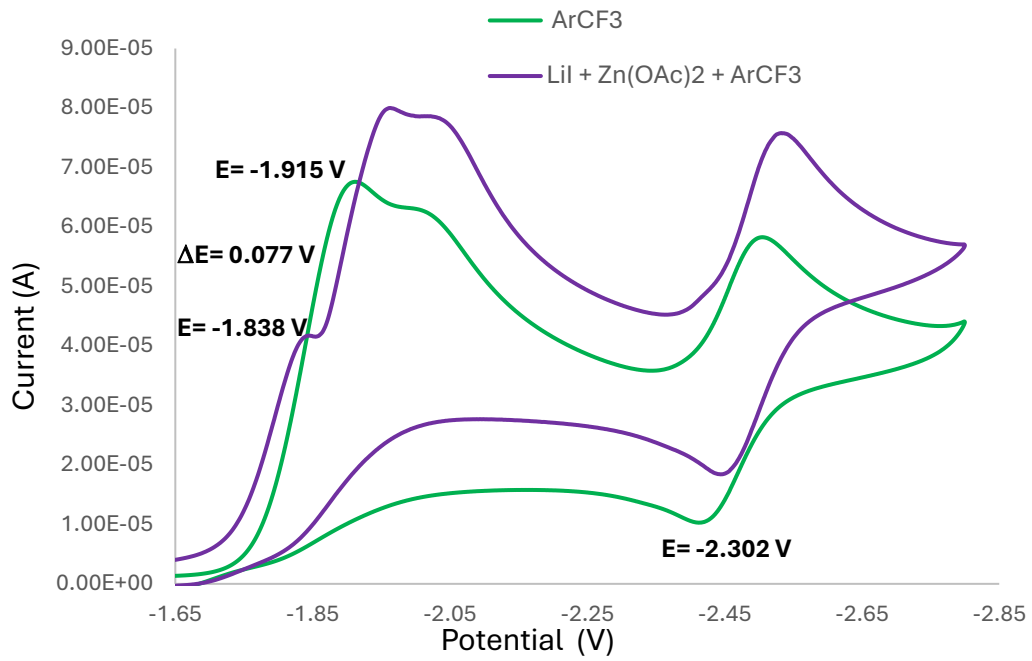

Figure 7. Cyclic voltammetry of **1a** and **1a** +LiI+ $Zn(OAc)_2$ in MeCN

Right: from 0.0 V to -3.0 V.

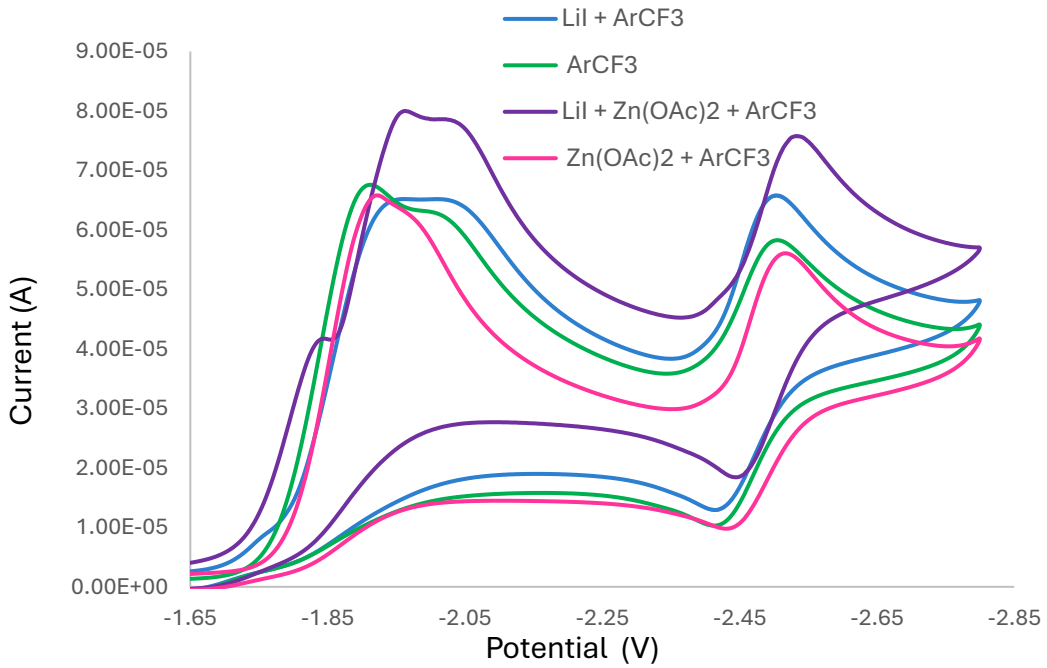

Figure 8. Cyclic voltammetry of **1a** with various additives in MeCN.

Right: from 0.0 V to -3.0 V.

UV-vis Absorption Spectroscopic Measurements

Addition of various reaction components to CuP2

Solutions containing 1.1 mM of each components were prepared in DCE and measured, except for CuI and dppbz, which were both at 0.11 mM. It was found that the mixture of **CuP2** + $Zn(OAc)_2$ + LiI gave apparent increase of absorption band corresponding to the emission wavelength of the applied light source (390 nm).

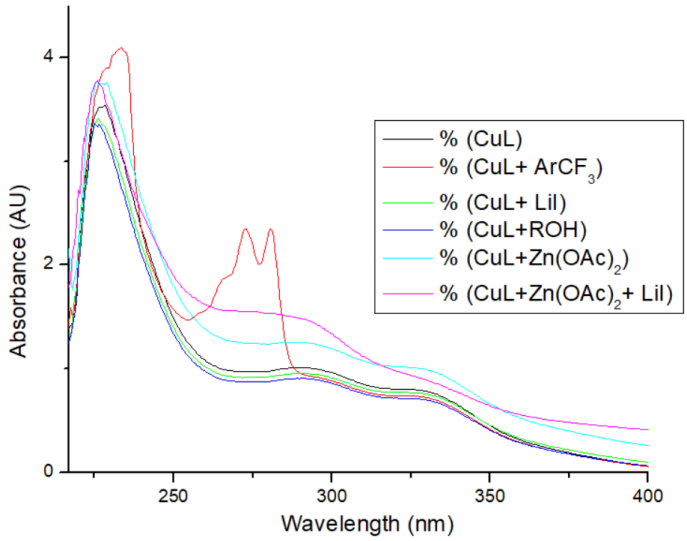

Figure 9. UV-vis spectroscopic absorption of **CuP2** with the various reaction components

Addition of $ArCF_3$ 1a to CuP4

The UV-absorption experiments were carried out with 2 x 10^{-4} M of **CuP4** in DCE along with various concentrations of **1a** in DCE. No apparent changes could be observed so the EDA formation between **CuP4** and **1a** is not plausible.

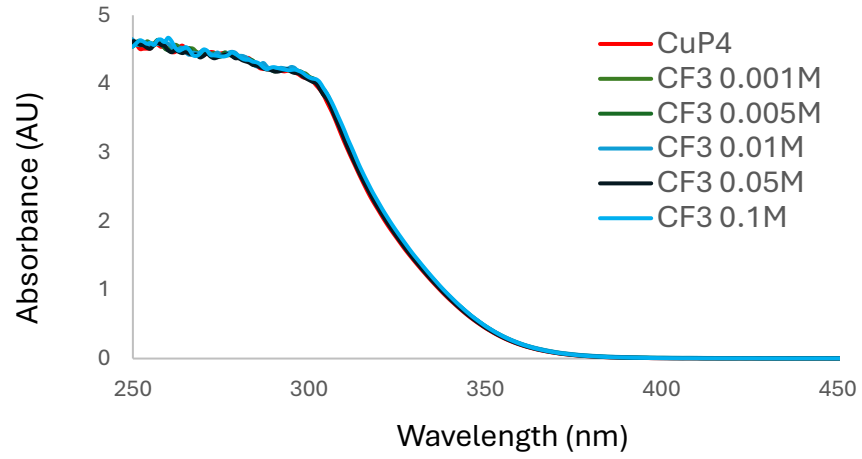

Figure 10. UV-vis spectroscopic absorption of **CuP4** with the different concentration of **1a**

Addition of tetrabutylammonium iodide (TBAI) to CuP4

The UV-absorption experiments were carried out with 2 x 10^{-4} M of (**CuP4**) in DCE along with various concentrations of TBAI.

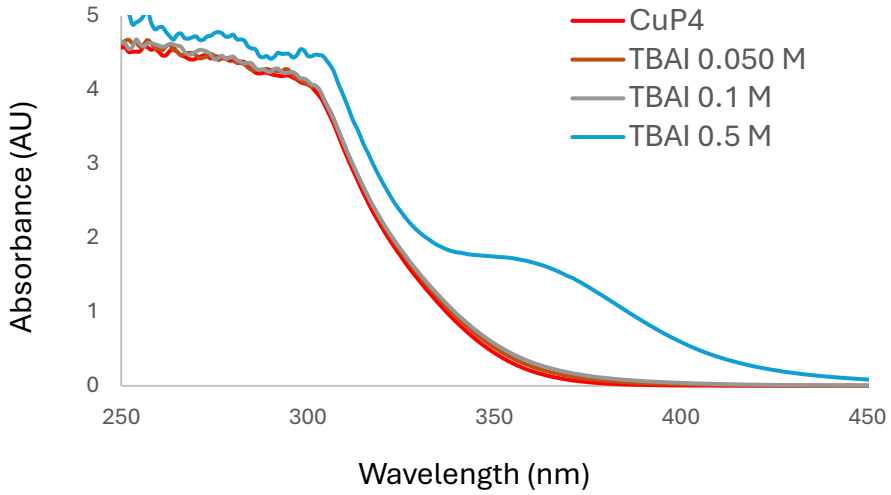

Figure 11. UV-vis spectroscopic absorption of **CuP4** with the different concentration of TBAI

Light On/off Experiment

In a nitrogen-filled glovebox, a catalyst solution was prepared in a 1-ml vial by vigorously stirring CuI (1.0 mg, 0.005 mmol, 0.10 equiv) and dppbz (1.8 mg, 0.004 mmol, 0.08 equiv) in DCE (0.3

mL) for 60 min. $Zn(OAc)_2$ (9.17 mg, 0.05 mmol, 1.00 equiv) and LiI (13.39 mg, 0.10 mmol, 2.00 equiv) were added to a 3-mL tube, followed by the addition of a stir bar and DCE (1 mL). The mixture was stirred for 30 min, and then $ArCF_3$ **1a** (0.05 mmol, 1.00 equiv), alcohol **2a** (1.25 mmol, 25.00 equiv) and the standard (trifluoromethoxy)benzene (0.1 mmol, 2.00 equiv) were added. The catalyst solution was added to the reaction mixture. The vial was rinsed with DCE (0.2 ml), and the rinse was transferred to the reaction mixture. The tube was sealed with a PTFE-lined septum cap removed from the glovebox. The tube was placed in a PhotoRedOx Box (HepatoChem) equipped with one 52 W 390-nm Kessil LED lamp. The mixture was virgously stirred with 30-min irradiation/dark intervals for 6 h. The tube was brought into the glovebox for sampling, and the progress was monitored by ^{19}F-NMR. It was found that the generation of product **3a** halted in the absence of light.

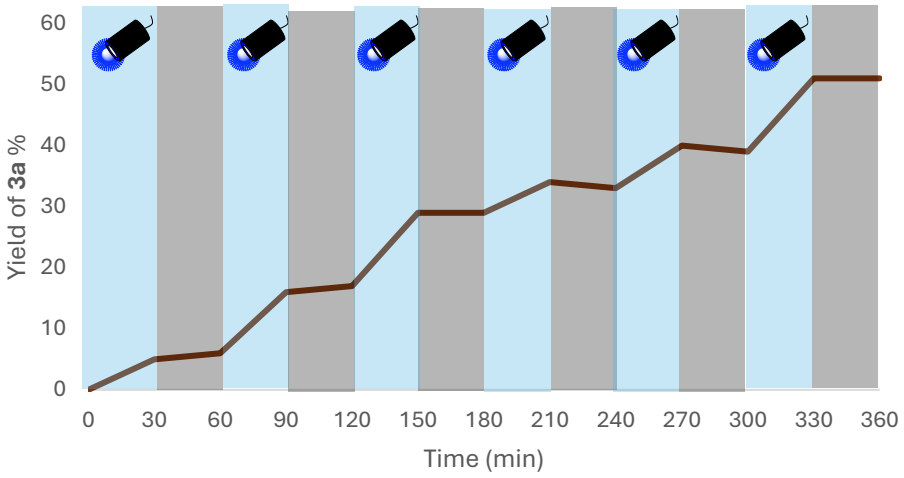

Figure 12. Light on/off experiment

Fluorescence Quenching Experiments

Fluorescence quenching experiment of CuP4

The experiments were carried out with 2 x 10^{-4} M of **CuP4** in DCE at 25°C. The excitation wavelength was 390 nm, and the emission intensity was monitored at 552 nm. The concentration of of quencher **1a** in DCE are shown in the table. Based on the below data, the photoexcited **CuP4** can be quenched by **1a**.

λ = 552 nm		
I	**1a** conc (M)	I_0/I
2271 (I_0)	0	1.00
1425	0.0008	1.59
1063	0.0014	2.14
817	0.0042	2.78
413	0.0100	5.49
306	0.0150	7.42
270	0.0200	8.41

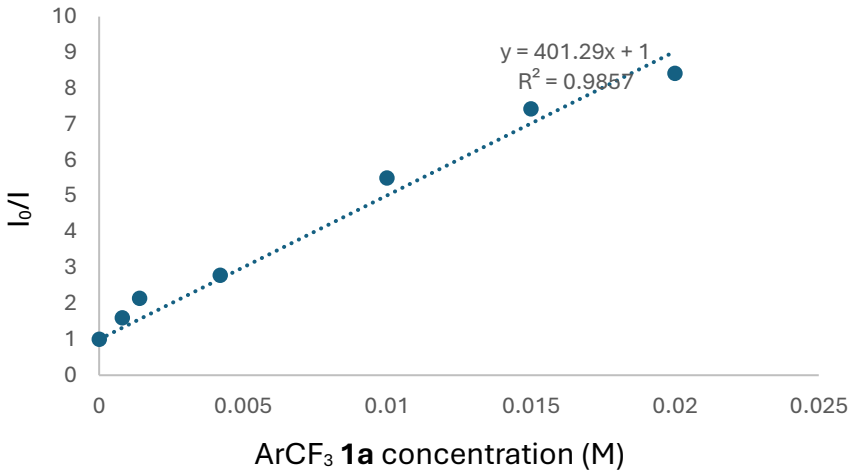

Figure 13. Fluorescence quenching experiment of **CuP4** with different concentration of **1a.**

The experiments were carried out with 2 x 10^{-4} M of **CuP4** in DCE at 25ºC. The excitation wavelength was 390 nm, and the emission intensity was monitored at 550 nm. The concentrations of quencher TBAI in DCE are shown in the table. Based on the below data, a combination of dynamic and static quenching may occur with TBAI

λ = 550 nm		
I	TBAI conc (M)	I_0/I
1564 (I_0)	0	1.00
1127	0.01	1.39

918	0.02	1.70
622	0.10	2.51
95	0.20	16.43

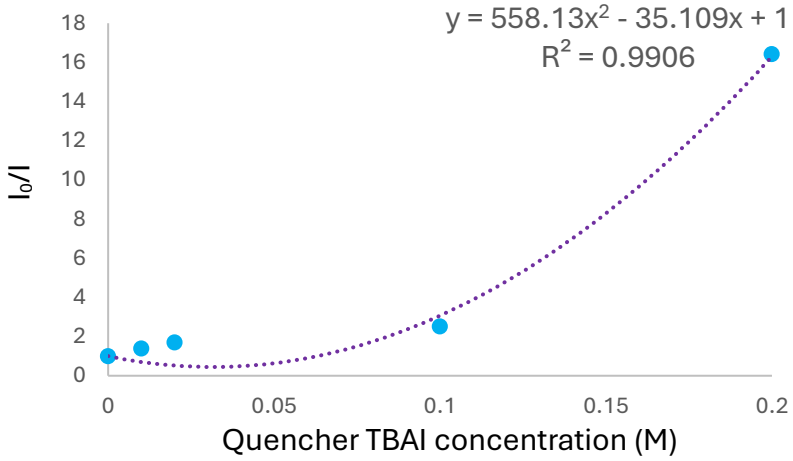

Figure 14. Luminescence quenching experiment of **CuP4** with different concentration of TBAI

Fluorescence quenching experiment of CuP2

The experiments were carried out with 2 x 10^{-4} M of **CuP2** in DCE at 25ºC. The excitation wavelength was 390 nm, and the emission intensity was monitored at 537 nm. The concentration of of quencher **1a** in DCE are shown in the table. Based on the below data, the photoexcited **CuP2** can be quenched by **1a**.

λ = 537 nm		
I	**1a** conc (M)	I_0/I
7459 (I_0)	0	1.00
6641	0.0025	1.12
5459	0.0050	1.37
2826	0.0100	2.64
2466	0.0150	3.02
1769	0.0200	4.22
1331	0.0300	5.60

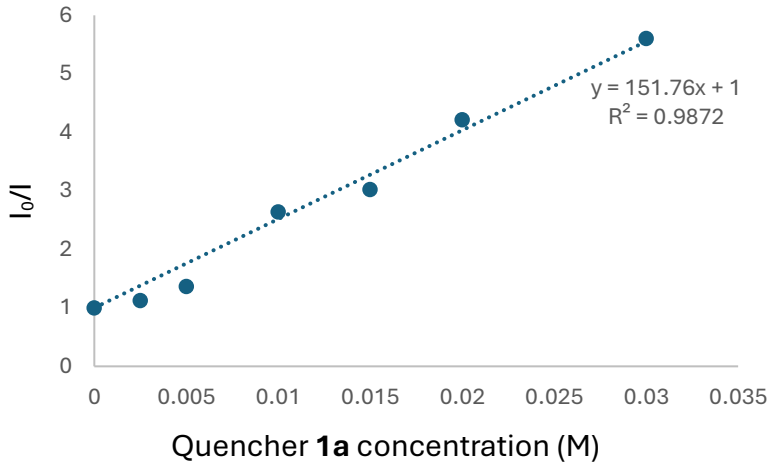

Figure 15. Fluorescence quenching experiment of **CuP2** with different concentration of **1a**

The experiments were carried out with 2 x 10^{-4} M of **CuP2** in DCE at 25 ºC. The excitation wavelength was 390 nm, and the emission intensity was monitored at 536 nm. The concentrations of quencher TBAI in DCE are shown in the table. Based on the below data, a combination of dynamic and static quenching may occur with TBAI.

λ = 536 nm		
I	TBAI conc (M)	I_0/I
7044 (I_0)	0	1.00
5649	0.0025	1.25
4460	0.0050	1.58
2048	0.0100	3.44
1230	0.0150	5.73
515.2	0.0200	13.67

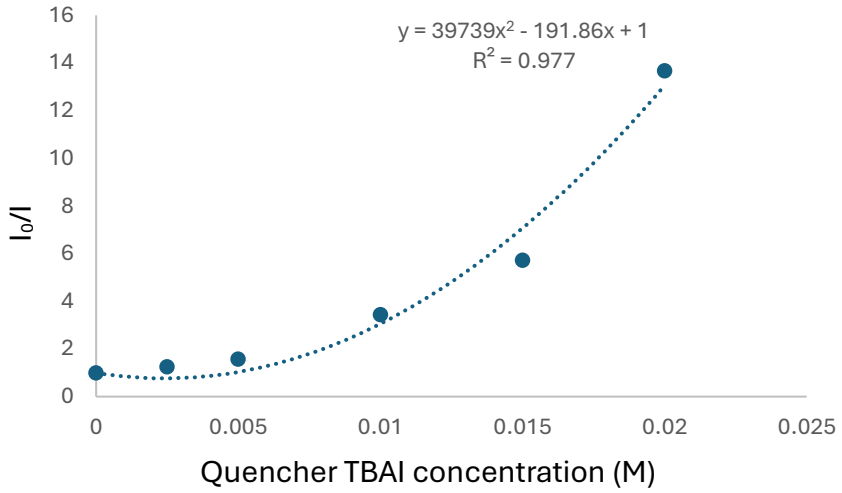

Figure 16. Luminescence quenching experiment of **CuP2** with different concentration of TBAI

^{31}P NMR Studies

In a nitrogen filled glovebox, 10-ml vials containing various reaction components were prepared as described in the table below. All vials were sealed with a rubber cap, and the mixture was stirred for 30 min. The vial **9** and **13** were removed from the glovebox, and the mixture was irradiated under 390 nm LED (40 W × 2) for 3 h at room temperature with virgous stirring. ^{31}P NMR studies were carried out for all the samples.

Vial No.	Components
1	1 equiv dppbz
2	1 equiv CuI + 1 equiv dppbz
3	1 equiv CuI + 1 equiv dppbz + 5 equiv **2a**
4	1 equiv CuI + 1 equiv dppbz + 5 equiv **1a**
5	1 equiv CuI + 1 equiv dppbz + 5 equiv $Zn(OAc)_2$
6	1 equiv CuI + 1 equiv dppbz + 5 equiv LiI
7	1 equiv CuI +1 equiv dppbz +5 equiv LiI+5 equiv $Zn(OAc)_2$
8	1 equiv CuI + 1 equiv dppbz + 5 equiv LiI+ 5 equiv $Zn(OAc)_2$+ 5 equiv **1a**+ 5 equiv **2a**
9	0.20 equiv CuI + 0.16 equiv dppbz + 2 equiv LiI+ 1 equiv $Zn(OAc)_2$+ 1 equiv **1a**+ 25 equiv **2a** (390nm)

10	1 equiv CuI + 1 equiv dppbz + 5 equiv LiOAc
11	1 equiv CuI + 1 equiv dppbz + 5 equiv ZnI_2
12	1 equiv CuI + 1 equiv dppbz + 5 equiv ZnI_2+ 5 equiv LiOAc
13	1 equiv CuI + 1 equiv dppbz + 5 equiv $Zn(OAc)_2$+ 25 equiv **2a** (390nm)

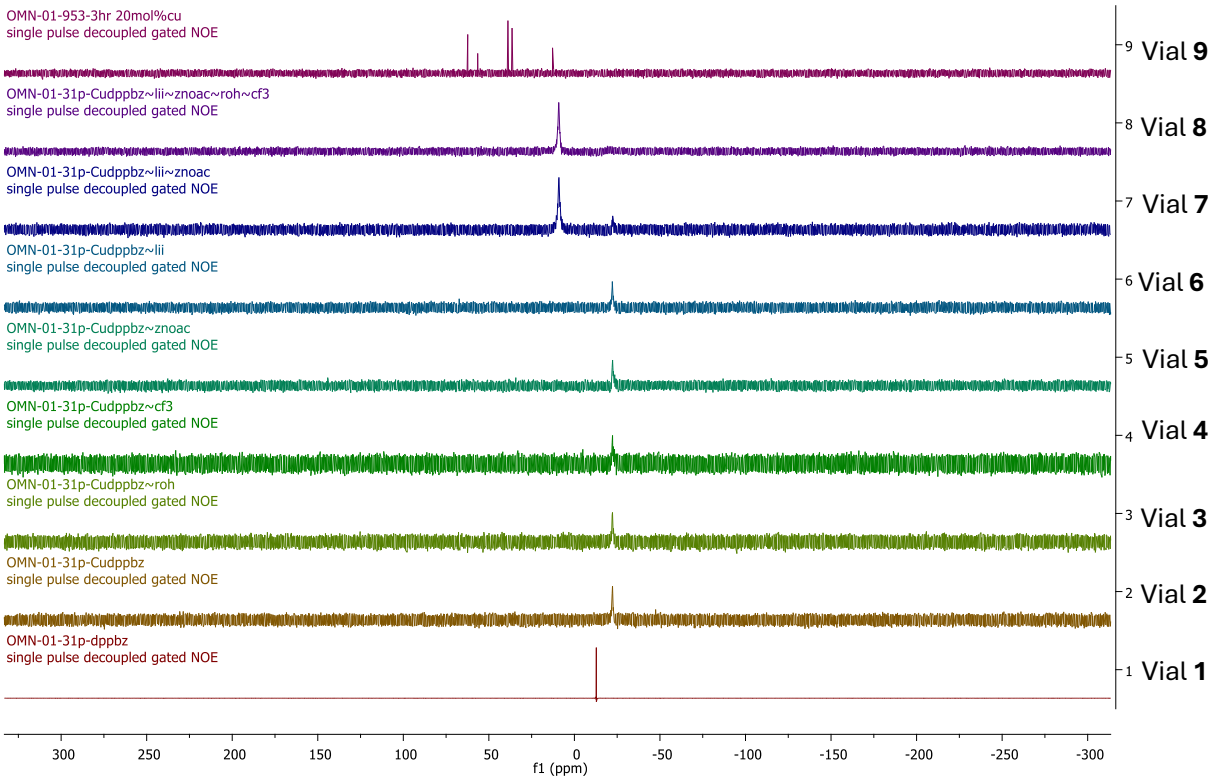

Figure 17. ^{31}P NMR study for vial **1-9**

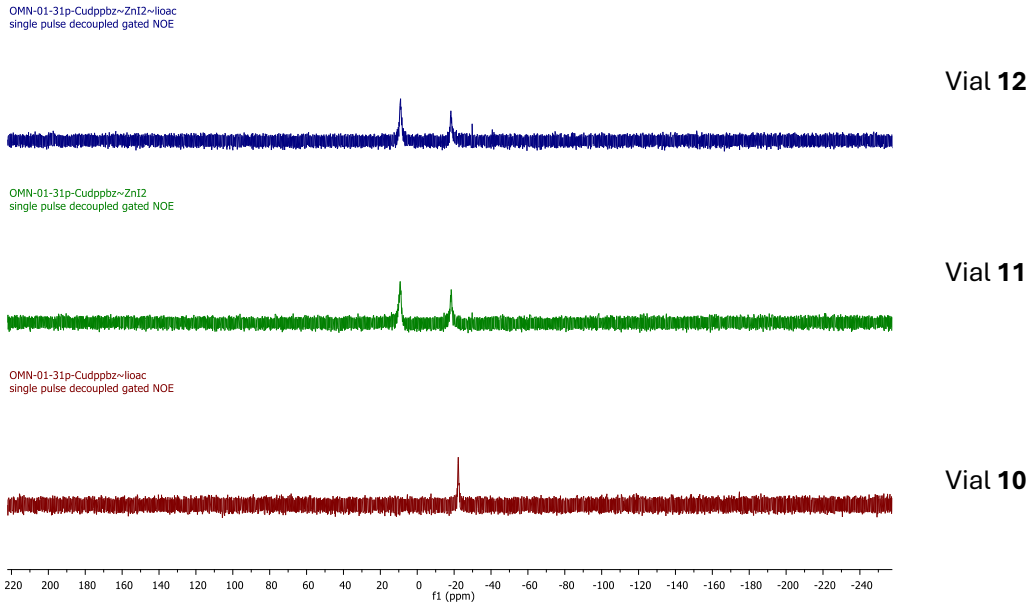

Figure 18. ^{31}P NMR study for vial **10-12**

Observataion of copper alkoxide complex 5

Vial **13**: In a nitrogen-filled glovebox, an oven-dried 9-mL flask equipped with a magnetic stir bar was charged with CuI (19.3 mg, 0.1 mmol, 1.0 equiv), dppbz (48.6 mg, 0.1 mmol, 1.0 equiv), and DCE (3 mL). The reaction mixture was then stirred at rt for 30 min. Then, $Zn(OAc)_2$ (5 equiv) and **2a** (25 equiv) was added to the reaction mixture. The tube was sealed and removed from the glovebox. The reaction mixture was vigorously stirred while irradiated with 390-nm LED lamp for 5 hr at room temperature. ^{31}P NMR and HRMS of this reaction mixture after irradiation was obtained.

HRMS (ESI) *m/z* calculated for $C_{37}H_{38}CuOP_2^+$ ($[M+H]^+$): 623.1688, found: 623.1689.

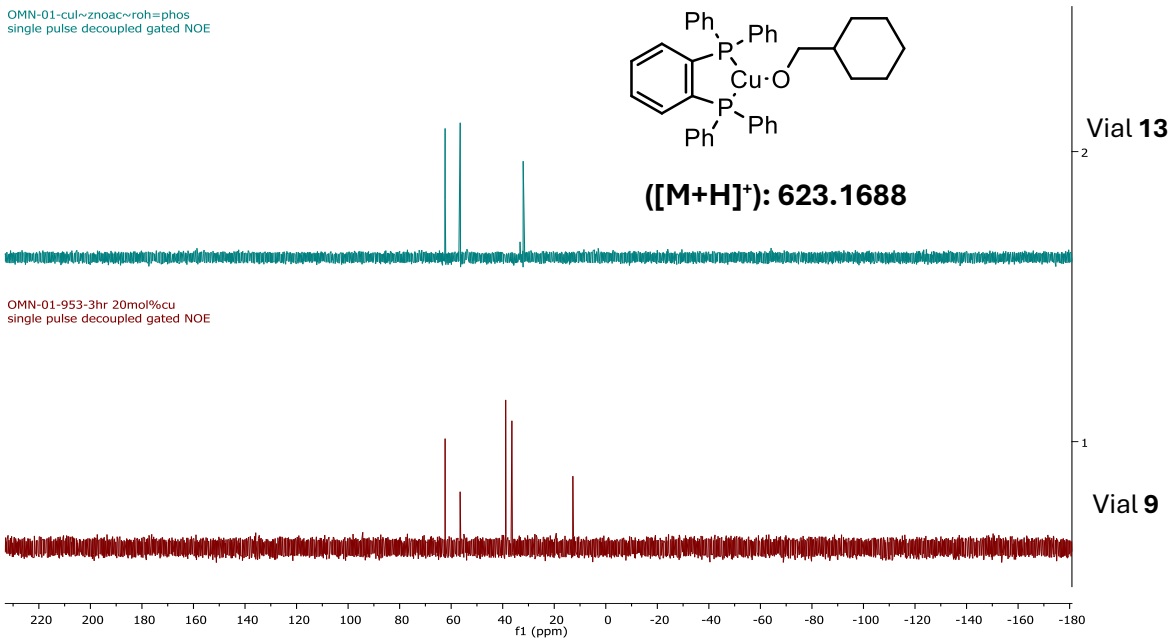

Figure 19. ^{31}P NMR study for vial **9** and **13**

<u>TEMPO Experiment</u>

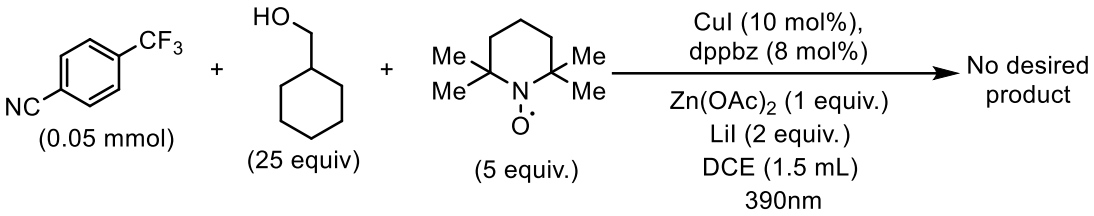

In a nitrogen-filled glovebox, a catalyst solution was prepared in a 3-ml vial by vigorously stirring CuI (1.0 mg, 0.005 mmol, 0.10 equiv) and dppbz (1.8 mg, 0.004 mmol, 0.08 equiv) in DCE (0.3 mL) for 60 min. $Zn(OAc)_2$ (9.2 mg, 0.05 mmol, 1.00 equiv) and LiI (13.4 mg, 0.10 mmol, 2.00 equiv) were added to a 5-mL tube, followed by the addition of a stir bar and DCE (1.0 mL). The mixture was stirred for 30 min, and then $ArCF_3$ **1a** (8.6 mg, 0.05 mmol, 1.00 equiv), alcohol **2a** (0.154 mL, 1.25 mmol, 25.00 equiv), and TEMPO(7.8 mg, 0.25 mmol, 5.0 equiv) were added. The catalyst solution was added to the reaction mixture. The vial was rinsed with DCE (0.2 ml), and the rinse was transferred to the reaction mixture. The tube was sealed with a PTFE-lined septum cap and removed from the glovebox. The tube was placed in a PhotoRedOx Box (HepatoChem) equipped with a 52 W 390-nm Kessil LED lamp, and the reaction mixture was vigorously stirred while irradiated at room temperature for 24 h. Then, (trifluoromethoxy)benzene (0.1 mmol)

standard and $CDCl_3$ were added to the crude reaction mixture. ^{19}F-NMR analysis indicated no formation of the $ArCF_2OR$ product.

Alkene Trapping Experiment

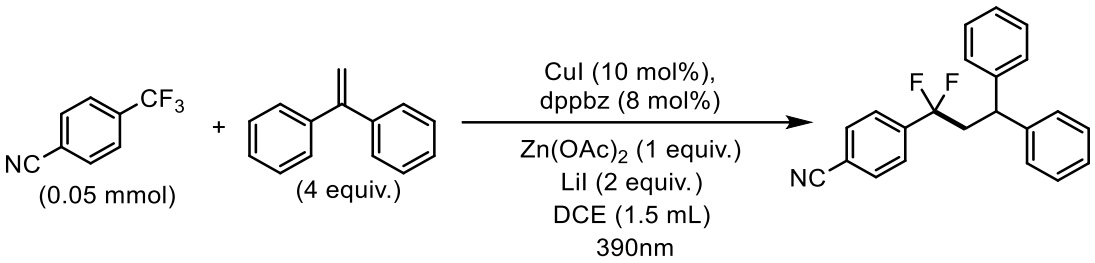

In a nitrogen-filled glovebox, a catalyst solution was prepared in a 3-ml vial by vigorously stirring CuI (1.0 mg, 0.005 mmol, 0.10 equiv) and dppbz (0.004 mmol, 0.08 equiv) in DCE (0.3 mL) for 60 min. $Zn(OAc)_2$ (0.05 mmol, 1.00 equiv) and LiI (0.10 mmol, 2.00 equiv) were added to a 5-mL tube, followed by the addition of a stir bar and DCE (1.0 mL). The mixture was stirred for 30 min, and then $ArCF_3$ **1a** (8.6 mg, 0.05 mmol, 1.00 equiv) and 1,1-Diphenylethylene (0.0353 mL, 0.20 mmol, 4.0 equiv) were added. The catalyst solution was added to the reaction mixture. The vial was rinsed with DCE (0.2 ml), and the rinse transferred to the reaction mixture. The tube was sealed with a PTFE-lined septum cap and removed from the glovebox. The tube was placed in a PhotoRedOx Box equipped with a 52 W 390-nm Kessil LED lamp, and the reaction mixture was vigorously stirred while irradiated at room temperature for 24 h. Then, (trifluoromethoxy)benzene (0.1 mmol) and $CDCl_3$ were added to the crude reaction mixture, which was subjected to ^{19}F NMR analysis (4% yield)

^{19}F NMR (376 MHz, $CDCl_3$) δ (ppm) -94.15 (t, J = 15.9Hz).

HRMS (EI) *m/z* calculated for $C_{23}H_{17}F_2N^+$ ($[M]^+$):333.1329, found: 333.1323.

Role of Alcohol

In a nitrogen-filled glovebox, a catalyst solution was prepared in a 3-ml vial by vigorously stirring CuI (1.0 mg, 0.005 mmol, 0.10 equiv) and dppbz (1.8 mg, 0.004 mmol, 0.08 equiv) in DCE (0.3 mL) for 60 min.

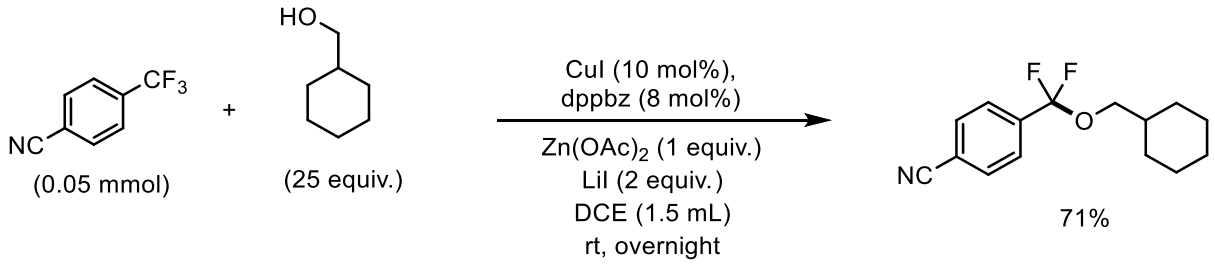

In the first 5-mL tube, $Zn(OAc)_2$ (9.2 mg, 0.05 mmol, 1.00 equiv) and LiI (13.4 mg, 0.10 mmol, 2.00 equiv) were added, followed by the addition of a stir bar and DCE (1.0 mL). The mixture was stirred for 30 min, and then $ArCF_3$ **1a** (0.05 mmol, 1.00 equiv) and alcohol **2a** (1.25 mmol, 25.00 equiv) were added. The catalyst solution was added to the reaction mixture. The vial was washed with DCE (0.2 ml), and the rinse was transferred to the reaction mixture.

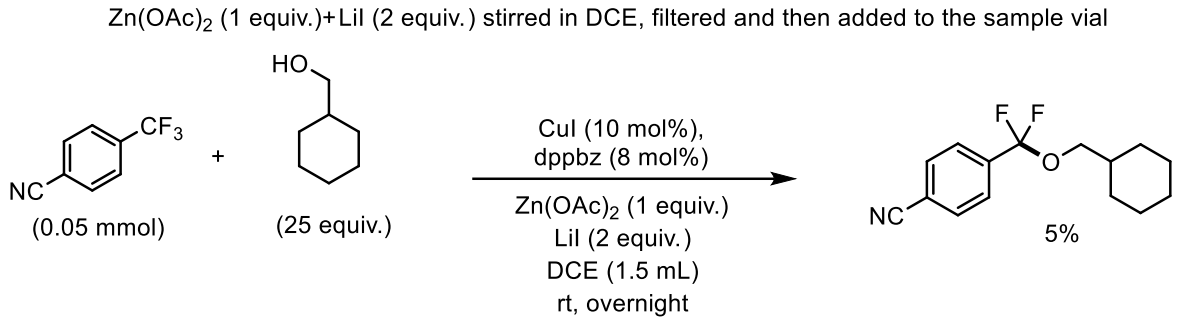

In the second 5-mL tube, the mixture of $Zn(OAc)_2$ (9.2 mg, 0.05 mmol, 1.00 equiv) and LiI (13.4 mg, 0.10 mmol, 2.00 equiv) in DCE (1.0 mL) was filtered after stirring. Then, $ArCF_3$ **1a** (0.05 mmol, 1.00 equiv) and alcohol **2a** (1.25 mmol, 25.00 equiv) were added . The catalyst solution was added to the reaction mixture. The vial was rinsed with DCE (0.2 ml), and the rinse was transferred to the reaction mixture.

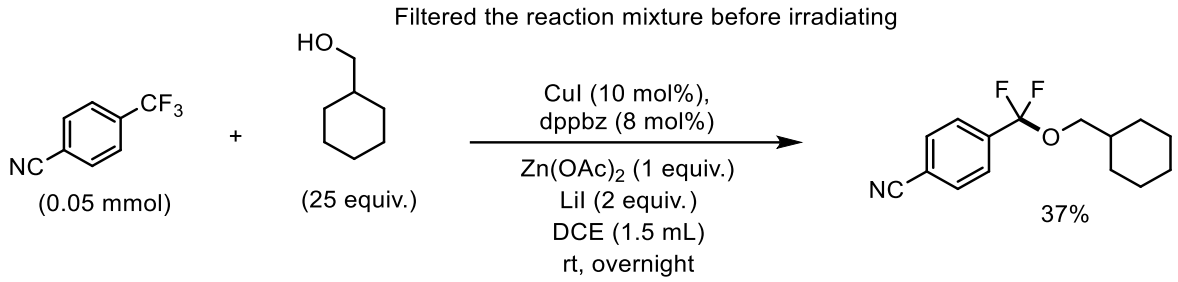

In the third 5-mL tube, all the reaction components were added in a similar way as the first tube. This reaction mixture was then filtered. All the tubes was sealed with a PTFE-lined septum cap

and removed the glovebox. The tubes were placed in a PhotoRedOx Box (HepatoChem) with a 52 W 390 nm Kessil LED lamp, and the reaction mixtures were vigorously stirred while irradiated at room temperature for 24 h. Then, (trifluoromethoxy)benzene (0.1 mmol) and $CDCl_3$ were added to the crude reaction mixture, which was subjected to ^{19}F NMR analysis.

Studies of $ArCF_2I$

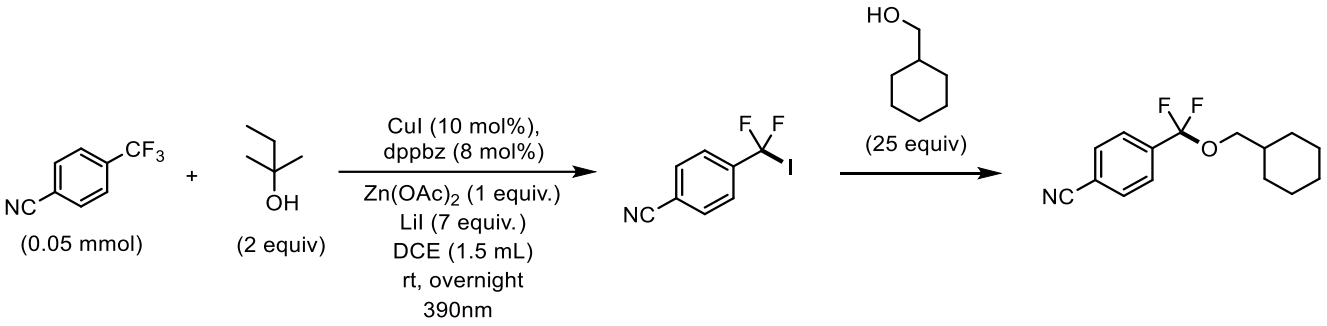

In a nitrogen-filled glovebox, a catalyst solution was prepared in a 9-ml vial by vigorously stirring CuI (4.8 mg, 0.025 mmol, 0.10 equiv) and dppbz (8.9 mg, 0.020 mmol, 0.08 equiv) in DCE (1.5 mL) for 60 min. $Zn(OAc)_2$ (45.9 mg, 0.25 mmol, 1.00 equiv), LiI (234.2 mg, 1.75 mmol, 7.00 equiv), $ArCF_3$ **1a** (0.25 mmol, 1.00 equiv), and *t*AmOH (0.054 mL, 0.50 mmol, 2equiv) were added, followed by the addition of a stir bar and DCE (5 mL). The catalyst solution was added to the reaction mixture. The vial was rinsed with DCE (0.5 ml), and the rinse was transferred to the reaction mixture. The tube was sealed with a PTFE-lined septum cap and removed from the glovebox. The tube was placed at ~5 cm from two 52 W 390-nm Kessil LED lamps, and the reaction mixture was virgously stirred while irradiated at room temperature for 24 h. Then, the tube was brought into the glovebox, and the mixture was filtered. The filtrate was evenly divided into sixvials, and each reaction mixture was prepared and allowed to react for 24 h according to the below table. Then, (trifluoromethoxy)benzene (0.1 mmol) as the standard and $CDCl_3$ were added to the crude reaction mixture, which was subjected to ^{19}F NMR analysis.

Vial	Components	Yield (%)
1	1.5 mL reaction mixture+ 25 equiv **2a**	0
2	1.5 mL reaction mixture+ 25 equiv **2a** + 390 nm	0
3	1.5 mL reaction mixture+ 25 equiv **2a**+ **CuP2**	0

4	1.5 mL reaction mixture+ 25 equiv **2a**+ **CuP2**+ 390 nm	0
5	1.5 mL reaction mixture+ 25 equiv **2a**+ **CuP2**+ 1.0 equiv $Zn(OAc)_2$	0
6	1.5 mL reaction mixture+ 25 equiv **2a**+ **CuP2**+ 1.0 equiv $Zn(OAc)_2$+ 390 nm	53

Light Intensity Screening

In a nitrogen-filled glovebox, a catalyst solution was prepared in a 3-ml vial by vigorously stirring CuI (1.0 mg, 0.005 mmol, 0.10 equiv) and dppbz (1.8 mg, 0.004 mmol, 0.08 equiv) in DCE (0.3 mL) for 60 min. $Zn(OAc)_2$ (9.2 mg, 0.05 mmol, 1.00 equiv) and LiI (13.4 mg, 0.10 mmol, 2.00 equiv) were added, followed by the addition of a stir bar and DCE (1.0 mL). The mixture was stirred for 30 min, and then $ArCF_3$ **1a** (0.05 mmol, 1.00 equiv) and alcohol **2a** (1.25 mmol, 25.00 equiv) were added. Then, (trifluoromethoxy)benzene (0.1 mmol) as the standard was added and the reaction mixture after 30 min irradiation with different intensity (25, 50, 75, 100% of full power) was monitored by ^{19}F NMR.

Entry	% Full power	%Yield of **3a** after 30 min	%Yield/min
1	0	0.0	0.000
2	25	4.7	0.157
3	50	7.0	0.233
4	75	8.6	0.287
5	100	13.3	0.443

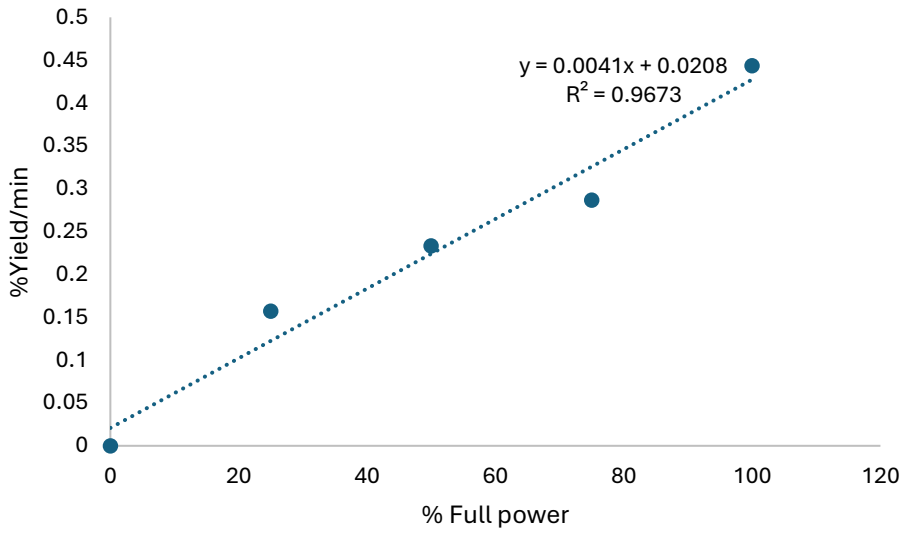

Studies of **3x** for Liquid Crystal Material

Synthesis

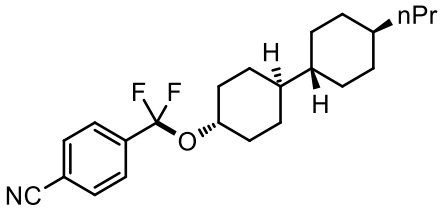

4-(difluoro(((1*r*,1'*s*,4*R*,4'*R*)-4'-propyl-[1,1'-bi(cyclohexan)]-4-yl)oxy)methyl)benzonitrile (3x). Prepared according to the general procedure described in Section 3 (30% of 5% EtOAc/pentane solution in hexane for column chromatography), and the title compound was obtained as a white solid (run 1: 107 mg, 7% ROAc, 28% hexane, 51% yield; ROAc: (1*r*,1'*s*,4*R*,4'*R*)-4'-propyl-[1,1'-bi(cyclohexan)]-4-yl acetate).

^{1}H NMR (400 MHz, $CDCl_3$) δ (ppm) 7.71 (s, 4H), 4.39 – 4.30 (m, 1H), 2.12 (d, J = 9.5 Hz, 2H), 1.84 – 1.66 (m, 8H), 1.51 – 1.39 (m, 2H), 1.35 – 1.25 (m, 3H), 1.19 – 1.09 (m, 8H), , 0.87 (t, J = 8.2, 6.3 Hz, 3H).

^{13}C NMR (101 MHz, $CDCl_3$) δ (ppm) 139.35 (t, J = 34.2 Hz), 132.35, 126.54 (t, J = 3.4 Hz), 122.16 (t, J = 253.4 Hz), 118.25, 114.47 (t, J = 1.3 Hz), 75.79 (t, J = 4.5 Hz), 42.85, 42.16, 39.90, 37.66, 33.74, 33.63, 30.31, 28.24, 20.17, 14.56.

^{19}F NMR (376 MHz, $CDCl_3$) δ (ppm) -66.33.

HRMS (ESI) *m/z* calculated for $C_{23}H_{31}F_2NNaO^+$ ($[M+Na]^+$): 398.2266, found: 398.2261.

Single crystal for X-ray analysis

3x obtained after column chromatography was mixed with 1.5 mL pentane, and the mixture was sonicated for 10 min. The resulting mixture was allowed to settle, and *ca.* 1.0 ml supernatant was transferred to another vial. A single crystal suitable for X-ray analysis was obtained by slow evaporation of pentane.

Table 16. The crystal data parameters obtained by single crystal XRD of 3x

Crystal name (CCDC #)	**3x** (2382839)
Empirical formula	$C_{23}H_{31}F_2NO$
Formula weight	375.49
Temperature/K	293
Crystal system	triclinic
Space group	*P*-1
a/Å	8.8140(2)
b/Å	10.2633(2)
c/Å	12.5161(2)
α/°	89.4310(10)
β/°	79.6300(10)
γ/°	74.918(2)
Volume/Å^3	1074.55(4)
Z	2
ρ_{calc}g/cm^3	1.161
μ/mm^{-1}	0.663
F(000)	404
Crystal size/mm^3	0.3 × 0.3 × 0.05
Radiation	Cu Kα (λ = 1.54184)
2Θ range for data collection/°	7.186 to 152.32
Reflections collected	38405
Independent reflections	4294 [R_{int} = 0.0425]
Data/restraints/parameters	4294/2/265
Goodness-of-fit on F^2	1.1

Final R indexes [I>=2σ (I)]	R_1 = 0.0697, wR_2 = 0.2256
Final R indexes [all data]	R_1 = 0.0788, wR_2 = 0.2363
Largest diff. peak/hole / e $Å^{-3}$	0.48/-0.30

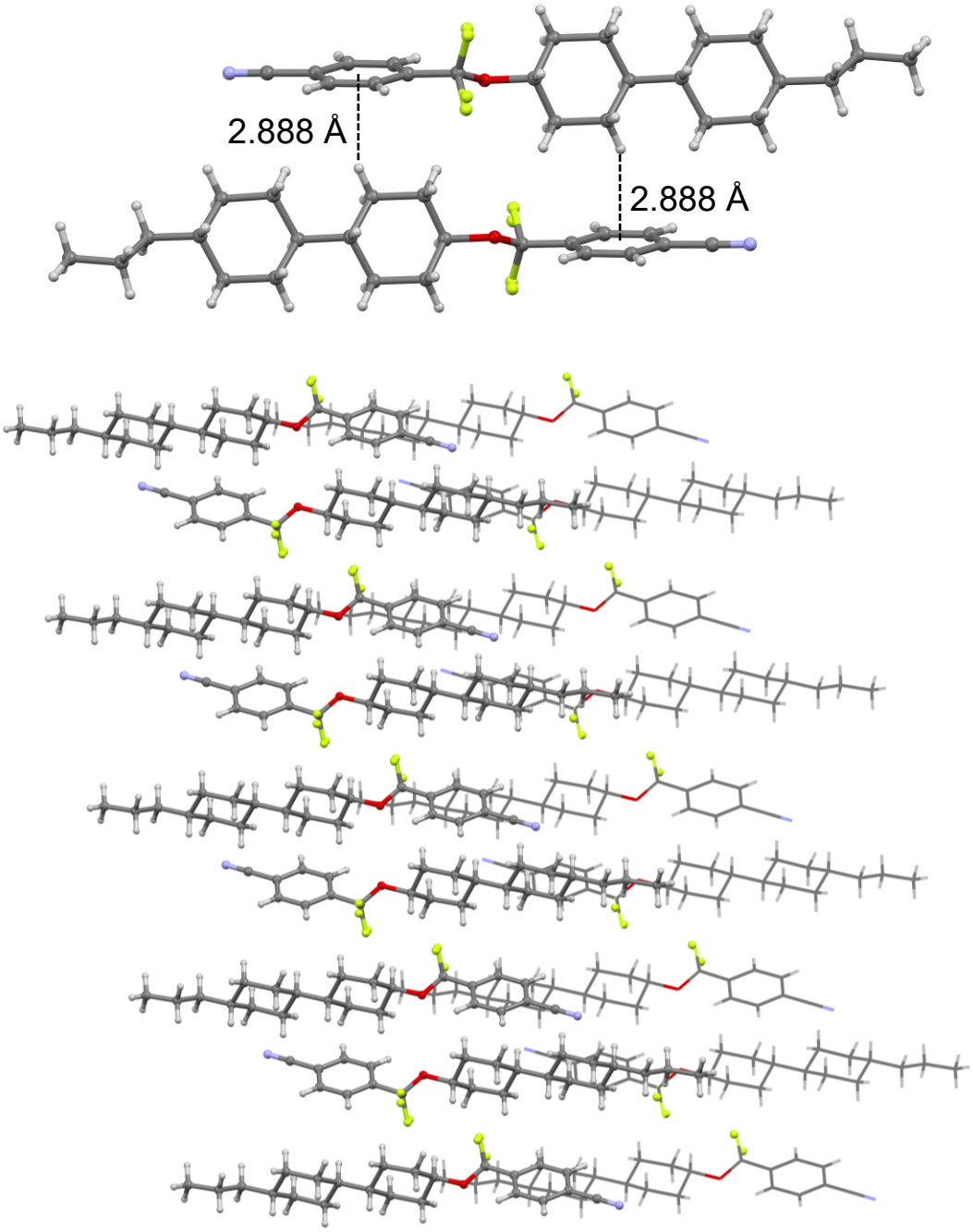

Figure 20. Single crystal structure of **3x** with intermolecular interactions displayed

Cross-polarized microscopy measurement

3x obtained after column chromatography was mixed with 1.5 mL pentane, and the mixture was sonicated for 10 min. The resulting mixture was allowed to settle, and the solution was decanted. The remaining solid was allowed to dry and used for cross-polarized microscopy measurement. Observation of liquid crystal of **3x** was carried out using Olympus BX51 microscopes with Olympus DP72 digital cameras under a cross-polarized light. Powder sample of **3x** was set on a thin glass plate on top of a thermal plate equipped in a chamber of temperature controller (Linkam LNP96). The solid at the room temperature appeared dark under the microscope, which indicates an amorphous solid phase. Upon heating to 140 ºC, bright image with a melted shape was observed, revealing that **3x** exhibits a liquid crystalline phase at this temperature.

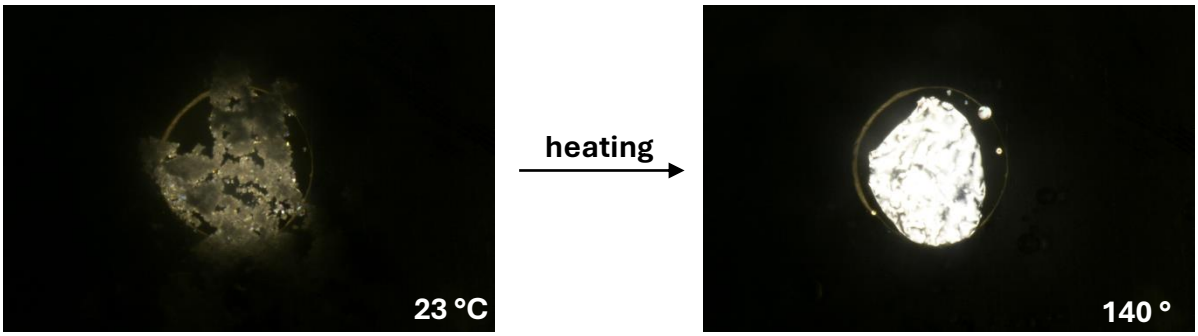

Chapter 3

Homoleptic Copper(I)-bisphosphine Complexes as Photoredox Catalysts

3.1 Introduction

Copper(I) complexes bearing closed-shell d^{10} configuration in the ground state are characterized by its sluggish nonradiative deactivation at the excited state due to their low-lying metal-centered states. They demonstrate high visible light responsiveness and suitable redox properties, enabling their broad use in organic transformations (please refer to Chapter 1 for complete discussions).[59]

Tetracoordinate copper complexes

Among all copper photocatalysts, tetracoordinate copper(I) complexes are the most extensively studied. Two principal categories dominate the field: homoleptic (**CuN4**) complex containing two identical bisimine ligands that surround the copper center and heteroleptic (**CuN2P2**) complexes containing one bisimine ligand and one bisphosphine ligand (Scheme 30).[60]

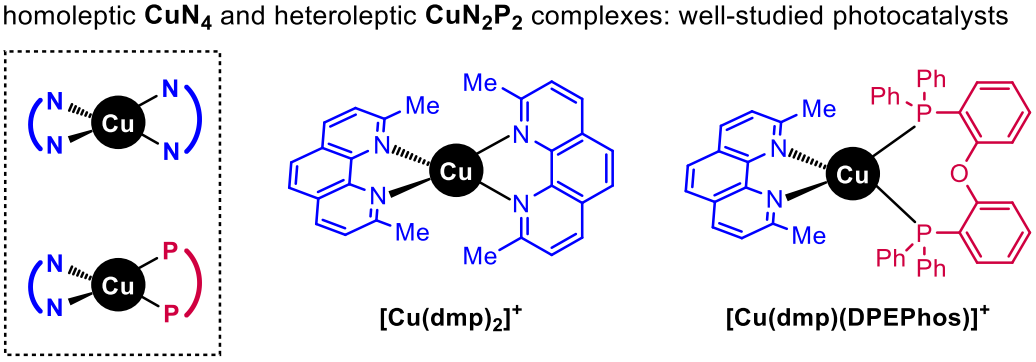

Scheme 30. Tetracoordinate Cu(I) complexes as photocatalysts.

Structural characteristics

The filled d^{10} electronic configuration of Cu(I) favors a pseudo-tetrahedral geometry. The structural adaptability of these complexes is influenced by ligand identity. For instance, the

[59] (a) Hossain, A.; Bhattacharyya, A.; Reiser, O. *Science*, **2019**, *364*, eaav9713. (b) Sandoval-Pauker, C.; Molina-Aguirre, G.; Pinter, B. *Polyhedron*, 2021, **199**, 115105−115127. (c) Beaudelot, J.; Oger, S.; Peruško, S.; Phan, T.-A.; Teunens, T.; Moucheron, C.; Evano, G. *Chem. Rev.*, **2022**, *122*, 16365−16609.

[60] (a) Hernandez-Perez, A. C.; Collins, S. K. *Acc. Chem. Res.,* **2016**, *49*, 1557–1565. (b) Zhang,Y.; Schulz, M.; Wächtler, M.; Karnahl, M.; Dietzek, B. *Coord. Chem. Rev.*, **2018**, *356*, 127–146.

HETPHEN (HETeroleptic PHENanthroline) strategy[61] engages one sterically demanding ligand and another less bulky ligand to stabilize the heteroleptic structures and prevent ligand exchange in solution. This approach also introduces directionality in electron transfer processes, enhancing catalytic efficiency.

Furthermore, the choice of ligands affects the excited-state dynamics. Bulky phosphine ligands with large bite angles can suppress flattening distortions in the excited state, thereby enhancing luminescent properties.[62] Such control over photophysical behavior is crucial for optimizing the performance of copper(I) complexes in photoredox applications (please refer to Chapter 1 for detailed discussion).

Absorption characteristics

These complexes display two main types of absorption bands. The bands in the UV region correspond to intense π–π* ligand-centered (LC) transitions. The bands in the visible region correspond to d–π* metal to ligand charge transfer (MLCT) transitions, particularly significant for photocatalysis.

Excited state properties and structural distortion

In the ^{1}MLCT excited state, the copper(I) ion is oxidized to copper(II) along with the reduction of ligands, generating a d^9 electronic configuration. This configuration is susceptible to a pseudo-Jahn−Teller flattening distortion. This flattening leads to a stabilized $MLCT_{flat}$, which then undergoes decay to regenerate the ground state. This geometrically distorted flattened state is also more susceptible to nucleophilic attack by coordinating solvent molecules, forming more stable excimer species that quench the luminescence.

[61] (a) Kohler, L.; Hayes, D.; Hong, J.; Carter, T. J.; Shelby, M. L.; Fransted, K. A.; Chen, L. X.; Mulfort, K. L. *Dalton Trans.* **2016**, *45*, 9871−9883. (b) Sandroni, M.; Kayanuma, M.; Planchat, A.; Szuwarski, N.; Blart, E.; Pellegrin, Y.; Daniel, C.; Boujtita, M.; Odobel, F. *Dalton Trans.* **2013**, *42*, 10818−10827.

[62] Beaudelot, J.; Oger, S.; Perusko, S.; Phan, T.-A.; Teunens, T.; Moucheron, C.; Evano, G. *Chem. Rev.* **2022**, *122*, 16365−16609.

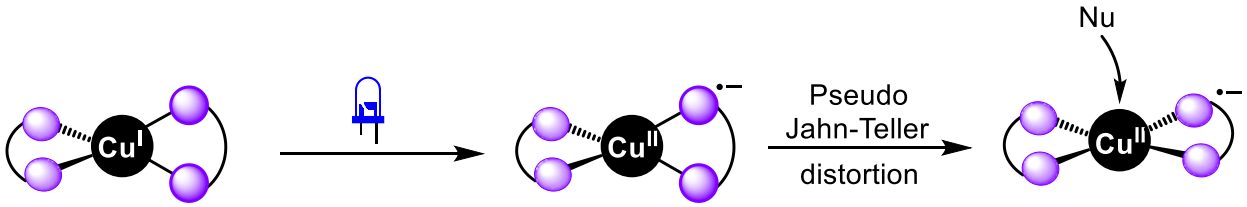

Scheme 31. Schematic representation of the pseudo-Jahn−Teller flattening distortion upon excitation in the MLCT excited state leading to an increased accessibility of the copper center to nucleophiles (Nu).

Intersystem crossing

The heavy atom effect of copper induces spin-orbit coupling, allowing an intersystem crossing (ISC) to occur from ^{1}MLCT to ^{3}MLCT state. However, this coupling is weaker in the flattened geometry, leading to the competition between both pathways: ^{1}MLCT →^{3}MLCT and ^{1}MLCT → ^{1}MLCT$_{flat}$.[63] Both ISC and the flattening distortion occur on ultrafast timescales, ranging from femtosecond to picoseconds. Following the ISC process, the populated ^{3}MLCT excited state also undergoes relaxing to ^{3}MLCT$_{flat}$ state lying below the ^{1}MLCTflat.

If the energy gap between the ^{1}MLCT$_{flat}$ and the ^{3}MLCT$_{flat}$ is smaller ($\Delta E_{S\text{-}T} < 0.37$ eV), the luminescence occurs predominately from ^{1}MLCT$_{flat}$ state through thermally activated delayed fluorescence (TADF).[64] If the $\Delta E_{S\text{-}T}$ is larger, then the observed luminescence mainly relates to the phosphorescence of the complex.

[63] Siddique, Z. A.; Yamamoto, Y.; Ohno, T.; Nozaki, K. *Inorg. Chem.* **2003**, *42*, 6366−6378.
[64] Czerwieniec, R.; Leitl, M. J.; Homeier, H. H. H.; Yersin, H. *Coord. Chem. Rev.* **2016**, *325*, 2−28.

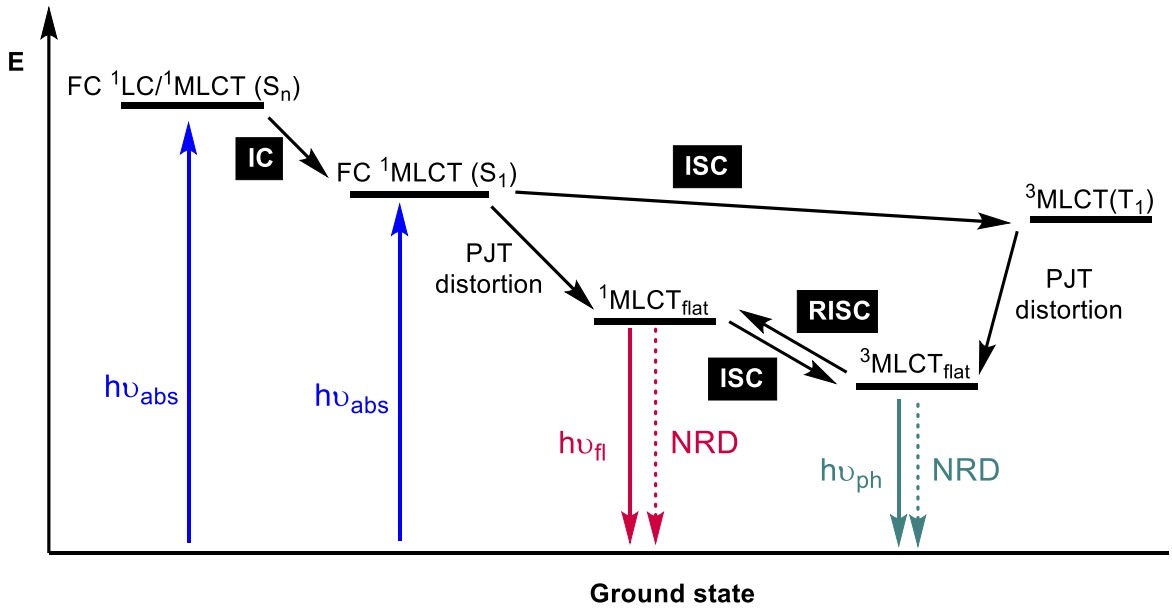

Scheme 32. General photophysical scheme of tetracoordinated copper(I) complexes: internal conversion (IC), intersystem crossing (ISC), Franck-Condon (FC), metal to ligand charge transfer (MLCT), nonradiative deactivation (NRD), pseudo-Jahn-Teller distortion (PJT distortion), reverse intersystem crossing (RISC), absorption (abs), fluorescence (fl), flattened geometry (flat), phosphorescence (ph).

Homolyptic **CuP4** complexes

Compared to homoleptic **CuN4** and heteroleptic **CuN2P2** systems, homoleptic copper-bisphosphine complexes (**CuP4**) have gained less attention. Initial studies on homoleptic **CuP4** complexes focused on their electronic structures and photophysical properties. Vogler and Perez groups studied luminescence properties and photophysical properties of $[Cu(BINAP)_2]^+$, respectively. Ueno, Esposti, Nierengarten and others examined the electronic properties of a homoleptic copper-bisphosphine complex, $Cu(dppbz)_2$, revealing insights into their absorption and emission characteristics. Cano group reported the influence of Xantphos ligands on the coordination effect in their copper(I) complexes. These early investigations highlighted the potential of **CuP4** complexes in photochemical applications but also underscored limitations such as short excited-state lifetimes and susceptibility to nonradiative decay. Further exploration could

lead to the development of cost-effective and efficient alternatives to noble-metal-based photocatalysts in sustainable chemical processes.[65]

CuP4 as photocatalyst

The application of homoleptic **CuP4** complexes as photocatalysts in organic synthesis was not reported until 2022, when the Ngai group introduced the effectiveness of $[Cu(BINAP)_2]^+$ in an olefin carbo-aroylation reaction. This method employs a combination of Cu(IPr)I and *rac*-BINAP ligand, which work cooperatively under visible-light irradiation to promote the reaction.[66] Very recently, our group highlighted the role of $[Cu(dppbz)_2]^+$ complexes in defluorinative C–O coupling reactions. This **CuP4** species acts as a photoredox catalyst, facilitating C–F activation, while a **CuP2** species serves as the cross-coupling catalyst for C–O bond formation (please refer to Chapter 2 for detailed discussion).

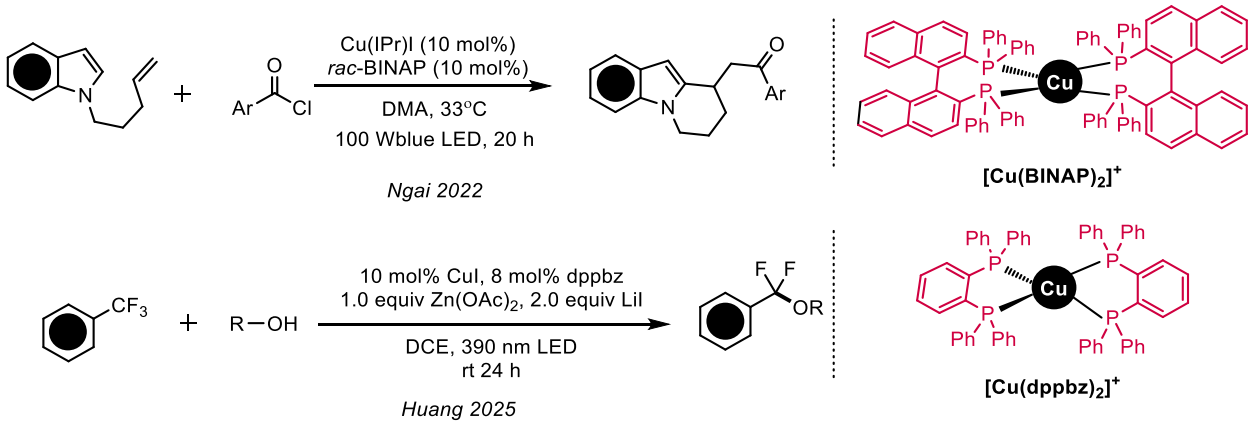

Scheme 33. CuP4 complexes as photocatalysts.

[65] (a) Black, J.; Levason, R. W.; Spicer, M. D.; Webster, M. *J. Chem. Soc. Dalton Trans.* **1993**, *20*, 3129−3134. (b) Szłyk, E.; Kucharek, R.; Szymańska, I.; Pazderski, L. *Polyhedron*, **2003**, *22*, 3389−3393. (c) Tsuboyama, A.; Kuge, K.; Furugori, M.; Okada, S.; Hoshino, M.; Ueno, K. *Inorg. Chem.*, **2007**, *46*, 1992–2001. (d) Venkateswaran, R.; Balakrishna, M. S.; Mobin, S. M.; Tuononen, H. M. *Inorg. Chem.*, **2007**, *46*, 6535–6541. (e) Moudam, O.; Kaeser, A.; Delavaux-Nicot, B.; Duhayon, C.; Holler, M.; Accorsi, G.; Armaroli, N.; Séguy, I.; Navarro, J.; Destruel, P.; Nierengarten, J.-F. *Chem. Commun.*, **2007**, 29, 3077–3079. (f) Kunkely, H.; Pawlowski, V.; Vogler, A. *Inorg. Chem. Commun.*, **2008**, *11*, 1003–1005. (g) Cain, M. F.; Reynolds, S. C.; Anderson, B. J.; Glueck, D. S.; Golen, J. A.; Moore, C. E.; Rheingold, A. L. *Inorg. Chim. Acta*, **2011**, *369*, 55–61. (h) Kaeser, A.; Mohankumar, M.; Mohanraj, J.; Monti, F.; Holler, M.; Cid, J.-J.; Moudam, O.; Nierengarten, I.; Karmazin-Brelot, L.; Duhayon, C.; Delavaux-Nicot, B.; Armaroli, N.; Nierengarten, J.-F. *Inorg. Chem.*, **2013**, *52*, 12140–12151. (i) Yuasa, J.; Dan, M.; Kawai, T. *Dalton Trans.*, **2013**, *42*, 16096–16101. (j) Kaeser, A.; Moudam, O.; Accorsi, G.; Séguy, I.; Navarro, J.; Belbarkra, A.; Duhayon, C.; Armaroli, N.; Delavaux-Nicot, B.; Nierengarten, J.-F. *Eur. J. Inorg. Chem.*, **2014**, *8*, 1345–1355. (k) Viciano-Chumillas, M.; Carbonell-Vilar, J. M.; Armentano, D.; Cano, J. *Eur. J. Inorg. Chem.*, **2019**, *25*, 2982–2989.

[66] Banerjee, A.; Sarkar, S.; Shah, J. A.; Frederiks, N. C.; Bazan-Bergamino, E. A.; Johnson, C. J.; Ngai, M.-Y. *Angew. Chem. Int. Ed.*, **2022**, ***61***, e202113841.

Despite these advancements, the field remains underexplored, and a systematic investigation on the photophysical and photochemical of **CuP4** complexes are necessary for their applications in photoredox reactions.

3.2 Preparations of CuP4 complexes

Synthesis

In our study, we synthesized a series of homoleptic copper(I)-bisphosphine (**CuP4**) complexes using readily available $Cu(MeCN)_4BF_4$ as the copper source and representative bisphosphine ligands in a 1:2 molar ratio. This approach yielded the desired **CuP4** complexes with ligands such as dppbz, (*R*)-BINAP, BIPHEP, DPEphos, and XantPhos (complexes **1**–**5**) with high efficiency (Scheme 34). We also achieved a multigram-scale synthesis of $[Cu(dppbz)_2]BF_4$ (**1**) with a 97% yield.

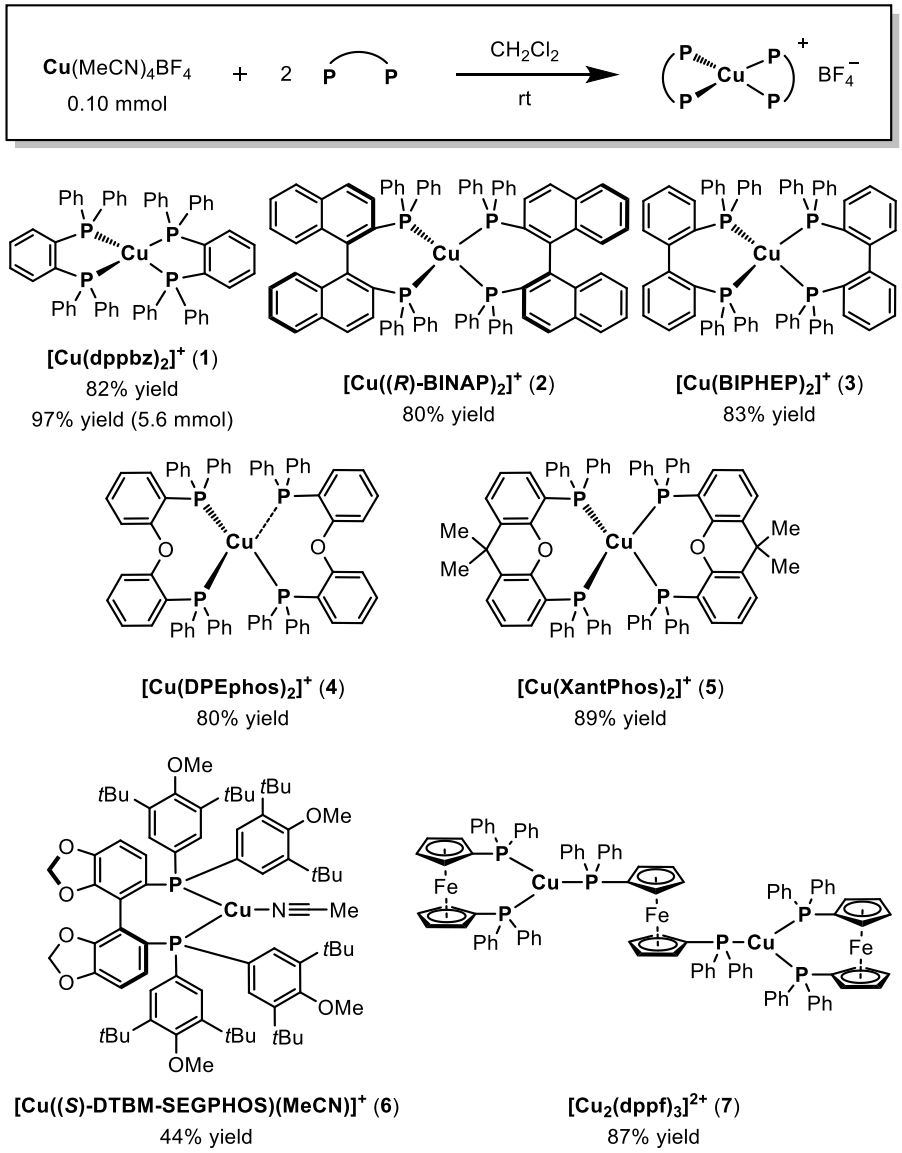

Scheme 34. Synthesis of **CuP4** complexes.

Coordination environment

Our findings revealed that the coordination environment of these **CuP4** complexes is significantly influenced by the nature of bisphosphine ligands. For instance, $[Cu(DPEphos)_2]^+$ (**4**) exists as **CuP3** in the solid state, with one phosphorus atom uncoordinated. However, its solution-phase ^{31}P NMR spectrum displays a single peak, indicating dynamic behavior. On the other hand, $[Cu((R)\text{-BINAP})_2]^+$ (**2**) maintains a **CuP4** structure in $CDCl_3$ but shifts to **CuP2** coordination in the coordinating CD_3CN with additional acetonitrile ligands, highlighting solvent-dependent

structural dynamics. In contrast, $[Cu(dppbz)_2]^+$ (**1**) retains its **CuP4** configuration in both solvents, consistent with its solid-state structure.

The steric properties of the ligands also play a crucial role in dictating the coordination geometry. For example, the bulky (*S*)-DTBM-SEGPHOS ligand leads to the formation of a **CuP2** complex (**6**) with one acetonitrile ligand. Additionally, using dppf as the ligand resulted in the formation of a dinuclear copper complex (**7**) bridged by one dppf moiety. These observations highlight the significant impact of ligand identity on the structural outcome of copper-bisphophine complexes, which in turn can influence their photophysical and catalytic properties.

3.3 Studies of CuP4 complexes

We choose 1,2-dichloroethane (DCE) as a suitable solvent for photophysical and electrochemical studies since **CuP4** complexes showed structural integrity in DCE.

UV-Vis absorption spectra

The UV-Vis absorption spectra for the five **CuP4** complexes showed two important features (Scheme 35). The band between 200–250 nm relates to intense ligand-centered (LC) π–π* transition, and a shoulder peak between 250–350 nm corresponds to MLCT transitions. These MLCT transitions result in the transfer of one electron from the copper center to the ligand, generating a charge-separated state capable of engaging in redox reactions.

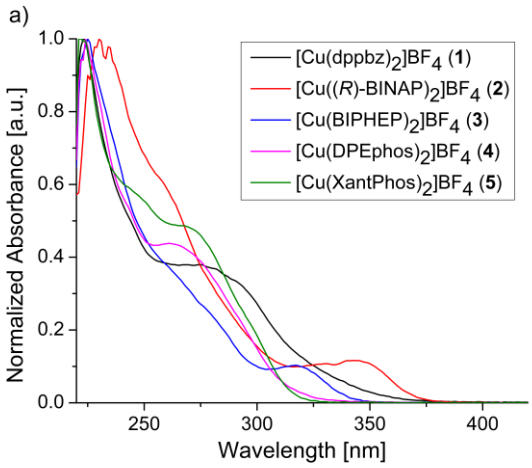

Scheme 35. Absorption spectra of **CuP4** complexes.

Emission Properties and Excited-State Lifetimes

Upon excitation at 390 nm, the emission spectra of complexes **1**–**5** gave rise to multiple peaks, including a broad band beyond 500 nm.

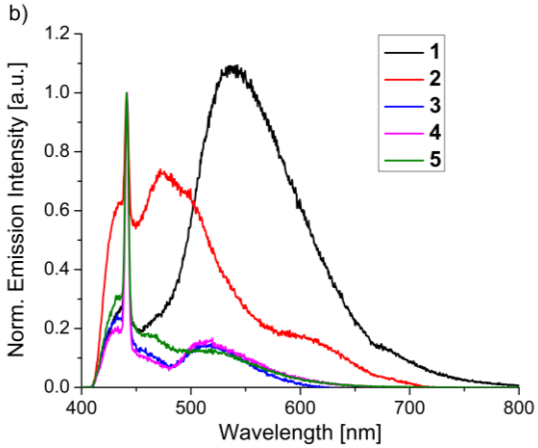

Scheme 36. Emission spectra (λ_{ex} = 390 nm) of **CuP4** complexes

Time-resolved photoluminescence measurements indicated that, except for complex **3**, these long-wavelength emissions have decay lifetimes exceeding 10 μs. Such prolonged excited-state lifetimes suggest that these complexes possess sufficiently persistent excited states to participate effectively in photoredox processes.

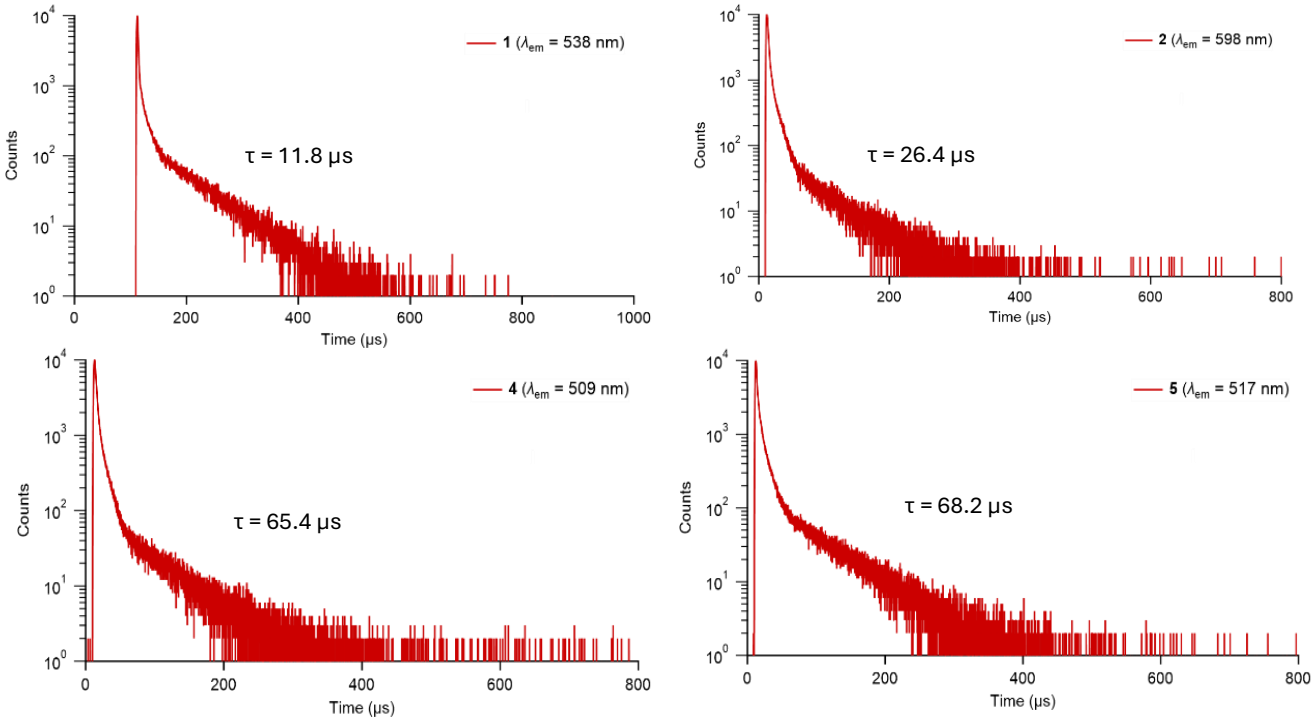

Scheme 37. Emission decay curves of complexes 1, 2, 4 and 5.

Electrochemical behavior

Cyclic voltammetry studies conducted in DCE revealed clear anodic peaks for all five complexes, ranging from 0.5-1.5 V vs. Fc^{+}/Fc (Scheme 38). These peaks are indicative of the Cu(I)/Cu(II) oxidation process, and the observed reversible behavior supports capability in photoredox cycles to facilitate electron transfer reactions.

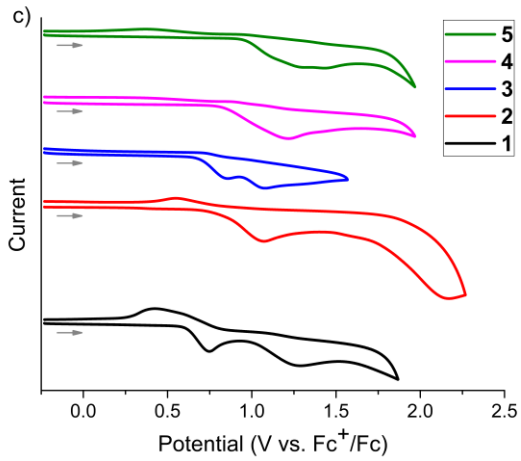

Scheme 38. Cyclic voltammogram of **CuP4** complexes.

Theoretical investigations

To elucidate the nature of the long-lived emission observed in $[Cu(dppbz)_2]^+$ (**1**), we performed time-dependent density functional theory (TD-DFT) calculations at the ωB97XD/cc-pVDZ/LanL2DZ(Cu)+CPCM(dichloroethane) level of theory. These calculations aimed to investigate the excited-state dynamics and provide insights into the photophysical behavior of the complex. The structural relaxation in the S_1 state lowers its excitation energy, which in turn reduces the energy of the triplet state (T_1) due to the similar electronic configurations of these states.[67] Consequently, ISC from the optimized S_1 structure to the T_1 state becomes energetically favorable. The T_1 state is calculated to have an excitation energy of 2.44 eV (508 nm), aligning well with the broad emission band observed experimentally between 500 and 700 nm. The long-lived nature of

[67] (a) Garakyaraghi, S.; Danilov, E. O.; McCusker, C. E.; Castellano, F. N. *J. Phys. Chem. A*, **2015**, *119*, 3181. (b) Garakyaraghi, S.; Crapps, P. D.; McCusker, C. E.; Castellano, F. N. *Inorg. Chem.*, **2016**, *55*, 10628. (c) Garakyaraghi, S.; Koutnik, P.; Castellano, F. N. *Phys. Chem. Chem. Phys.*, **2017**, ***19***, 16662.

this emission, with a measured lifetime of 26.4 μs for complex **1**, is consistent with the triplet state character and the reduced oscillator strength resulting from the structural reorganization.

Thus, upon photoexcitation, the complex transitions to the first singlet excited state ^{1}MLCT. This process involves the transfer of electron density from the copper(I) center to the ligand, effectively oxidizing Cu(I) to Cu(II) and reducing the ligand. The redistribution of electron density induces a significant structural reorganization from the ground-state geometry to a more stabilized S_1 structure. This reorganization is accompanied by a marked decrease in oscillator strength, which correlates with the experimentally observed prolonged excited-state lifetime.

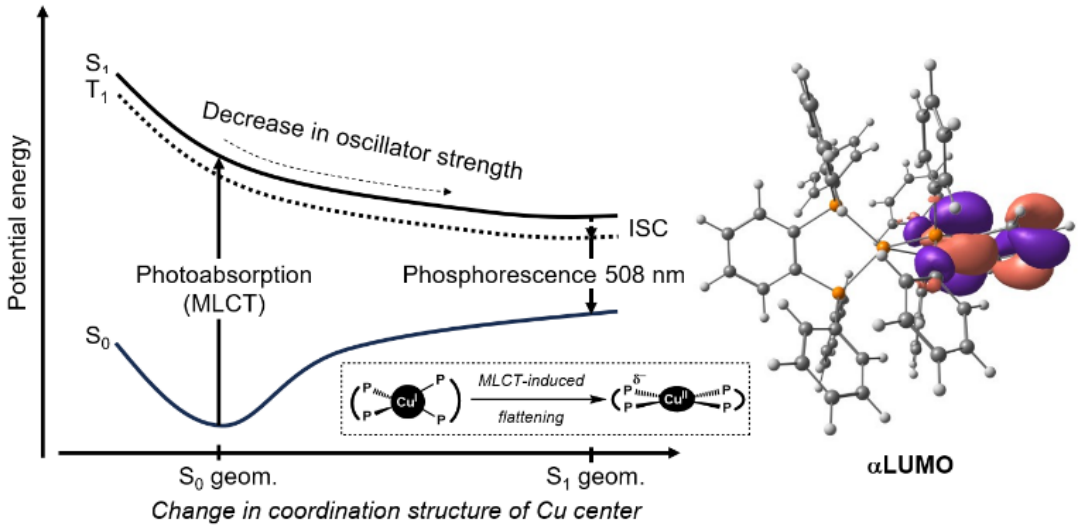

Scheme 39. Electronic transition and structural rearrangement of $[Cu(dppbz)_2]BF_4$ (**1**).

Implications for photoredox activity

The ability of $[Cu(dppbz)_2]^+$ to undergo efficient ISC and form a long-lived triplet state with significant MLCT character is crucial for its function as a photoredox catalyst. The extended lifetime of the excited state provides a sufficient window for engaging in electron transfer processes with substrates, a key requirement for effective photoredox catalysis. These findings underscore the importance of excited-state dynamics and structural flexibility in designing copper(I)-based photoredox catalysts.

3.4 Applications of CuP4 in organic transformations

In our investigation of the photocatalytic capabilities of homoleptic copper(I)-bisphosphine (CuP_4) complexes, we focused on evaluating the effect of five isolated **CuP4** complexes, (**1**-**5**).

Defluorinative C–I coupling of trifluoromethylarenes

This reaction is significant for synthesizing difluorobenzyl iodides ($ArCF_2I$), an underexplored class of fluorinated compounds with potential applications in pharmaceuticals and materials. Our previous studies suggest that the excited-state **CuP4** complex could act as a reductant, facilitating the conversion of $ArCF_3$ into the key $ArCF_2$• radical intermediate. This radical then reacts with an iodine source to form the desired $ArCF_2I$ product. Among all **CuP4**, We observed that $[Cu(dppbz)_2]^+$ (**1**) expressed superior catalytic activity as compared to other candidates.

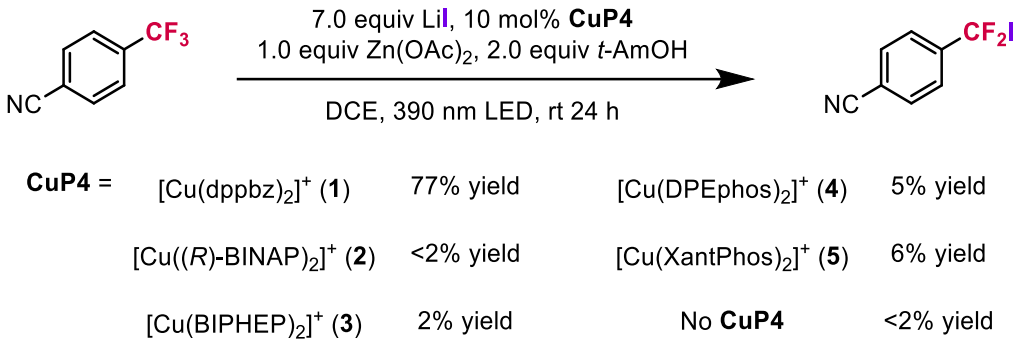

Scheme 40. Defluorinative C–I coupling with $ArCF_3$.

Hydrodeiodination of Aryl Iodides

In the presence of tert-amyl alcohol (*t*AmOH) and *N*,*N*-diisopropylethylamine (DIPEA) as well as photoirradiation, all **CuP4** complexes facilitated the hydrodehalogenation of aryl iodides, with $[Cu(dppbz)_2]^+$ (**1**) yielding the highest efficiency (Table 17). [68]Remarkably, similar results were achieved with *in situ* generated catalysts. Control experiments suggested that both *t*AmOH and DIPEA could serve as hydrogen donors. Reactions conducted in the dark or under 440 nm light showed diminished or no yields, highlighting the necessity of appropriate light irradiation. A

[68] Alonso, F.; Beletskaya, I. P.; Yus, M. *Chem. Rev.*, **2002**, *102*, 4009–4092.

brief substrate scope revealed that aryl iodides bearing electron-withdrawing groups, such as esters or quinazolines, reacted efficiently, whereas electron-rich substrates exhibited lower reactivity (Scheme 41). The protocol was also extended to aryl bromides, with electron-deficient arenes providing better yields.

Table 17. Control experiment for hydrodeiodination of ArI

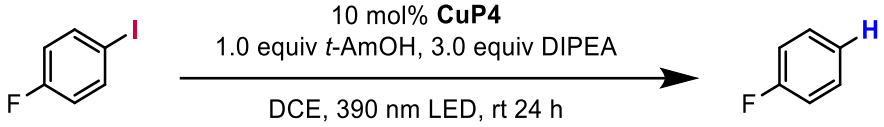

Entry	Conditions	Yield (%)[a]
1	**CuP4** = $[Cu(dppbz)_2]BF_4$ (**1**)	98
2	**CuP4** = $[Cu((R)\text{-BINAP})_2]BF_4$ (**2**)	47
3	**CuP4** = $[Cu(BIPHEP)_2]BF_4$ (**3**)	24
4	**CuP4** = $[Cu(DPEphos)_2]BF_4$ (**4**)	17
5	**CuP4** = $[Cu(XantPhos)_2]BF_4$ (**5**)	35
6	10 mol% $Cu(MeCN)_4BF_4$ + 20 mol%	>99
7	As entry 6, no *t*AmOH	72
8	As entry 6, no DIPEA	24
9	As entry 6, no light, rt or 60 °C	<3
10	As entry 6, 440 nm instead of 390 nm	15
11	No Cu/L	14

[a]Determined by ^{19}F-NMR analysis of the crude mixture with (trifluoromethoxy)benzene as the standard.

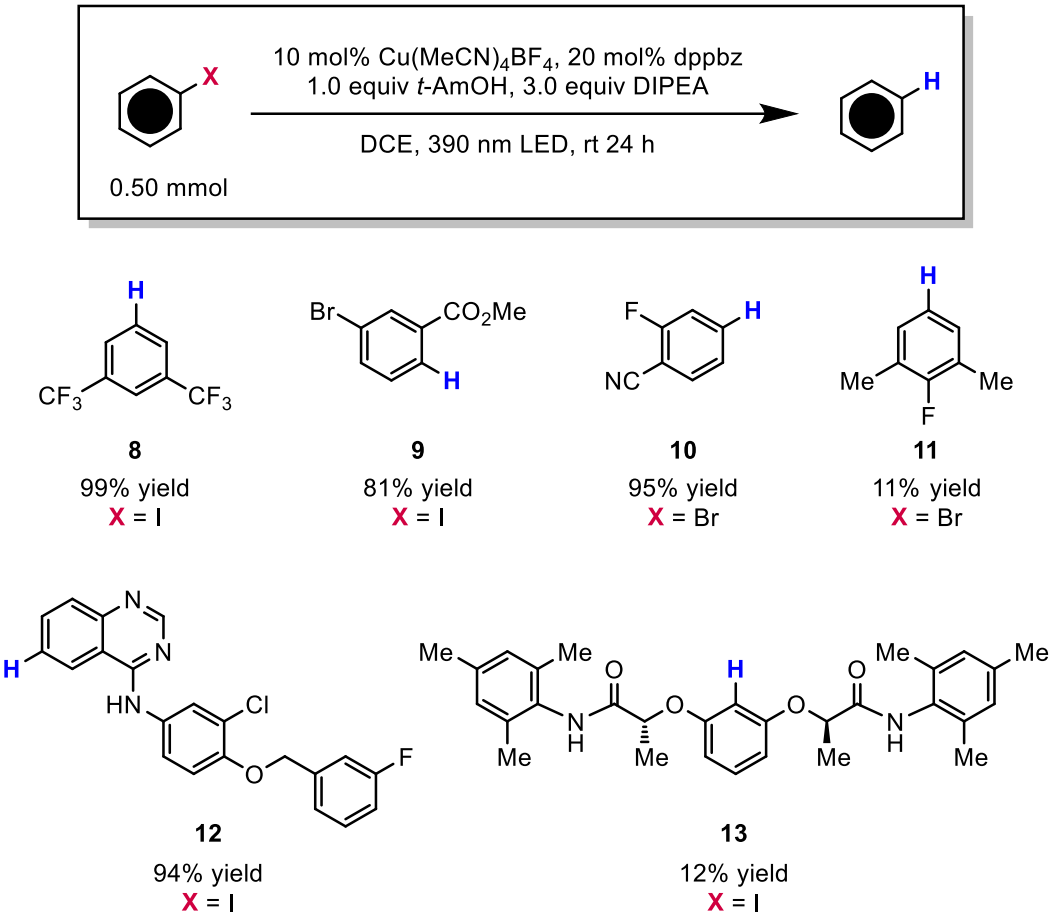

Scheme 41. Scope of photoinduced Cu-catalyzed hydrodehalogenation reactions.

Photocatalytic C–S Coupling

We studied the application of complex **1** in photocatalytic C–S coupling reactions. In the presence of $[Cu(dppbz)_2]^+$ (**1**), the coupling of aryl halides with thiols proceeded with good efficiency, achieving up to 92% isolated yield on a 0.50 mmol scale. Control experiments showed non-negligible yields without **1**, presumably due to the known electron donor-acceptor (EDA) mechanism.[69] The method was successfully applied to the coupling with 2-mercaptobenzothiazole (MBT), a compound utilized as an accelerant in rubber vulcanization processes.

[69] Liu, B.; Lim, C.-H.; Miyake, G. M. *J. Am. Chem. Soc.*, **2017**, *139*, 13616–13619.

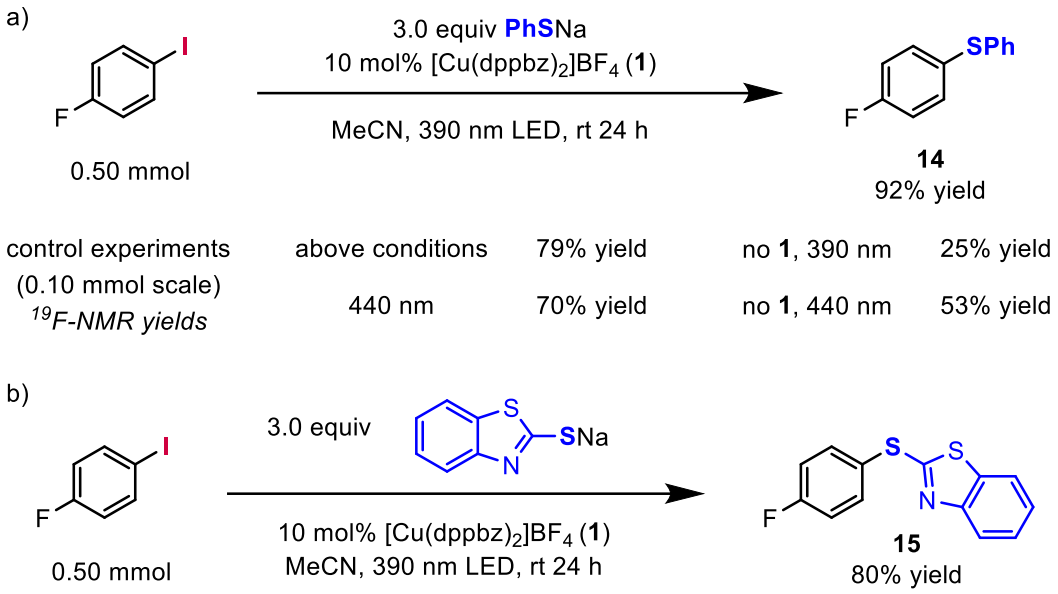

Scheme 42. Photoinduced Cu-catalyzed C–S coupling reactions.

3.5 Conclusion

These findings underscore the potential of homoleptic **CuP4** complexes, particularly $[Cu(dppbz)_2]^+$, as versatile photocatalysts in various organic transformations. Their tunable photophysical properties and redox potential, influenced by ligand modifications, offer promising possibilities for the development of efficient and sustainable photoredox catalytic systems.

3.6 Outlook

Modification of dppbz for electronic and steric tuning

Introducing electron-donating or electron-withdrawing groups on the phenyl rings of dppbz can modulate the electron density at the copper center, thereby affecting the redox potential and excited-state energy and lifetime of the complexes. Introducing steric bulk on dppbz by incorporating substituents at strategic positions can influence the geometry and thus the stability of the complexes.

Exploration of diverse organic transformations

With tailored electronic and steric properties, the modified **CuP4** complexes can be evaluated in a broader range of photoredox-catalyzed transformations, providing a valuable alternative to noble-metal-based photocatalysts.

Development of enantioselective photocatalysis

Incorporating chiral elements into the dppbz ligand framework can pave the way for enantioselective photoredox catalysis. Chiral **CuP4** complexes can have the potential to induce asymmetry in the generation or functionalization of radical intermediates, leading to the formation of enantioenriched products.

Investigation of excited state redox potential

A comprehensive understanding of the excited-state redox potential of **CuP4** complexes is crucial for optimizing their photocatalytic performance, and advanced spectroscopical, electrochemical, as well as computational approaches are expected to be informative.

3.7 Experimental section

General Methods

Starting materials and reagents were commercially available and used as obtained from Wako Pure Chemical, Kanto Chemical, Sigma-Aldrich, or Tokyo Chemical Industry (TCI) without further purification. Tetrakis(acetonitrile)copper(I) tetrafluoroborate, dppbz, DPEphos, XantPhos, (*S*)-DTBM-SEGPHOS, dppf was obtained from TCI. (*R*)-(+)-BINAP, BIPHEP, anhydrous DCM, anhydrous ACN, anhydrous DCE was obtained from Kanto Chemical. NMR spectra were recorded on a JEOL ESZ-400S spectrometer at 25 °C using residual protonated solvent signals as internal standards for ^{1}H- and ^{13}C-spectra chemical shifts are denoted in δ (ppm). Coupling constants *J*, are denoted in Hz. The splitting patterns are designated as follows: s (singlet); d (doublet); t (triplet); q (quartet); m (multiplet); dd (doublet of doublets); ddd (doublet of doublets of doublets); dt (doublet of triplets); td (triplet of doublets) and br (broad). The UV-vis experiments were performed on an F-7000 FL spectrophotometer (Hitachi, Japan) with a quartz cuvette (10 mm path length). High-resolution mass spectra were measured at the Instrumental Analysis Division of Global Facility Center in Hokkaido University. Thin-layer chromatography (TLC) was performed on commercial Merck 60F, 254 silica gel plates and compounds were visualized with naked eyes or UV light (λ = 254 nm). Kessil PR160L-390nm LED lamps were used for the photoreaction. Single-crystal X-ray diffraction (XRD) analyses were carried out on a Rigaku XtaLAB Synergy diffractometer using graphite monochromated Cu-Kα radiation. The structures were solved with the SHELXT structure solution program using Intrinsic Phasing incorporated in the OLEX2

program package[70] and refined with the SHELXL package[71]. Hydrogen atoms were refined using the riding model.

Synthesis of CuP4

[Cu(dppbz)$_2$]BF$_4$ (1)

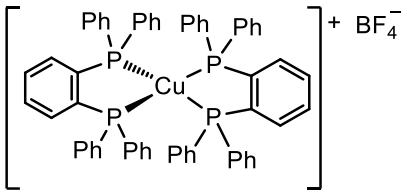

In an argon-filled glovebox, a 9-mL vial equipped with a magnetic stir bar was charged with tetrakis(acetonitrile)copper(I) tetrafluoroborate (31.5 mg, 0.1 mmol, 1.0 equiv), dppbz (89.3 mg, 0.2 mmol, 2.0 equiv), and CH_2Cl_2 (5 mL). The reaction mixture was allowed to stir at rt overnight. To the reaction mixture, hexane was added dropwise until the solution became turbid. The resulting solution was stirred for 2 h to fully precipitate the solid, which was then filtered, washed with 0.5 mL hexane, and dried to afford the desired complex. The title compound was obtained as an off-white solid (86.7 mg, 3% hexane, 3% DCM, 82% yield).

^{1}H NMR (400 MHz, $CDCl_3$) δ (ppm) 7.55 – 7.45 (m, 8H), 7.29 (t, *J* = 7.4 Hz, 8H), 7.06 (t, *J* = 7.6 Hz, 16H), 6.97 – 6.90 (m, 16H).

^{13}C NMR (101 MHz, $CDCl_3$) δ (ppm) 134.28 – 134.11 (m), 132.70 – 132.50 (m), 131.80 (bs), 131.36, 130.37, 129.26 – 129.01 (m).

^{31}P NMR (162 MHz, $CDCl_3$) *δ* (ppm) 8.76.

HRMS (ESI) *m/z* calculated for $C_{60}H_{48}CuP_4^+$ ([M]$^+$): 955.1997, found: 955.1988.

Gram scale synthesis

A 300 mL oven-dried two-neck round bottom flask equipped with a stirring bar was charged with tetrakis(acetonitrile)copper(I) tetrafluoroborate (1.76 g, 5.6 mmol, 1.0 equiv), dppbz (5.00 g, 11.2 mmol, 2.0 equiv). The flask was sealed and subjected to three vacuum/nitrogen cycles before CH_2Cl_2 (60 mL) was added. The reaction mixture was allowed to stir at rt under nitrogen for 24 hr. To the reaction mixture, 80 ml hexane was added dropwise through an additional funnel until the solution became turbid (cloud point). The solution was stirred for 2 h to fully precipitate the

[70]Dolomanov, O. V.; Bourhis, L. J.; Gildea, R. J.; Howard, J. A. K; Puschmann, H. J. *Appl. Crystallogr.* **2009**, *42*, 339−341.
[71]Sheldrick, G. M. *Acta Crystallogr., Sect. A.* **2015**, *71*, 3−8.

solid. Then 100 mL hexane was added to the resulting solution, which was stirred for 1 h. Upon completion, the product was collected by filtration, washed with hexane, and dried under high vacuum. The title compound was obtained as an off-white solid (5.69 g, 97% yield).

[Cu((*R*)-BINAP)$_2$]BF$_4$ (2)

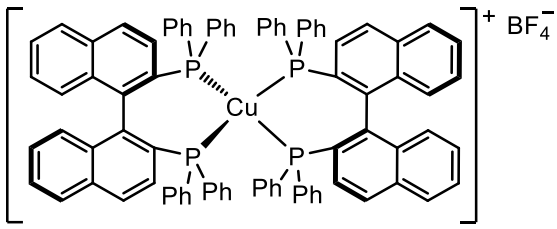

In an argon-filled glovebox, a 9-mL vial equipped with a magnetic stir bar was charged with tetrakis(acetonitrile)copper(I) tetrafluoroborate (31.5 mg, 0.1 mmol, 1.0 equiv), (*R*)-(+)-BINAP (124.5 mg, 0.2 mmol, 2.0 equiv), and CH_2Cl_2 (5 mL). The reaction mixture was allowed to stir at rt overnight. To the reaction mixture, hexane was added dropwise until the solution became turbid. The resulting solution was stirred for 2 h to fully precipitate the solid, which was then filtered, washed with 0.5 mL hexane, and dried to afford the desired complex. The title compound was obtained as a yellow solid (117.8 mg, 15% hexane, 10% CH_2Cl_2, 80% yield). The solid was further dried under vacuum before usage.

^{1}H NMR (400 MHz, $CDCl_3$) δ (ppm) 7.82 (d, *J* = 6.9 Hz, 8H), 7.68 (d, *J* = 8.8 Hz, 4H), 7.63 – 7.50 (m, 13H), 7.42 – 7.36 (m, 11H), 7.18 – 7.13 (m, 4H), 7.02 (d, *J* = 6.8 Hz, 8H), 6.95 (d, *J* = 8.7 Hz, 4H), 6.41 (t, *J* = 7.4 Hz, 4H), 5.91 (t, *J* = 7.6 Hz, 8H).

^{13}C NMR (101 MHz, $CDCl_3$) δ (ppm) 139.97 – 139.78 (m), 136.97 – 136.65 (m), 133.97 – 133.72 (m), 133.33, 133.30 – 133.22 (m), 131.91 (t, *J* = 16.6 Hz), 131.71, 131.12, 129.11, 128.94 (t, *J* = 5.1 Hz), 128.81 – 128.69 (m), 128.63 – 128.51 (m), 128.41, 128.32, 127.39, 126.98 – 126.84 (m), 126.62.

^{31}P NMR (162 MHz, $CDCl_3$) *δ* (ppm) 8.77.

HRMS (ESI) *m/z* calculated for $C_{88}H_{64}CuP_4^+$ ($[M]^+$)1307.3254, found: 1307.3222.

[Cu(BIPHEP)$_2$]BF$_4$ (3)

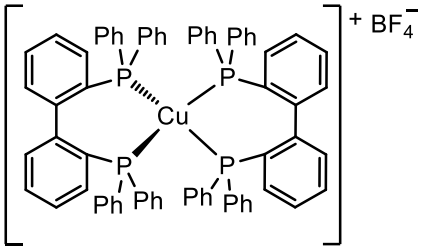

In an argon-filled glovebox, a 9-mL vial equipped with a magnetic stir bar was charged with tetrakis(acetonitrile)copper(I) tetrafluoroborate (31.5 mg, 0.1 mmol, 1.0 equiv), 2,2'-bis(diphenylphosphino)-1,1'-biphenyl (BIPHEP) (104.5mg, 0.2 mmol, 2.0 equiv), and DCE (5 mL). The reaction mixture was allowed to stir at rt overnight. To the reaction mixture, hexane was added dropwise until the solution became turbid. The resulting solution was stirred for 2 h to fully precipitate the solid, which was then filtered, washed with 0.5 mL hexane, and dried to afford the desired complex. The title compound was obtained as an off-white solid (102.1 mg, 25% DCE, 8% hexane, 9% EtOAc, 83% yield). The solid was further dried under vacuum before usage.

^{1}H NMR (400 MHz, CDCl$_3$) δ (ppm) 7.66 – 7.60 (m, 8H), 7.48 (t, J = 7.4 Hz, 4H), 7.29 – 7.22 (m, 8H), 7.21 – 7.11 (m, 16H), 7.06 – 7.01 (m, 4H), 6.97 (t, J = 7.4 Hz, 4H), 6.79 (d, J = 7.6 Hz, 4H), 6.56 (t, J = 7.6 Hz, 8H).

^{13}C NMR (101 MHz, CDCl$_3$) δ (ppm) 144.57 – 144.39 (m), 136.98 – 136.56 (m), 134.96, 134.83 – 134.57 (m), 132.09 – 131.77 (m), 131.79 – 131.71 (m), 131.68, 131.48 – 131.12 (m), 131.11 – 130.72 (m), 130.43, 130.19, 128.86 (dt, J = 5.2, 2.7 Hz), 128.02 (dt, J = 4.7, 2.4 Hz), 127.14.

^{31}P NMR (162 MHz, CDCl$_3$) δ (ppm) 4.95.

HRMS (ESI) *m/z* calculated for $C_{72}H_{56}CuP_4^+$ ([M]$^+$):1107.2628, found: 1107.2655.

[Cu(DPEphos)$_2$]BF$_4$ (4)

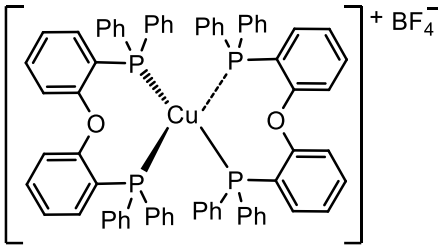

In an argon-filled glovebox, a 9-mL vial equipped with a magnetic stir bar was charged with tetrakis(acetonitrile)copper(I) tetrafluoroborate (31.5 mg, 0.1 mmol, 1.0 equiv), DPEphos (107.7mg, 0.2 mmol, 2.0 equiv), and CH_2Cl_2 (5 mL). The reaction mixture was allowed to stir at rt overnight. The reaction mixture was concentrated under vacuum. The title compound was obtained as an off-white solid (102.6 mg, 47% hexane, 22% CH_2Cl_2, 80% yield). The solid was further dried under vacuum before usage.

^{1}H NMR (400 MHz, $CDCl_3$) δ (ppm) 7.29 – 7.23 (m, 12H), 7.14 (t, *J* = 7.6 Hz, 4H), 6.99 (t, *J* = 7.5 Hz, 18H), 6.76 (d, *J* = 7.0 Hz, 19H), 6.44 (d, *J* = 7.9 Hz, 3H).

^{13}C NMR (101 MHz, $CDCl_3$) δ (ppm) 158.40 – 158.19 (m), 134.43, 133.77 (t, *J* = 6.9 Hz), 132.21, 131.23 – 130.90 (m), 130.46, 128.86, 124.84 , 124.80 – 124.69 (m), 119.42 – 119.26 (m).

^{31}P NMR (162 MHz, $CDCl_3$) *δ* (ppm) -13.05.

HRMS (ESI) *m/z* calculated for $C_{72}H_{56}CuO_2P_4^+$ ($[M]^+$): 1139.2522, found: 1139.2519.

[Cu(XantPhos)$_2$]BF$_4$ (5)

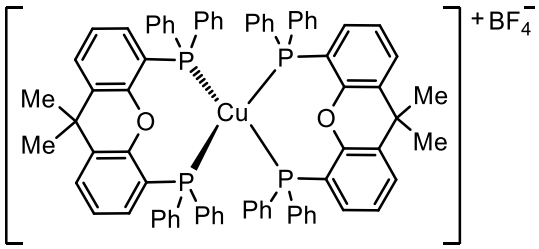

In an argon-filled glovebox, a 9-mL vial equipped with a magnetic stir bar was charged with tetrakis(acetonitrile)copper(I) tetrafluoroborate (31.5 mg, 0.1 mmol, 1.0 equiv), XantPhos (115.7mg, 0.2 mmol, 2.0 equiv), and CH_2Cl_2 (5 mL). The reaction mixture was allowed to stir at rt overnight. To the reaction mixture, hexane was added dropwise until the solution became turbid. The resulting solution was stirred for 2 h to fully precipitate the solid, which was then filtered, washed with 0.5 mL hexane, and dried to afford the desired complex. The title compound was obtained as an off-white solid (116.8 mg, 5% hexane, 89% yield).

Note: presumably due to the dynamic nature in solution, the NMR peaks appear broad and cannot be clearly assigned.

^{1}H NMR (400 MHz, $CDCl_3$) δ (ppm) 7.80 – 7.35 (br), 7.35 – 6.05 (br), 2.07 – 0.58 (br).

^{13}C NMR (101 MHz, $CDCl_3$) δ (ppm) 153.56 (br), 133.64 (br), 133.05 (br), 130.09 (br), 128.83 (br), 127.34 (br), 124.76, 35.33.

^{31}P NMR (162 MHz, $CDCl_3$) *δ* (ppm) -12.76.

HRMS (ESI) *m/z* calculated for $C_{78}H_{64}CuO_2P_4^+$ ($[M]^+$):1219.3148, found: 1219.3140.

[Cu((*S*)-DTBM-SEGPHOS)(MeCN)]BF_4 (6)

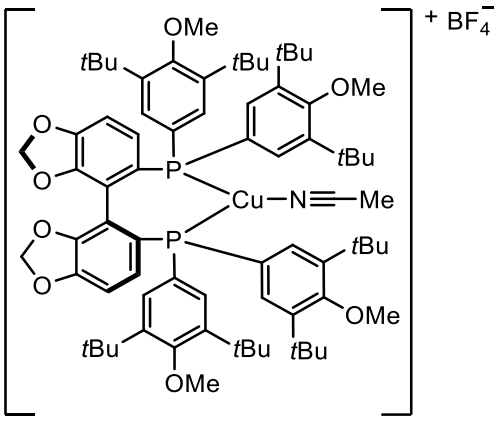

In an argon-filled glovebox, a 9-mL vial equipped with a magnetic stir bar was charged with tetrakis(acetonitrile)copper(I) tetrafluoroborate (31.5 mg, 0.1 mmol, 1.0 equiv), (*S*)-DTBM-SEGPHOS (235.9 mg, 0.2 mmol, 2.0 equiv), and CH_2Cl_2 (5 mL). The reaction mixture was allowed to stir at rt overnight. To the reaction mixture, hexane was added dropwise until the solution became turbid. The resulting solution was stirred for 2 h to fully precipitate the solid, which was then filtered, washed with 0.5 mL hexane, and dried to afford the desired complex. The title compound was obtained as an off-white solid (60.2 mg, 2% hexane, 44% yield).

^{1}H NMR (400 MHz, $CDCl_3$) δ (ppm) 7.55 (t, *J* = 6.1 Hz, 4H), 7.27 – 7.26 (m, 1H), 7.26 – 7.25 (m, 2H), 7.24 – 7.23 (m, 1H), 6.52 (d, *J* = 8.1 Hz, 2H), 6.39 (dt, *J* = 8.1, 5.0 Hz, 2H), 5.60 (d, *J* = 1.2 Hz, 2H), 5.47 (d, *J* = 0.9 Hz, 2H), 3.75 (s, 6H), 3.63 (s, 6H), 2.53 (s, 3H), 1.43 (s, 36H), 1.30 (s, 36H).

^{13}C NMR (101 MHz, $CDCl_3$) δ (ppm) 162.46 (d, *J* = 6.1 Hz), 148.31 (s), 147.48 (t, *J* = 6.4 Hz), 145.31 (t, *J* = 5.5 Hz), 144.27 (t, *J* = 5.7 Hz), 133.43 – 133.16 (m), 132.73 – 132.42 (m), 125.42 (t, *J* = 4.1 Hz), 124.49 (t, *J* = 17.9 Hz), 122.99 (t, *J* = 23.4 Hz), 118.01 (t, *J* = 11.0 Hz), 108.32 (t, *J* = 3.8 Hz), 100.76, 64.69, 64.42, 36.25, 35.87, 32.15, 31.96.

^{31}P NMR (162 MHz, $CDCl_3$) *δ* (ppm) 0.54.

HRMS (ESI) *m/z* calculated for $C_{76}H_{103}CuNO_8P_2^+$ ($[M]^+$): 1282.6455, found: 1282.6436.

Synthesis of $[Cu_2(dppf)_3](BF_4)_2$ (7)

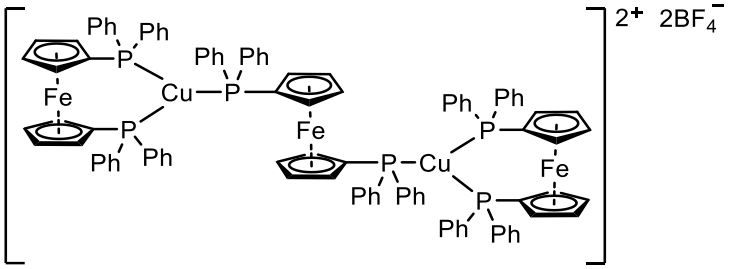

In an argon-filled glovebox, a 9-mL vial equipped with a magnetic stir bar was charged with tetrakis(acetonitrile)copper(I) tetrafluoroborate (31.5 mg, 0.1 mmol, 1.0 equiv), dppf (110.9 mg, 0.2 mmol, 2.0 equiv), and CH_2Cl_2 (5 mL). The reaction mixture was allowed to stir at rt overnight. To the reaction mixture, hexane was added dropwise until the solution became turbid. The resulting solution was stirred for 2 h to fully precipitate the solid, which was then filtered, washed with 0.5 mL hexane, and dried to afford the desired complex. The title compound was obtained as an off-white solid (92.4 mg, 74% hexane, 87% yield).

^{1}H NMR (400 MHz, DMSO-d6) δ (ppm) 7.51 – 7.43 (m, 18H), 7.39 (s, 42H), 4.36 (s, 12H), 4.01 (s, 12H).

^{13}C NMR (101 MHz, DMSO-d6) δ (ppm) 133.40 – 133.07 (m), 130.12 – 129.97 (m), 128.92 – 128.51 (m), 73.71 – 73.46 (m), 72.42 – 72.24 (m).

^{31}P NMR (162 MHz, DMSO-d6) δ (ppm) -15.08.

^{31}P NMR (162 MHz, $CDCl_3$) δ (ppm) -9.03 – -9.25 (m), -16.52 – -16.81 (m).

^{31}P NMR (162 MHz, Toluene-d8) δ (ppm) -16.68.

HRMS (ESI) *m/z* calculated for $C_{68}H_{56}CuFe_2P_4^+$ ($[M]^+$): 1171.1349, found: 1171.1301.

^{31}P NMR studies of **CuP4** complexes in CD_3CN and $CHCl_3$ solution

CuP4	$CDCl_3$ (δ ppm)	CD_3CN (δ ppm)
$[Cu(dppbz)_2]^+BF_4^-$ (**1**)	8.71	9.31
$[Cu((R)\text{-BINAP})_2]^+BF_4^-$ (**2**)	8.77	-0.81, -15.95
$[Cu(BIPHEP)_2]^+BF_4^-$ (**3**)	4.95	5.66, -4.37, -14.49
$[Cu(DPEphos)_2]^+BF_4^-$ (**4**)	-13.05	-13.46
$[Cu(XantPhos)_2]^+BF_4^-$ (**5**)	-12.76	-9.63, -13.74, -18.16

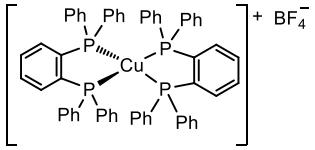
Ph Ph Ph Ph
P
Cu
P
P
P
Ph Ph Ph Ph
+ BF4−

1

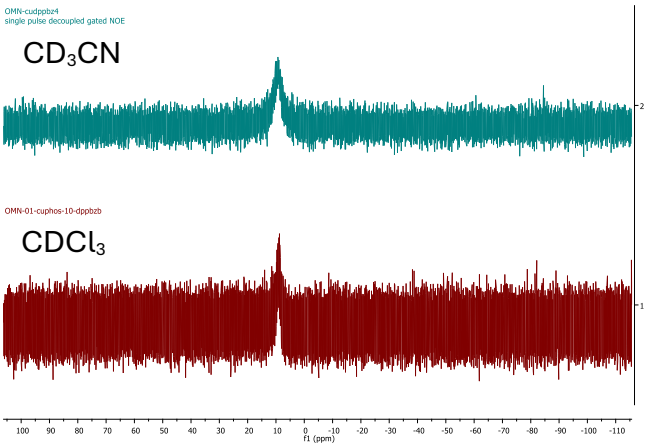
OMN-cudppbz4
single pulse decoupled gated NOE
CD3CN
OMN-01-cuphos-10-dppbzb
CDCl3
f1 (ppm)

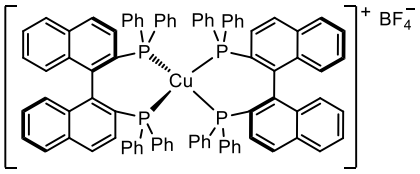
Ph Ph Ph Ph
P
Cu
P
P
P
Ph Ph Ph Ph
+ BF4−

2

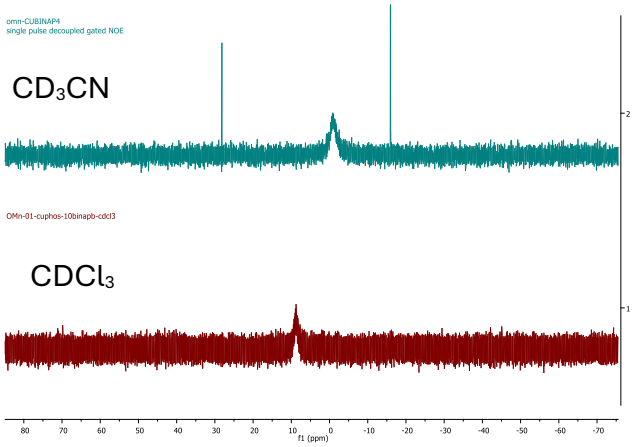
omn-CUBINAP4
single pulse decoupled gated NOE
CD3CN
OMn-01-cuphos-10binapb-cdcl3
CDCl3
f1 (ppm)

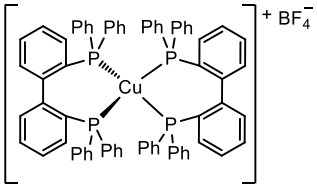
Ph Ph Ph Ph
P
Cu
P
P
P
Ph Ph Ph Ph
+ BF4−

3

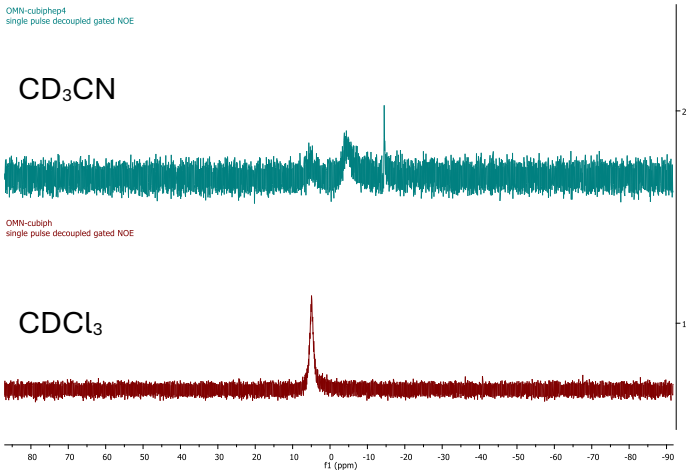
OMN-cubiphep4
single pulse decoupled gated NOE
CD3CN
OMN-cubiph
single pulse decoupled gated NOE
CDCl3
f1 (ppm)

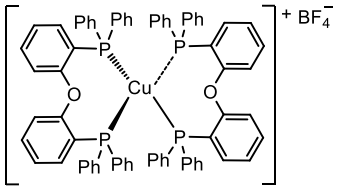

4

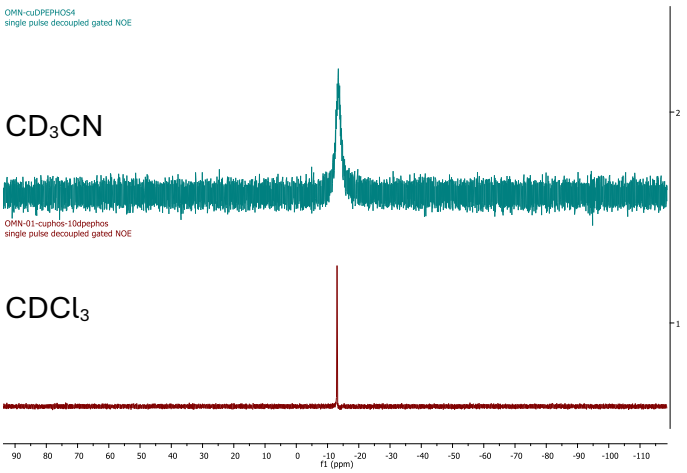

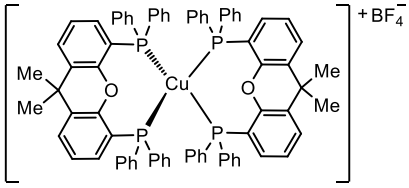

5

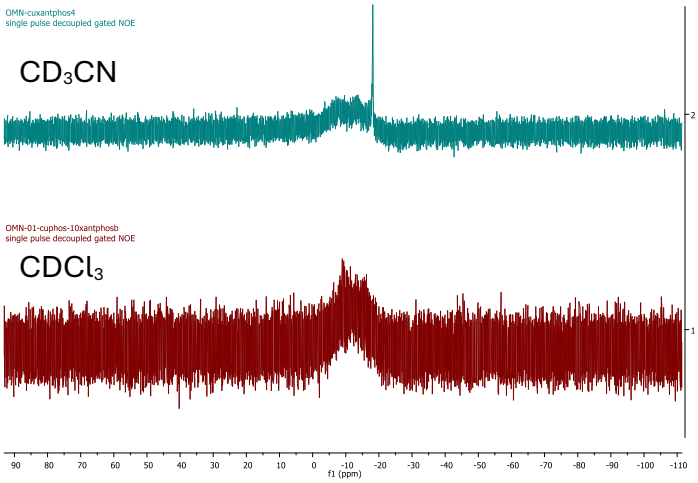

Cyclic Voltammetry Analysis

1,2-dichloroethane (DCE)

All the cyclic voltammetry experiments were performed in a batch setup. The analysis was performed with a PalmSens EmStat3+ instrument equipped with a glassy carbon working electrode (3 mm), a platinum wire counter electrode, and an Ag wire reference electrode (Ag/Ag^{+}). Ferrocene (Fc) was added as an internal standard. All measurements were carried out at the analyte concentration of 0.0005 M in anhydrous degassed DCE in the presence of an electrolyte ($n$$Bu_4NPF_6$, 0.05 M) and with a scan rate of 100-400 mV/s as mentioned.

MeCN

All the cyclic voltammetry experiments were performed in a batch setup. The analysis was performed with a PalmSens EmStat3+ instrument equipped with a glassy carbon working electrode (3 mm), a platinum wire counter electrode, and a SCE reference electrode. All measurements were carried out at the analyte concentration of 0.0006 M in anhydrous degassed MeCN in the presence of an electrolyte (nBu$_4$NPF$_6$, 0.06M) and with a scan rate of 100 mV/s.

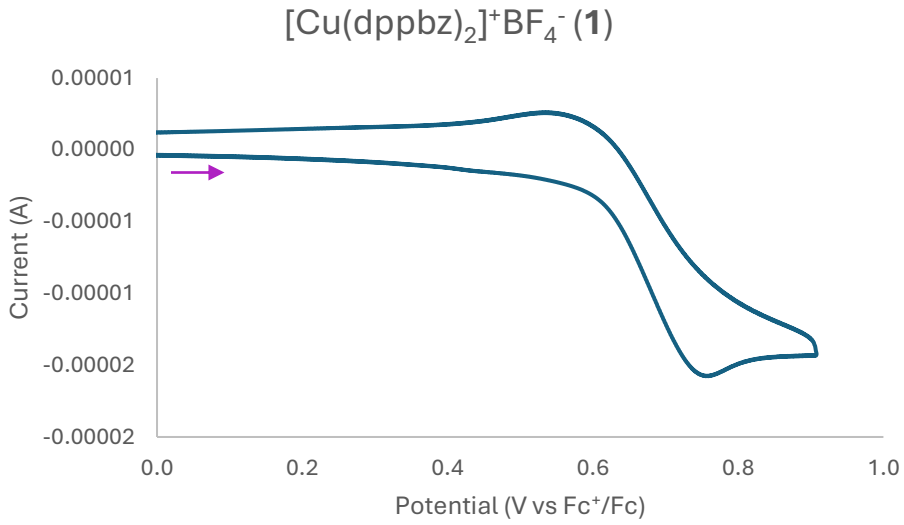

Figure 21. Cyclic voltammetry of $[Cu(dppbz)_2]^+BF_4^-$ (**1**) in DCE at a scan rate of 100 mVs^{-1}. Right: from 0 V to +1.0 V.

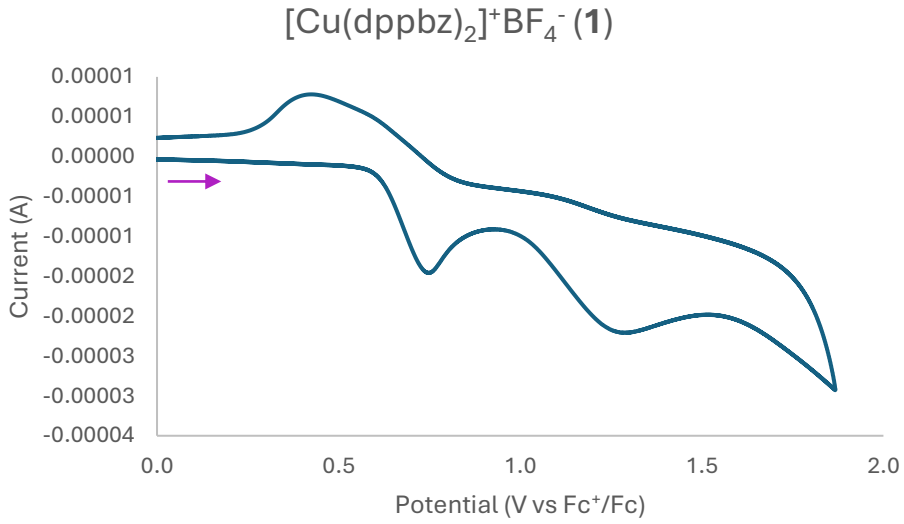

Figure 22. Cyclic voltammetry of $[Cu(dppbz)_2]^+BF_4^-$ (**1**) in DCE at a scan rate of 400 mVs^{-1}. Right: from 0 V to +2.0 V.

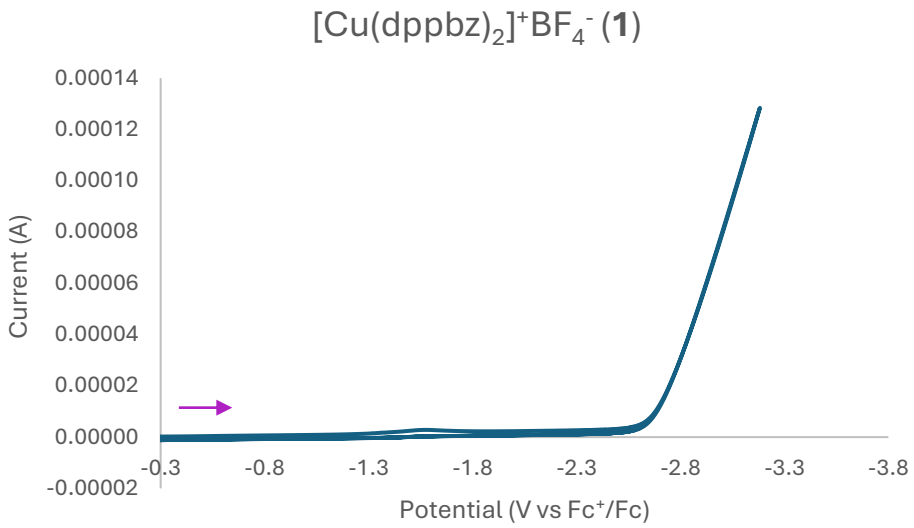

Figure 23. Cyclic voltammetry of $[Cu(dppbz)_2]^+BF_4^-$ (**1**) in DCE at a scan rate of 100 mVs^{-1}. Right: from -0.25 V to -3.5 V.

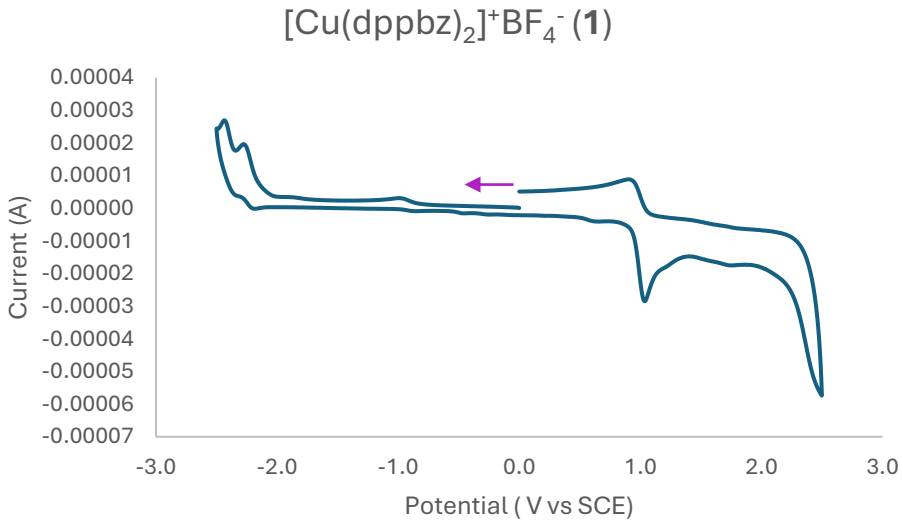

Figure 24. Cyclic voltammetry of $[Cu(dppbz)_2]^+BF_4^-$ (**1**) in MeCN at a scan rate of 100 mVs^{-1}. Right: from -3.0 V to +3.0 V.

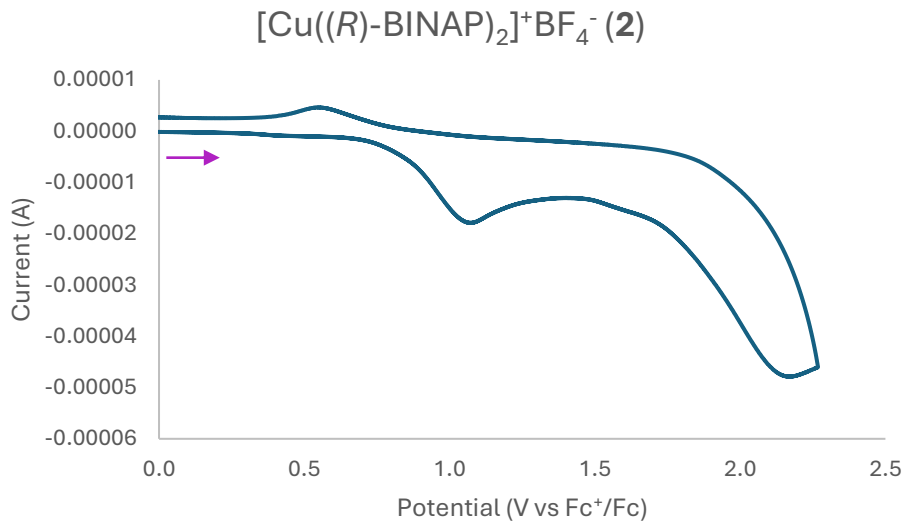

Figure 25. Cyclic voltammetry of $[Cu((R)\text{-}BINAP)_2]^+BF_4^-$ (**2**) in DCE at a scan rate 100 mVs^{-1}. Right: from 0 V to +2.5 V.

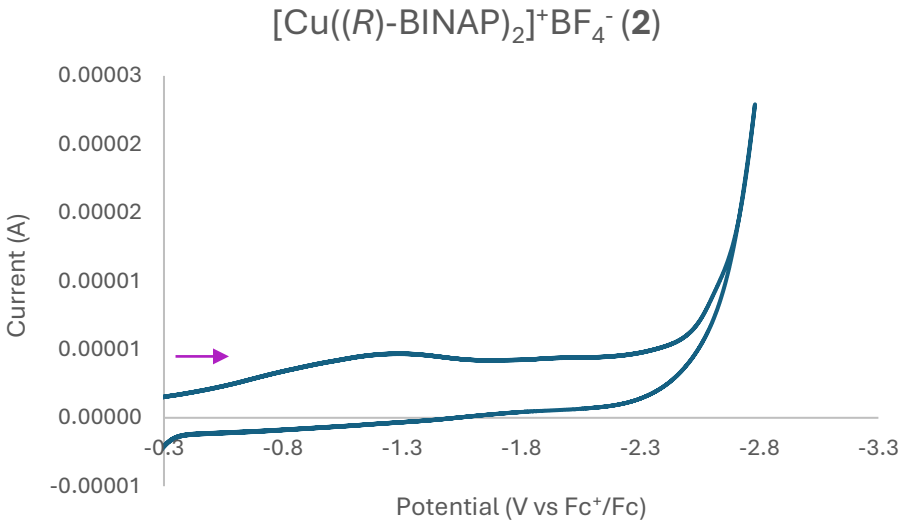

Figure 26. Cyclic voltammetry of $[Cu((R)\text{-}BINAP)_2]^+BF_4^-$ (**2**) in DCE at a scan rate 100 mVs^{-1}. Right: from -0.25 V to -3.0 V.

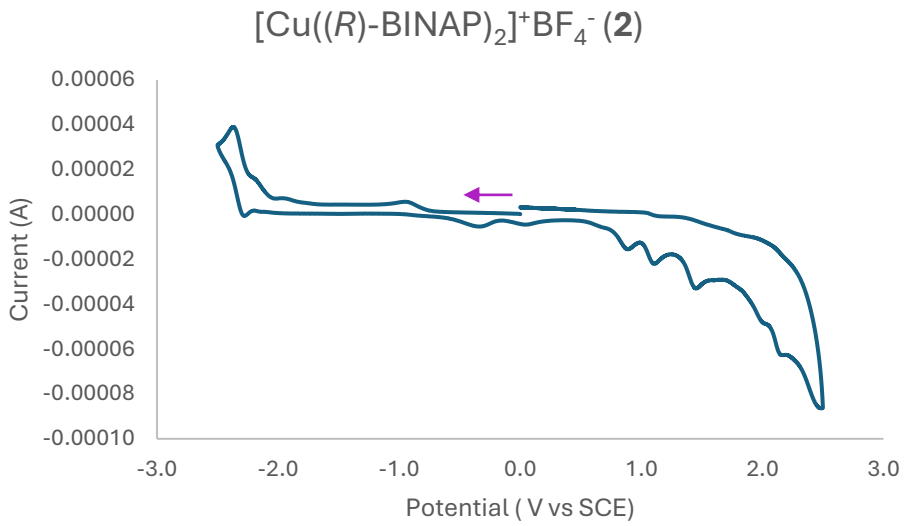

Figure 27. Cyclic voltammetry of $[Cu((R)\text{-BINAP})_2]^+BF_4^-$ (**2**) in MeCN at a scan rate100 mVs^{-1}. Right: from -3.0 V to +3.0 V.

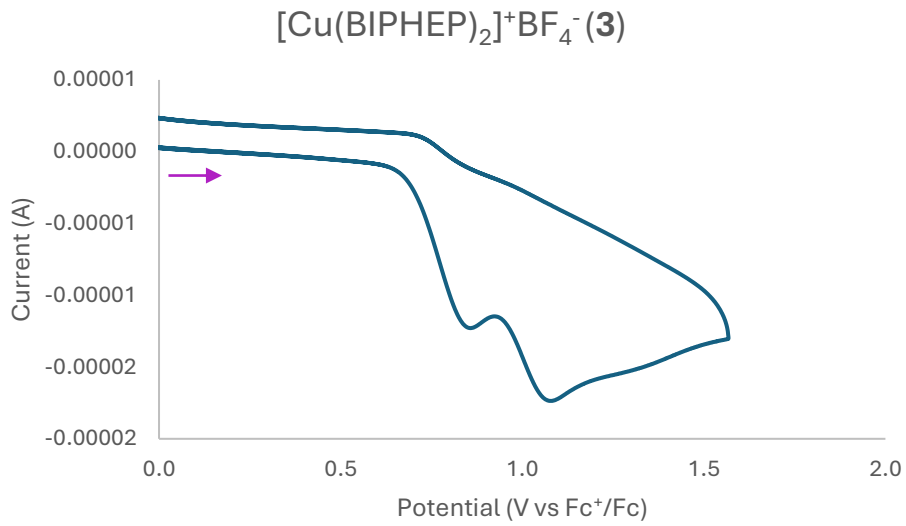

Figure 28. Cyclic voltammetry of $[Cu(BIPHEP)_2]^+BF_4^-$ (**3**) in DCE at a scan rate of 100 mVs^{-1}. Right: from 0 V to +2.0 V.

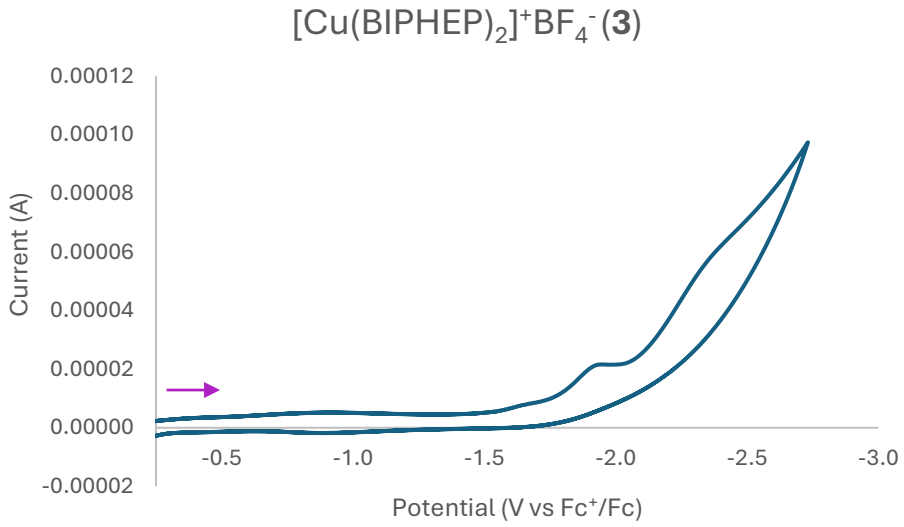

Figure 29. Cyclic voltammetry of $[Cu(BIPHEP)_2]^+BF_4^-$ (**3**) in DCE at a scan rate of 100 mVs^{-1}. Right: from -0.25 V to -3.0 V.

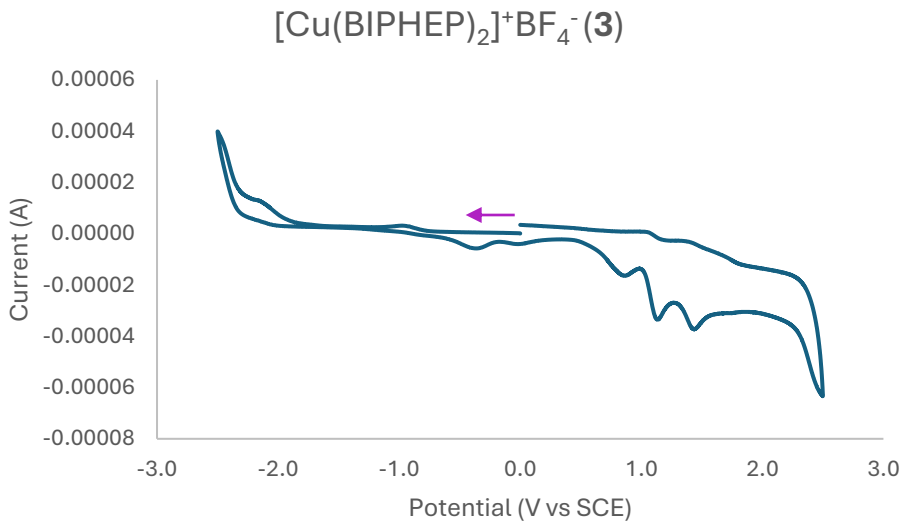

Figure 30. Cyclic voltammetry of $[Cu(BIPHEP)_2]^+BF_4^-$ (**3**) in MeCN at a scan rate 100 mVs^{-1}. Right: from -3.0 V to +3.0 V.

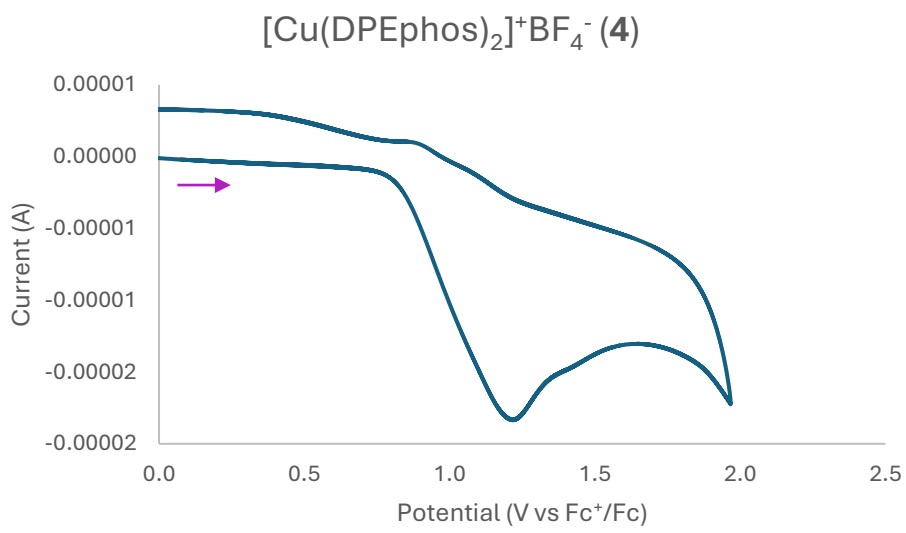

Figure 31. Cyclic voltammetry of $[Cu(DPEphos)_2]^+BF_4^-$ (**4**) in DCE at a scan rate 100 mVs^{-1}. Right: from 0 V to +2.5 V.

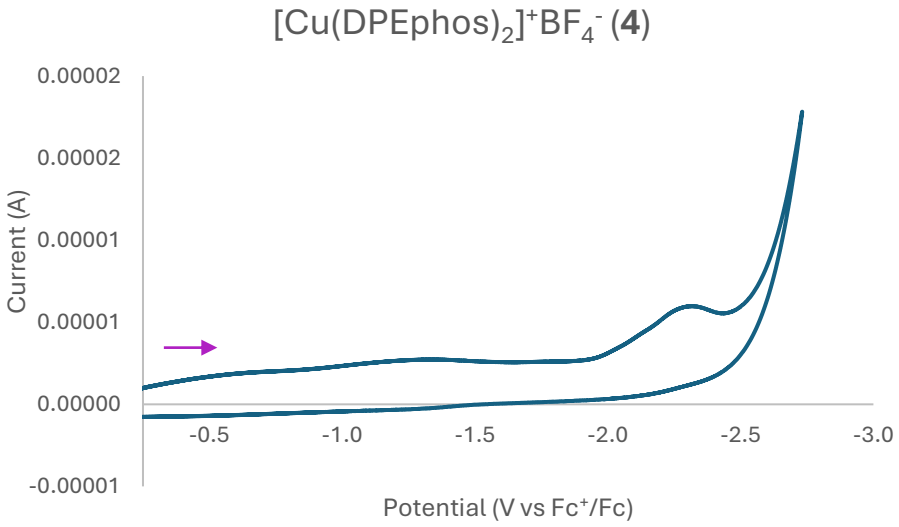

Figure 32. Cyclic voltammetry of $[Cu(DPEphos)_2]^+BF_4^-$ (**4**) in DCE at a scan rate 100 mVs^{-1}. Right: from -0.25 V to -3.0 V.

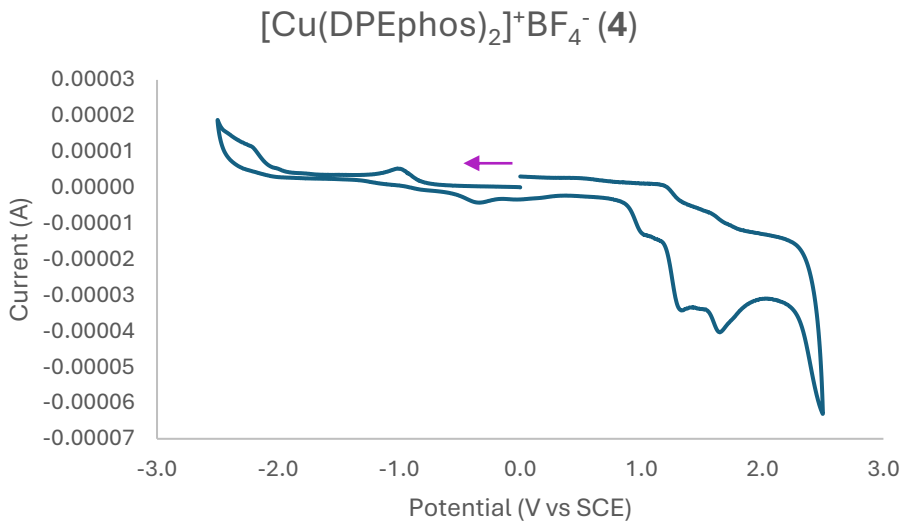

Figure 33. Cyclic voltammetry of $[Cu(DPEphos)_2]^+BF_4^-$ (**4**) in MeCN at a scan rate 100 mVs^{-1}. Right: from -3.0 V to +3.0 V.

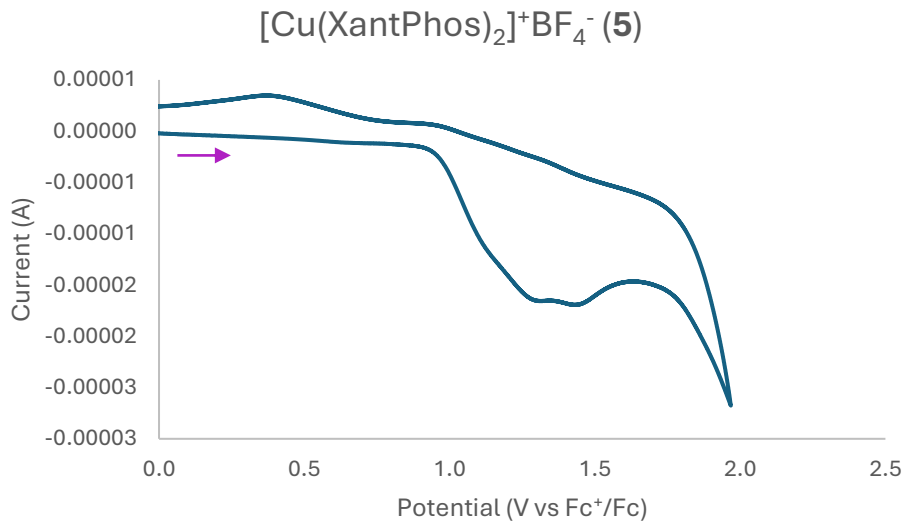

Figure 34. Cyclic voltammetry of $[Cu(XantPhos)_2]^+BF_4^-$ (**5**) in DCE at a scan rate 100 mVs^{-1}. Right: from 0 V to +2.5 V.

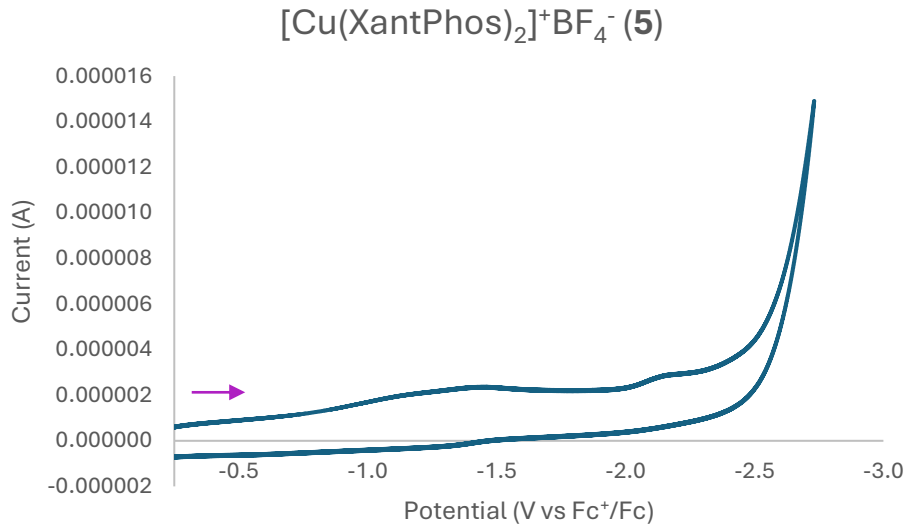

Figure 35. Cyclic voltammetry of $[Cu(XantPhos)_2]^+BF_4^-$ (**5**) in DCE at a scan rate 100 mVs^{-1}. Right: from -0.25 V to -3.0 V.

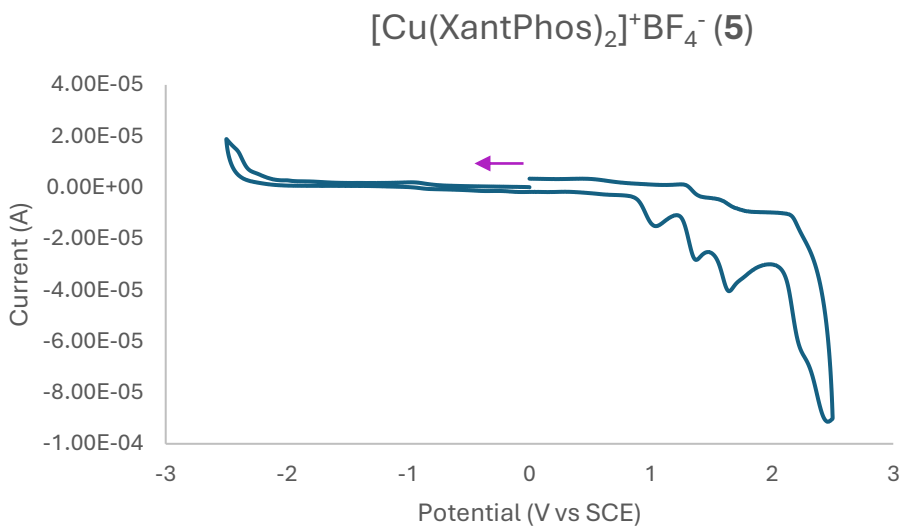

Figure 36. Cyclic voltammetry of $[Cu(XantPhos)_2]^+BF_4^-$ (**5**) in MeCN at a scan rate 100 mVs^{-1}. Right: from -3.0 V to +3.0 V.

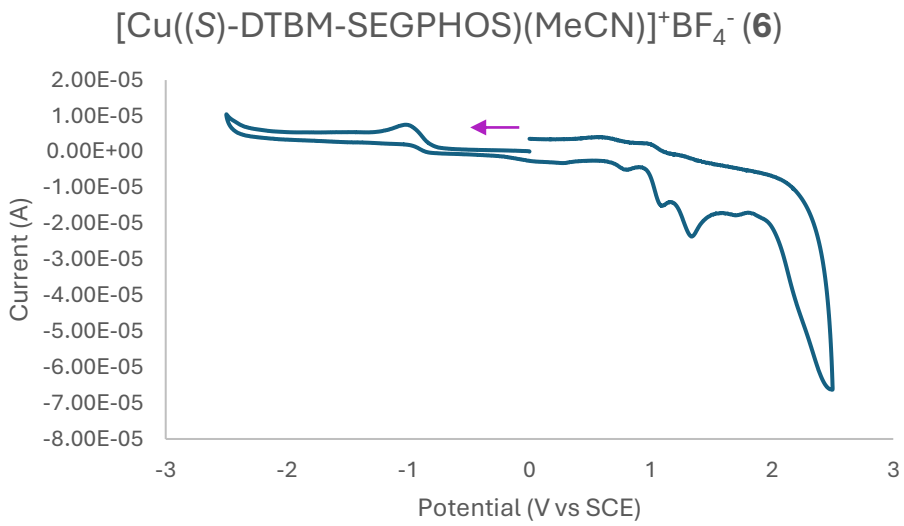

Figure 37. Cyclic voltammetry of $[Cu((S)\text{-DTBM-SEGPHOS})(MeCN)]^+BF_4^-$ (**6**) in MeCN at a scan rate of 100 mVs^{-1}.
Right: from -3.0 V to +3.0 V.

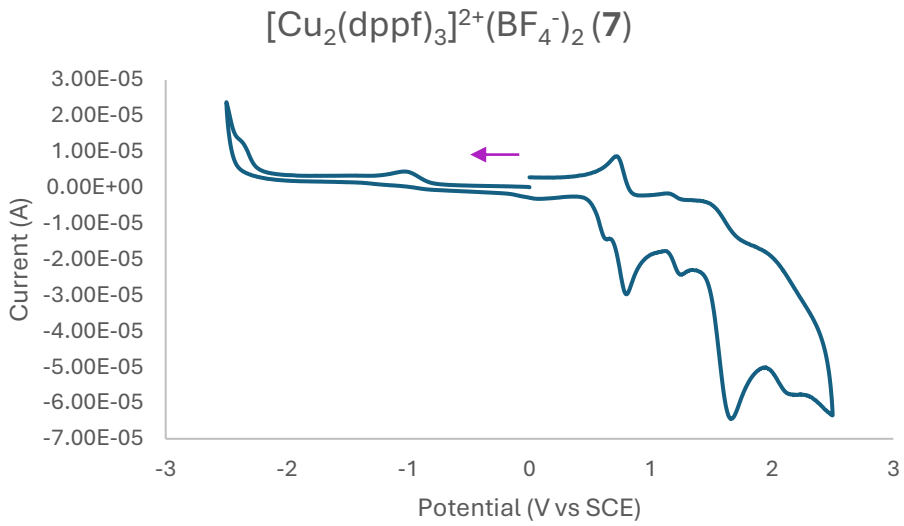

Figure 38. Cyclic voltammetry of $[Cu_2(dppf)_3]^{2+}(BF_4^-)_2$ (**7**) in MeCN at a scan rate 100 mVs^{-1}. Right: from -3.0 V to +3.0 V.

UV-vis Absorption Spectra

The UV-absorption experiments were carried out with 2.5 x 10^{-5} M of copper complexes in DCE. Note: a small peak at ~370 nm is a result of an artifact from the spectrometer that appeared even in the blank.

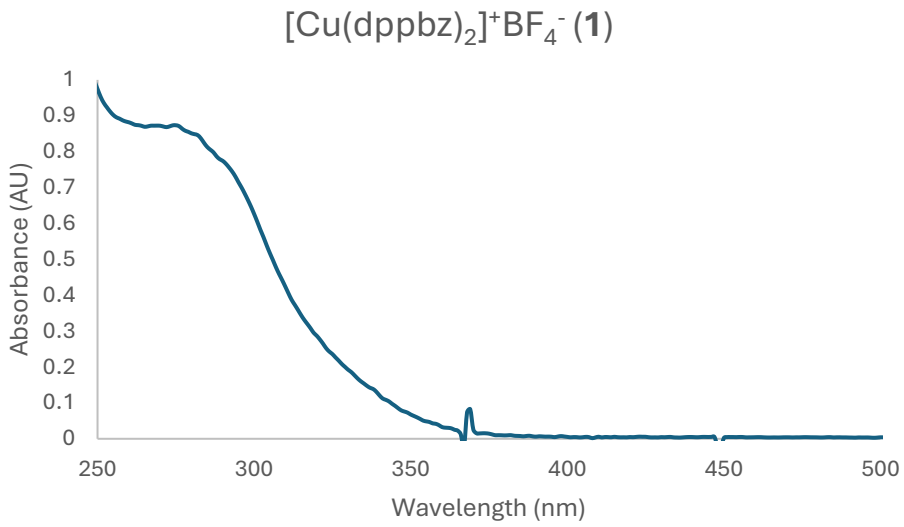

Figure 39. UV-vis spectroscopic absorption of $[Cu(dppbz)_2]^+BF_4^-$ (**1**)

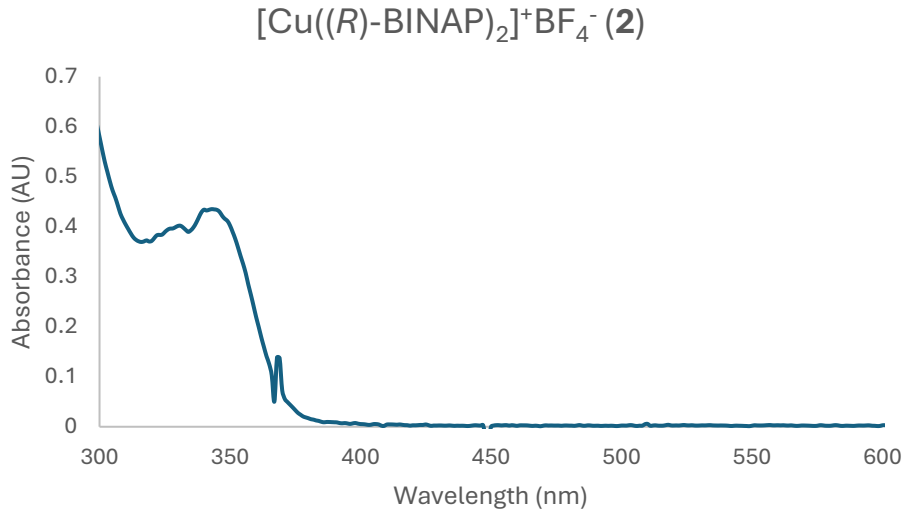

Figure 40. UV-vis spectroscopic absorption of $[Cu((R)\text{-BINAP})_2]^+BF_4^-$ (**2**)

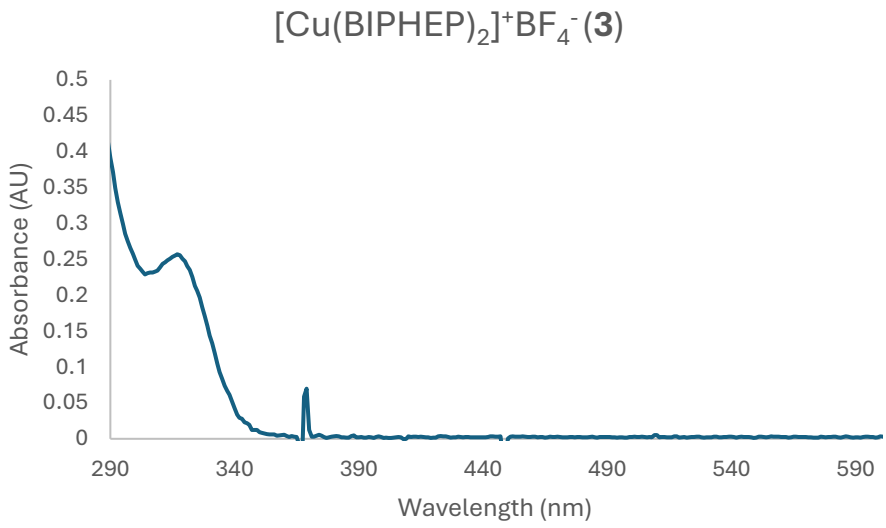

Figure 41. UV-vis spectroscopic absorption of $[Cu(BIPHEP)_2]^+BF_4^-$ (**3**)

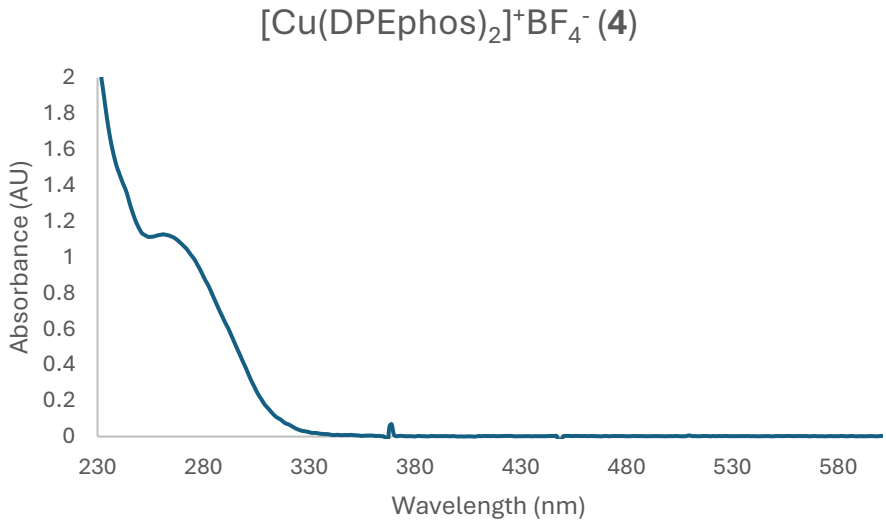

Figure 42. UV-vis spectroscopic absorption of $[Cu(DPEphos)_2]^+BF_4^-$ (**4**)

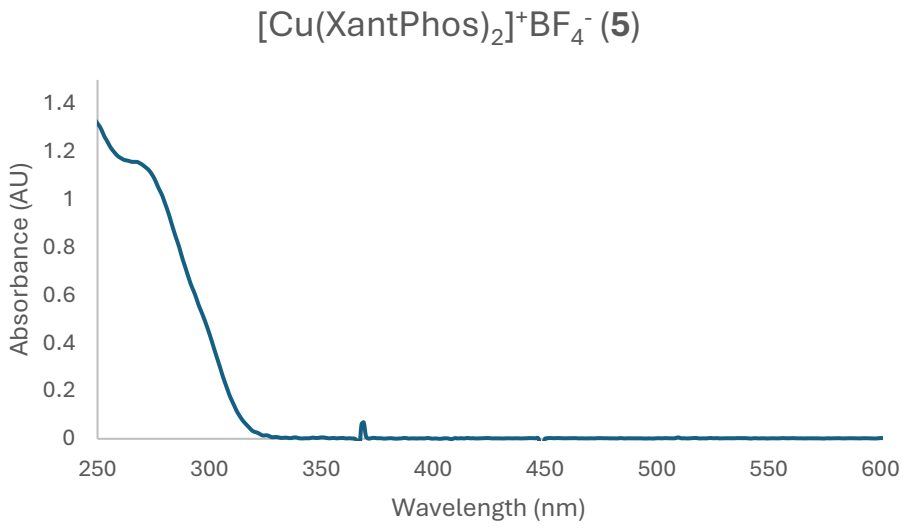

Figure 43. UV-vis spectroscopic absorption of $[Cu(XantPhos)_2]^+BF_4^-$ (**5**)

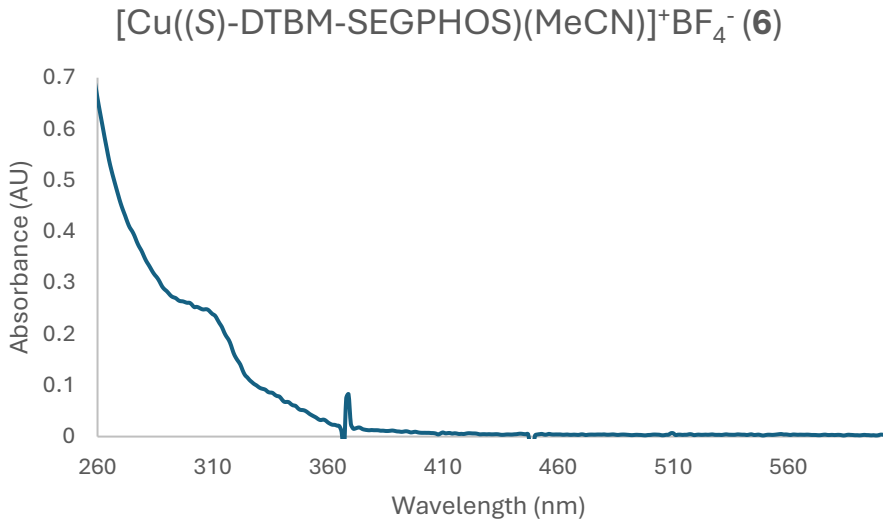

Figure 44. UV-vis spectroscopic absorption of $[Cu((S)\text{-DTBM-SEGPHOS})(MeCN)]^+BF_4^-$ (**6**)

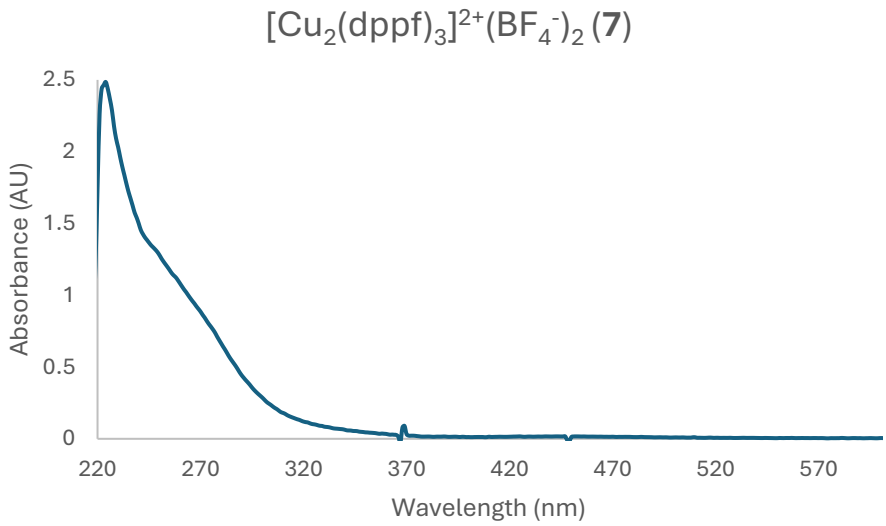

Figure 45. UV-vis spectroscopic absorption of $[Cu_2(dppf)_3]^{2+}(BF_4^-)_2$ (**7**)

Emission Spectra

The emission experiments were performed on a F-7000 FL Spectrophotometer (Hitachi). The measurement were carried out with 2.5 x 10^{-4} M of copper complexes in DCE.

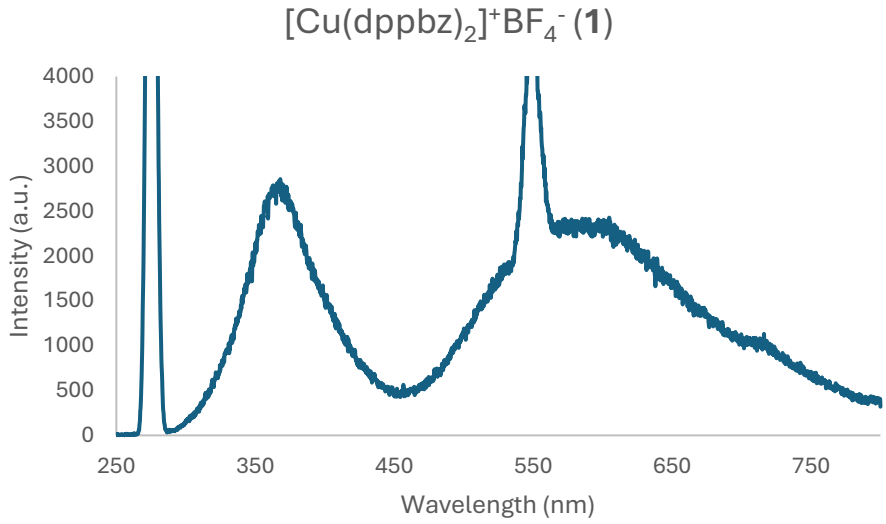

Figure 46. Emission spectrum of $[Cu(dppbz)_2]^+BF_4^-$ (**1**) (λ_{ex} = 276 nm)

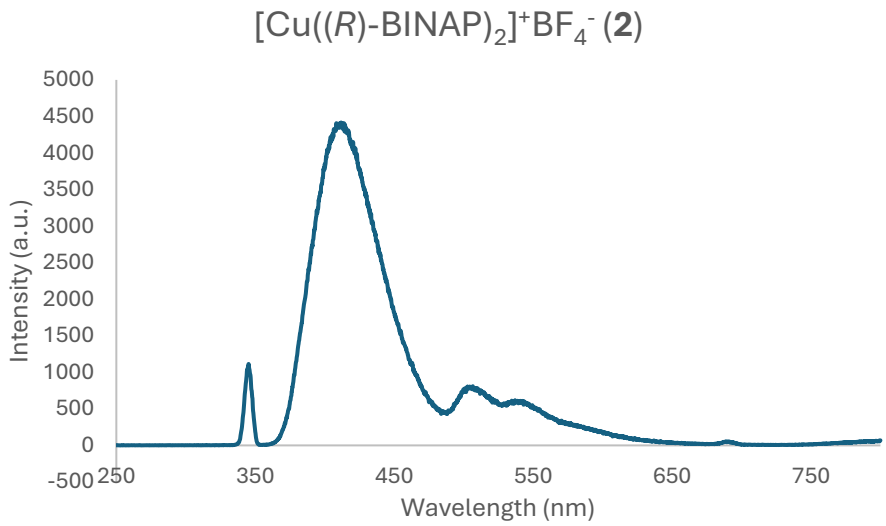

Figure 47. Emission spectrum of $[Cu((R)\text{-}BINAP)_2]^+BF_4^-$ (**2**) (λ_{ex} = 343 nm)

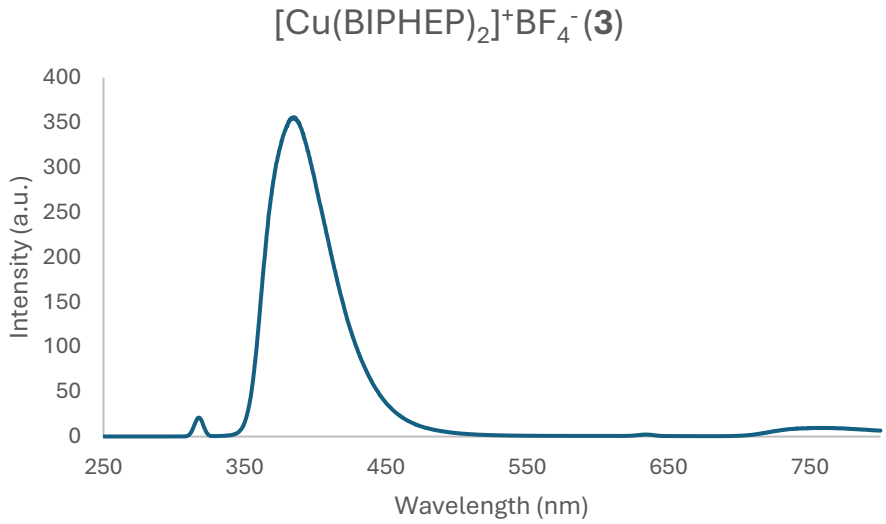

Figure 48. Emission spectrum of $[Cu(BIPHEP)_2]^+BF_4^-$ (**3**) (λ_{ex} = 317 nm)

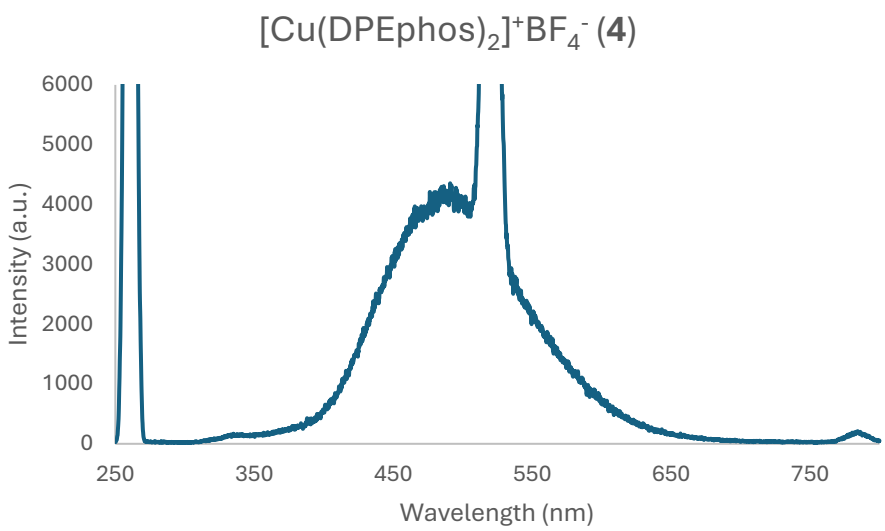

Figure 49. Emission spectrum of $[Cu(DPEphos)_2]^+BF_4^-$ (**4**) (λ_{ex} = 261 nm)

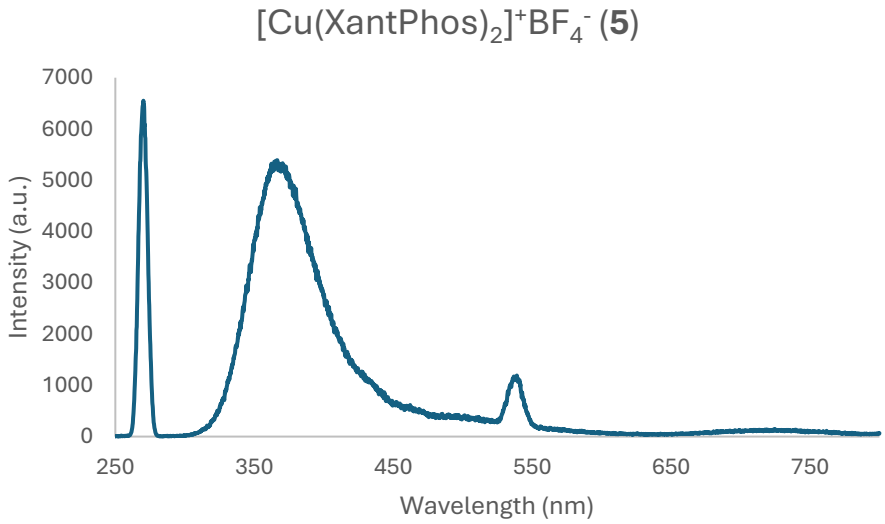

Figure 50. Emission spectrum of $[Cu(XantPhos)_2]^+BF_4^-$ (**5**) (λ_{ex} = 270 nm)

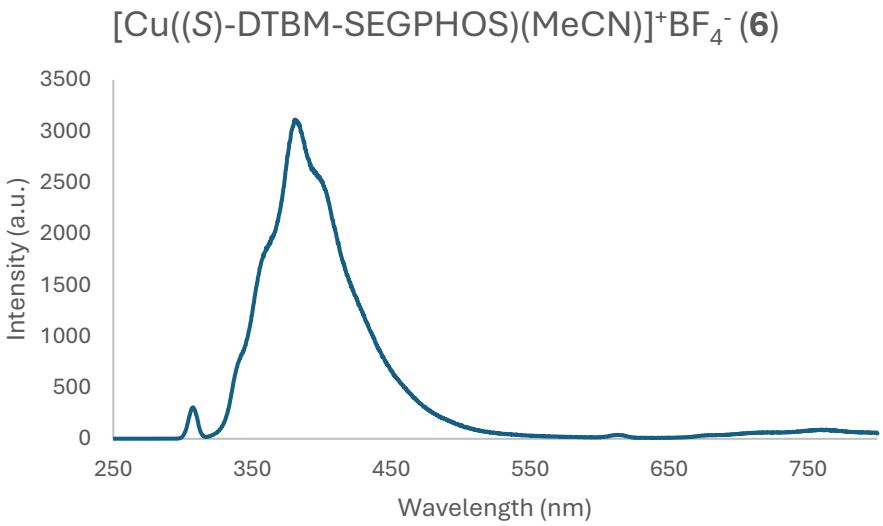

Figure 51. Emission spectrum of [Cu((*S*)-DTBM-SEGPHOS)(MeCN)]$^{+}BF_4^{-}$ (**6**) (λ_{ex} = 307 nm)

Measurements of Emission Decay

Emission and excitation spectra were measured on an Edinburgh Instruments FLS1000 Photoluminescence Spectrometer. Emission decay profiles were obtained using an Edinburgh Instruments FLS1000 Photoluminescence Spectrometer with the EPL series picosecond pulsed diode laser.

Table 18. Emission lifetimes fitted from the emission decays of the Cu complexes **1**–**5** in solution.

Entry	λ_{ex}[a]	λ_{em}[b]	τ_1 / ns (A_1 / -)	τ_2 / ns (A_2 / -)	τ_3 / ns (A_3 / -)	τ_{av} / ns[c]	χ^2
	375	433	1.436 (0.91)	12.7827 (0.09)	-	2.4853	1.0026
1	375	441	1.446 (0.91)	13.2695 (0.09)	-	2.4908	1.1602
	390	538	1453.4 (0.42)	10017.2 (0.27)	75137 (0.31)	26429.8	1.0034
	375	433	0.0900 (0.64)	2.0647 (0.15)	12.4768 (0.20)	2.9079	1.0783
	375	441	0.0904 (0.61)	1.9228 (0.18)	12.2114 (0.19)	2.7682	1.1142
2	375	473	0.1378 (0.40)	1.9631 (0.46)	12.1271 (0.14)	2.6643	1.1353
	390	598	2072.2782 (0.51)	9961.2076 (0.38)	62788.0384 (0.11)	11778.6943	1.0021
3	375	432	1.3787 (0.81)	2.3205 (0.12)	14.9311 (0.07)	2.4848	1.1186

	375	441	1.4589 (0.93)	13.1968 (0.07)	-	2.2228	1.0088
	375	455	1.4755 (0.94)	12.2857 (0.06)	-	2.0975	1.0776
	375	512	0.8401 (0.21)	1.7505 (0.74)	11.6023 (0.05)	2.0329	1.1252
	375	430	1.3717 (0.36)	5.7109 (0.33)	14.3693 (0.31)	6.7798	1.0442
	375	441	1.2961 (0.38)	5.0670 (0.30)	14.1484 (0.32)	6.5024	1.1376
4	375	456	1.6681 (0.40)	9.3746 (0.51)	24.5619 (0.09)	7.5972	1.1934
	390	509	2284.7981 (0.46)	9492.5896 (0.41)	65452.1801 (0.13)	13228.5234	1.0027
	375	432	1.5477 (0.23)	12.8115 (0.77)	-	10.2277	1.068
	375	441	1.4981 (0.26)	12.7874 (0.74)	-	9.8648	1.0598
5	375	468	1.3597 (0.23)	11.4131 (0.67)	18.4121 (0.10)	9.7627	1.0752
	390	517	1557.3953 (0.28)	8459.1394 (0.50)	68214.8935 (0.22)	19733.2168	1.0052

[a]Irradiated light wavelength. [b]Monitored wavelength. [c]$\tau_{av} = \Sigma\tau_n A_n$. All emission decay was fitted by tail fitting.

$[Cu(dppbz)_2]^+BF_4^-$ (1)

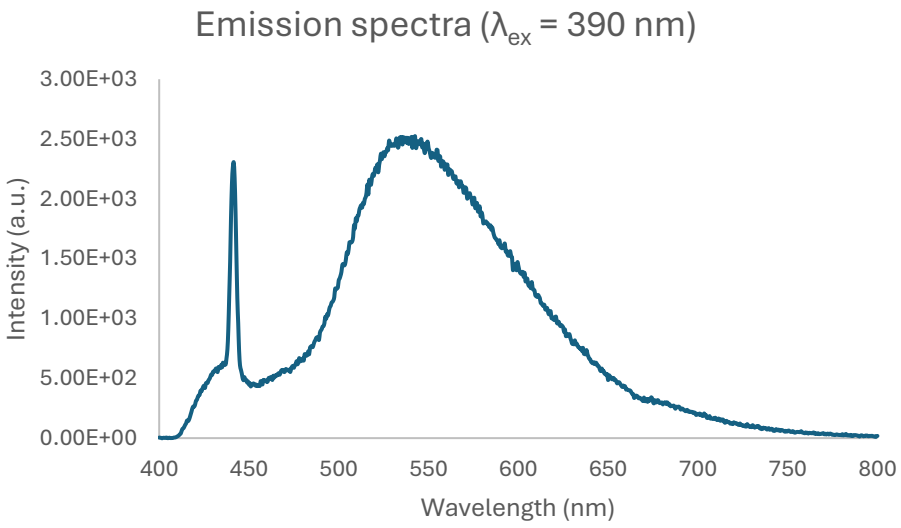

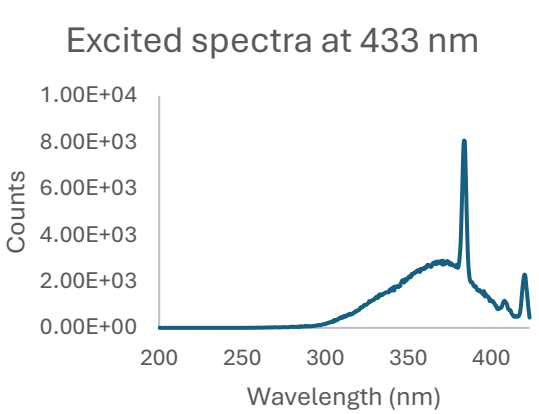
Excited spectra at 433 nm
1.00E+04
8.00E+03
6.00E+03
4.00E+03
2.00E+03
0.00E+00
Counts
200
250
300
350
400
Wavelength (nm)

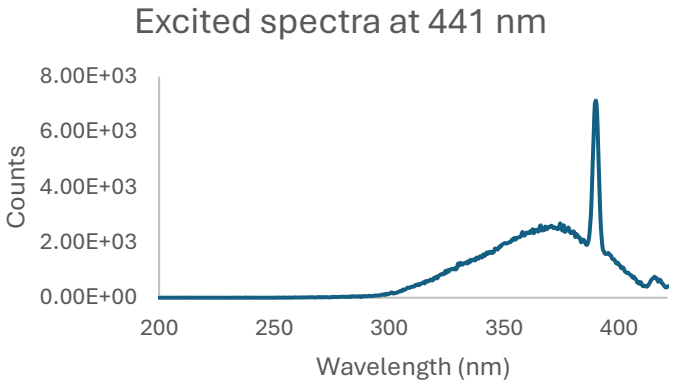
Excited spectra at 441 nm
8.00E+03
6.00E+03
4.00E+03
2.00E+03
0.00E+00
Counts
200
250
300
350
400
Wavelength (nm)

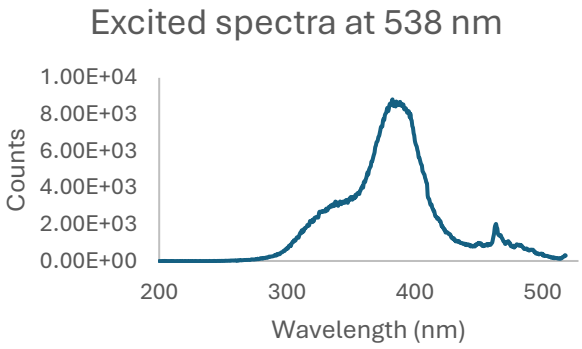
Excited spectra at 538 nm
1.00E+04
8.00E+03
6.00E+03
4.00E+03
2.00E+03
0.00E+00
Counts
200
300
400
500
Wavelength (nm)

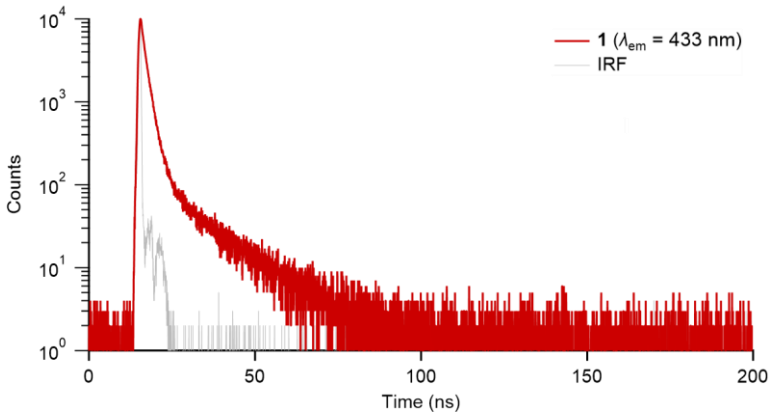
1 (λem = 433 nm)
IRF
Counts
Time (ns)
0
50
100
150
200

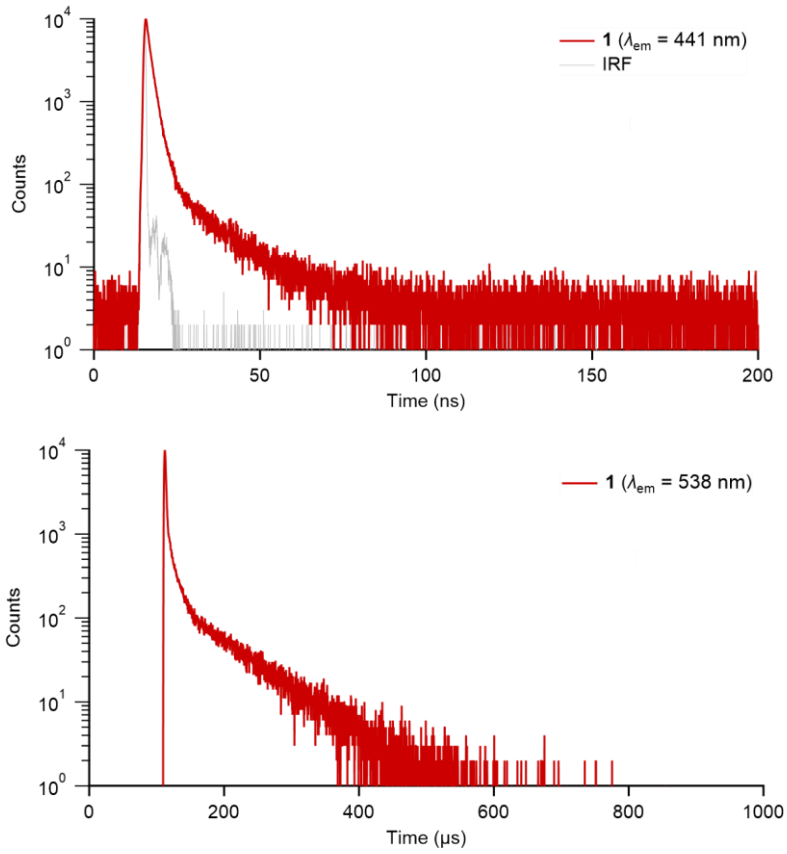

[Cu((*R*)-BINAP)$_2$]$^+$BF$_4^-$ (2)

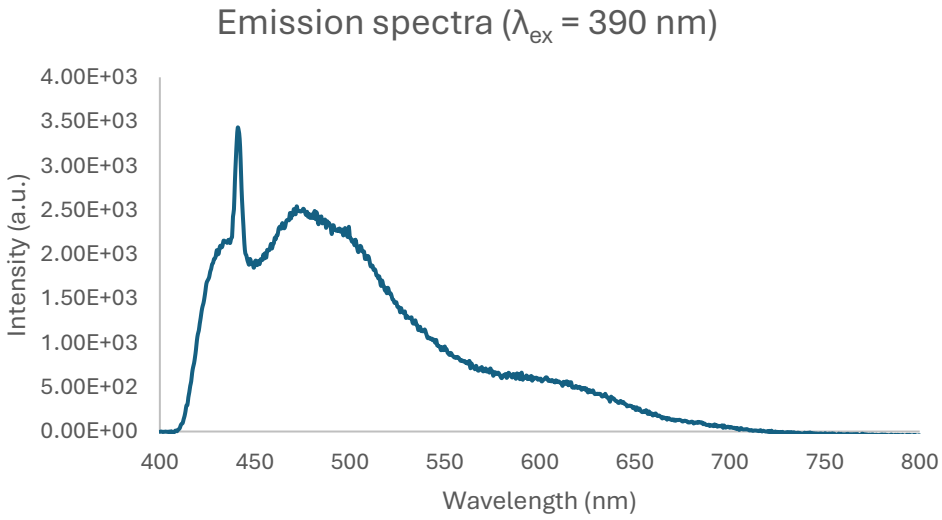

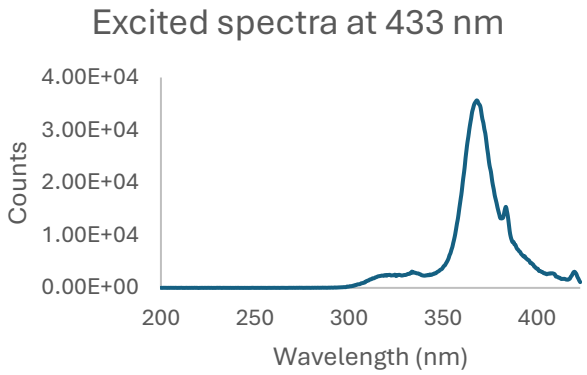
Excited spectra at 433 nm
Counts
4.00E+04
3.00E+04
2.00E+04
1.00E+04
0.00E+00
200
250
300
350
400
Wavelength (nm)

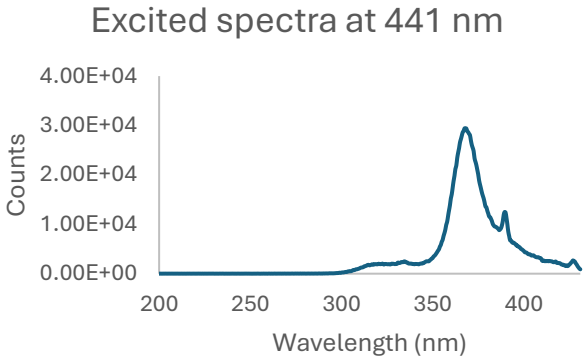
Excited spectra at 441 nm
Counts
4.00E+04
3.00E+04
2.00E+04
1.00E+04
0.00E+00
200
250
300
350
400
Wavelength (nm)

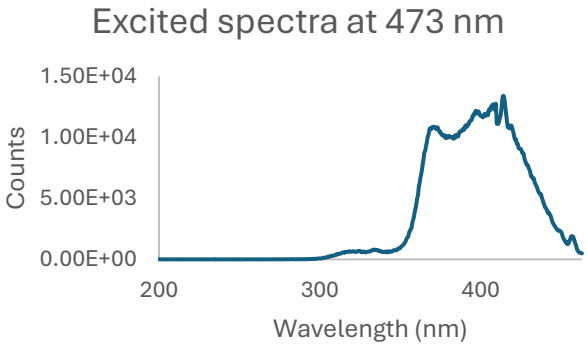
Excited spectra at 473 nm
Counts
1.50E+04
1.00E+04
5.00E+03
0.00E+00
200
300
400
Wavelength (nm)

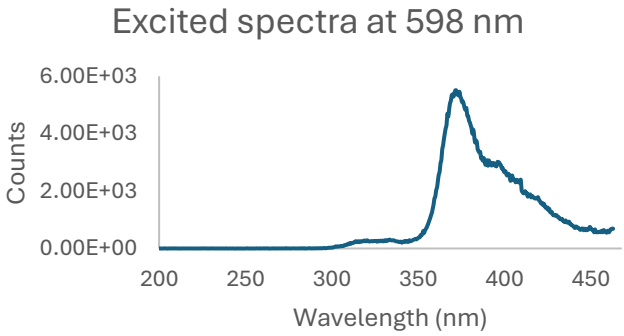
Excited spectra at 598 nm
Counts
6.00E+03
4.00E+03
2.00E+03
0.00E+00
200
250
300
350
400
450
Wavelength (nm)

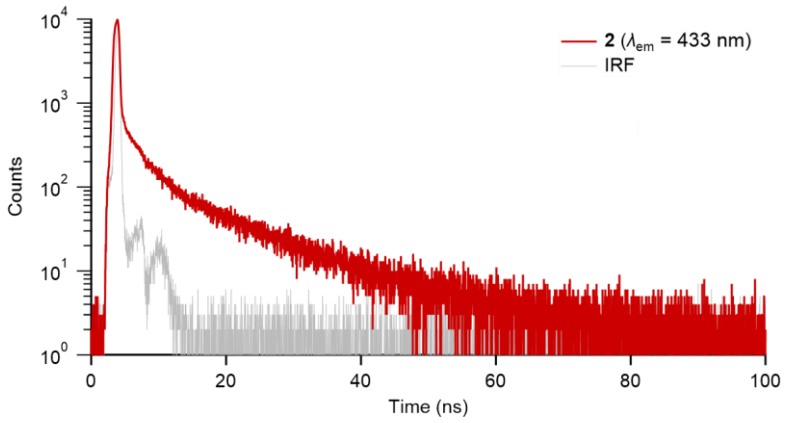
2 (λem = 433 nm)
IRF
Counts
10^4
10^3
10^2
10^1
10^0
0
20
40
60
80
100
Time (ns)

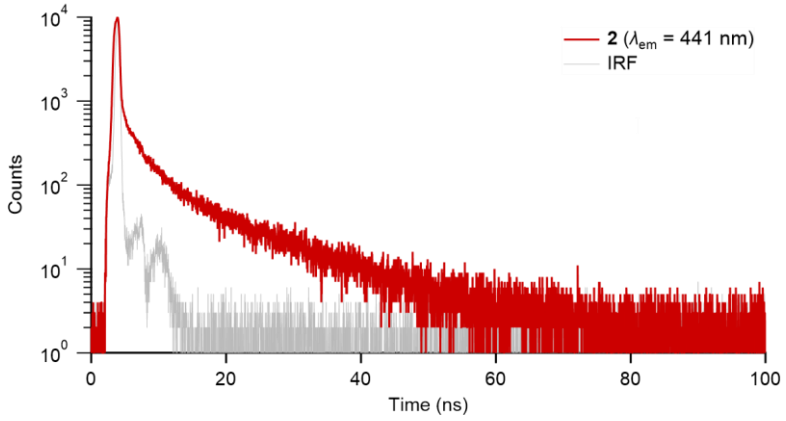
2 (λ_{em} = 441 nm)
IRF
Counts
Time (ns)

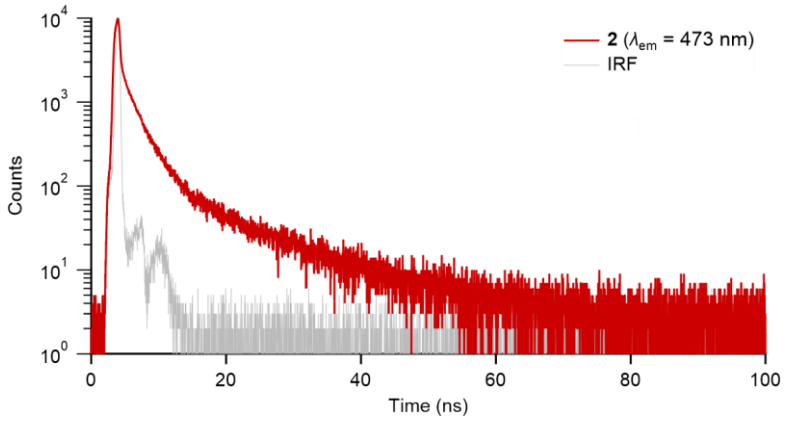
2 (λ_{em} = 473 nm)
IRF
Counts
Time (ns)

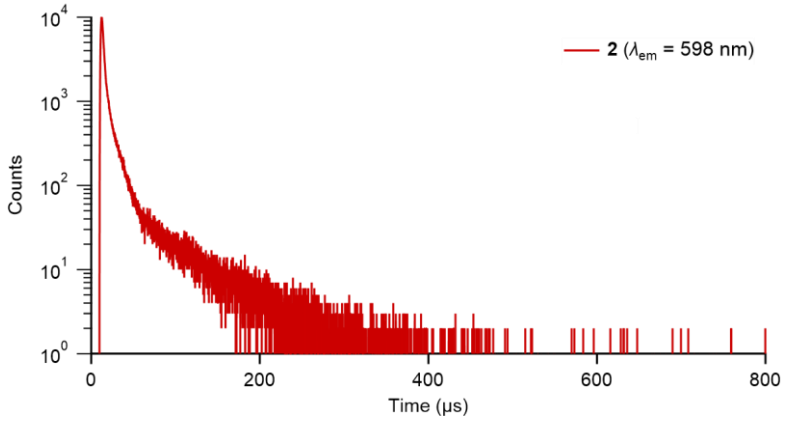
2 (λ_{em} = 598 nm)
Counts
Time (µs)

[Cu(BIPHEP)$_2$]$^+$BF$_4^-$ (3)

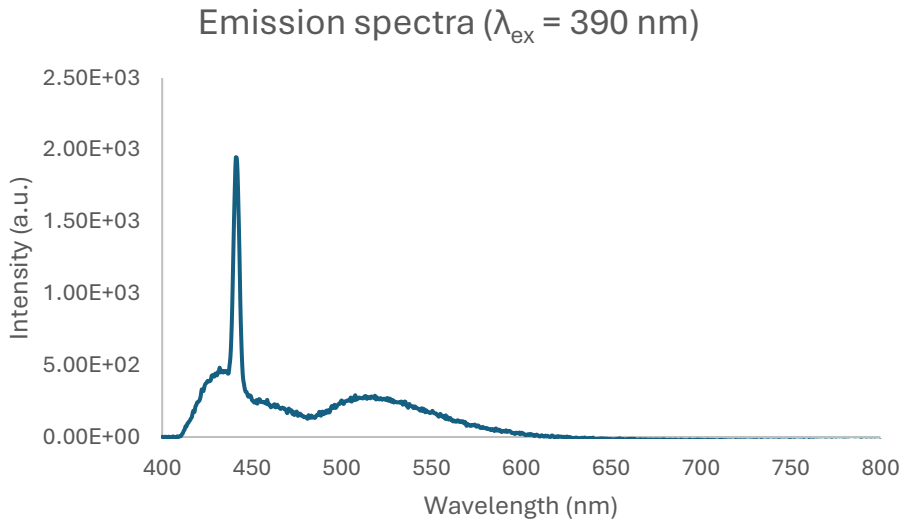

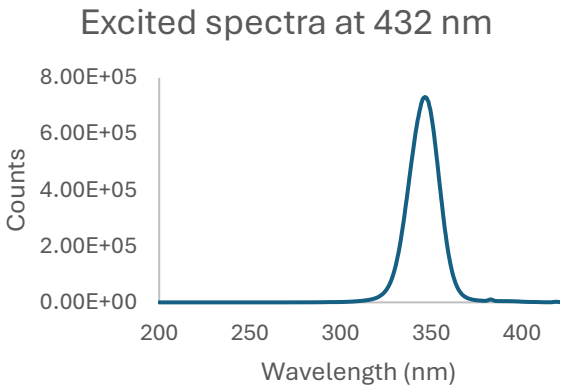

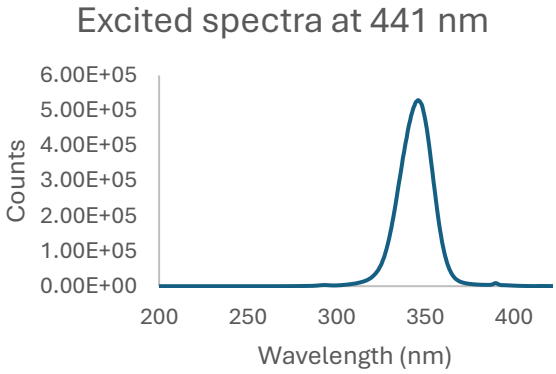

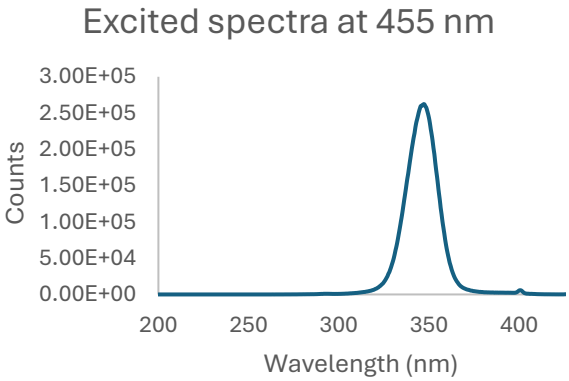

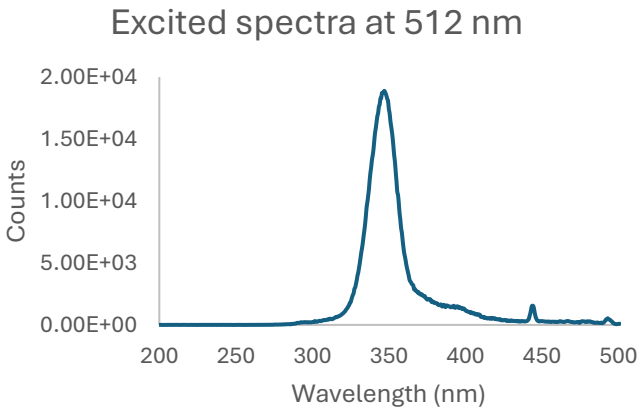

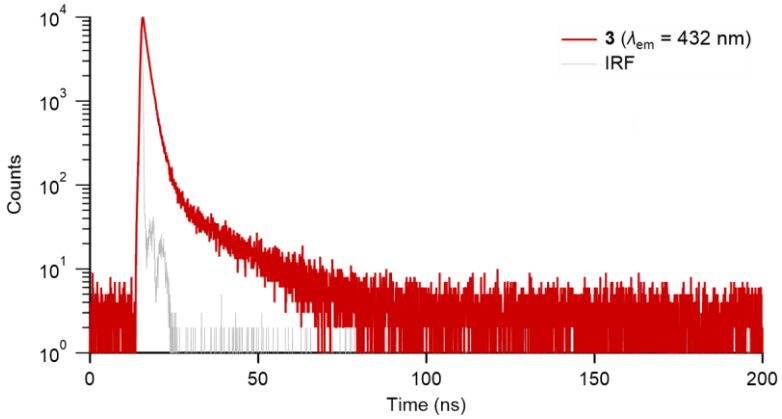
3 (λ_{em} = 432 nm)
IRF
Counts
Time (ns)

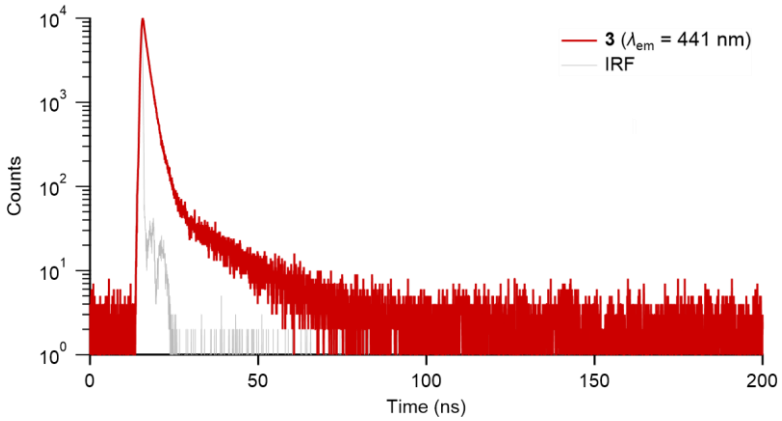
3 (λ_{em} = 441 nm)
IRF
Counts
Time (ns)

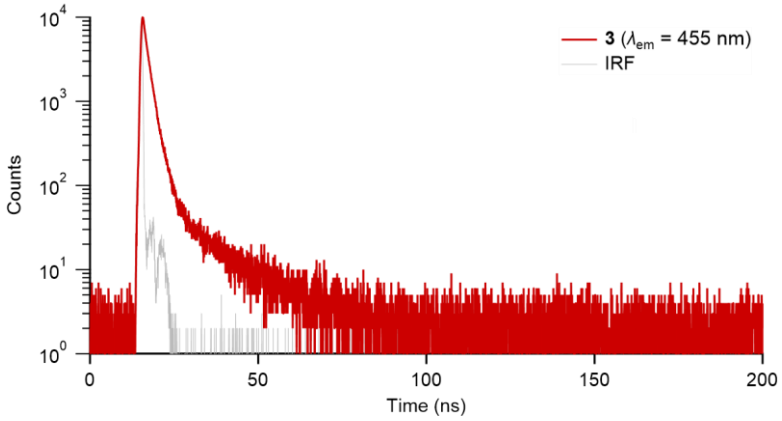
3 (λ_{em} = 455 nm)
IRF
Counts
Time (ns)

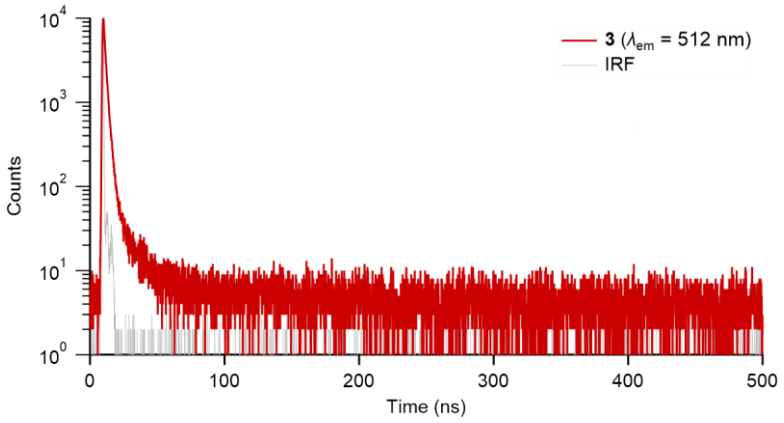

[Cu(DPEphos)$_2$]$^+$BF$_4^-$ (4)

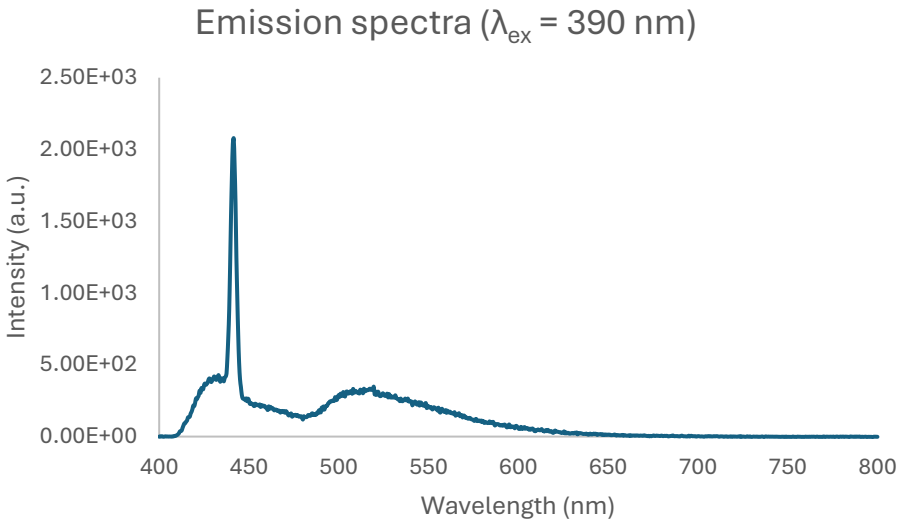

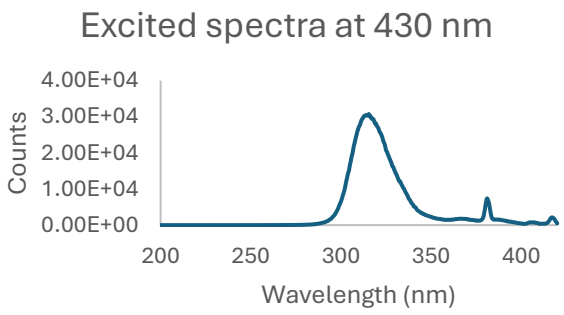

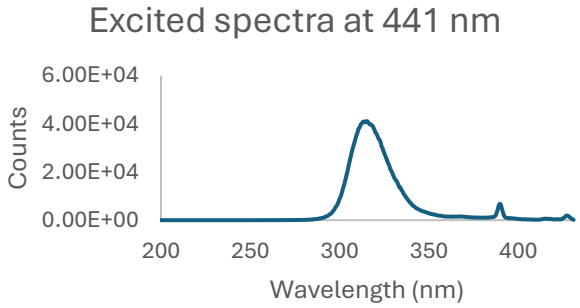

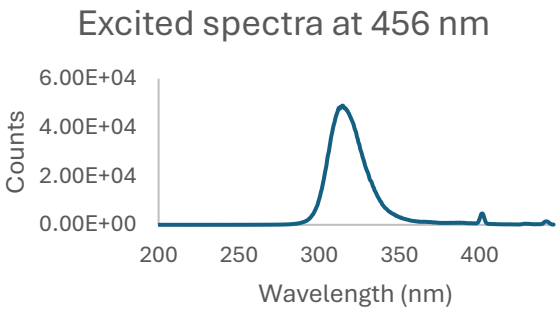
Excited spectra at 456 nm
Counts
6.00E+04
4.00E+04
2.00E+04
0.00E+00
200
250
300
350
400
Wavelength (nm)

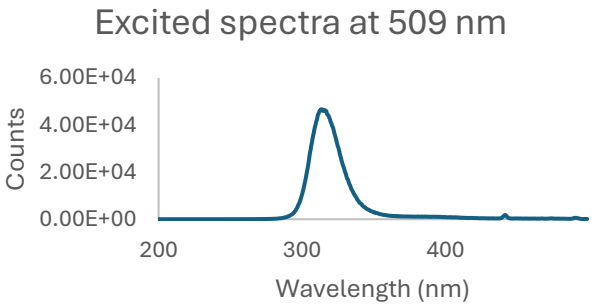
Excited spectra at 509 nm
Counts
6.00E+04
4.00E+04
2.00E+04
0.00E+00
200
300
400
Wavelength (nm)

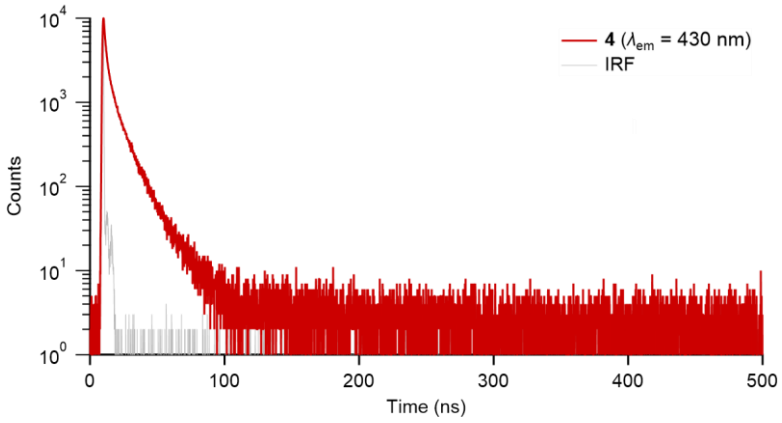
4 (λem = 430 nm)
IRF
Counts
10^4
10^3
10^2
10^1
10^0
0
100
200
300
400
500
Time (ns)

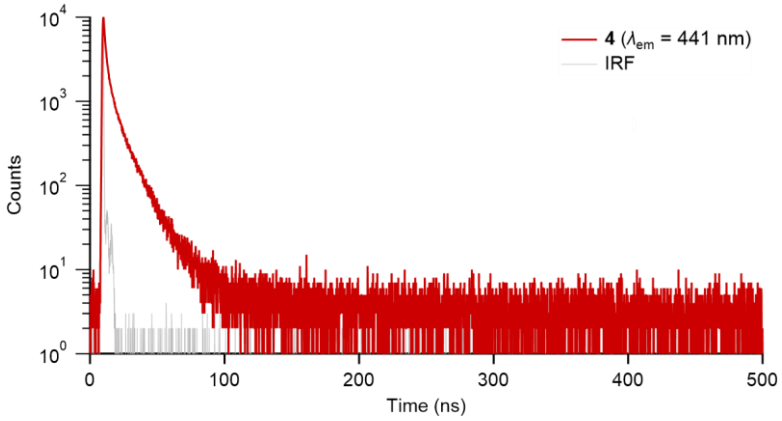
4 (λem = 441 nm)
IRF
Counts
10^4
10^3
10^2
10^1
10^0
0
100
200
300
400
500
Time (ns)

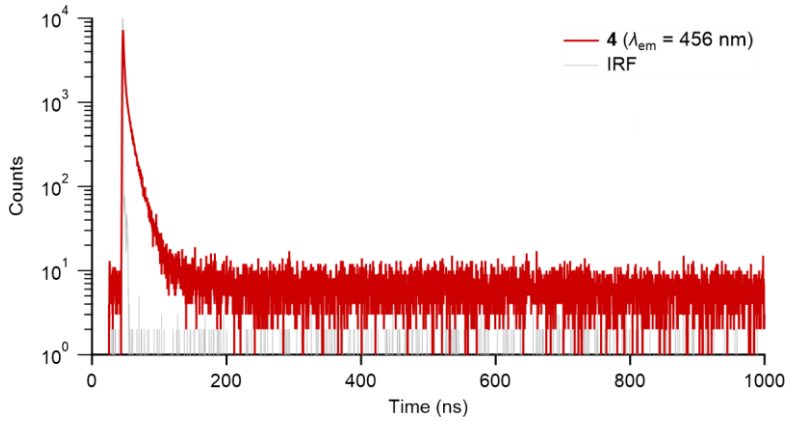

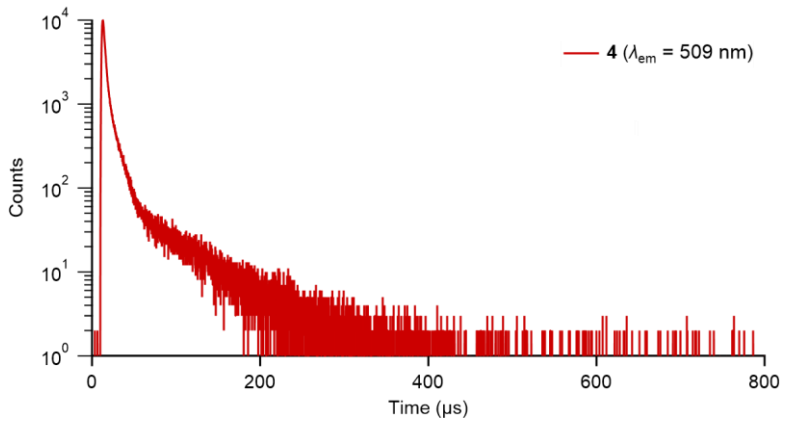

[Cu(XantPhos)$_2$]$^+$BF$_4^-$ (5)

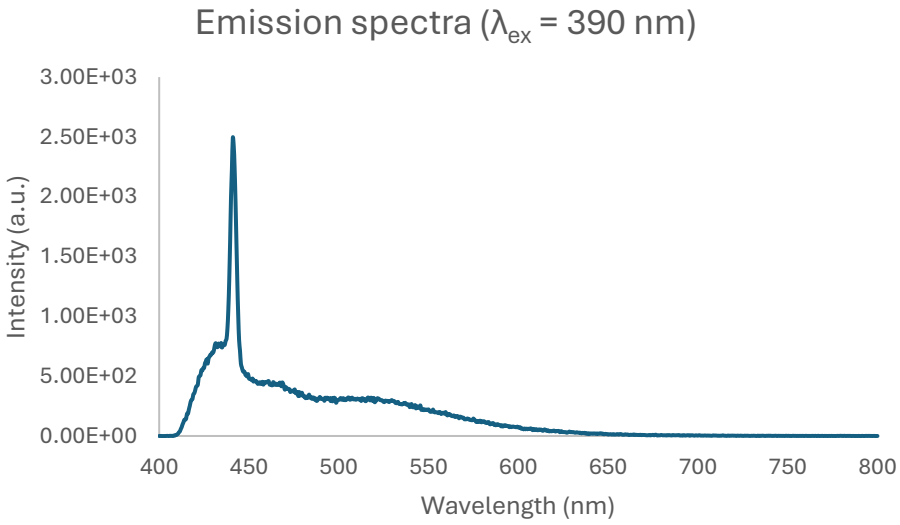

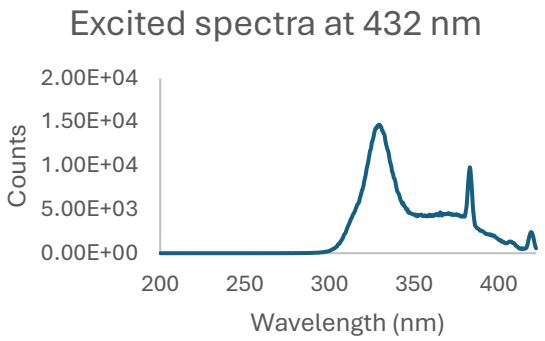
Excited spectra at 432 nm
Counts
2.00E+04
1.50E+04
1.00E+04
5.00E+03
0.00E+00
200
250
300
350
400
Wavelength (nm)

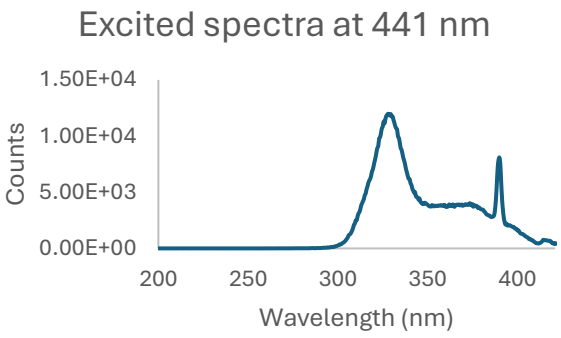
Excited spectra at 441 nm
Counts
1.50E+04
1.00E+04
5.00E+03
0.00E+00
200
250
300
350
400
Wavelength (nm)

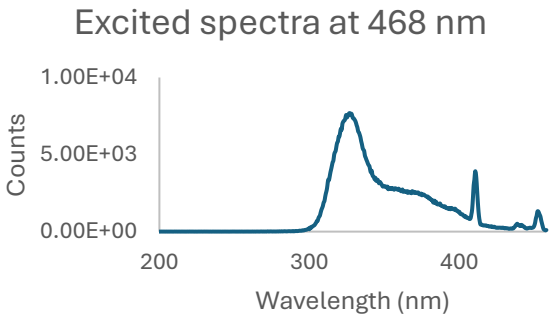
Excited spectra at 468 nm
Counts
1.00E+04
5.00E+03
0.00E+00
200
300
400
Wavelength (nm)

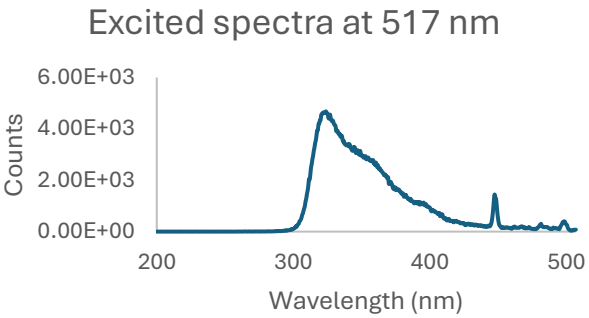
Excited spectra at 517 nm
Counts
6.00E+03
4.00E+03
2.00E+03
0.00E+00
200
300
400
500
Wavelength (nm)

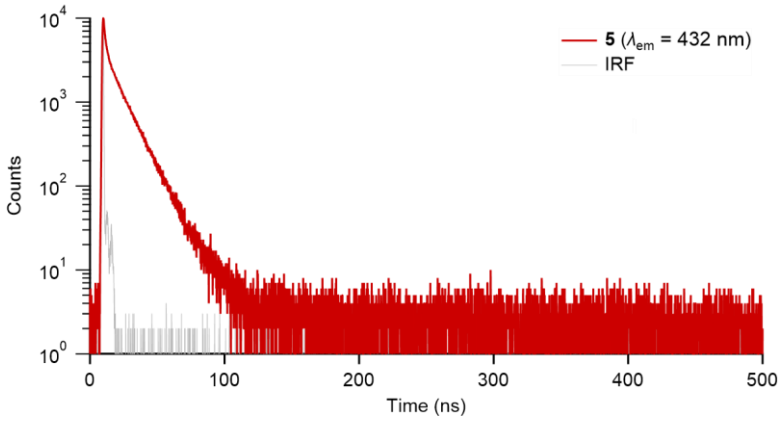
5 (λem = 432 nm)
IRF
Counts
10^4
10^3
10^2
10^1
10^0
0
100
200
300
400
500
Time (ns)

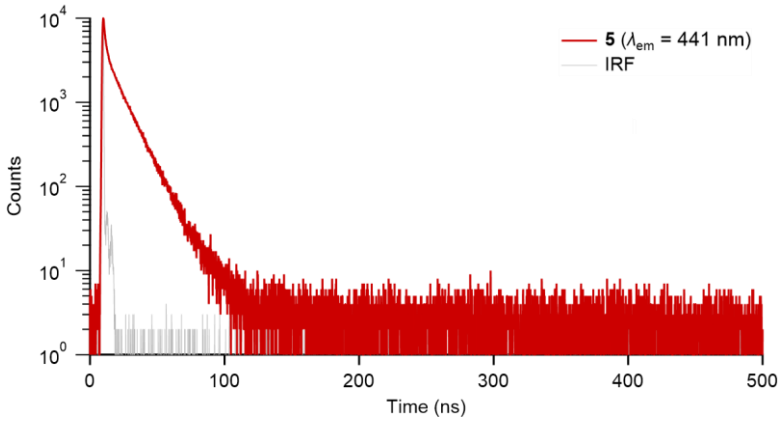
5 (λ_{em} = 441 nm)
IRF
Counts
Time (ns)

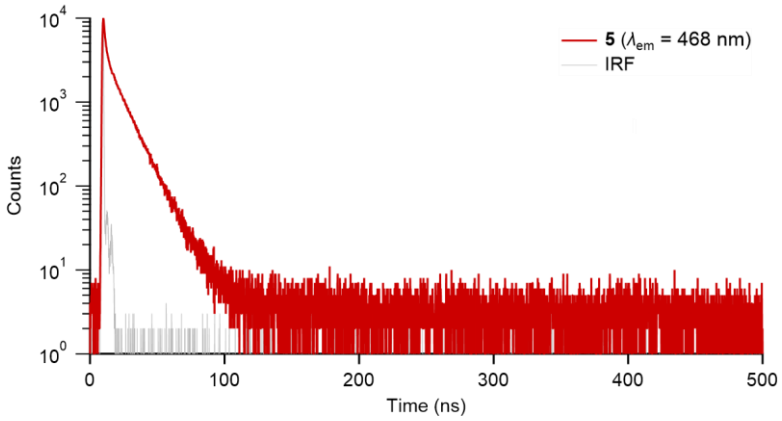
5 (λ_{em} = 468 nm)
IRF
Counts
Time (ns)

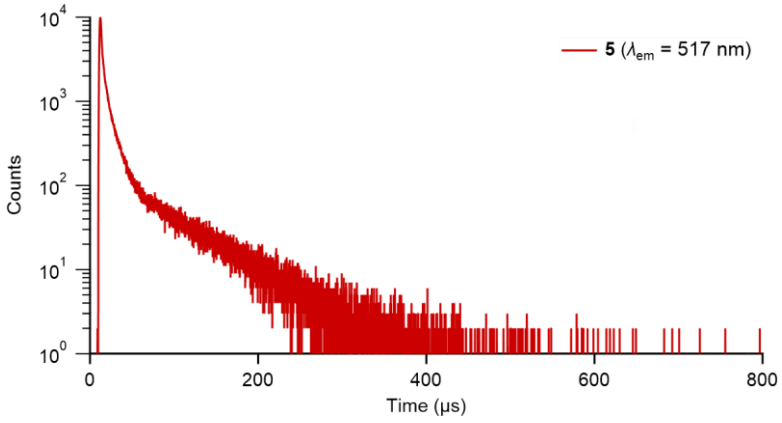
5 (λ_{em} = 517 nm)
Counts
Time (μs)

[Cu((*S*)-DTBM-SEGPHOS)(MeCN)]$^{+}BF_4^{-}$ (6)

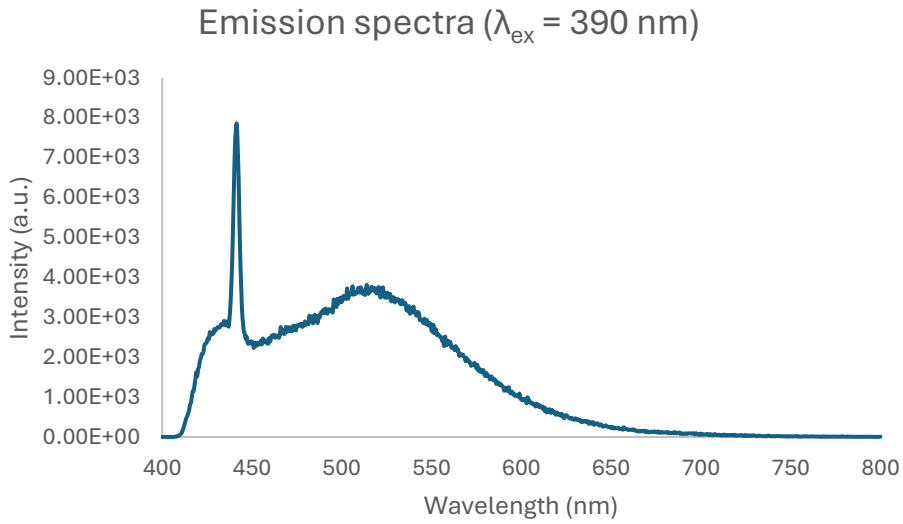

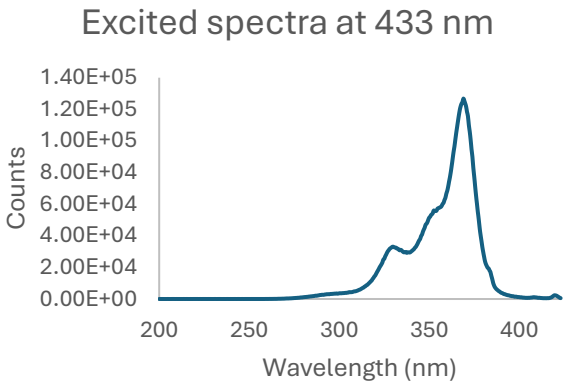

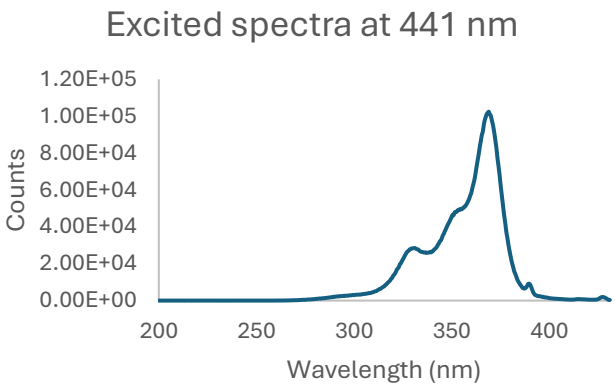

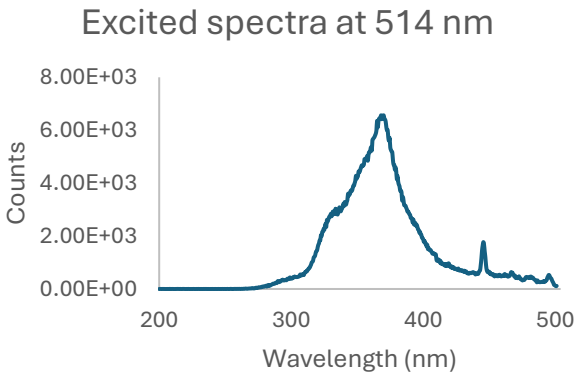

[$Cu_2(dppf)_3]^{2+}(BF_4^-)_2$ (7)

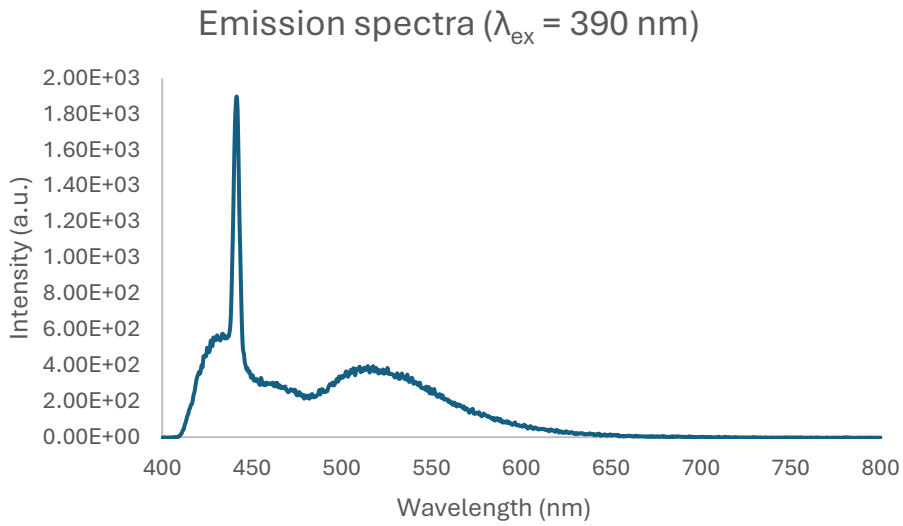

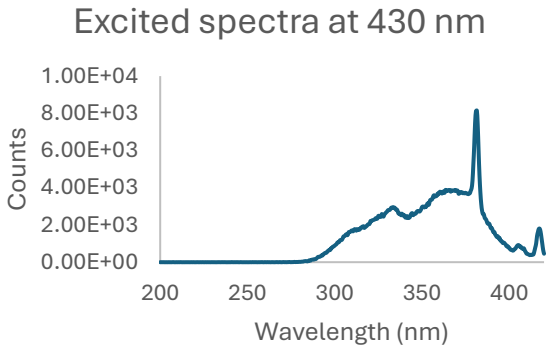

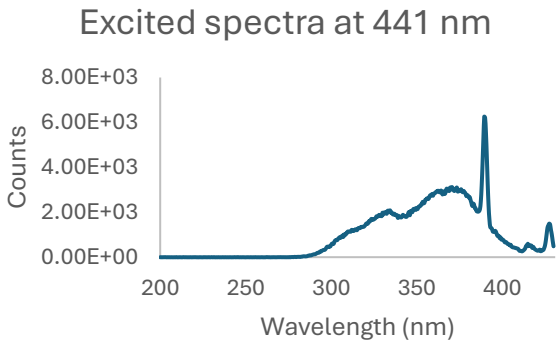

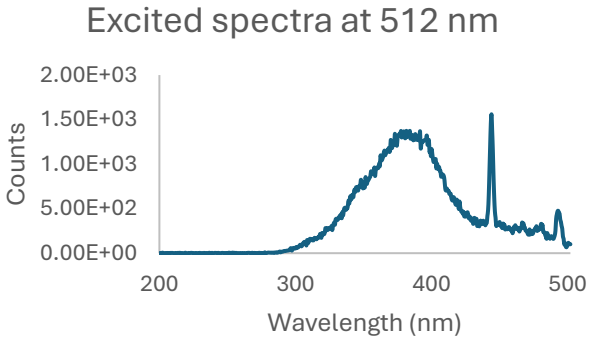

Emission Quenching Studies

Emission spectra were measured on an Edinburgh Instruments FLS1000 Photoluminescence Spectrometer. Quenching experiments were carried out using an 8 x 10^{-4} M solution of $[Cu(dppbz)_2]BF_4$ (**1**) in DCE (excitation wavelength: 390 nm, monitoring wavelength: 568 nm).

Quenching with 4-fluoroiodobenzene (ArI)

ArI concentration	Emission intensity @ 568 nm (I)	I_0/I
0.0000 M	40713	1.00
0.0001 M	34996	1.16
0.0002 M	18606	2.19
0.0010 M	10045	4.05
0.0016 M	8449	4.82

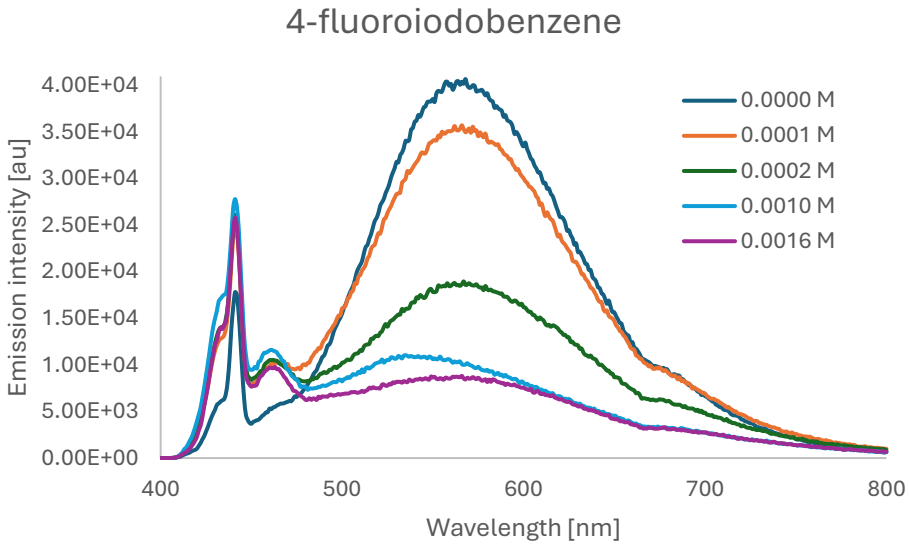

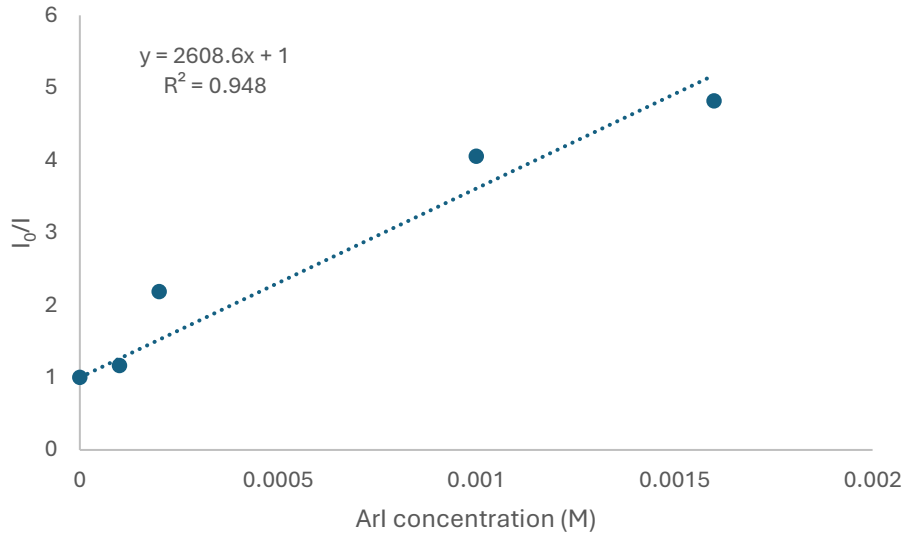

Quenching with DIPEA

DIPEA concentration	Emission intensity @ 568 nm (I)	I_0/I
0.0000 M	40713	1.00
0.0001 M	25376	1.60
0.0002 M	15631	2.60
0.0010 M	12712	3.20
0.0020 M	7810	5.21

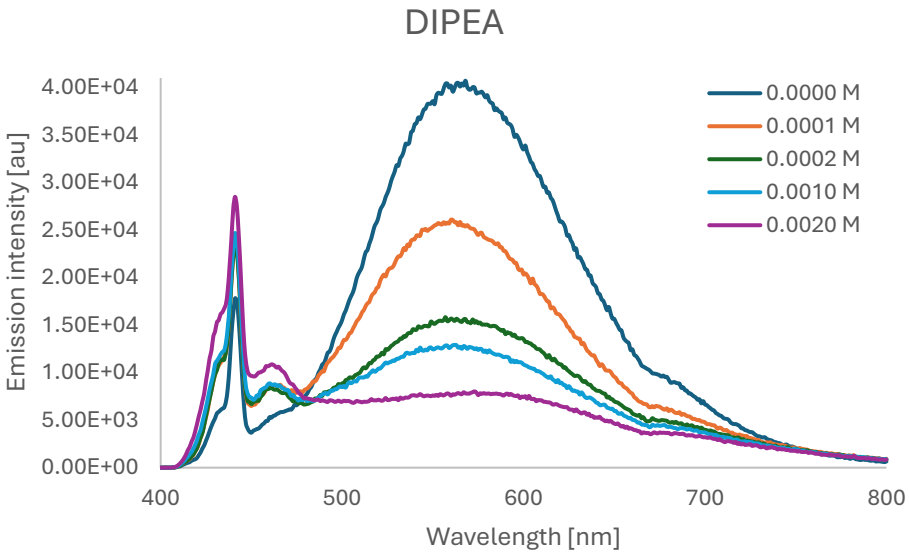

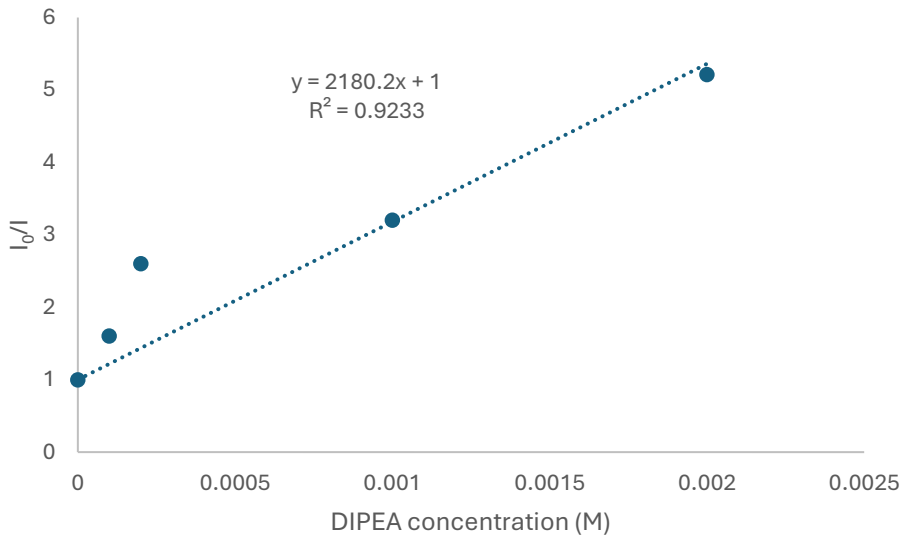

X-ray Single Crystal Analysis of CuP

Single-crystal X-ray diffraction (XRD) analyses were carried out on a Rigaku XtaLAB Synergy diffractometer using graphite monochromated Cu-Kα radiation. The structures were solved with the SHELXT structure solution program using Intrinsic Phasing incorporated in the OLEX2 program package[72] and refined with the SHELXL package[73]. Hydrogen atoms were refined using the riding model. The crystal data parameters are given in **Table 19** & **20**, and the crystal structures are shown in **Figure 52~56.**

Complex	Crystallization method
$[Cu(dppbz)_2]^+BF_4^-$ (**1**)	vapor diffusion of hexane to **1** in EtOAc solution
$[Cu(BIPHEP)_2]^+BF_4^-$ (**3**)	vapor diffusion of hexane to **3** in 20/3 EtOAc/acetone solution
$[Cu(DPEphos)_2]^+BF_4^-$ (**4**)	vapor diffusion of hexane to **4** in CH_2Cl_2 solution
$[Cu(XantPhos)_2]^+BF_4^-$ (**5**)	vapor diffusion of hexane to **5** in 20/3 EtOAc/acetone solution
$[Cu_2(dppf)_3]^{2+}(BF_4^-)_2$ (**7**)	vapor diffusion of hexane to **7** in CH_2Cl_2 solution

[72]Dolomanov, O.V.; Bourhis, L.J.; Gildea, R.J.; Howard, J.A.K; Puschmann, H.J. *Appl. Crystallogr.* **2009**, *42*, 339-341.
[73]Sheldrick, G. M. *Acta Crystallogr., Sect. A.* **2015**, *71*, 3-8.

Table 19. Summary of X-ray crystallographic data of the crystals **1**, **3**, and **4**.

compound	$[Cu(dppbz)_2]BF_4$ (**1**)	$[Cu(BIPHEP)_2]BF_4$ (**3**)	$[Cu(DPEphos)_2]BF_4$ (**4**)
CCDC Number	2445751	2445749	2445750
Empirical Formula	$C_{60}H_{48}BCuF_4P_4$	$C_{75}H_{62}BCuF_4OP_4$	$C_{72}H_{56}BCuF_4O_2P_4$
Formula Weight	1043.21	1253.47	1227.39
Crystal System	monoclinic	monoclinic	orthorhombic
Crystal Size / mm	0.2 × 0.2 × 0.1	0.1 × 0.1 × 0.1	0.1 × 0.1 × 0.1
a / Å	13.55730(10)	13.19360(10)	20.13810(10)
b / Å	12.57930(10)	22.87260(10)	24.51420(10)
c / Å	14.98090(10)	20.81060(10)	24.82890(10)
α / °	90	90	90
β / °	100.5330(10)	100.1510(10)	90
γ / °	90	90	90
V / Å3	2511.81(3)	6181.75(6)	12257.27(9)
Space Group	*P*2/n	*P*2/n	*P*bcn
Z value	2	4	8
D_{calc} / g cm^{-3}	1.379	1.347	1.330
Temperature / K	153	153	153
2θmax / °	152.640	152.720	152.666
μ(Cu K$_\alpha$) / mm^{-1}	2.265	1.948	1.967
No. of Reflections	Total: 46771 Unique: 5203 Rint = 0.0330	Total: 117182 Unique: 12831 Rint = 0.0369	Total: 113670 Unique: 12719 Rint = 0.0309
R_1[a]	0.0331	0.0526	0.0365
wR_2[b]	0.0847	0.1545	0.0975
GOF[c]	1.029	1.043	1.042
Max./Mini. peak *I*[d] / Å^3	0.70 e$^-$/-0.56 e$^-$	2.54 e$^-$/-0.77 e$^-$	0.79 e$^-$/-0.48 e$^-$
Flack Parameter	-	-	-

[a]:$I > 2.00\sigma(I)$. [b]:All reflections. [c]:Goodness of Fit Indicator. [d]: in Final Diff. Map.

Table 20. Summary of X-ray crystallographic data of the crystals **5** and **7**

compound	$[Cu(XantPhos)_2]BF_4$ (**5**)	$[Cu_2(dppf)_3]_2BF_4$ (**7**)
CCDC Number	2445752	2445753
Empirical Formula	$C_{78}H_{64}BCuF_4O_2P_4$	$C_{52}H_{42}BCuF_4Fe_{1.5}NP_3$
Formula Weight	1307.52	1007.90
Crystal System	orthorhombic	monoclinic
Crystal Size / mm	0.2 × 0.05 × 0.05	0.05 × 0.05 × 0.01
a / Å	18.27100(10)	32.6597(9)
b / Å	18.39760(10)	14.7589(2)
c / Å	18.61640(10)	25.9972(7)
α / °	90	90
β / °	90	128.916(4)
γ / °	90	90
V / Å3	6257.76(6)	9750.1(6)
Space Group	*P*bcn	*C*2/c
Z value	4	8
D_{calc} / g cm^{-3}	1.388	1.373
Temperature / K	153	153
2*θ*max / °	155.952	150.492
μ(Cu K$_\alpha$) / mm^{-1}	1.961	5.417
No. of Reflections	Total: 56712 Unique: 6486 Rint = 0.0229	Total: 16913 Unique: 8451 Rint = 0.0220
R_1[a]	0.0781	0.0568
wR_2[b]	0.1626	0.1849
GOF[c]	1.226	1.070
Max./Mini. peak *I*[d] / Å^3	0.91 e$^-$/-0.68 e$^-$	1.52 e$^-$/-0.48 e$^-$
Flack Parameter	-	-

[a]:$I > 2.00\sigma(I)$. [b]:All reflections. [c]:Goodness of Fit Indicator. [d]: in Final Diff. Map.

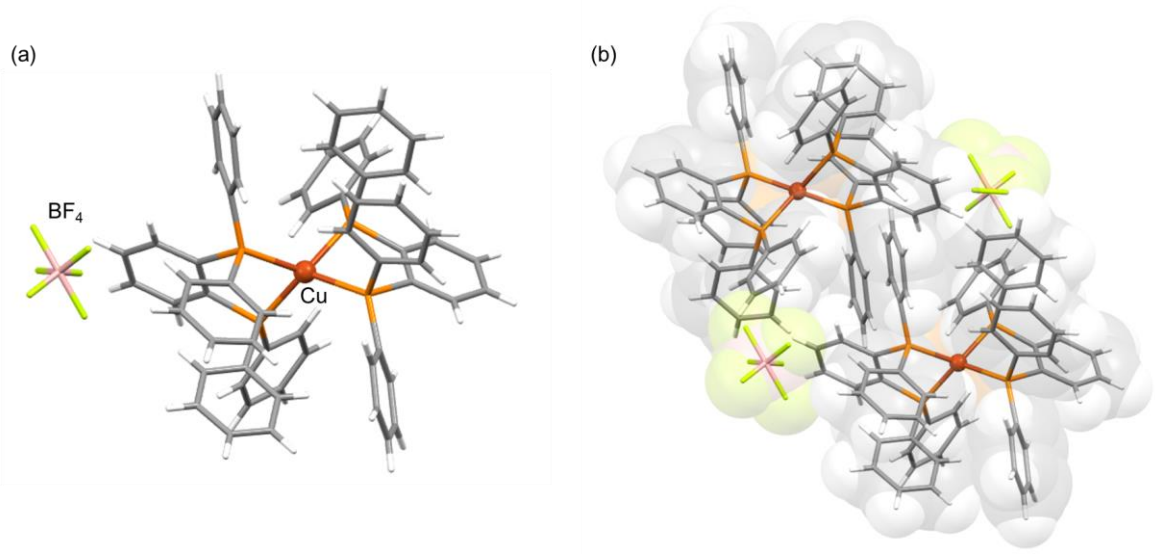

Figure 52. Single-crystal structure of $[Cu(dppbz)_2]BF_4$ (**1**) at 153 K. (a) Illustration of the single molecule. (b) Intermolecular packing structure.

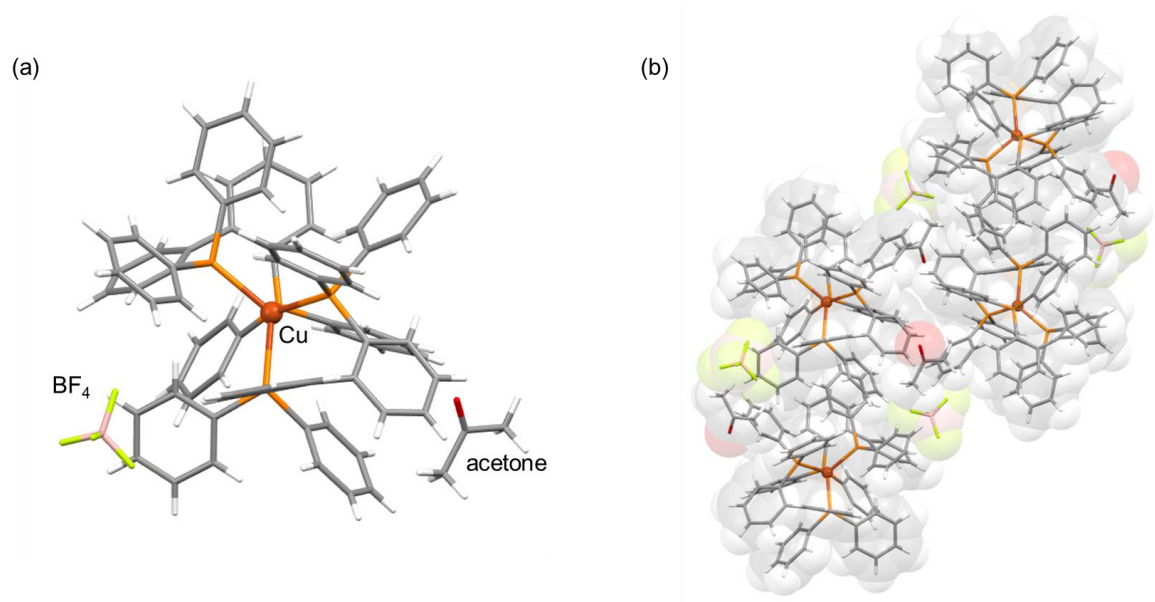

Figure 53. Single-crystal structure of $[Cu(BIPHEP)_2]BF_4$ (**3**) at 153 K. (a) Illustration of the single molecule. (b) Intermolecular packing structure.

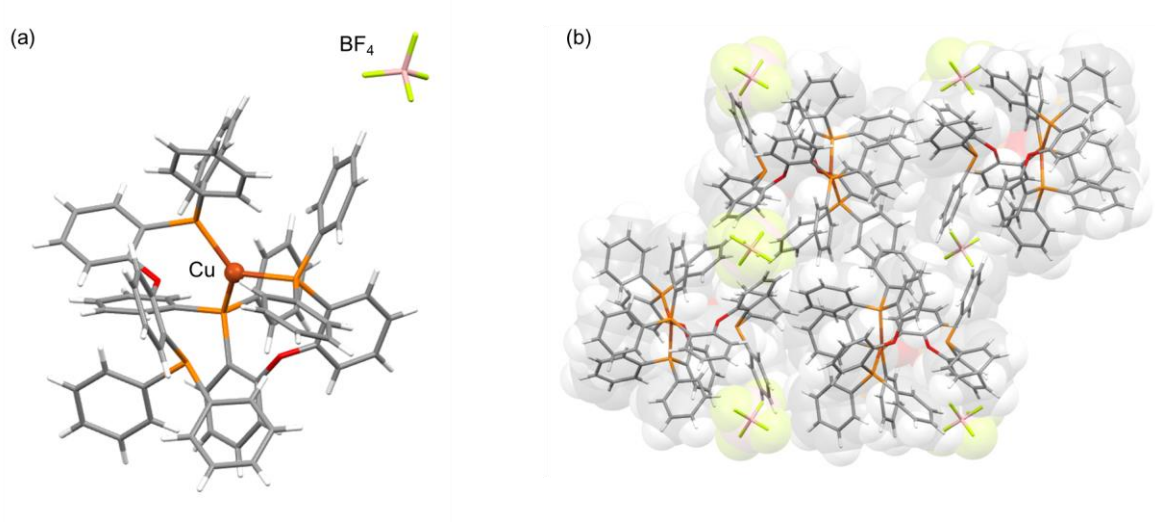

Figure 54. Single-crystal structure of $[Cu(DPEphos)_2]BF_4$ (**4**) at 153 K. (a) Illustration of the single molecule. (b) Intermolecular packing structure.

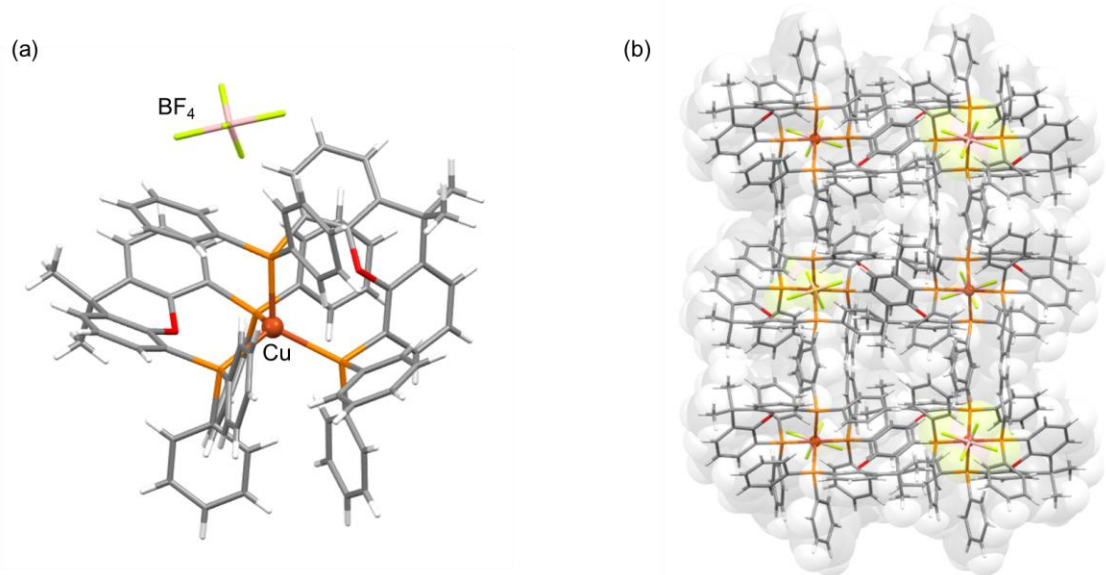

Figure 55. Single-crystal structure of $[Cu(XantPhos)_2]BF_4$ (**5**) at 153 K. (a) Illustration of the single molecule. (b) Intermolecular packing structure.

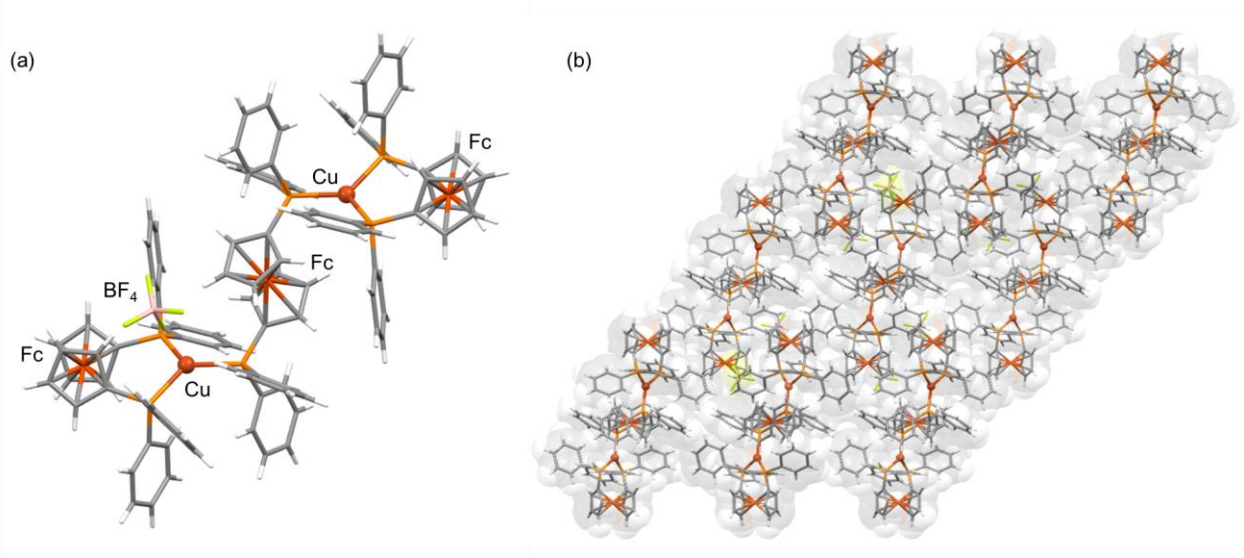

Figure 56. Single-crystal structure of $[Cu_2(dppf)_3]_2BF_4$ (**7**) at 153 K. The disordered *n*-hexane molecules could not be modeled due to multiple orientations and partial occupancies. A solvent mask was applied using the Olex2 MASK routine. *N*-hexane molecules are omitted for clarity. (a) Illustration of the single molecule. (b) Intermolecular packing structure.

Stability Studies

In an argon-filled glovebox, a catalyst solution was prepared in a 3 ml vial with a magnetic stirrer by vigorously stirring $Cu(MeCN)_4BF_4$ (31.4 mg, 0.10 mmol, 1.0 equiv) and dppbz (89.3 mg, 0.20 mmol, 2.0 equiv) in DCE (2.0 mL) for 60 min. The tube was sealed with a PTFE-lined septum cap, removed from the glovebox, and then placed at ~5 cm from two 52 W 390nm Kessil LED lamps. The reaction mixture was vigorously stirred while irradiated at room temperature (with fan cooling). For each time interval (5 h, 10 h , 36 h), 0.3 mL of the solution was transferred to the NMR tube, along with the addition of 0.2 mL of $CDCl_3$. ^{31}P-NMR analysis was performed at each time interval.

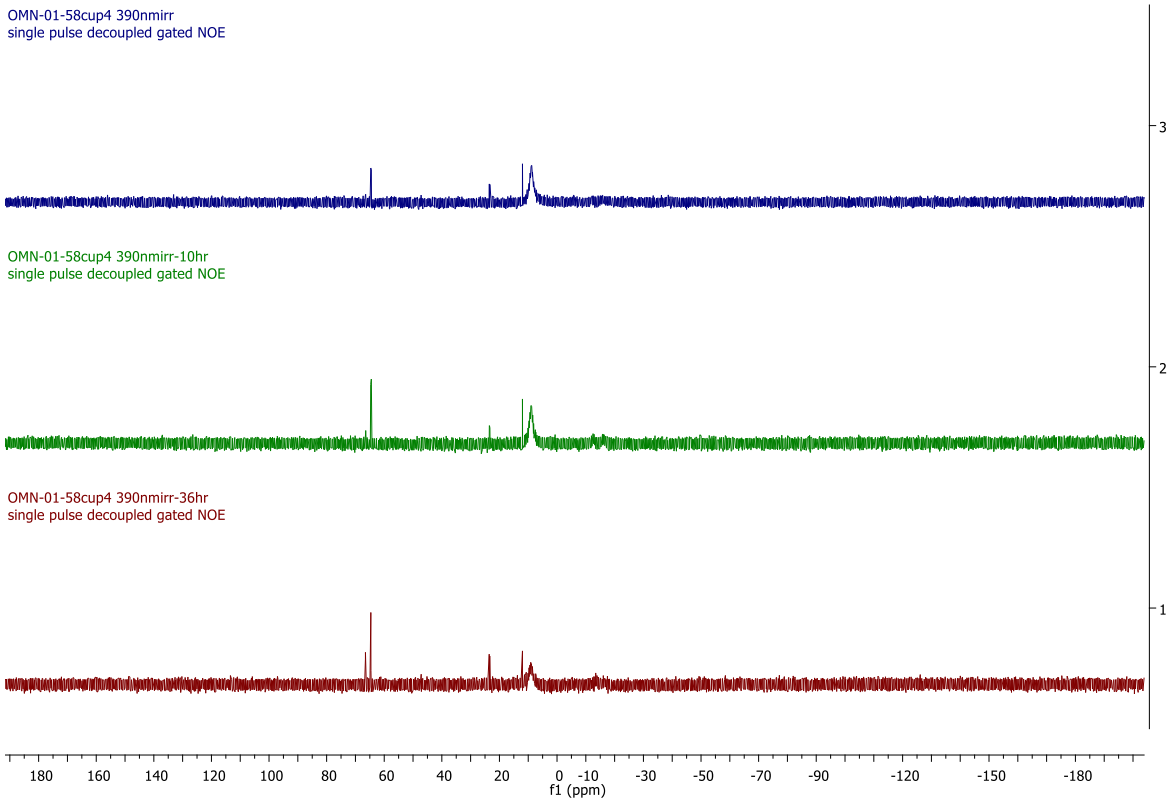

In an argon-filled glovebox, $[Cu(dppbz)_2]^+BF_4^-$ (**1**, 73.0 mg, 0.07 mmol, 1equiv) was added to a 3 ml vial with a magnetic stirrer, followed by the addition of DCE (2.0 mL). The tube was sealed with a PTFE-lined septum cap, removed from the glovebox, and then placed at ~5 cm from two 52 W 390nm Kessil LED lamps. The reaction mixture was vigorously stirred while irradiated at room temperature (with fan cooling). For each time interval (1 h, 3 h , 10 h, and 24 h), 0.3 mL of the solution was transferred to the NMR tube, along with the addition of 0.2 mL of $CDCl_3$. ^{31}P-NMR analysis was performed at each time intervals.

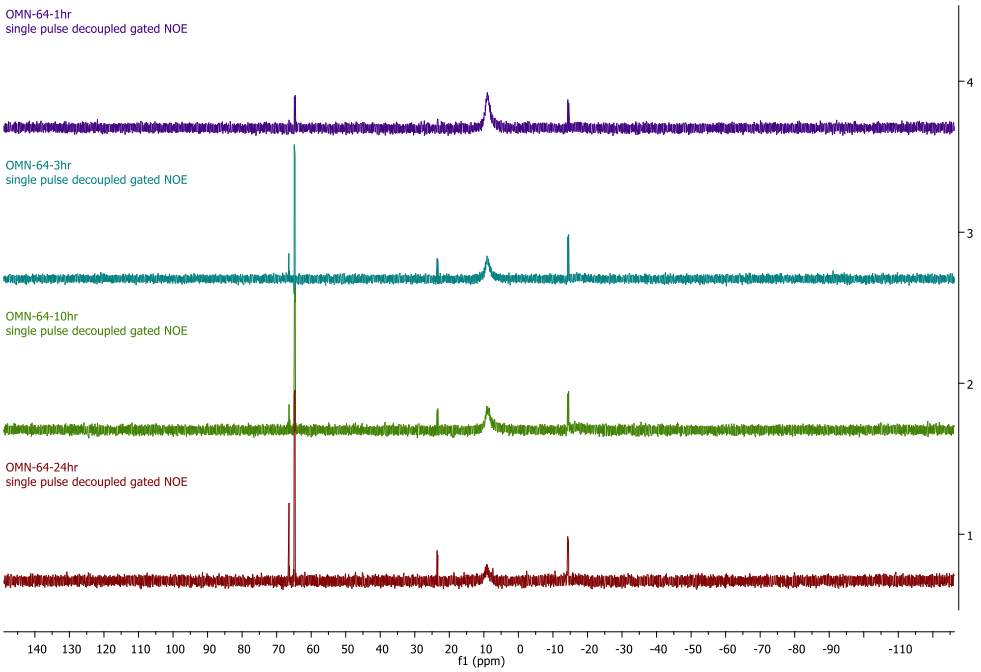

Cu-catalyzed C–I Coupling of Trifluoromethylarenes

In an argon-filled glovebox, a catalyst solution was prepared in a 3-ml vial by vigorously stirring **CuP4** (0.005 mmol, 0.10 equiv) in DCE (0.50 mL) for 60 min. To this solution were added $Zn(OAc)_2$ (9.2 mg, 0.05 mmol, 1.00 equiv), LiI (46.8 mg, 0.35 mmol, 7.00 equiv), 4-(trifluoromethyl)benzonitrile (8.6 mg, 0.05 mmol, 1.00 equiv), and *tert*-amyl alcohol (10.8 mL, 0.1 mmol, 2.00 equiv), followed by the addition of a stir bar and DCE (1.00 mL). The tube was sealed with a PTFE-lined septum cap, removed from the glovebox, and placed at ~5 cm from two 52 W 390-nm Kessil LED lamps. The reaction mixture was vigorously stirred while irradiated for 24 h at room temperature (with fan cooling). For the determination of ^{19}F-NMR yields, (trifluoromethoxy)benzene (0.1 mmol, 2.00 equiv) was added to the reaction mixture as the standard.

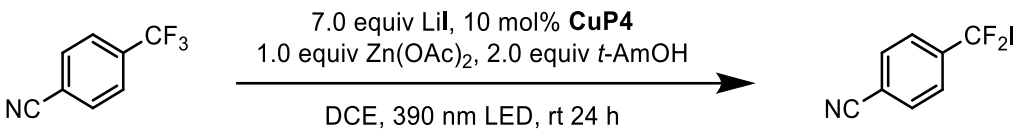

Entry[a]	CuL	Yield (%)[b]
1	$[Cu(dppbz)_2]^+BF_4^-$ (**1**)	77
2	$[Cu((R)\text{-}BINAP)_2]^+BF_4^-$ (**2**)	<5
3	$[Cu(BIPHEP)_2]^+BF_4^-$ (**3**)	2
4	$[Cu(DPEphos)_2]^+BF_4^-$ (**4**)	5
5	$[Cu(XantPhos)_2]^+BF_4^-$ (**5**)	6
6	None	<5

Cu-catalyzed Hydrodehalogenation of Aryhalides

Screening of base

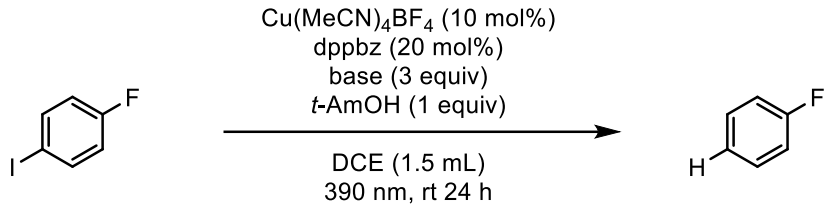

Entry[a]	Base	Yield (%)[b]
1	None	35
2	Et_3N	90
3	HMDS	39
4	DBU	85
5	DIPEA	>99
6	NaOtBu	58
7	K_2CO_3	35
8	Cs_2CO_3	42

Table 21. [a]Reactions were carried out using 0.1 mmol of iodide, 3 equiv of base, and 1 equiv of *t*-AmOH in DCE under irradiation with violet LEDs (390 nm) for 24 h at rt. [b]Yields were determined by ^{19}F-NMR analysis of the crude mixture using (trifluoromethoxy)benzene as the standard.

Screening of copper complexes

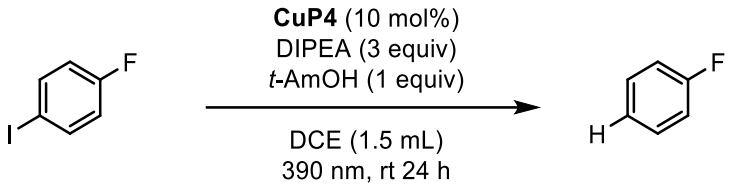

Entry[a]	CuP4	Yield (%)[b]
1	$[Cu(dppbz)_2]^+BF_4^-$ (**1**)	98
2	$[Cu((R)\text{-}BINAP)_2]^+BF_4^-$ (**2**)	47
3	$[Cu(BIPHEP)_2]^+BF_4^-$ (**3**)	24
4	$[Cu(DPEphos)_2]^+BF_4^-$ (**4**)	17
5	$[Cu(XantPhos)_2]^+BF_4^-$ (**5**)	35

Table 22. [a]Reactions were carried out using 0.1 mmol of iodide, 3 equiv of DIPEA, and 1 equiv of *t*-AmOH in DCE under irradiation with violet LEDs (390 nm) for 24 h at rt. [b]Yields were determined by ^{19}F-NMR analysis of the crude mixture using (trifluoromethoxy)benzene as the standard.

Control experiments

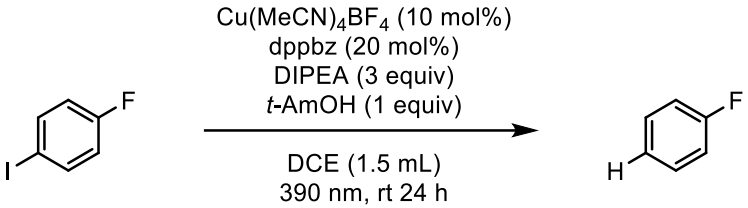

Entry	Conditions	Yield (%)[a]
1	standard conditions	>99
2	Isolated $[Cu(dppbz)_2]^+BF_4^-$ (**1**)	83
3	no Cu/L	14
4	no *t*-AmOH	72
5	no DIPEA	24
6	no light, rt or 60 ºC	<5
7	440 nm	15

Table 23. [a]Yields were determined by ^{19}F-NMR analysis of the crude mixture using (trifluoromethoxy)benzene as the standard.

General procedure for hydrodehalogenation reactions

In an argon-filled glovebox, a catalyst solution was prepared in a 50-ml vial with a magnetic stirrer by vigorously stirring $Cu(MeCN)_4BF_4$ (15.7 mg, 0.05 mmol, 0.10 equiv) and dppbz (44.6 mg, 0.10 mmol, 0.20 equiv) in DCE (2.5 mL) for 60 min. To the above solution were added aryl iodide/bromide (0.50 mmol, 1.00 equiv), DIPEA (261.28 mL, 1.50 mmol, 3.00 equiv), *tert*-amyl alcohol (54.41 mL, 0.50 mmol, 1.00 equiv), and DCE (5 mL). The tube was sealed with a PTFE-lined septum cap, removed from the glovebox, and then placed at ~5 cm from two 52 W 390-nm Kessil LED lamps. The reaction mixture was vigorously stirred while irradiated for 24 h at room temperature (with fan cooling). The resulting mixture was quenched with 20 ml saturated NH_4Cl solution, extracted with EtOAc (30 mL), and washed with water and brine. The organic phase was dried with Na_2SO_4, and the filtrate was concentrated under reduced pressure. The crude was purified by flash column chromatography (Biotage, 100-g silica gel column, EtOAc in pentane/hexane as the eluent). For the determination of ^{19}F-NMR yields, (trifluoromethoxy)benzene (0.50 mmol, 1.00 equiv) was added to the reaction mixture as the standard.

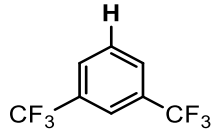

1,3-Bis(trifluoromethyl)benzene (3a). Prepared according to the general procedure, and the title compound was obtained in 99% NMR yield with spectroscopic characterization consistent with the literature.[74]

^{19}F NMR (376 MHz, $CDCl_3$) δ (ppm) -63.21.

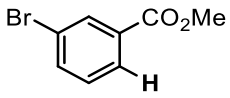

Methyl 3-bromobenzoate (3a). Prepared according to the general procedure (3-10% EtOAc solution in hexane for column chromatography), and the title compound was obtained as a

[74] Qi, J.; Xu, J.; Ang, H. T.; Wang, B.; Gupta, N. K.; Dubbaka, S. R.; O'Neill, P.; Mao, X.; Lum, Y.; Wu, J. *J. Am. Chem. Soc.* **2023**, *145*, 24965– 24971.

colorless oil (139.5 mg, 6% hexane, 81% yield) with spectroscopic characterization consistent with the literature.[75]

^{1}H NMR (400 MHz, $CDCl_3$) δ (ppm) 8.17 (t, *J* = 1.8 Hz, 1H), 7.97 – 7.94 (m, 1H), 7.69 – 7.65 (m, 1H), 7.31 (t, *J* = 7.9 Hz, 1H), 3.91 (s, 3H).

^{13}C NMR (101 MHz, $CDCl_3$) δ (ppm) 165.85, 135.97, 132.71, 132.15, 130.06, 128.26, 122.56, 52.53.

HRMS (APCI) *m/z* calculated for $C_8H_8BrO_2^+$ ($[M+H]^+$): 214.9697, found: 214.9700.

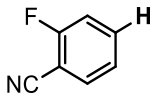

2-Fluorobenzonitrile (3a). Prepared aryl bromide according to the general procedure, and the title compound was obtained in 95% NMR yield with spectroscopic characterization consistent with the literature.[76]

^{19}F NMR (376 MHz, $CDCl_3$) *δ* (ppm) -106.76 – 106.97 (m).

HRMS (EI) *m/z* calculated for $C_7H_4FN^+$ ($[M]^+$): 121.0328, found: 121.0321.

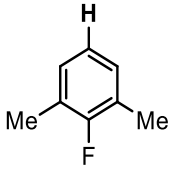

2-Fluoro-1,3-dimethylbenzene (3a). Prepared from aryl bromide according to the general procedure, and the title compound was obtained in 11% NMR yield with spectroscopic characterization consistent with the literature.[77]

^{19}F NMR (376 MHz, $CDCl_3$) *δ* (ppm) -124.25 – 124.33 (m).

HRMS (EI) *m/z* calculated for $C_8H_9F^+$ ($[M]^+$): 124.0688, found: 124.0682.

[75] Shao, C.; Lu, A.; Wang, X.; Zhou, B.; Guan, X.; Zhang, Y. *Org. Biomol. Chem.* **2017**, *15*, 5033–5040.

[76] Mudshinge, S. R.; Potnis, C. S.; Xu, B.; Hammond, G. B. *Green Chem.* **2020**, *22*, 4161–4164.

[77] Gatenyo, J.; Vints, I.; Rozen, S. *J. Org. Chem.* **2013**, *78,* 23, 11794–11797.

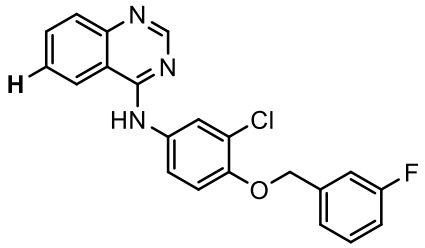

***N*-(3-chloro-4-((3-fluorobenzyl)oxy)phenyl)quinazolin-4-amine (3a).** Prepared according to the general procedure (3-15% EtOAc solution in hexane for column chromatography), and the title compound was obtained as a colorless oil (192.19 mg, 21% hexane, 13% EtOAc, 94% yield).

^{1}H NMR (400 MHz, $CDCl_3$) δ (ppm) 8.76 (s, 1H), 7.90 (dd, *J* = 14.1, 8.3 Hz, 2H), 7.84 – 7.77 (m, 2H), 7.58 – 7.49 (m, 3H), 7.38 – 7.33 (m, 1H), 7.25 – 7.19 (m, 2H), 7.05 – 6.99 (m, 1H), 6.96 (d, *J* = 8.9 Hz, 1H), 5.14 (s, 2H).

^{13}C NMR (101 MHz, $CDCl_3$) δ (ppm) 164.37 (s), 159.82 (d, *J* = 422.7 Hz), 155.05 (s), 151.26 (s), 150.11 (s), 139.17 (d, *J* = 7.3 Hz), 133.20 (s), 132.25 (s), 130.34 (d, *J* = 8.3 Hz), 129.16 (s), 126.89 (s), 124.93 (s), 123.76 (s), 122.57 (d, *J* = 3.0 Hz), 121.95 (s), 120.39 (s), 115.08 (d, *J* = 21.2 Hz), 115.04 (s), 114.54 (s), 114.12 (d, *J* = 22.3 Hz), 70.56 (d, *J* = 2.0 Hz).

^{19}F NMR (376 MHz, $CDCl_3$) *δ* (ppm) -112.40 – -112.53 (m).

HRMS (ESI) *m/z* calculated for $C_{21}H_{16}ClFN_3O^+$ ($[M+H]^+$): 390.0961, found: 390.0955.

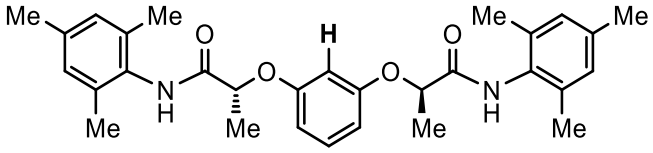

(2*R*,2'*R*)-2,2'-(1,3-phenylenebis(oxy))bis(N-mesitylpropanamide) (3a). Prepared according to the general procedure (10-45% EtOAc/hexane for column chromatography), and the title compound was obtained as a brown solid (25 mg, 15% (SM+EtOAc), 12% yield).

^{1}H NMR (400 MHz, $CDCl_3$) δ (ppm) 7.51 (s, 2H), 7.28 (m, 1H), 6.85 (s, 4H), 6.69 (m, 3H), 4.85 (q, *J* = 6.7 Hz, 2H), 2.24 (s, 6H), 2.05 (s, 12H), 1.73 (d, *J* = 6.7 Hz, 2H).

^{13}C NMR (101 MHz, $CDCl_3$) δ (ppm) 170.68, 158.51, 137.39, 135.16, 130.95, 129.93, 129.17, 108.71, 104.00, 75.57, 21.04, 19.46, 18.23.

HRMS (ESI) *m/z* calculated for $C_{30}H_{36}N_2O_4Na^+$ ($[M+Na]^+$): 511.2568, found: 511.2557.

Cu-catalyzed C–S Coupling

Control experiments

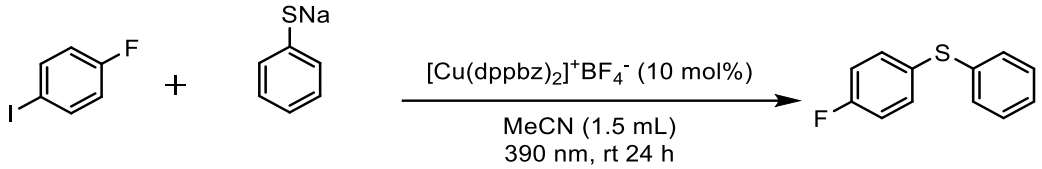

Entry[a]	Experiments	Yield (%)[b]
1	standard conditions	79
2	no $[Cu(dppbz)_2]^+BF_4^-$ (**1**), 390 nm	25
3	with **1**, 440 nm	70
4	no **1**, 440 nm	53
5	no light, rt or 80 °C	0

Table 24. [a]Reactions were carried out using 0.1 mmol of iodide, 3 equiv of sodium phenyl thiolate in MeCN under irradiation with violet LEDs (390 nm) for 24 h at rt. [b]Yields were determined by ^{19}F-NMR analysis of the crude mixture using (trifluoromethoxy)benzene as the standard.

Screening of solvents

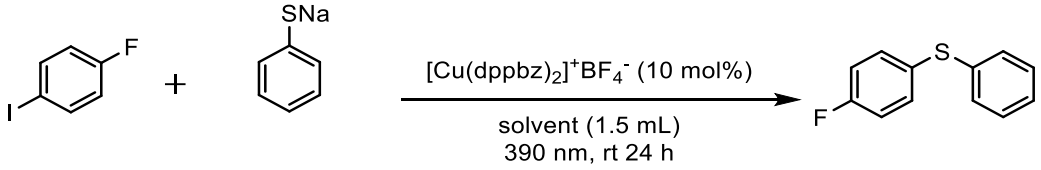

Entry[a]	Solvents	Yield (%)[b]
1	MeCN	88
2	THF	54
3	1,4-Dioxane	0
4	Toluene	5
5	DCE	2
6	Et_2O	25
7	Benzene	6

Table 25. [a]Reactions were carried out using 0.1 mmol of iodide and 3 equiv of sodium phenyl thiolate in above mentioned solvents under irradiation with violet LEDs (390 nm) for 24 h at rt. [b]Yields were determined by ^{19}F-NMR analysis of the crude mixture using (trifluoromethoxy)benzene as the standard.

General procedure for C–S coupling reaction

To a 50 ml round-bottomed flask with a magnetic stirrer were added $[Cu(dppbz)_2]^+BF_4^-$ (**1**) (15.7 mg, 0.05 mmol, 0.10 equiv), 4-fluoroiodobenzene (0.50 mmol, 1.00 equiv), and MeCN (7.5 mL). The tube was sealed with a PTFE-lined septum cap, removed from the glovebox, and then placed at ~5 cm from two 52 W 390-nm Kessil LED lamps. The reaction mixture was vigorously stirred while irradiated for 24 h at room temperature (with fan cooling). The resulting yellow turbid mixture was concentrated, and the crude was purified by flash column chromatography (Biotage, 100-g silica gel column, EtOAc in pentane/hexane as the eluent).

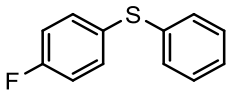

(4-Fluorophenyl)(phenyl)sulfane (3a). Prepared according to the general procedure (0-7% EtOAc solution in hexane for column chromatography), and the title compound was obtained as a colorless oil (95.1 mg, 2.3% EtOAc, 92% yield) with spectroscopic characterization consistent with the literature.

^{1}H NMR (400 MHz, $CDCl_3$) δ (ppm) 7.54 – 7.50 (m, 1H), 7.43 – 7.20 (m, 7H), 7.07 – 7.01 (m, 1H).

^{19}F NMR (376 MHz, $CDCl_3$) *δ* (ppm)) -113.80 – -113.93 (m).[78]

HRMS (EI) *m/z* calculated for $C_{12}H_9FS^+$ ($[M]^+$): 204.0409, found: 204.0403.

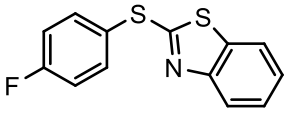

2-((4-Fluorophenyl)thio)benzo[d]thiazole (3a). Prepared according to the general procedure (5% EtOAc solution in hexane for column chromatography), and the title compound was obtained as a colorless oil (120.1 mg, 5% hexane, 5% EtOAc, *ca* 90% pure, 80% yield).

^{1}H NMR (400 MHz, $CDCl_3$) δ (ppm) 7.89 – 7.86 (m, 1H), 7.76 – 7.72 (m, 2H), 7.67 (ddd, *J* = 8.0, 1.2, 0.6 Hz, 1H), 7.41 (ddd, *J* = 8.3, 7.3, 1.2 Hz, 1H), 7.31 – 7.27 (m, 1H), 7.21 – 7.16 (m, 2H).

[78] Wang, X.; Cuny, G. D.; Noël T. *Angew. Chem., Int. Ed.* **2013**, *52*, 7860–7864.

^{13}C NMR (101 MHz, $CDCl_3$) δ (ppm) 169.68 (d, *J* = 2.0 Hz), 164.36 (d, *J* = 252.1 Hz), 154.07, 137.94 (d, *J* = 8.8 Hz), 135.60, 126.40, 125.24 (d, *J* = 3.5 Hz), 124.55, 122.13, 120.96, 117.40 (d, *J* = 22.2 Hz).

^{19}F NMR (376 MHz, $CDCl_3$) *δ* (ppm) -108.76 – -108.84 (m).

HRMS (ESI) *m/z* calculated for $C_{13}H_9FNS_2^+$ ($[M+H]^+$): 262.0155, found: 262.0150.

Publication list

Publications included in the thesis:

[1] **Priya Saha**, Mingoo Jin, Dennis Chung Yang Huang. Defluorinative C−O Coupling between Trifluoromethylarenes and Alcohols via Copper Photoredox Catalysis. *Angew. Chem. Int. Ed.* **2025***, 64*, e202419591.

[2] **Priya Saha**, Ryunosuke Tomita, Takao Tsuneda, Tetsuya Taketsugu, Mingoo Jin, Dennis Chung-Yang Huang. Homoleptic Copper(I)-bisphosphine Complexes as Photoredox Catalysts. *manuscript submitted*.

Publications not included in the thesis:

[1] Amit K. Jaiswal, **Priya Saha**, Julong Jiang, Kimichi Suzuki, Anna Jasny, Bernd M. Schmidt, Satoshi Maeda, Stefan Hecht, Dennis Chung-Yang Huang. Accessing a Diverse Set of Functional Red-Light Photoswitches by Selective Copper-Catalyzed Indigo *N*-Arylation. *J. Am. Chem. Soc.* **2024**, *146,* 21367–21376.

Acknowledgement

The research mentioned in this thesis was carried out under the supervision of Prof. Dr. Dennis Chung-Yang Huang at Institute for Chemical Reaction Design and Discovery (ICReDD), Hokkaido University from September 2022 to September 2025.

I would like to express my sincere and heartfelt thanks to Prof. Dr. Dennis Chung-Yang Huang for his unwavering support, kind encouragement, and generous guidance which have been invaluable throughout the course of my research. It has been a great privilege to learn under his mentorship, and this achievement would not have been possible without his dedicated supervision, and I will always be grateful for his mentorship.

I would like to sincerely thank Prof. Mingoo Jin and his research group for their generous support and collaboration. Their assistance in performing the single-crystal X-ray diffraction measurements, studying liquid crystal molecules, and guiding the emission decay measurements has been invaluable to this work. I am also deeply grateful to Prof. Takao Tsuneda and Prof. Tetsuya Taketsugu for their contributions in carrying out the theoretical calculations presented in this thesis. Their expertise added great depth and clarity to the study. I would also like to express my appreciation to Prof. Dr. Masaya Sawamura, Prof. Dr. Yusuke Masuda, Prof. Dr. Yohei Shimizu, and Prof. Dr. Min Gao for the thoughtful and insightful discussion.

I am truly grateful to the committee members of my doctoral thesis for their time, thoughtful evaluation, and valuable feedback. The insightful suggestions and comments from Prof. Dr. Hajime Ito, Prof. Dr. Yasuhide Inokuma, Prof. Dr. Kazuki Sada, Prof. Dr. Yohei Shimizu, and Prof. Dr. Mingoo Jin have been influential in improving the quality and clarity of this thesis.

I would also like to thank the MEXT doctoral program for providing generous scholarship support throughout the course of my Ph.D. studies. This support has been essential in allowing me to fully dedicate myself to my research.

I would like to express my deepest gratitude to my family for their unwavering support, love, and encouragement. My father, Late Parimal Saha, my mother, Shyamoli Saha, and my sister, Riya Saha, have stood by me every step of the way, offering constant motivation and care. This journey was not mine alone, it was also their dream to see me complete my Ph.D. and graduate, and I carry their hopes with me in every achievement. I also remember with love and gratitude my grandmothers, Late Parul Saha and Late Rekha Rani Saha, whose words and strength inspired me to grow into a resilient and compassionate person. Their blessings continue to guide me.

I would also like to thank the alumni of Huang Lab, Dr. Amit Kumar Jaiswal and Kai Sun for their guidance, support, and helpful discussions during the early stages of my research. My sincere thanks also go to the present lab members, especially Dr. Vishal Jyoti Roy, for his camaraderie and continued support. I am grateful to Dr. Ervin Kovács, visiting scientist, and Anna Nožičková, visiting student, for their collaboration and valuable input during their time in the lab. Their presence enriched both the academic environment and the experience of working together.

I would like to sincerely thank Prof. Dr. Maya Shankar Singh, Prof. Dr. Asok Kumar Basak, and Prof. Dr. Vinod Prasad Singh for their valuable guidance and encouragement. Their insights and mentorship, especially during my formative academic years, have played a meaningful role in shaping my journey in research and chemistry.

I would like to extend my heartfelt thanks to my dear friends Irtaza Qureshi, Emna Mejri, Mahesh Dubey, Jyoti Singh, Sheetal Jaiswal, Saumya Singh, Shivam Jaiswal, Sundari Kumari, Ganesh Kumar Bindra, Akash Dweep, Saurabh Pandey, and Jaishree Mishra. Their friendship, encouragement, and constant support have meant a great deal to me throughout this journey. In times of stress and joy alike, their presence has brought comfort, laughter, and strength.

Above all, I would like to thank God for constant guidance, strength, and blessings throughout this journey. In moments of doubt and difficulty, faith has been my anchor, and I am deeply grateful for the grace that has carried me through.

सर्वेभ्यः कृतज्ञता

Sarvebhyaḥ kṛtajñatā

Gratitude to all**.**

Priya Saha